ANTIMICROBIAL MECHANISM OF *TRANS*-CINNAMALDEHYDE AND OTHER ESSENTIAL OIL COMPOUNDS IN *LISTERIA MONOCYTOGENES*

Gil ROGIERS

Supervisor:
Prof. Chris Michiels

Co-supervisor:
Prof. Abram Aertsen

Members of the Examination Committee:
Prof. Johan Buyse, chairman, KU Leuven
Prof. Rob Lavigne, KU Leuven
Prof. Marc Hendrickx, KU Leuven
Prof. Stanley Brul, Universiteit van Amsterdam
Dr. Rob Van Houdt, SCK-CEN

Dissertation presented in partial fulfilment of the requirements for the degree of Doctor of Bioscience Engineering

September 2017

Doctoraatsproefschrift nr. 1449 aan de faculteit Bio-ingenieurswetenschappen van de KU Leuven

Uitgegeven in eigen beheer, Gil Rogiers, Korte Heistraat 36 B-2800 Mechelen

Preface – Acknowledgements

Na 4 jaar onderzoek, 4 jaar focus op één en hetzelfde onderwerp en het ontrafelen van mysterieuze waarnemingen en raadsels, is nu de tijd gekomen om definitief een punt achter mijn carrière als doctoraatsonderzoeker te zetten. De deur van het labo Levensmiddelenmicrobiologie van de KU Leuven kan ik echter niet achter mij toe trekken zonder eerst nog een aantal mensen uitvoerig te bedanken.

Eerst en vooral wil ik de jury, prof. Marc Hendrickx, prof. Rob Lavigne, dr. Rob Van Houdt en prof. Stanley Brul bedanken voor de suggesties en het kritisch nalezen en becommentariëren van mijn manuscript. Special thanks to dr. Biniam T. Kebede, former member of the Lab of Food Technology, and dr. Bram Van den Bergh from CMPG, who both helped me with experiments that delivered new insights into our research and took it to a higher level. Biniam, thanks for showing me the potential of HS-SPME-GC-MS measurements and the assistance during the experiments. We have had a very pleasant and fruitful cooperation. Bram Van den Bergh, ik wil je van harte bedanken voor de assistentie bij de analyse van de whole-genome sequencings en de tijd die je vrijmaakte om de analyse uit te voeren, grondig uit te leggen en te verduidelijken waar nodig.

Van het labo Levensmiddelenmicrobiologie zou ik graag als eerste persoon mijn promotor prof. Chris Michiels willen bedanken. Bedankt voor de kans die je mij hebt gegeven om onderzoek uit te voeren in het Labo Levensmiddelenmicrobiologie en het vertrouwen waarmee je me vanaf het begin zelfstandig onderzoek hebt laten uitvoeren. Je deur stond altijd open en je was altijd geïnteresseerd om resultaten te bespreken. Hierdoor overlegde we bijna dagelijks resultaten, waardoor we kort op de bal konden spelen en wat uiteindelijk tot een zeer constructieve en aangename samenwerking heeft geleid. Op wetenschappelijk vlak heb ik veel van je geleerd en dit uiteraard ook proberen toe te passen in mijn onderzoek, blijkbaar zodanig veel dat sommige mensen me zelfs begonnen te vertellen dat ik op je begon te lijken. Blijkbaar heeft de kalmte waarmee ook ik zaken aanpak en uitleg er iets mee te maken. Ik sta soms nog steeds versteld van je brede wetenschappelijke kennis, ook buiten (levensmiddelen)microbiologie, en de gave die je hebt om zeer genuanceerd maar toch beknopt een wetenschappelijke theorie op papier te zetten. Dit bleek telkens opnieuw uit de verbeteringen van een paper of mijn doctoraat. Ik wil je dan zeker en vast ook bedanken voor

de tijd die je hebt gestoken in het nalezen van mijn manuscript. Ik wil je ook bedanken om me ook buiten mijn eigen onderzoek te betrekken bij grotere en kleinere industriële projecten. Dit heeft mijn kennis in de levensmiddelenmicrobiologie zeker en vast verbreed met ervaring uit de industriële praktijk, kennis die me later nog van pas zal komen.

Naast mijn promotor, wil ik ook mijn copromotor prof. Abram Aertsen bedanken. Hoewel ons aantal wetenschappelijke discussies eerder beperkt bleven tot de lab meetings en een paar eenzame middagmaaltijden waarop je me vergezelde, zetten deze korte maar krachtige discussies me toch telkens weer op scherp en gaven ze me vaak nieuwe inspiratie, waarvoor dank.

Hoewel het grootste deel van de bevolking meent dat wij als doctoraatstudenten zeer solitair werken (als het al als werken beschouwd wordt en niet als studeren of gratis en voor niets experimentjes uitvoeren voor het belang van de wetenschap), toch kan je als onderzoeker niet elk gek experiment zelf bedenken en uitvoeren en hebben ook wij collega's en vrienden nodig die ons doorheen de moeilijke tijden helpen. Moeilijke tijden wanneer je zoveelste experiment mislukt, wanneer je nog maar eens een irrelevante waarneming doet die niet publiceerbaar blijkt te zijn, wanneer je de relevantie van je onderzoek in twijfel trekt of wanneer die ene reviewer je manuscript van die broodnodige paper onterecht verwerpt. Ik ben er dan ook van overtuigd dat ik niet aan dit voorwoord toe was gekomen zonder mijn familie, maar zeker ook niet zonder mijn vrienden-collega's uit het labo die van de afgelopen vier jaar vooral een zeer aangename periode gemaakt hebben. Door hen kwam ik bijna alle dagen met plezier naar het labo.

De persoon die indirect, maar vaak ook wel direct, een van de grootste bijdragen levert aan alle doctoraten die in het Labo Levensmiddelenmicrobiologie worden behaald, is onze onmisbare laborant Kristof. Eigenlijk past de titel van lab manager hem veel beter, want Kristof - en het kan niet voldoende gezegd worden - je bent het fundament van het labo. Je zorgt ervoor dat het labo blijft functioneren door logistieke en technische ondersteuning en door altijd paraat te staan tijdens noodgevallen. Bovendien heb je altijd praktische raad bij de start van een nieuw experiment. Ik ben overigens uiterst blij dat ik vier jaar dezelfde hoek in het labo heb kunnen delen met jou en Charlien. Gezien we beide (en Charlien stiekem ook wel) liefhebbers zijn van hetzelfde genre humor, was plezier steeds gegarandeerd. Ik ben je trouwens nog steeds dankbaar dat je die kleine incubator tussen mij en Charlien hebt gezet.

Het mag nu eindelijk gezegd worden, die incubator is eigenlijk gewoon aangekocht als buffer om Charlien haar uitbreidingsdrang in te perken en mij ook nog wat werkplaats te gunnen. Helaas ben je noodgedwongen de laatste jaren wat meer achter de kast in jouw bureau verzeild geraakt door verbouwingsplannen en toenemende regeltjes en administratie aangeboden door je goede vrienden bij VGM. Maar ook in je bureau wisten we je te vinden voor een goede babbel, wat raad, een mop of wat geklaag en gezaag. Ik hoop overigens van harte dat we elkaar nog af en toe terugzien op een quiz of op een koersfietstocht. Hoewel je enorm benadeeld bent door je rug- en nekklachten, slaagde je er toch als enige in om mij pijn te doen op de hellingen. Kristof, bedankt voor alles!

Charlien en Alexander zijn de volgende twee collega's, die ondertussen echt goede vrienden geworden zijn en die ieder gedurende de afgelopen vier jaar toch wel hun eigen paragraaf in dit dankwoord verdiend hebben. We zijn samen aan het doctoraatsavontuur gestart en hebben tezamen 6 nederlagen bij het IWT kunnen verteren. What doesn't kill you makes you stronger zeggen ze dan… Gelukkig heeft de intelligentste van ons drie dan toch nog een FWO-aspirantenmandaat gehaald. Samen zweten schept een band zo was het klavertje drie (het beter klinkende triumviraat was helaas reeds in gebruik) geboren en hebben we er samen een schitterende tijd van gemaakt. Charlien, we hebben elkaar een beetje toevallig leren kennen, toen je me tijdens je thesisjaar bij je wekelijkse replica-plate sessie elke keer opnieuw vroeg of ik ook naar het vak Religie ging (voor de allerlaatste keer, ik heb dat vak niet gevolgd) en ik stilaan begon te twijfelen of je misschien wel jongdement was. Uiteindelijk belandden we bij dezelfde promotor voor ons doctoraat en nadat *Clostridium*, gelukkig, uit mijn eerste projectvoorstel geschrapt werd, belandde het op jouw bord. Eerlijk gezegd denk ik dat er niemand beter in staat zou geweest zijn om het *Clostridium*-project uit de grond te stampen dan jij. Het mag gezegd worden, het begin van je doctoraat was een kruistocht, maar ik vind dat je zeer trots mag zijn op het werk dat je afgeleverd hebt. Jouw vastberadenheid, ondernemerschap en assertiviteit heb ik altijd enorm bewonderd en heeft me ook zelf aangezet om aan die eigenschappen te werken. Daarnaast ben je rechtuit en eerlijk, een echte team player en heb je de laatste vier jaar voor veel sfeer in het labo en op de bureau gezorgd door af en toe spontaan een danske te placeren of een stukje mee te zingen met je idool Biebs. We hebben gedurende vier jaar samen het practicum microbiologie van de levensmiddelen gegeven en de combinatie van onze beide karakters maakte ons team een geoliede machine.

Ik ben zeer blij dat we 4 jaar samen onderzoek hebben uitgevoerd en ik wens je dan ook nog heel veel succes en plezier in het verre Bocholt met Koen en je huisje, pluisje (dit is voor alle duidelijkheid een hamster), tuintje, hondje,…

Alexander, jou kende ik niet voor je aan je doctoraat startte en gezien je imposant voorkomen had ik toch wel een klein beetje angst of we het wel met elkaar zouden vinden. Na verloop van tijd bleek de heer Cambré vooral ruw van buiten maar zacht vanbinnen. Voor Alexander was geen genetische vraag te veel of wetenschappelijk paper onbekend, Cambré was altijd mee. Jouw werkijver en passie voor onderzoek heb ik steeds bewonderd. Je hield me geregeld up to date van de wetenschappelijke literatuur met je "FYI" mails en zette me daardoor ook aan om net die paper extra te lezen. Bovendien overtuigde je me ook van het nut van fundamentele wetenschap die in eerste instantie niet echt relevant lijkt. Je overtuigde me dan ook van mijn resultaten in crisistijden, waarin ik de relevantie van mijn onderzoek in twijfel trok en het allemaal niet meer zo goed zag zitten. Gezien je brede genetische kennis ben je een echt meerwaarde geweest tijdens mijn doctoraat en dat ben je zeker en vast nog steeds voor het volledige labo. Blijf vooral kritisch tijdens de lab meetings, want ik heb er zelf altijd veel uit geleerd. Ik wens je nog het allerbeste in het verdere verloop van je doctoraat, maar ook daarbuiten.

Voorts wil ik alle overige collega-vrienden uit het labo bedanken. Aurélie, je bent een echte meerwaarde voor de groepssfeer in het labo doordat je regelmatig een etentje of andere activiteit organiseert of doordat je iedereen er regelmatig op wijst dat het nog eens tijd is om een pint te gaan pakken. Ik ben je enorm dankbaar dat je dit jaar een groot deel van het practicum op je schouders hebt genomen, zodat Charlien en ik ons doctoraat met iets meer gemoedsrust konden afwerken. Ik wens je nog veel succes met de verderzetting van het uitdagende *Clostridium* onderzoek en het practicum. Sanne, met jou erbij was plezier gegarandeerd. Je had altijd wel een straf, bizar en/of grappig verhaal en ik bewonder je openheid en eerlijkheid. Oscar, I have the feeling that I got to learn you a bit late, as you are a truly funny and helpful guy. I would like to thank you for the tips and tricks for difficult genetic constructs and your advice when it came to protein functionality. Your knowledge on protein structures and functionality is of great value for the lab! Ines, persoonlijk ken ik je niet zo goed, maar je opgewektheid en je woensdagse quote "het is bijna weekend", vrolijkte ook mijn humeur op. Hyacintha, eigenlijk zou jij mij moeten bedanken aangezien ik je samen met

Chris heb aangenomen voor je huidige job in het labo (mopje…), maar ik ga je toch bedanken voor je ongezouten meningen, hulp in het labo en om waakhond te spelen over de regels in het labo. Julien, Tom, Elisa and Wubishet, it was nice working with you and I wish you all the best in your future (academic) careers. Maarten, ik draag bij deze officieel mijn bacteriën aan jou over. Verzorg ze goed, ontrafel hun geheimen en hou me op de hoogte. Lut, hartelijk bedankt voor de altijd vriendelijke administratieve hulp.

Één van de bepalende factoren die me uiteindelijk overtuigd hebben om aan een doctoraat in het Labo Levensmiddelenmicrobiologie te starten, zijn een aantal ex-collega's. Julie, door jou uitstekende begeleiding van mijn thesis en de inhoud van mijn thesis kreeg ik de smaak voor onderzoek in het domein van levensmiddelenmicrobiologie te pakken wat mij uiteindelijk tot dit punt heeft gebracht. Bram, van jou heb ik de onmisbare genetische basisvaardigheden geleerd volgens de regels van de kunst in het eerste jaar van mijn doctoraat. Ik heb het altijd jammer gevonden dat je niet aan een postdoc bent begonnen in het labo. Niet alleen omdat je net zoals ik veel belang hecht aan regels en structuur en ook steevast tussen 12u en 12u15 ging lunchen, maar vooral omdat jouw gestructureerde aanpak van experimenten en plichtsbewustheid een echte meerwaarde waren geweest voor het labo. William, Sander en Johan, jullie werkijver en passie voor jullie onderzoek hebben mezelf ook gestimuleerd om af en toe nog een tandje bij te steken en nu en dan in het weekend een experiment op te volgen. Angela, your ability to keep on working hard and holding on in difficult times, while keeping a smile on your face and staying super gentle to everyone was just admirable and inspiring.

Als laatste medewerker aan mijn doctoraat wil ik mijn enige thesisstudent Sofie nog bedanken. Je had de niet zo leuke taak om tussen een slordige 8000 mutanten op zoek te gaan naar een aantal interessante mutanten voor ons onderzoek. Gelukkig heb je er een aantal zeer interessante gevonden, waarop in de toekomst zeker nog verder onderzoek zal uitgevoerd worden. Bedankt voor het werk dat je geleverd hebt en de fijne samenwerking.

Tot slot wil ik mijn eigen naaste familie en die van Jitka bedanken voor de steun en interesse in mijn doctoraat. In het bijzonder bedank ik Jitka, mijn ouders, broer en zus, bomma & bompa en oma, maar ook opa van wie ik zeker weet dat hij enorm trots was geweest en dit graag had meegemaakt. Hun rol in mijn leven en de kansen die ze mij geven zijn van onschatbare waarde en hun steun is onvoorwaardelijk. We zijn een kleine maar zeer hechte familie en het is altijd fijn om thuis te komen. Het is een cliché omdat het waar is, maar ik zou een doctoraat niet behaald hebben zonder jullie.

Bedankt iedereen!

Gil

Summary

Natural antimicrobials enjoy an increasing interest in view of the trend towards healthy, minimally processed food that has a natural image and a conveniently long shelf life. They can be integrated in a hurdle concept of multiple mild food preservation strategies, which address the challenges of this trend in terms of microbiological stability and safety. Studies on natural food preservatives have so far been mainly descriptive, reporting the antimicrobial activity of different extracts and compounds against a range of food spoilage bacteria and pathogens in pure culture and in foods, sometimes in combination with other (natural) antimicrobials or processing and preservation methods. Studies on the mode of action of these compounds are however scarce. Yet, this knowledge is important to understand why some combinations of hurdles are more effective than others and it thus forms the rational basis for the development of more effective hurdle applications. Therefore, the objective of this work was to investigate the mode of action of *trans*-cinnamaldehyde (t-CIN) and allyl isothiocyanate (AIT), which were previously shown to synergistically reinforce bacterial inactivation by high pressure treatment in our laboratory. *Listeria monocytogenes* was chosen as a model organism for this work, since it is one of the most important food-borne pathogens in minimally treated, refrigerated ready-to-eat foods.

First, a genome-wide transposon mutant library of *L. monocytogenes* Scott A was constructed and screened for t-CIN and AIT sensitive mutants. The transposon insertion was identified in t-CIN and AIT sensitive mutants, which resulted in a total of eleven different mutants. After cross-testing the isolated mutants for both compounds, all mutants were found to be hypersensitive to t-CIN and seven out of eleven mutants to AIT. The hypersensitivity was primarily the result of an extended lag phase in the presence of the compounds, while the exponential growth rate and stationary-phase cell density was less affected, with exception for one mutant which had a reduced growth rate but an unaltered lag phase and stationary-phase cell density. Detailed analysis of the WT lag phase in t-CIN revealed no significant bacterial degradation of t-CIN and no transient inactivation. Moreover, resistant mutants did not arise after subculturing the WT strain four times in the presence of t-CIN. Therefore, we concluded that t-CIN induces a transient growth inhibition that cells can overcome after an adaptation phase and that the mutants require a longer time for this adaptation.

One of the most t-CIN and AIT sensitive mutants, which also showed a slightly different colony morphology and attenuated growth at 10 °C, has a disabled branched-chain amino acid aminotransferase, IlvE, which reversibly catalyzes the deamination of branched-chain amino acids to the corresponding α-ketoacids. The latter in turn are substrates for the synthesis of branched-chain fatty acids (BCFAs), which make up more than 90% of the fatty acids found in membranes of *L. monocytogenes.* They are indispensable for its growth at low temperature due to their low phase transition temperature. Both t-CIN tolerance and growth at low temperatures could be restored by genetic complementation and by supplementation of α-ketoacids to the growth medium. Membrane fatty acid analyses revealed that the BCFA content was strongly reduced in the *ilvE* mutant as a result of an almost complete loss of anteiso-BCFAs. This in turn also explains the observed reduced growth rate at 10 °C. Membrane fatty acid analyses after growth in the presence of t-CIN showed that *L. monocytogenes* modulates its membrane fatty acid composition in a way that the membranes become less fluid, suggesting an adaptation to compensate for the membrane fluidizing effect of t-CIN.

While growth of the WT strain in the presence of t-CIN did not yield mutants with increased tolerance, revertants of the *ilvE* mutant with increased t-CIN tolerance could be isolated. Whole-genome sequencing allowed to assign reversion mutations to three genes: three revertants had a mutation in *codY*, four in *argR* and three in *ack.* All *codY* and *argR* revertants displayed, besides increased t-CIN tolerance, a reverted WT colony morphology and partially restored growth at 10 °C. All mutations in the transcriptional regulator CodY are single amino acid substitutions and are predicted to derepress the *ilv-leu* operon, allowing IlvE-independent synthesis of α-ketoacids via threonine and pyruvate. This was confirmed by fatty acid analysis. CodY was previously shown to regulate flagellar synthesis and motility. Interestingly, it was found during motility analysis that the *ilvE* mutant was completely non-motile, and that motility was restored by α-ketoacid supplementation. This strongly suggests that membrane fluidity affects motility, a link that is not yet well established. Furthermore, the CodY revertants had partially restored motility that could also be completely restored to WT level by α-ketoacid supplementation. Together, these results suggested that the CodY variant proteins have lost the ability to repress the IlvE operon (BCFA synthesis), but retained their ability to activate the flagellar operon. All mutations in *argR*, encoding a transcriptional

regulator controlling arginine metabolism, abort translation and were predicted to cause loss of function. These revertants had strongly increased levels of iso-C15:0 fatty acid, suggesting a yet unknown role of ArgR in the regulation of BCFA synthesis. In contrast, both amino acid substitutions and frameshifts were found in the *ack* revertants. These revertants grew even slower at 10 °C than the original *ilvE* mutant and, in accordance with this observation, showed no clear changes in the membrane fatty composition. Nevertheless, they had the highest t-CIN tolerance of all identified revertants, indicating a membrane unrelated tolerance mechanism. *ack* encodes acetate kinase and is thus closely linked to the central carbon metabolism, energy production and generation of reducing power. This may possibly explain the regained t-CIN tolerance in these revertants, because t-CIN is a thiol-reactive compound predicted to disturb the intracellular redox homeostasis.

Finally, the interplay between the serine/threonine PASTA kinase PrkC and YvcK was investigated. YvcK is known to be phosphorylated by PrkC and t-CIN and AIT sensitive transposon mutants in both genes encoding these proteins, were isolated during the screen. The *prkC* mutant displayed moderate hypersensitivity, while the *yvcK* mutants were strongly hypersensitive to both compounds. A phosphoablative T252A/T256A mutant of YvcK, in which the threonine residues that are phosphorylated by PrkC have been replaced by alanine residues, and which can therefore be regarded the equivalent of a *yvcK* knockout strain in terms of phosphorylation, was indistinguishable from WT for growth in t-CIN. In contrast, a phosphomimetic T252E/T256E mutant of YvcK, mimicking a constitutively phosphorylated state of YvcK, showed intermediate t-CIN sensitivity compared to WT and a *yvcK* knockout. We therefore conclude that the sensitivity of the *prkC* mutant cannot be attributed to disabled phosphorylation of YvcK, and that it is probably related to disabled phosphorylation of one or more of the other effector proteins. Nonetheless, the phosphorylation state of YvcK also affected the sensitivity of *L. monocytogenes* for t-CIN.

In summary, this thesis revealed some of the most important proteins and metabolic pathways used by *L. monocytogenes* to cope with the detrimental effects of t-CIN, which will help to better understand the impact of similar essential oils compounds on bacterial metabolism and develop innovative food preservation strategies.

Samenvatting

Door de toenemende vraag naar meer gezonde en minimaal bewerkte levensmiddelen met een natuurlijk imago en voldoende lange houdbaarheid, neemt de belangstelling voor natuurlijke antimicrobiële componenten toe. Deze trend gaat echter gepaard met uitdagingen op vlak van microbiologische stabiliteit en veiligheid. Natuurlijke antimicrobiële componenten hebben het potentieel om tegemoet te komen aan deze uitdagingen wanneer ze in levensmiddelen toegepast worden in een concept van hordentechnologie. Hierbij worden meerdere conserveringsstrategieën gecombineerd om de groei van bacteriën in levensmiddelen efficiënter te onderdrukken en tegelijk de impact op de kwaliteit van het levensmiddel zo klein mogelijk te houden. De meeste studies over deze natuurlijke componenten en combinaties van componenten en bewaringstechnieken zijn eerder beschrijvend, waarbij de antimicrobiële activiteit wordt onderzocht tegen een reeks voedselpathogenen en -bedervers in zuivere culturen en in levensmiddelen. Het werkingsmechanisme van deze natuurlijke componenten wordt echter zelden onderzocht, hoewel dit cruciaal is om te begrijpen waarom sommige combinaties effectiever zijn dan andere. Deze kennis vormt dus de rationele basis voor de ontwikkeling van meer doeltreffende hordenstrategieën. Daarom werd in dit werk het werkingsmechanisme van *trans*-kaneelaldehyde (t-CIN) en allylisothiocyanaat (AIT) onderzocht. Van deze componenten werd eerder in ons laboratorium aangetoond dat ze bacteriële inactivatie door hoge druk op een synergetische manier versterken. Gezien het belang van *Listeria monocytogenes* in minimaal bewerkte, gekoelde kant-en-klare levensmiddelen, werd deze bacterie gebruikt in dit werk als modelorganisme.

Als startpunt werd een genoomwijde transposonmutantenbank van *L. monocytogenes* Scott A aangemaakt en gescreend voor mutanten die gevoelig zijn voor t-CIN en AIT. Lokalisatie van het transposoninsert in zowel de t-CIN als AIT gevoelige mutanten, leverde een totaal van elf mutanten op. Na bepaling van de gevoeligheid van deze mutanten voor beide componenten, bleken alle mutanten gevoelig te zijn voor t-CIN en zeven van de elf voor AIT. De gevoeligheid van de mutanten is voornamelijk zichtbaar in de lagfase, terwijl exponentiële groeisnelheid en celdensiteit in stationaire fase minder getroffen worden. Dit met uitzondering van één mutant die een verlaagde groeisnelheid vertoont, maar een ongewijzigde lagfase en celdensiteit in

stationaire fase. Een gedetailleerde analyse van de lagfase van de wild type (WT) toont aan dat er geen significante bacteriële degradatie van t-CIN plaatsvindt, alsook geen transiënte inactivatie. Daarenboven, ontstaan er geen resistente mutanten wanneer de WT opeenvolgend viermaal wordt opgegroeid in aanwezigheid van t-CIN. Omwille van deze observaties besluiten we dat t-CIN een transiënte groei-inhibitie induceert, die cellen kunnen overwinnen na een aanpassingsfase. De mutanten hebben hiervoor meer tijd nodig, wat resulteert in een verlengde lagfase.

In een van de meest gevoelige mutanten voor t-CIN en AIT, die ook een licht afwijkende koloniemorfologie bezit en verzwakte groei bij 10 °C, is het vertakte-keten aminozuur-aminotransferase, IlvE, uitgeschakeld. Dit enzym katalyseert de deaminatie van vertakte-keten aminozuren tot de overeenkomstige α-ketozuren, dewelke als substraten dienen voor de synthese van vertakte-keten vetzuren (VKVZ). Deze vertegenwoordigen meer dan 90% van de vetzuren in de membranen van *L. monocytogenes* en zijn onmisbaar voor groei bij lage temperaturen. Zowel tolerantie voor t-CIN als groei bij lage temperaturen kan hersteld worden door genetische complementatie en toevoeging van α-ketozuren aan het groeimedium. De hoeveelheid VKVZ bleek na vetzuuranalyse sterk gereduceerd te zijn in de *ilvE* mutant door een bijna volledig verlies van anteiso-VKVZ. Dit verklaart meteen ook de verzwakte groei bij 10 °C. Vetzuuranalyse na groei in aanwezigheid van t-CIN toont aan dat *L. monocytogenes* de membranen aanpast zodat deze minder vloeibaar worden, waardoor het fluïdiserend effect van t-CIN in de membranen wordt tegengewerkt.

In tegenstelling tot de WT, konden van de *ilvE* mutant wel revertanten met verhoogde tolerantie voor t-CIN geïsoleerd worden. Sequentieanalyse van de volledige genomen van deze revertanten bracht mutaties aan het licht in drie genen: drie revertanten met een mutatie in *codY*, vier met een mutatie in *argR* en drie met een mutatie in *ack*. Naast verhoogde tolerantie voor t-CIN vertonen alle *codY* en *argR* revertanten ook een gereverteerde koloniemorfologie en deels herstelde groei bij 10 °C. Alle mutaties in de transcriptieregulator CodY zijn enkelvoudige aminozuursubstituties, die ertoe leiden dat de transcriptie van het *ilv-leu* operon niet meer wordt onderdrukt. Hierdoor is synthese van α-ketozuren op een IlvE-onafhankelijke manier mogelijk en dit werd bevestigd door vetzuuranalyse. Omdat van CodY eerder werd aangetoond dat het de flagelsynthese reguleert, werd ook dit fenotype onderzocht. De *ilvE* mutant is volledig immobiel, maar motiliteit kan volledig hersteld worden

door toevoeging van α-ketozuren. Deze waarneming suggereert dat membraanfluïditeit bepalend is voor motiliteit. Daarenboven bezitten de *codY* revertanten een deels herstelde motiliteit die ook kan hersteld worden door toevoeging van α-ketozuren. Tezamen wijzen deze resultaten erop dat de CodY varianten de capaciteit hebben verloren om het *ilv-leu* operon (VKVZ-synthese) te onderdrukken, maar dat ze de capaciteit hebben behouden om het flagellair operon te activeren. ArgR is een transcriptionele regulator van het argininemetabolisme. Alle geïdentificeerde mutaties in *argR* zijn leesraamverschuivingen die leiden tot niet-functionele proteïnen. Opvallend genoeg bezitten de membranen van deze revertanten sterk verhoogde hoeveelheden van het iso-C15:0 vetzuur, wat erop wijst dat ArgR een tot hiertoe onbekende rol speelt in de regulatie van de synthese van VKVZ. De revertanten in *ack*, dat codeert voor acetaat kinase, zijn gekenmerkt door zowel aminozuursubstituties als leesraamverschuivingen. Deze revertanten groeien zelfs trager bij 10 °C dan de originele *ilvE* mutant en vertonen overeenkomstig geen veranderingen in de vetzuursamenstelling. Toch vertonen deze revertanten de hoogste graad van tolerantie voor t-CIN in vergelijking met de overige revertanten. Dit betekent dat er ook tolerantiemechanismen bestaan die niet het gevolg zijn van membraanaanpassingen. Acetaat kinase is nauw verbonden aan het centraal koolstofmetabolisme, energieproductie en de ontwikkeling van reducerend vermogen, wat mogelijk de herwonnen tolerantie voor t-CIN kan verklaren, aangezien t-CIN een thiolreactieve molecule is waarvan verondersteld wordt dat het de intracellulaire redoxhomeostase verstoort.

Tot slot werd de interactie tussen het serine/threonine PASTA kinase PrkC en YvcK onderzocht. Van PrkC is bekend dat het YvcK fosforyleert en transposonmutanten in beide genen, coderend voor deze proteïnen, werden geïsoleerd zowel tijdens de screen met t-CIN als met AIT. De *prkC* mutant vertoont een matige gevoeligheid, terwijl de *yvcK* mutant hypergevoelig is voor beide componenten. Een fosfoablatieve T252A/T256A mutant van YvcK was niet te onderscheiden van een WT tijdens groei in aanwezigheid van t-CIN. In deze mutant zijn threonineresiduen, die door PrkC gefosforyleerd worden, vervangen door alanineresiduen, waardoor deze op het niveau van fosforylatie kan beschouwd worden als het equivalent van een *yvcK* knockout. De stam waarin constitutieve fosforylatie wordt nagebootst door een T252E/T256E mutatie, vertoonde daarentegen een intermediaire gevoeligheid voor t-CIN in vergelijking met de WT en de *yvcK* knockout. De gevoeligheid van de *prkC* mutant kan dus niet

worden toegeschreven aan de uitgeschakelde fosforylatie van YvcK, maar vermoedelijk aan verstoorde fosforylatie van één of meerdere van de andere gekende effectoren van PrkC. Niettemin speelt de fosforyleringstoestand van YvcK een rol in de gevoeligheid voor t-CIN.

Samengevat heeft deze thesis een aantal van de meest belangrijke proteïnen en metabolismen blootgelegd, die voor *L. monocytogenes* nodig zijn om de schadelijke effecten van t-CIN op te vangen. Deze informatie zal bijdragen tot het beter begrijpen van de impact van gelijkaardige componenten uit essentiële oliën op het bacterieel metabolisme en daardoor ook aan de ontwikkeling van innovatieve strategieën voor voedselconservering.

List of abbreviations

μ_{max}	maximum growth rate
AIT	allyl isothiocyanate
ATP	adenosine triphosphate
AMP	adenosine monophosphate
BCAA(s)	branched-chain amino acid(s)
BCFA(s)	branched-chain fatty acid(s)
BCKD	branched-chain α-keto acid dehydrogenase
BHI	brain heart infusion
Cfu	colony forming unit
Cm	chloramphenicol
CoA	coenzyme A
DNA	deoxyribonucleic acid
Em	erythromycin
EO	essential oil
FASII	type II fatty acid biosynthesis
GAF	cGMP-specific phosphodiesterases, adenyl cyclases and bacterial transcription regulator FhlA
GABA shunt	*gamma*-aminobutyric acid
GTP	guanosine triphosphate
HS-SPME-GC-MS	headspace – solid-phase micro-extraction – gas chromatography – mass spectrometry
Ile	isoleucine
IlvE	branched-chain amino acid aminotransferase
KIC	α-ketoisocaproate
KIV	α-ketoisovalerate
Km	kanamycine
KMV	α-ketomethylvalerate
LB	lysogeny broth
Leu	leucine

logP	logarithm of the partition coefficient of the compound between n-octanol and water
MIC	minimal inhibitory concentration
OD	optical density
PASTA	Penicillin-Binding Protein And Serine/Threonine Kinase-Associated
PBP	penicillin binding protein
PPB	potassium phosphate buffer
QAC	quaternary ammonium compound
REPFED	refrigerated processed foods of extended durability
RNA	ribonucleic acid
RTE	ready-to-eat
TCA	tricarboxylic acid
t-CIN	*trans*-cinnamaldehyde
Val	valine
VP	Voges-Proskauer
WGS	whole-genome sequencing
wHTH	winged helix-turn-helix
WT	wild-type
α-KA	α-ketoacids
λ	lag phase

Table of contents

Chapter 1

Literature review

1.1. *Listeria monocytogenes*: a food-borne pathogen

Listeria monocytogenes is a low G+C Gram-positive, non-sporeforming, rod-shaped bacterium belonging to the *Firmicutes* phylum. *L. monocytogenes* is an opportunistic intracellular food-borne pathogen of several warm-blooded animals, that can cause severe invasive listeriosis in humans. Besides causing septicemia, the pathogen often also targets the central nervous system leading to meningitis. Furthermore, *L. monocytogenes* can pass the placental barrier, causing abortion, stillbirth or fetal death in pregnant woman. The majority of human cases occurs in neonatal, elderly or immunocompromised individuals [1].

According to the most recent epidemiological data, there is a steady but significant (*p*-value < 0.1) increasing trend of listeriosis in the EU since 2008 [2].Twenty-seven member states of the EU reported a total of 2161 confirmed cases of listeriosis in 2014, with a hospitalization rate of 98.9% and a mortality rate among the confirmed cases of 15%. This was the highest mortality rate observed between 2009 and 2014. With 62.3% of the reported cases in 2014, the incidence of listeriosis was highest in the elderly population (> 65 years). The increase of

L. monocytogenes infections may therefore be partially explained by the increasing elderly population.

L. monocytogenes is, due to its capacities to proliferate over a wide range of conditions, ubiquitous in various natural environments such as water, soil, and the gastrointestinal tract of various animals, but also in man-made environments like wastewater treatment plants and water drains in the household and in the food industry. Therefore, the organism is not only commonly found in raw materials used for food production, it is also a common contaminant at various later stages of food production. The foods that are most implicated in human listeriosis are ready-to-eat (RTE) foods including meat, dairy, fish, fruit and vegetable products. Even though the incidence of human listeriosis increased year after year in the period 2008-2014, the proportion of non-compliant food units on the market in 2014 remained at a comparable low level to previous years (< 1%). Non-compliance at the retail level was highest (4.7% of single samples and 10.8% of batches) for fishery products, especially smoked fish [2].

Besides its widespread occurrence, *L. monocytogenes* combines several other properties that make it successful in many refrigerated foods. First, it is a psychrotrophic bacterium that grows over a wide temperature range of about 1 - 45 °C. For some strains growth has even been observed at -0.4 °C [3,4]. The psychrotrophic nature provides a competitive advantage over several microbial competitors, making *L. monocytogenes* an important bacterial threat especially in the so-called refrigerated processed foods of extended durability (REPFED). Besides at low temperature, growth of *L. monocytogenes* has been reported down to a pH of 4.5 [5,6], a water activity of 0.90 [7] and a salt (NaCl) concentration up to 10% [8]. As such, *L. monocytogenes* can grow at lower water activity than most other food-borne pathogens, and this has been attributed to its ability to accumulate a range of compatible solutes [9,10]. Moreover *L. monocytogenes* can grow both aerobically and anaerobically, it has a relative high tolerance to elevated CO_2 concentrations as used in modified atmosphere packaging and to commonly used preservatives such as nitrite [11,12]. Altogether, the potential of *L. monocytogenes* to grow under a wide variety of stressful conditions allow it to subsist in food processing plants, to endure and survive different food preservation hurdles and to become one of the most important hazards in REPFEDs.

For heated foods, post-process contamination from equipment and environment is the main concern when it comes to prevention of *L. monocytogenes* [13]. *L. monocytogenes* is

frequently found on conveyor belts, cutting boards, floors and in drains in the production environment [14], and this has been ascribed at least in part to the ability of *L. monocytogenes* to form biofilms on a variety of materials commonly used in food processing environments [15–17]. Bacteria in biofilms are often hard to eliminate, because their resistance is increased by specific physiological adaptations and because they often exist in difficult to clean locations in the machinery. Persistent biofilms therefore constitute a permanent source of contamination in the food production process [18].

Food producers, in particular those producing REPFEDs, have to control the hazard of *L. monocytogenes* by implementing control measures in the context of their Hazard Analysis and Critical Control Points (HACCP) and Good Hygienic Practices (GHP) programs. These control measures are aimed at reducing pathogen levels in the raw materials and contamination during the production process, pathogen elimination by processing and/or formulation and conditioning of the food product to prevent outgrowth. Post-packaging heat treatments are very effective to eliminate *L. monocytogenes* from REPFEDs, since *L. monocytogenes* are heat-sensitive and easily inactivated by commercial heat treatments typically used for RTE foods. Exposure for 2 min at 70 °C will cause a six decimal (6-D) reduction of *L. monocytogenes* and is commonly considered as the minimal heat treatment required for the safety of pasteurized foods [19].

Consumers increasingly demand minimally processed, nutritionally healthy and fresh foods without artificial preservatives or other technological additives. The food industry has responded to this by attempting to replace “artificial” preservatives like nitrite by “natural” alternatives like plant extracts [20,21]. However, it needs to be emphasized that “artificial” and “natural” in this context are not clearly defined, and that “natural” alternatives are not necessarily healthier than the compounds they replace. For many plant extracts and their constituents, little or no safety studies are available. Nevertheless, plants constitute a vast reservoir of potentially useful antimicrobials that can help to make foods safer and healthier by suppressing growth of *L. monocytogenes* and other pathogens, especially in minimally treated and refrigerated ready-to-eat foods, which is one of the strongest growing and innovative segments in the food industry.

To address the microbial safety challenges that come along with the demand for less processed food that nevertheless has a longer shelf-life, food scientists are looking for

solutions based on hurdle technology. Hurdle technology implies the combination of two or more gentle processing and preservation techniques to obtain maximal control of microbial safety and stability with a minimal loss of food quality [22]. It can be a very effective approach because some hurdles have a synergistic effect on microbial inactivation or growth inhibition. Although the concept of hurdle technology has been known for almost half a century, it is receiving renewed attention because of the development of novel processing and preservation technologies that can be used as new hurdles. One such hurdle that is showing much promise in the context of mildly processed and natural foods are plant essential oils and their major components, which are investigated to improve the safety and extend the microbiological shelf-life of foods without the use of traditional 'chemical' preservatives. Besides, new hurdle technology concepts with natural antimicrobials and especially the ones that lead to synergistic bacterial inactivation or growth suppression, can also contribute to the development of healthier food products with reduced amounts or intensities of classic hurdles like salt, lowered pH and heat treatment [20,23].

1.2. Plant essential oils and their constituents as natural food preservatives

Essential oils are aromatic volatile liquids extracted from plant material such as flowers, roots, bark, leaves, seeds, peel, fruits, wood or whole plants. They are complex mixtures of plant secondary metabolites, many of which play a role in the plant defense system. Their constituents are usually low molecular weight compounds displaying a wide diversity in reactivity, water and fat solubility, smell and aroma. Dozens of essential oils and their constituents have been documented to have antimicrobial activity. They generally have a wide activity spectrum including both Gram-positive and Gram-negative bacteria, yeasts and molds, and this makes them potentially useful for food applications. A range of the essential oil compounds are registered as permitted food flavorings in the EU, such as linalool, carvacrol, vanillin, cinnamaldehyde and citral (Regulation (EU) No. 872/2012). The potential use of essential oils and their purified major constituents as natural food preservatives has gained a lot of interest since at least a decade, driven by the increasing negative consumer perception towards artificial, classic food preservatives [20,23]. However, the use of these substances as food preservatives is not allowed under the current EU legislation regarding food additives (Regulation (EU) No 1333/2008).

The major constituents and active compounds of essential oils can be divided into four groups according to their biosynthetic pathways and chemical structure: terpenes, terpenoids, phenylpropenes and a diverse group of molecules. Terpenes are hydrocarbons produced from a combination of isoprene units, and are designated as monoterpenes, sesquiterpenes, diterpenes etc. depending on the number of composing units. Terpenes in general do not possess high antimicrobial activities [23].

Terpenoids are terpenes that have been enzymatically modified by addition of oxygen atoms and/or addition or removal of methyl groups. The group of terpenoids is further subdivided depending on whether the oxygen-containing functional group is an alcohol, ester, aldehyde, ketone, ether, phenol or epoxide. These functional groups are often linked to their antimicrobial activity. Some terpenoids that have been widely studied for their antimicrobial activity are carvacrol, thymol and linalool [23].

Phenylpropenes are a subfamily of the group of organic compounds called phenylpropanoids, which are derived from the amino acid phenylalanine in plants. Their antimicrobial capacities stem from the functional groups on the propene side chain and the kind and number of functional groups on the aromatic ring. One of the most extensively investigated compounds of this class is *trans*-cinnamaldehyde, mainly for its rather strong and broad antimicrobial activity [23]. This compound will be studied in this PhD thesis as a model for thiol-reactive, hydrophobic, low molecular weight compounds from plant essential oils.

Finally, the diverse group of compounds consists of various degradation products from unsaturated fatty acids, lactones, glycosides and sulfur and nitrogen containing compounds. A much studied group of such molecules are the isothiocyanates, characterized by a R-N=C=S functional group and causing the pungent taste of vegetables and spices from the *Brassicaceae* family such as mustard, broccoli, Brussels sprouts and horseradish [23]. These compounds are mostly present in the vacuoles in the form of a non-reactive glucosinolate. Isothiocyanates are released after tissue damage by enzymatic cleavage of the glucosinolate by myrosinase, which is located in the cytoplasm or cell wall [24,25].

It is useful to note that the above classification of plant essential oil compounds is not necessarily consistent with their mode of antibacterial action. In fact, the mode of action of most compounds has only been studied superficially, and several compounds may display

multiple activities, including general effects like disturbance of membrane structure and functionality. On the other hand, some compounds may share a similar mode of action despite being structurally different. For example, the antimicrobial activity of *trans*-cinnamaldehyde (and other α, β-unsaturated aldehydes) and of isothiocyanates is believed to be at least partly based on their reactivity to cellular thiol groups (see 1.3).

Although many essential oil compounds have a wide activity spectrum including Gram-positive and Gram-negative bacteria and yeasts and molds, their application as food preservatives is often limited by their low water solubility and strong sensory impact. Different strategies can be used to circumvent these problems, including the use of essential oil compounds in active packaging, edible coatings or sachets that provide slow release to the food surface or headspace of the package, and formulation in nanoemulsions added to the food product [23]. Nanoemulsions seem to be the most promising delivery system for food applications due to the unique properties inherent to their nanometric size. They allow to use compounds at concentrations above their maximum solubility, while at the same time reducing the sensory impact. Further, nanoemulsions are less subject to aggregation compared to regular emulsions and are transparent or only slightly turbid because the diameter of the droplets (20-200 nm) is smaller than the wavelength of light which greatly reduces light scattering. Yet, the effect of nanoemulsification on the antimicrobial activity of a compound is not entirely understood and strongly depends on a number of factors like the physicochemical characteristics of the essential oils or compounds, the used emulsifier, the droplet size, the properties of the microbial strains and the food matrix [26]. Both increased antimicrobial activity [27–29] and decreased activity [30,31] due to encapsulation or nanoemulsification of essential oils or their compounds have been reported.

Another attractive approach to overcome the limitations of essential oil based antimicrobials is the use of hurdle technology, as stated before. Hurdle technology becomes most effective when it combines techniques that reinforce each other in a synergistic fashion, because this allows to maximally reduce the intensity of the individual hurdles. In the case of essential oil compounds, this can make them effective at lower concentrations and thus reduce their sensory impact and possible solubility problems. In addition, lower concentrations also contribute to cost reduction. Finally, a multiple hurdle preservation system may be more robust than a single hurdle because it makes the development of microbial resistance less

likely, particularly if the hurdles rely on different microbial inactivation or inhibition mechanisms.

A variety of hurdle applications with essential oil compounds have been investigated. As an example, the inactivation of *Escherichia coli* O157:H7 and *L. monocytogenes* EGD-e by mild heat treatment (54 °C, 10 min) was shown to be synergistically enhanced by citrus fruit essential oils at rather low concentrations (0.2 µl/ml) [32]. A promising combination is the synergistic inactivation of bacteria by the combination of high hydrostatic pressure and different small molecule antimicrobials from essential oils, as reported by several research groups [33–35]. In a recent study in our own research group, a variety of essential oil compounds from different classes with diverse functional groups were screened at sub minimal inhibitory concentrations (MIC) concentrations for synergistic inactivation of several Gram-positive and Gram-negative bacteria [35]. Less than half of the tested compounds displayed synergy with high pressure treatment, the strongest synergy being observed with α, β-unsaturated aldehydes (*trans*-cinnamaldehyde, *trans*-2-hexenal), isothiocyanates (allyl isothiocyanate, sulforaphane) and reuterin. These compounds are all electrophilic and show reactivity towards thiol groups [36,37]. It was therefore hypothesized that thiol reactivity might be the cause of synergy with high pressure treatment. In addition, these thiol-reactive compounds share hydrophobic properties, with exception of reuterin. Two examples of the observed synergistic effect are shown in Fig. 1.1.

Besides combinations with processes, the mutual combination of two or more essential oil compounds or the combination with other natural antimicrobials or antibiotics can also result in a synergistic effect. For example, the combination of *trans*-cinnamaldehyde and carvacrol exerted a synergistic bactericidal effect on *E. coli* and *S. aureus*. Time-kill curves showed a significant faster inactivation of both micro-organisms when *trans*-cinnamaldehyde and carvacrol were combined at 0.16 mg/ml compared to the separate treatments with concentrations twice as high (0.32 mg/ml). Moreover, a synergistic growth-inhibitory effect was observed on various other Gram-positive and Gram-negative food-borne pathogens, determined via the checkerboard assay [38]. The combination of a nisin variant (nisin V) in the form of a fermentate with thymol, carvacrol or *trans*-cinnamaldehyde elongated the lag phase of *L. monocytogenes* in a synergistic way [39]. Finally, allyl isothiocyanate and phenylethyl isothiocyanate displayed synergy with the antibiotic streptomycin [40–42].

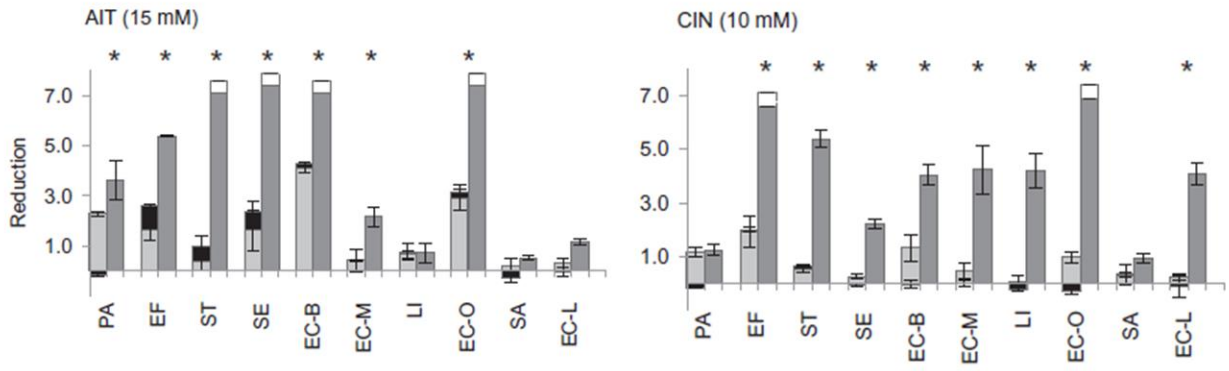

Fig. 1.1. Feyaerts *et al.* (2016) [35]: Two examples of synergistic bacterial inactivation of ten different bacteria by the combined treatment of allyl isothiocyanate (AIT) or *trans*-cinnamaldehyde (CIN) in potassium phosphate buffer (pH 7.0, 10 mM). Cell suspensions (approx. 9.5 log cfu/ml) in potassium phosphate buffer (10 mM, pH 7.0) were treated with high pressure (20 °C; 15 min; 150–300 MPa), with AIT/CIN, and with high pressure + AIT/CIN. Reduction by the different treatments (log N0/N) is represented in pale grey (high pressure), black (AIT or CIN) and dark grey (high pressure + AIT or CIN). The bars representing high pressure and AIT or CIN inactivation are stacked to facilitate visual assessment of synergy, which is the difference in inactivation achieved in the combined treatment and the sum of the inactivation achieved by high pressure and AIT or CIN separately. Results are presented as means ± standard deviations of three independent experiments. Dashed lines at the top of the bars indicate that the treatment resulted in complete inactivation and that the real reduction may be higher than represented. * Synergistic combinations based on statistical analysis ($p < 0.05$). The pressure levels used were: *P. aeruginosa* PAO1 (PA; 150 MPa), *E. fergusonii* ATCC 35469 (EF) and *S.* Typhimurium LT2 (ST; 225 MPa), *S.* Enteritidis ATCC 13076 (SE) and *E. coli* BL21 DE3 (EC-B; 250 MPa), *E. coli* MG1655 (EC-M; 275 MPa), *L. innocua* CIP 8012 (LI), *E. coli* O157:H7 ATCC 43888 (EC-O), *S. aureus* LMG 8064 (SA) and *E. coli* LMM1010 (EC-L; 300 MPa).

However, it is currently not understood what determines the outcome of the interaction of two or more treatments. The identification of synergistic combinations that are potentially useful for food applications currently depends on a process of trial and error. Studies on the cellular or molecular mode of action of essential oil compounds are necessary to advance our understanding of how they interact with each other and with other hurdles, and this could in turn contribute to a more rational design of effective hurdle combinations using these compounds. Within this broad framework, the main objective of this PhD thesis is to advance the insight in the cellular mode of action of small hydrophobic thiol-reactive molecules from essential oils because of their promising synergistic interaction with high pressure inactivation. Therefore, the following section discusses the state of the knowledge on this matter, with a focus on *trans*-cinnamaldehyde and *L. monocytogenes*, which will be used as a model in the experimental work.

1.3. Antibacterial mode of action of hydrophobic and thiol-reactive small molecules

Among the thiol-reactive compounds of natural origin, *trans*-cinnamaldehyde (t-CIN, Fig. 1.2), is one of the most investigated regarding both its antibacterial mode of action and its potential food applications. It is the major constituent of cinnamon bark essential oil. t-CIN has an α, β-unsaturated aldehyde functional group which is responsible for the molecule's electrophilic properties. In general, a C=C double bond next to a carbonyl group (aldehyde or ketone), transmits the electrophilic character from the carbonyl carbon atom to the β-carbon of the double bond, based on the formation of a resonance system presented in Fig. 1.3a.

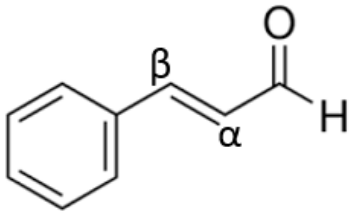

Fig. 1.2. The structure of *trans*-cinnamaldehyde, characterized by its reactive α, β-unsaturated aldehyde group.

a.

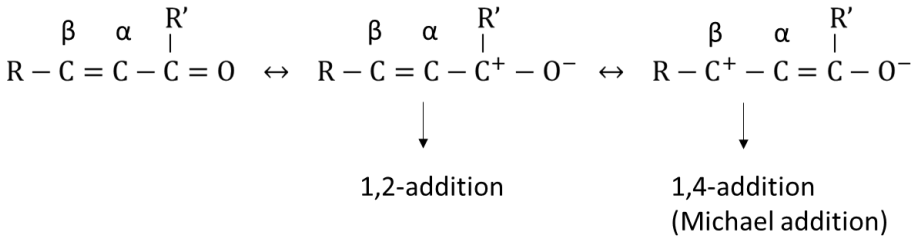

b.

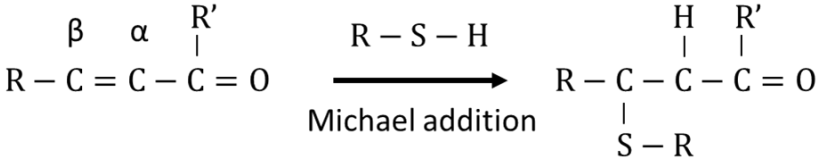

Fig. 1.3. (a) α, β-unsaturated carbonyl resonance system; (b) Michael addition reaction of an α, β-unsaturated carbonyl compound with a thiol residue.

In view of the resonance system, α, β-unsaturated aldehydes can react with a nucleophile according to two competing reaction schemes, a 1,2-addition and a 1,4-addition reaction (Michael addition) respectively (Fig. 1.3). Which of both will dominate is mostly determined by the nature of the nucleophile. If the nucleophile is a weak base, such as alcohols, amines and thiols, both addition reactions are reversible. This means that the competition between the 1,2-addition and 1,4-addition is thermodynamically controlled and that, as a consequence, the 1,4-addition will dominate because the stable carbonyl group is retained (Conjugate addition reactions, Chemistry Libretexts (website); Little *et al.* 1995). Several natural compounds with an α, β-unsaturated carbonyl group are biologically active, displaying anti-inflammatory, anti-oxidative, anti-mitotic, bactericidal, antifungal and chemoprotective activity. Their biological activity is mostly based on the Michael acceptor activity of the α, β-unsaturated carbonyl system and the reaction with amines and/or thiol groups from cellular nucleophiles [36].

Besides being electrophilic, t-CIN is hydrophobic like most essential oil compounds. The $logP_{oct}$ (logarithm of the partition coefficient of the compound between n-octanol and water) value of t-CIN is 2.12 (PubChem). In general, hydrophobic or lipophilic small molecules are anticipated to accumulate in the hydrophobic core of bacterial membranes [20]. Research on *in vitro* membrane model systems such as *E. coli* phospholipid liposomes [44] and monolayers of bacterial phospholipids [45] have documented this membrane partitioning. The results of the latter study further indicate that geraniol, carvacrol and t-CIN also modify lipid monolayer structures by reducing the lipid packing effectiveness, increasing membrane fluidity and altering the dipole moment. In addition, partitioning and hydrophobic interactions may distort lipid-protein interactions and alter protein and enzyme functionality by direct interaction with the hydrophobic parts of membrane proteins [44].

Whether the electrophilic properties of t-CIN contribute to its antimicrobial activity has not been directly demonstrated, but there are indirect indications that this is the case. *E. coli* O157:H7 has been shown to be able to reduce the aldehyde group of t-CIN, leading to the formation of cinnamyl alcohol (phenyl-2-propen-1-ol). Although cinnamyl alcohol is still a hydrophobic molecule, with a $logP_{oct}$ of 1.70, it is no longer reactive with thiol or amino groups, and the MIC for *E. coli* O157:H7 of this compound is four times less than for t-CIN [46]. Stronger evidence for a role of thiol-reactivity in antimicrobial activity exists for reuterin (3-

hydroxypropionaldehyde), a water-soluble metabolite produced by *Lactobacillus reuteri*. This compound induced an oxidative stress response in *E. coli*, and was much more active against *oxyR* mutants of *E. coli*, which are defective in developing such an oxidative stress response [47].

However, the primary cellular targets of α, β-unsaturated carbonyl compounds, and the bacterial stress response and adaptation potential upon exposure to these compounds are not fully understood. This basic knowledge will be important for the further development of intelligent hurdle technology applications of this class of natural compounds in combination with other natural compounds or mild food processing and preservation techniques. Therefore, the following section reviews the existing knowledge on the effects of membrane disturbing and/or electrophilic natural antimicrobial compounds, food preservatives and disinfectants, with a focus on *L. monocytogenes*.

1.4. Stress response and adaptation to membrane perturbing antimicrobial compounds

1.4.1. Bacterial homeoviscous adaptation and membrane characteristics of *L. monocytogenes*

One of the pillars supporting bacterial survival and growth in different environmental conditions is membrane lipid homeostasis. Bacteria can modulate their membrane composition by varying the types of fatty acids that are produced by the fatty acid biosynthetic pathway and incorporated into phospholipids, in order to maintain a constant membrane fluidity in response to changing environments. The process is therefore also referred to as homeoviscous adaptation. These adaptations minimize the cell energy expenditure and optimize growth to the existing environmental conditions. Well-known environmental parameters that can induce membrane fatty acid alterations are temperature, osmolarity, salinity and pH [48].

Bacterial membranes consist of a phospholipid bilayer with embedded proteins. Phospholipids are together with membrane proteins important determinants of the membrane biophysical properties. Phospholipids are the main determinants of membrane viscosity, which in turn determines the passive membrane permeability for small and hydrophobic compounds, but also indirectly affects membrane proteins involved in active transport and other membrane activities. Most bacterial phospholipids are

glycerophospholipids, composed of two fatty acids linked to a polar glycerol phosphate head group. Fatty acid biosynthesis in bacteria starts from various acyl-CoA substrates (Fig. 1.4) which are subsequently polymerized and reduced to different fatty acids in a process called type II fatty acid biosynthesis (FASII). The genes encoding the enzymes of this pathway are highly conserved [49].

Different mechanisms are used to adjust membrane fluidity depending on the species. Bacteria that contain primarily unbranched fatty acids, like most Gram-negative and some Gram-positive bacteria, alter their membrane fluidity predominantly by changing the acyl chain length and the ratio of saturated to unsaturated fatty acids [49]. On the other hand, bacteria that contain primarily branched-chain fatty acids (BCFAs), like *L. monocytogenes* and several other Gram-positive bacteria, alter their membrane fluidity by changing the iso/anteiso fatty acid ratio and the acyl chain length [50]. *L. monocytogenes* membranes are almost exclusively made up of anteiso- and iso-BCFAs (> 90%), mainly anteiso-C15:0, anteiso-C17:0, iso-C15:0 and iso-C17:0 (Fig. 1.4 and 1.5). The major phospholipid structures in *L. monocytogenes*, as determined by Verheul *et al.* (1997) [51], are phosphatidylglycerol (~ 62%), diphosphatidylglycerol (~ 13%), a phosphoglycolipid (~ 10%) and a group of different minor phospholipids.

Growth of *L. monocytogenes* at low temperatures results in a reduction in chain length (e.g. from C17 to C15), and a shift in relative abundance from iso to anteiso. This adaptation is critical to maintain an appropriate membrane fluidity at low temperatures and is one of the mechanisms underlying the ability of *L. monocytogenes* to grow at temperatures approaching the freezing point [52,53]. More specifically, branching of fatty acids increases the occupied area per lipid in the membrane, reduces the bilayer thickness, lowers chain ordering and favors formation of kinks at the branching point. All these effects result in a gain in membrane fluidity [54]. Moreover, the fluidity varies with the position of the methyl side chain, because it determines the phase-transition temperature of the fatty acid. For example, the phase-transition temperature of iso-C15:0 (methyl on the penultimate carbon, Fig. 1.5) is 52.2 °C, while the anteiso-C15:0 (methyl on the antepenultimate carbon, Fig. 1.5) has a phase-transition temperature of 25.8 °C [50]. It follows that, even though both iso and anteiso fatty acids contribute to membrane fluidity compared to unbranched fatty acids, the contribution of anteiso forms is considerably greater.

Membrane fatty acid adaptation in *L. monocytogenes* has been mainly studied as a response to changing environmental temperatures [52,53,55]. Yet other environmental stresses and antimicrobial compounds also cause membrane stress and trigger cells to adapt membranes to remain metabolically functional. Because of its small structure and lipophilicity ($logP_{oct}$ 2.12), the antimicrobial mode of action of t-CIN, which is the major subject of this work, is predicted to be at least partially based on its membrane partitioning and perturbing effect. Therefore, the stress response and subsequent adaptation upon challenge with membrane disruptive and perturbing compounds, both natural antimicrobials and conventional 'chemical' preservatives and disinfectants, will be discussed in the next sections.

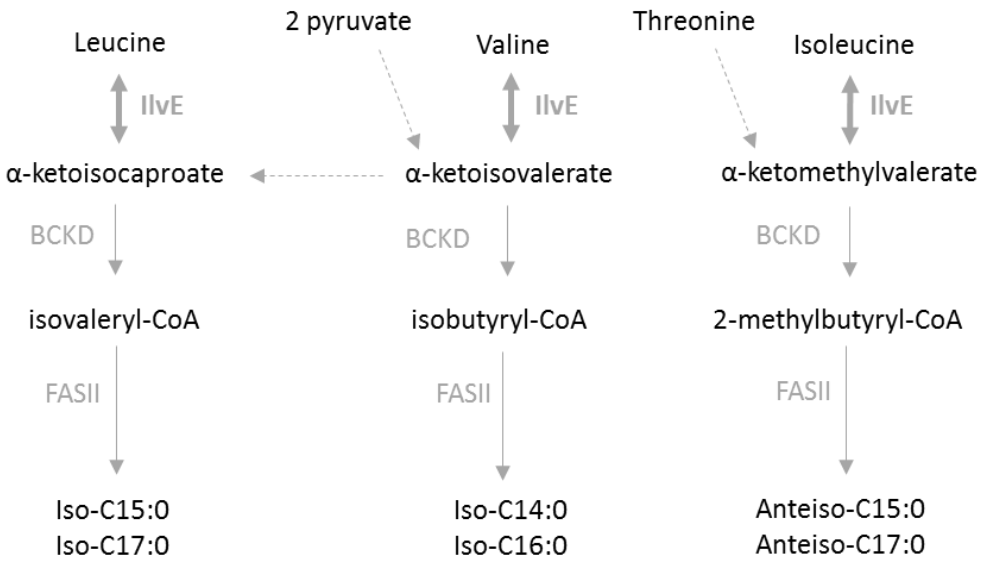

Fig. 1.4. Generalized scheme of the predicted branched-chain fatty acid biosynthesis pathway in *L. monocytogenes* (based on Zhu *et al.* 2005 and Biocyc database collection). Branched-chain amino acid aminotransferase, annotated as IlvE; BCKD: branched-chain keto acid dehydrogenase (enzyme complex); FASII: fatty acid synthase (enzyme complex).

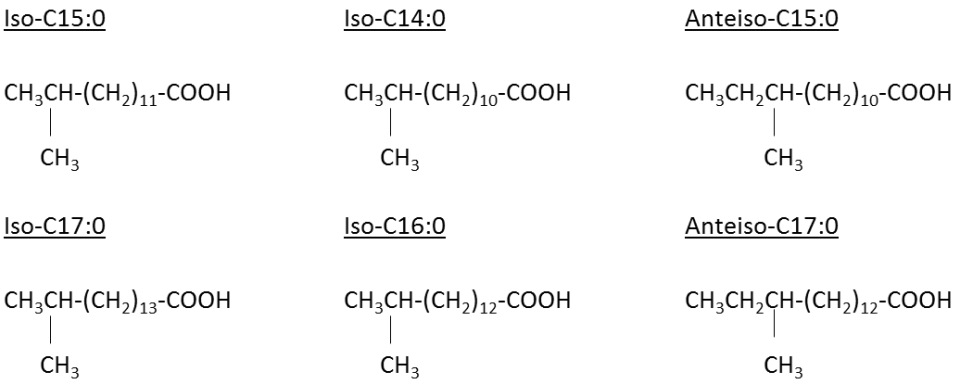

Fig. 1.5. Chemical structure of the major branched-chain fatty acids of *L. monocytogenes*.

1.4.2. Conventional food preservatives: sorbic acid, benzoic acid and parabens

Sorbic acid (*trans-trans*-2,4-hexadienoic acid, Fig. 1.6a), and benzoic acid (Fig. 1.6b) are weak acids and are worldwide among the most used preservatives in a wide variety of foods. They have a broad antimicrobial activity against bacteria, yeasts and molds. Although both compounds have been applied for decades as food preservatives, their antimicrobial mode of action is still not entirely understood and no single mechanism appears to explain the antimicrobial activity. Sorbic acid and benzoic acid are moderately hydrophobic with $logP_{oct}$ values of 1.3 and 1.9 respectively (PubChem) and have acid dissociation constants (pK_a) at 25 °C of 4.8 and 4.2 respectively (PubChem). In solution, weak acids exist in a pH-dependent equilibrium between the undissociated and dissociated state. Sorbic acid and benzoic acid exist mainly in the dissociated state in foods with a pH > pK_a, and in the undissociated state in foods with a pH < pK_a. Because of their moderately lipophilic properties and relatively small size, the undissociated and uncharged state of both acids can diffuse through microbial membranes, as opposed to the negatively charged dissociated state. Since the cytoplasm of most bacteria is near-neutral (pH 6 - 7), the incoming acids will dissociate because the intracellular pH is higher than the pK_a and cause intracellular acidification. This protonophore effect is regarded as one of the major antimicrobial mechanisms of sorbic acid, benzoic acid and other lipophilic weak acids [56–58].

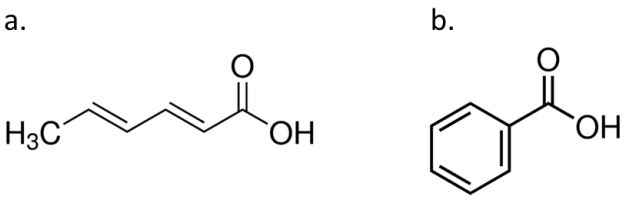

Fig. 1.6. Chemical structure of sorbic acid (a) and benzoic acid (b)

In addition, the lipophilic tail of sorbic acid has been shown to perturb the membrane and interfere with membrane proteins [59]. Together with the acidification of the cytoplasm this could lead to loss of the proton motive force and affect nutrient transport across the membrane [60]. Using genome-wide transcriptional analysis, Ter Beek *et al.* (2008) [57] showed that mild sorbic acid stress induced a stress response, characteristic of nutrient limitation in *Bacillus subtilis*, as indicated by a strong derepression of transcriptional regulators such as CcpA and CodY, induction of genes related to the tricarboxylic acid cycle, SigL- and SigH-dependent genes and the stringent response. Interestingly, also an activation of the *fab* genes, encoding the FASII enzyme complex and the BCKD complex (Fig. 1.4), was observed immediately after exposure to sorbic acid, suggesting an increased production of branched-chain fatty acids. This may reflect a response to counter the disturbance in membrane fluidity that may have been caused by accumulation of sorbic acid in the membrane [57]. Since the fatty acid composition after exposure to sorbic acid was not determined, the effect of mild sorbic acid stress on the phase-transition temperature remain unresolved. Similar to *B. subtilis*, also the yeast *Zygosaccharomyces rouxii* was shown to change its fatty acid composition in response to potassium sorbate [61].

Benzoic acid also induces changes in the membrane composition of *L. monocytogenes* [62,63]. In the presence of 1 g/l benzoic acid in Brain Heart Infusion (BHI) medium at neutral pH, when benzoic acid is mainly present in its dissociated anionic form, the proportion of saturated unbranched-chain fatty acids C16:0 and C18:0 increased at the expense of the BCFAs anteiso-C15:0 and anteiso-C17:0. In addition, the relative quantity of cardiolipin and phosphatidylglycerol decreased by 39.8% and 37.6%, respectively, causing an overall reduction in negative head group charges.

The hypothesis that sorbic and benzoic acid do not solely exert their antimicrobial activity on the basis of their protonophore activity was further supported by Heavin *et al.* (2009) [58] in a comparative study with benzoic, sorbic and acetic acid. Growth experiments with *L. monocytogenes* were performed in a defined growth medium at pH 6.4 and the amounts of undissociated acid was calculated according to the equation of Henderson-Hasselbach. To reduce the growth rates by 50%, cultures had to be exposed to 4 mM benzoic acid (0.02 mM undissociated), 10 mM sorbic acid (0.22 mM undissociated) and 50 mM acetic acid (1.07 mM undissociated). These results indicated that benzoic acid was the most potent of the investigated acids, despite having the lowest concentration of undissociated acid under the conditions of the experiment. Besides, Heavin *et al.* (2009) investigated the role of the glutamate decarboxylation system and the role of the stress inducible sigma factor B in response to acetic, sorbic and benzoic acid. Glutamate decarboxylation consumes intracellular protons and this reaction is thought to contribute to intracellular pH homeostasis in *L. monocytogenes* [64]. Glutamate supplementation in the growth medium could therefore offer some protection against acidic environments. Yet, a *gadAB* deletion mutant, deficient in the glutamate decarboxylase AB system, did not grow slower than the corresponding isogenic strain in a defined medium containing glutamate, adjusted to pH 6.4, in the presence of acetic, benzoic or sorbic acid. Therefore, the proton consuming GadAB system does not seem to protect the cells against the action of these weak acids. However, these observations do not allow to conclude that internal acidification is not important for the antimicrobial action of sorbic, acetic or benzoic acid, because other pH homeostasis systems exist in *L. monocytogenes*, like the GadD glutamate decarboxylase [65] and the arginine deiminase system [66]. The stress inducible sigma factor B, controlling the general stress response in *L. monocytogenes*, is also known to play an important role in surviving strong acidic conditions [67]. Yet, in the presence of sorbic or benzoic acid (3 mM each) a *sigB* deletion mutant showed only a very small decrease in the growth rate [58]. All results from these different studies indicate that cytoplasmic acidification might not be the main cause of the antibacterial action of sorbic and benzoic acid (and possibly other lipophilic weak acids) at a pH well above the pK_a. Other mechanisms like membrane perturbing effects, caused by their lipophilic nature, might play an additional role in their mode of action.

Food preservatives that are often applied in combination with sorbic acid and sorbates, are the *p*-hydroxy benzoic acid esters or parabens. Parabens approved in some food applications in the European Union are the methyl-, ethyl and propyl parabens. These molecules are uncharged over a wide pH range of 3 to 8, which covers almost all types of foods. Like sorbic and benzoic acid they are lipophilic and can traverse the plasma membrane into the cytoplasm, where they are hydrolyzed by non-specific esterases to *p*-hydroxybenzoic acid and a remaining alcohol. Because of the near-neutral intracellular pH, *p*-hydroxybenzoic acid will dissociate and cause acidification of the cytoplasm. Besides, parabens also have been shown to disrupt membrane transport processes and to cause cell membrane damage, loss of intracellular compounds and dissipation of the proton gradient [60], inhibit DNA and RNA synthesis [68] and inhibit key enzymes such as ATPases and phosphotransferase [69]. Propylparaben ($logP_{oct}$ 3.04, PubChem) is considered to have stronger antimicrobial capacity than ethylparaben ($logP_{oct}$ 2.47, PubChem) and methylparaben ($logP_{oct}$ 1.87, PubChem) due to its higher hydrophobicity and, consequently, higher membrane perturbing effect. On the other hand, more hydrophobic parabens tend to accumulate in the fat or oil phase of foods, and this will reduce their active concentration in the water phase. Therefore, mixtures of two parabens are often used to increase the antimicrobial effect [70].

1.4.3. Cationic antiseptics and disinfectants

Cationic surfactants have been used for over a century as antiseptics and disinfectants in the food industry. Commonly used compounds include the monocationic quaternary ammonium compounds and the polycationic biguanides, both of which are lipophilic and positively charged. Their positive charge allows them to interact and bind to the negatively charged cell wall and surface of the cell membrane of bacteria. On the other hand, the lipophilic domains of the molecules can penetrate the interior of the cell membrane. As a result, these molecules perturb the cell membrane structure which ultimately leads to leakage of intracellular compounds and cell death. Despite these similarities in their mode of action, both types of compounds differ substantially in the nature of their interactions with the cell membrane and the way bacteria respond and try to adapt to these molecules [71,72].

Quaternary ammonium compounds (QACs) are widely used as disinfectants in food production settings, creating a hygienic environment and preventing the persistence of environmental food-borne pathogens such as *L. monocytogenes*. Commonly used QACs

include benzalkonium chloride (Fig. 1.7a) and cetrimide, a mixture of different quaternary ammonium salts including cetrimonium bromide (Fig 1.7b) [73]. QACs are amphoteric surfactants, containing one positively charged quaternary nitrogen associated with at least one major hydrophobic constituent which is an alkyl or an aryl group (Fig. 1.7). Both the strong positive charge and the hydrophobic moiety are necessary to interact with the cell surface and penetrate the cell membrane. For aliphatic QACs, the antimicrobial activity against different bacterial species depends on the length and hydrophobicity of the alkyl chain. In order to achieve a broad spectrum activity, different QACs are often mixed in commercial preparations [71].

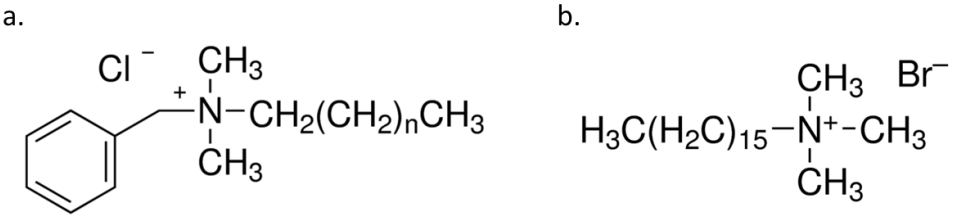

Fig. 1.7. Chemical structure of benzalkonium chloride (a) and cetrimonium bromide (b).

Fig. 1.8 shows the stepwise membrane disruptive mode of action of QACs. The initial interaction starts with the displacement of Mg^{2+} and Ca^{2+} cations, that neutralize and cross-bridge the negatively charged phospholipid head groups at the outer membrane surface, by the positively charged quaternary nitrogen group of the QACs. At low concentrations, the hydrophobic alkyl chain subsequently interdigitates into the hydrophobic membrane core, leading to a decrease in membrane fluidity. This transition implies a loss of the membrane osmoregulatory and physiological functions and the creation of hydrophilic domains in the membrane. This transition also causes phospholipids to tend towards a stable hexagonal arrangement. The functionality of membrane embedded proteins will consequently be disturbed or be completely lost. At higher concentrations, as used in industrial disinfectant formulations, the membrane disruptive actions will eventually lead to the formation of micellar QAC aggregates that solubilize hydrophobic membrane components such as phospholipids. This action leads to leakage of cytoplasmic molecules and eventually cell lysis [71].

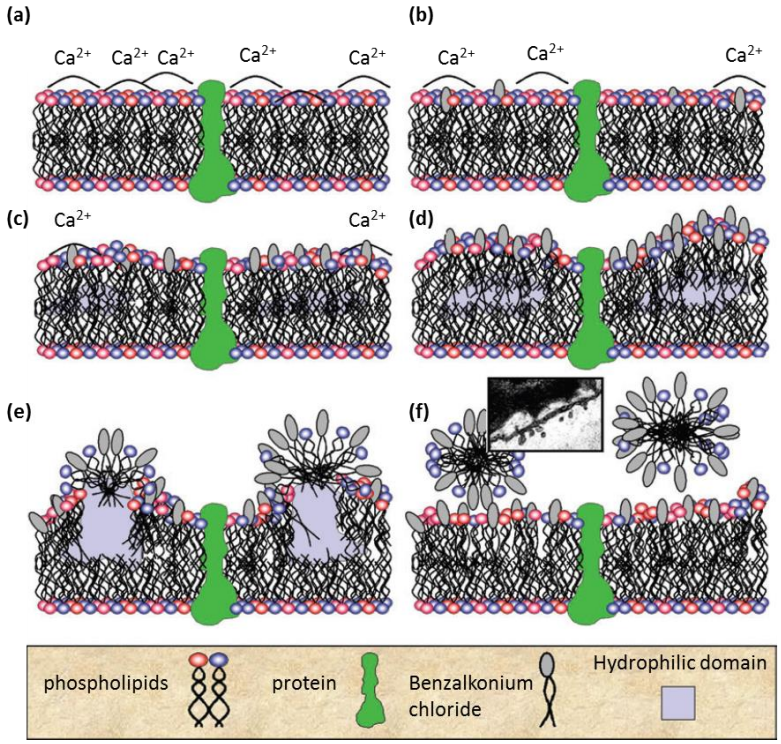

Fig. 1.8 [71]. Cartoon showing the mechanism of action for quaternary ammonium biocides. The segments (a–f) show progressive adsorption of the quaternary head group to acidic phospholipids in the membrane with increasing QAC exposure/concentration. This leads to decreased fluidity of the bilayers and the creation of hydrophilic domains in the membrane. Protein function is perturbed with an eventual lysis of the cell, and solubilization of phospholipids and proteins into QAC-phospholipid micelles. Inset micrograph shows vesicle formation from outer membrane caused by QAC treatment.

Bacteria that are repeatedly exposed to sublethal concentrations of disinfectants in food processing environments due to dosage failure, inadequate rinsing after cleaning or persistence in biofilms, may become less sensitive over time to those disinfectants. *L. monocytogenes* strains with increased minimal inhibitory concentrations (MICs) for benzalkonium chloride have been isolated from food production sites, as reported in different studies. In general, *L. monocytogenes* developed only a moderate, two- to eightfold increase of the MIC. These increased MICs are not anticipated to increase the risk of *L. monocytogenes* outbreaks, since they do not exceed the concentrations of benzalkonium chloride that are usually applied to sanitize food processing environments (200-1000 mg/l) [74].

Specific adaptations in cellular phospholipids and in membrane fatty acid composition as a response to QACs have been documented [75,76]. Bisbiroulas *et al.* (2011) reported minor increases in the amounts of saturated straight-chain fatty acids C16:0 and C18:0 in the membranes of early stationary-phase cultures of *L. monocytogenes*, cultured in the presence

of 2.5 mg/l benzalkonium chloride in BHI broth, which was the highest concentration allowing growth. The increases took place at the expense of anteiso-C15:0 and anteiso-C17:0. To *et al.* (2002) [75] used a different approach whereby two originally benzalkonium chloride resistant and four originally sensitive strains from different sources were repeatedly subcultured in increasing sublethal concentrations of benzalkonium chloride. The strains were allowed to adapt to increasing concentrations until the point where ten consecutive transfers resulted in no further adaptation. After adaptation, the originally sensitive strains showed at least a fivefold increase of the MIC and the originally resistant strains a twofold increase. Only one evolved strain, derived from an originally resistant strain, showed a slight change in fatty acid profile compared to its ancestor. Its fatty acid composition was characterized by a decrease in the amounts of iso- and anteiso-C15:0 from 16.77% and 38.67% of total fatty acids in the parental strain to 8.32% and 21.50%, respectively, in the evolved strain. These reductions were almost entirely compensated by increased amounts of iso- and anteiso-C17:0, from 6.38% and 21.67% in the parental strain to 13.93% and 42.24% in the adapted strain, respectively. These changes are predicted to reduce membrane fluidity and increase membrane thickness.

Both studies also investigated whether the membrane surface structure or properties had been altered upon adaptation to benzalkonium chloride. To *et al.* (2002) hypothesized that a change in the surface hydrophobicity might repel the water soluble benzalkonium chloride, but no differences between the evolved, more tolerant strains and their parental progenitors could be observed. On the other hand, transmission electron microscopy revealed morphological differences after exposure to benzalkonium chloride. For both an originally sensitive and resistant strain the outer layers of adapted cells grown in the presence of benzalkonium chloride were more undulating and rougher than the outer layers of their parental strains and showed on top of that increased filamentation and elongation.

An essential feature of the mode of action of benzalkonium chloride is the interaction with phospholipids of the cytoplasmic membrane. Bisbiroulas *et al.* (2011) [76] therefore also analyzed the phospholipid profile after exposure to benzalkonium chloride. An increase in the amounts of cardiolipin (31%,) and a decrease in the amounts of phosphoaminolipids (32.7%), phosphatidylinositol (34.1%,) and phosphatidylglycerol (8.3%) was observed compared to the control strain. The observed changes in phospholipid composition led to an increase of 9.4%

of the anionic phospholipid fraction, which includes cardiolipin, phosphatidylinositol and phosphatidylglycerol. Yet, the role of these adaptations in response to benzalkonium chloride remains inconclusive.

The observations in both studies allow to conclude that the fatty acid profile and changes in the polarity of the phospholipid head groups affect the physicochemical cell surface properties and may alter the susceptibility of *L. monocytogenes* to benzalkonium chloride. However, these changes do not seem to be essential for increased benzalkonium chloride tolerance since they do not occur in all evolved strains, suggesting that additional mechanisms exist.

A remarkable observation in the study of Mereghetti *et al.* (2000)[77] is the association of increased benzalkonium chloride tolerance with non-typeability by serological techniques in *L. monocytogenes*. Mereghetti *et al.* (2000) isolated seven strains with increased QAC resistance from various ecosystems. Five of the resistant strains were non-typeable by phage typing, which suggests structural changes in the cell walls. The role of cell wall modifications in response to QACs was further supported by a study performed by Fox, Leonard, and Jordan (2011)[78] who characterized persistent and non-persistent isolates of *L. monocytogenes* from farmhouse cheese production facilities, by phenotype microarray, growth curve analyses and transcriptome sequencing. Persistent strains exhibited higher tolerance for the QACs benzethonium chloride and cetylpyridinium chloride than the non-persistent strains. Transcriptomic analyses of a persistent and a non-persistent strain, in the presence of sublethal concentrations of benzethonium chloride, revealed in comparison to unexposed strains significant upregulation in both strains of genes involved in peptidoglycan synthesis, from initial sequestration of carbohydrates from the environment and biosynthesis of peptidoglycan precursors to assembly of peptidoglycan in the cell wall. Since QACs have a membrane disruptive mode of action, regeneration or reorganization of peptidoglycan, possibly leading to increased peptidoglycan thickness and/or cross-linking layer may prevent accumulation or passage of QACs through the peptidoglycan layer. In this way, the access of QACs to the cell membrane target is more restricted. However, these observations occurred in both a persistent and non-persistent strain. This means that the role of peptidoglycan modifications as an adaptation strategy against QACs is not restricted to persistent strains only, but seems to be a general adaptation of *L. monocytogenes.* It can therefore be concluded that peptidoglycan modifications are not the main contributors to increased QAC tolerance.

To elucidate the molecular response of *L. monocytogenes* to QACs, Casey *et al.* (2014)[79] also performed a transcriptome analysis on a persistent *L. monocytogenes* strain isolated from a farmhouse cheese production facility. The strain was grown statically at 14 °C in tryptic soy broth to early stationary phase in the presence or absence of 4 ppm benzethonium chloride. The analysis identified approximately 600 genes which demonstrated a 4-fold or greater change in relative expression in the presence of benzethonium chloride, and over 141 genes with a 7.5-fold change or more. Multiple genes of the following functional groups were considerably upregulated: peptidoglycan biosynthesis, chemotaxis, flagellar assembly, fatty acid metabolism and biosynthesis, phosphotransferase system and cobalamin synthesis. Genes from the peptidoglycan biosynthesis, fatty acid metabolism and biosynthesis and the phosphotransferase system were also found to be upregulated in the earlier transcriptome study of Fox *et al.* (2011) [78].

Besides cell wall and membrane modifications, efflux pumps are reported to be activated after repeated exposure to benzalkonium chloride, thus suggesting that these contribute to increased tolerance for QACs [75,80]. Two efflux pumps, MdrL and the multi-drug transporter Lde, have been described in *L. monocytogenes*. Both are known to extrude a variety of structurally unrelated toxic compounds such as antibiotics, heavy metals and ethidium bromide [81,82] Aase *et al.* (2000) [80] subcultured both benzalkonium resistant and sensitive environmental isolates as soon as growth was recorded, in increasing concentrations of benzalkonium chloride until there was no growth within 7 days. 50% of the benzalkonium chloride resistant isolates also showed cross-resistance towards ethidium bromide, which was the result of ethidium bromide efflux, meaning that efflux pumps were already activated in the benzalkonium resistant isolates. The efflux of ethidium bromide was also found in originally sensitive isolates that were gradually adapted to benzalkonium chloride, but not in their sensitive parental strains. These results therefore indicate that efflux pumps can be activated upon exposure to benzalkonium chloride and that this activation can induce a broad-spectrum resistance mechanism based on efflux pumps. No indication was found that this type of resistance was related to antibiotic resistance. As described earlier, To *et al.* (2002) exposed the parental strains to increasing concentrations of benzalkonium chloride. The cultures were allowed to adapt to increasing concentrations until the point where ten consecutive transfers resulted in no further adaptation. Ethidium bromide efflux was

observed in benzalkonium adapted originally sensitive isolates, while efflux pump activity was absent in adapted originally resistant isolates. The role of efflux pumps in adaptation and resistance of *L. monocytogenes* to benzalkonium chloride was more rigorously investigated by Romanova *et al.* (2006)[83], using the potent efflux pump inhibitor reserpine. Efflux pump inhibition by reserpine led to decreased MIC values of laboratory adapted strains with increased tolerance for benzalkonium chloride, but not for naturally isolated resistant strains. Gene expression profiling of naturally resistant isolates showed only low levels of expression of the genes encoding the MdrL and Lde efflux pumps, while the evolved, but originally sensitive strains, showed increased expression of the MdrL, but not the Lde efflux pump. Just like membrane and cell surface modifications, efflux pumps therefore only seem to be partly or in some cases responsible for adaptation to benzalkonium chloride. The studies of To *et al.* (2002) and Romanova *et al.* (2006) indicate that especially for naturally resistant isolates, the upregulation of efflux pump activity in acquiring resistance seems to be very limited.

Next to monocationic QACs, polycationic biguanides are widely used cationic disinfectants. This group can be subdivided in bisbiguanides like chlorohexidine (Fig. 1.9a) and alexidine (Fig. 1.9b), and polymeric biguanides like polyhexamethylene biguanide (Fig. 1.9c). The latter are used in particular by the food industry, while the bisbiguanides are more applied as biocides in hand washing and oral products[72].

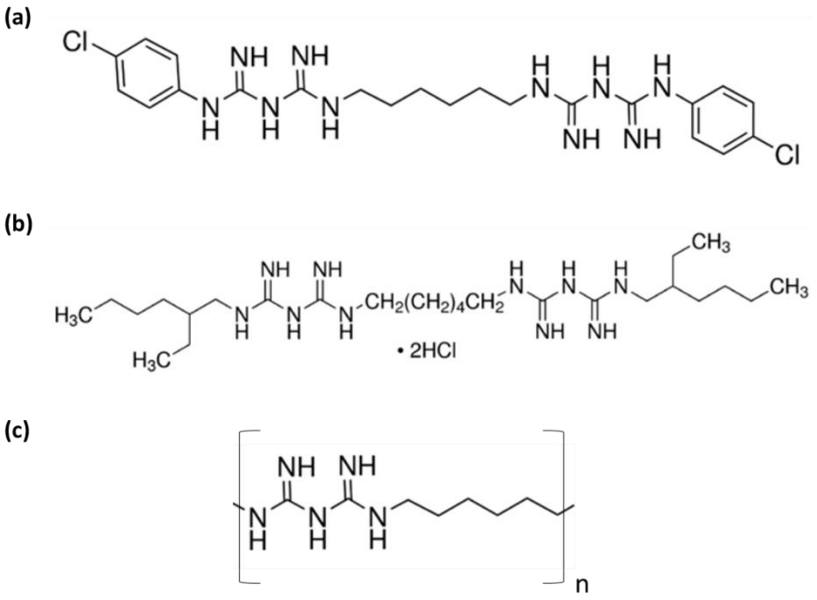

Fig 1.9. The chemical structure of the bisbiguanides chlorhexidine (a) and alexidine (b) and the polymeric biguanide polyhexamethylene biguanide (c).

The mode of action of biguanides is similar to that of QACs in that the biguanide cationic functional groups strongly associate with exposed anionic sites on the cell membrane and cell wall, particularly acidic phospholipids and proteins. There is, however, also a major difference which is visualized in Fig. 1.10. While the hydrophobic acyl chain of QACs becomes solubilized within the hydrophobic core of the membrane, the hydrophobic regions of biguanides do not interdigitate because they are somewhat inflexible and incapable of folding sufficiently to interdigitate into the phospholipid layer. Bisbiguanides act by bridging adjacent phospholipid head groups being bound to a biguanide moiety and displace the membrane stabilizing Ca^{2+} ions. Just like in the interaction between QACs and membranes, these membrane disruptive interactions result already at low concentrations in a reduction of the membrane fluidity, which in turn disturbs the metabolic and osmoregulatory functions of the cell membrane and its embedded proteins and enzymes. At higher concentrations, as used in practical applications, the interactions between biguanides and phospholipids are stronger and cause the membrane to adopt a liquid crystalline state and lose its integrity. This will eventually lead to cell leakage and lysis [71]. Although this mode of action has always been the prevailing model for their antibacterial mode of action, Chindera *et al.* (2016)[84] recently discovered that polyhexamethylene biguanide surprisingly also enters different Gram-positive and Gram–negative cells when applied at low µg/ml concentrations. Once inside the cell, this compound causes condensation of bacterial chromosomes and cell division arrest. Their results suggest an alternative and complementary antimicrobial mode action of biguanides. So far, no mutants with acquired resistance to biguanides have been reported or could be isolated [84].

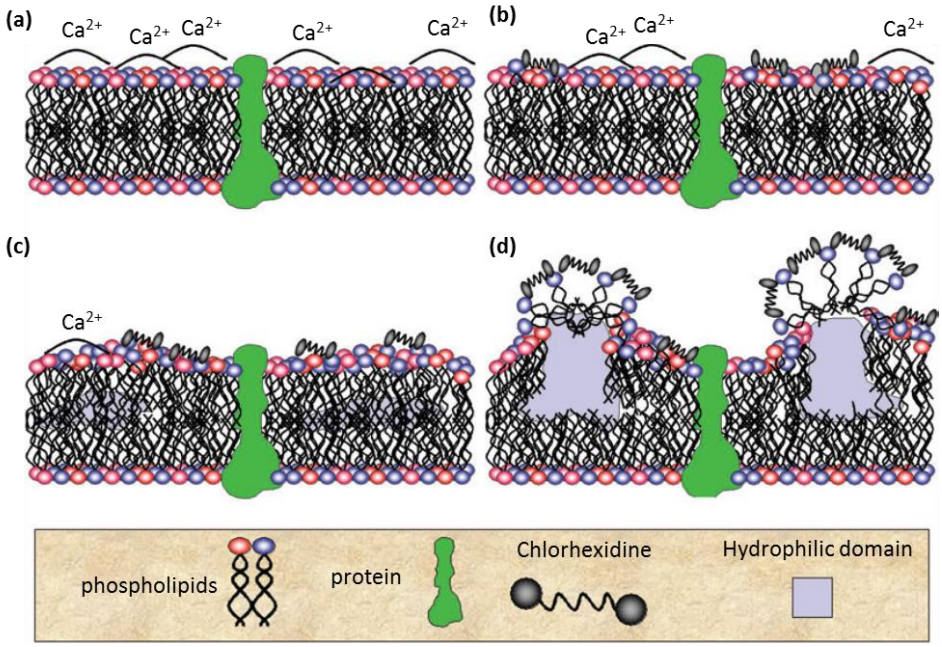

Fig. 1.10. [71]. Cartoon showing the interaction of chlorhexidine with the bacterial cytoplasmic membrane. Steps (a-d) represent progressive decrease in fluidity of the outer leaflet with increasing exposure to the bisbiguanide.

1.4.4. Triclosan

The bisphenol compound triclosan (Fig. 1.11) is used in many household products such as soaps, detergents and cosmetics to prevent bacterial contamination and deterioration. Triclosan has also been incorporated in a variety of food contact materials like storage containers and chopping boards, to prevent long-term survival and biofilm formation. Triclosan is also used as an antiseptic agent in surgical scrubs and soaps and to wash patients that are carriers of methicillin-resistant *S. aureus* prior to surgery [85]. While most biocides, antiseptics and detergents have multiple cellular targets and often cause multiple stresses, triclosan has a specific cellular target to which it owes it antibacterial activity. It was first discovered by McMurry, Oethinger, and Levy (1998) [86] that triclosan, already at low concentrations, blocks lipid synthesis in *E. coli* by specifically inhibiting FabI. This enzyme is the enoyl-acyl carrier protein reductase subunit of the FASII complex (Fig. 1.4). It is an essential enzyme in the fatty acid elongation cycle.

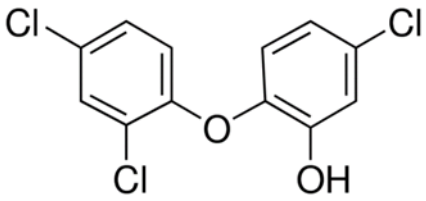

Fig. 1.11. The chemical structure of triclosan.

The specific interaction between triclosan and its target FabI was discovered by the characterization of five independent *E. coli* mutants with different levels of triclosan resistance. Sequencing analysis revealed that three mutants each contained a different single amino acid substitution in the *fabI* gene. Expression of the wild type *fabI* in the two remaining, but unsequenced mutants, led to loss of the triclosan-resistant phenotype indicating that mutations in *fabI* are also at the base of the resistant phenotype.

To prove that triclosan indeed inhibits lipid synthesis, McMurry *et al.* (1998) performed a lipid synthesis assay with [1-^{14}C]-acetate on logarithmically growing cells in LB broth supplemented with triclosan. For comparison, the same experiments were performed with diazaborine, which is a specific inhibitor of FabI in *E. coli* and *Salmonella* Typhimurium [87]. Its binding with FabI depends on the presence of the co-factor NADH [87,88]. Diazaborine reduced acetate incorporation into lipids by 93%, compared to 92% for 0.24 µg/ml triclosan, while two control compounds chloramphenicol, a protein synthesis inhibitor, and ciprofloxacin, a DNA synthesis inhibitor, reduced the incorporation only by 19% and 2% respectively. In the mutant that was most resistant to triclosan (FabI Gly93Val), lipid synthesis was blocked by only 2% with 0.24 µg/ml triclosan and by 75% with 26 µg/ml triclosan. Moreover, the Gly93Val mutation in *E. coli* FabI, also generated diazaborine resistance, reduced binding of diazaborine to the enzyme and lowered the specific activity of the enzyme [87,89]. It was later demonstrated by Heath *et al.* (1999) [90] that triclosan forms a tight non-covalent ternary complex with FabI and NAD^+. More specifically, triclosan binds to the enoyl substrate site on FabI, but a tight binding of triclosan requires interactions between both the protein and the NAD^+ cofactor, eventually blocking enzyme activity [90,91]. The Gly93Ser mutation in the active site of *E. coli* FabI interferes with the formation of this stable ternary complex, leading to resistance.

Triclosan can also lead to lysis at higher concentrations. As an example, McMurry *et al.* (1998) [86] determined that the *E. coli* AG100 needed 0.15 µg/ml triclosan to inhibit the growth rate by 50%, but that 8 µg/ml was needed for lysis. The Gly93Val triclosan resistant mutant required 13 µg/ml of the drug to inhibit the growth rate by 50%, while no lysis could be observed up to a concentration of 256 µg/ml, which exceeds the solubility of triclosan.

By now several other Gram-positive and Gram-negative bacteria have been documented to develop increased tolerance and resistance to triclosan by point mutations in *fabI* or overexpression of *fabI*, but also by increased efflux pump activity [85,92]. Besides mutations in the *fabI* gene, mutations in another gene of the FASII enzyme complex for lipid biosynthesis, *fabD,* can increase resistance to triclosan. These mutations lead to a by-pass of the normal biosynthetic pathway via FabI, which is inhibited in the presence of triclosan, by enhancing incorporation of exogenous fatty acids. This was discovered by Morvan *et al.* (2016) [93], who observed that triclosan resistant colonies arose at about 100-fold higher frequencies (~10^{-6}) on BHI agar in the presence of a cocktail of fatty acids. The triclosan resistant mutants could be divided into two groups based on their fatty acid requirements: a group of fatty acid prototrophs and group that had become fatty-acid dependent for normal growth and thus showing poor growth in BHI without supplemented fatty acids. Among the prototrophs, three out of sixteen mutants had unaltered fatty acid profiles, indicating that the FASII pathway was still active. The other thirteen prototrophic mutants incorporated both exogenously supplied and endogenously synthesized fatty acids in their membranes. Since all of these resistant mutants still carried a wild type *fabI* gene, these results suggest that these mutants are able to bypass a FASII triclosan induced block in FabI by incorporating exogenous fatty acids. Whole-genome sequencing of three mutants revealed *fabD* mutations. FabD is the FASII initiation enzyme which loads acyl carrier protein to generate malonyl-acyl carrier protein, which is used further downstream in the fatty acid elongation cycle. Further sequencing of *fabD* in all other resistant mutants revealed mutations, mainly at positions G196 and Q265. The causality between the observed phenotypes and the *fabD* mutations was confirmed via complementation experiments with the wild type *fabD* gene in the mutant strain background. Altogether the results of Morvan *et al.* (2016) [93] show that FASII blockage can be bypassed by mutations in *fabD* and the use of diverse fatty acid combinations and that the emergence of triclosan resistant bacteria can be nutrient dependent.

In *L. monocytogenes*, four cycles of growth (24h, 37 °C) in sublethal concentrations of triclosan (1 and 4 μg/ml) , did not lead to altered MIC values, but instead induced resistance to aminoglycoside antibiotics [94]. Two types of triclosan-induced aminoglycoside resistant isolates could be distinguished based on colony morphology. A pinpoint colony phenotype seemed to be caused by mutations in the heme genes. Mutations were found both in the ferrochelatase gene (*hemH*) and in the glutamyl-tRNA reductase gene (*hemA*). Addition of hemin restored the colony size. However, the link between the emergence of antibiotic resistance, the pinpoint morphology and triclosan activity remains unclear. The isolates with a normal colony size had mutations affecting ATP synthase subunits or ABC transporters involved in active transport systems. This could possibly explain the link with aminoglycoside resistance, since active transport is necessary for the uptake and antibiotic activity of this type of antibiotics [95].

1.4.5. Nisin

Nisin is 34-amino acid polypeptide bacteriocin produced by *Lactococcus lactis* subsp. *lactis*, and belonging to the group of lantibiotics (lanthionine functional group, i.e. Alanine-S-Alanine). Since its discovery in the 1920s, nisin has proven to be an effective antimicrobial agent, especially against Gram-positive bacteria. Nisin is produced commercially with a legal status for usage as food additive (E234 in the EU). Two nisin variants are known, nisin A and nisin Z. The only difference is the presence of a histidine residue at position 27 in nisin A, compared to an asparagine at the same position in nisin Z. Nisin is an amphiphilic polypeptide with a relatively hydrophobic N-terminal part and a net positive charge at physiological pH, mainly in the C-terminal domain due to three lysine residues and one (nisin Z) or two (nisin A) histidine residues and the absence of negatively charged glutamate and aspartate residues. The primary target of nisin in bacterial vegetative cells is the cytoplasmic membrane. The mode of action is primarily based on the incorporation in the membrane and subsequent pore formation, caused by the binding of nisin with lipid II, the bactoprenol lipid anchor that translocates disaccharide-pentapeptide building blocks across the membrane during peptidoglycan synthesis. Pore formation eventually leads to leakage of intracellular compounds and dissipation of the proton gradient. At higher concentrations nisin also inhibits the peptidoglycan synthesis. Nisin resistance has been reported in several Gram-positive species, like *L. monocytogenes, B. cereus and S. aureus* [96].

In *L. monocytogenes*, nisin resistance is linked predominantly to membrane composition modifications. Ming and Daeschel (1993, 1995) [97,98] were one of the first to report the correlation between membrane modifications and nisin resistance in *L. monocytogenes*. They obtained a nisin-resistant isolate of *L. monocytogenes* Scott A after seven transfers in BHI broth at 37 °C, containing increasing amounts of nisin, from 400 U/ml to 2000 U/ml. Eventually the MIC of the nisin-resistant strain was tenfold increased. The resistance was stable after three passages, approximately 30-35 generations, in nisin-free broth. No nisin degradation was observed by the resistant strain as nisin activity remained stable in culture supernatants. The membrane phase-transition temperature in the resistant strain, determined on whole cells by differential scanning calorimetry, had increased from 37.4 °C to 44.4 °C. The subsequent fatty acid analysis was consistent with this observation, showing an increased proportion of straight-chain over branched-chain fatty acids. Significant differences were found within the fatty acid fractions C14:0, iso-C15:0, anteiso-C15:0 and iso-C17:0. As expected, the specific growth rate of the resistant mutant, especially at low temperature, was reduced due to the lower amounts of branched-chain fatty acids. At 37 °C, the specific growth rate of the resistant strain was 86.7% of that of the parent, while at 20 °C it was only 40.9%. In conclusion, Ming and Daeschel (1993) hypothesized that the altered fatty acid composition may make the membrane somehow less susceptible for the action of nisin. Whether this is a consequence of reduced binding to lipid II, or of the increased rigidity of the membrane, or an indirect effect related to possible changes in presence or distribution of membrane proteins, is unknown. In a follow-up study Ming and Daeschel (1995) investigated the correlation of cellular phospholipid content with the nisin resistance of *L. monocytogenes* Scott A. The stable nisin-resistant mutant isolated in their previous study, also had a significantly lower total phospholipid content (31.3 in the mutant vs. 46.1 mg/g dry weight cells in the parent), which was caused by significant reductions in the amounts of all three major types of phospholipids, phosphatidylglycerol, diphosphatidylglycerol and bis-phosphatidylglyceryl phosphate.

The interaction of nisin with membranes depends not only on the hydrophobic interaction of amino acid residues of nisin and the fatty acids of the membranes, but also on the electrostatic attraction between the net positive charge of the amphiphilic nisin molecule and the negatively charged phospholipids. Ming and Daeschel (1995) found that less nisin was associated with resistant cells, which may be a consequence of the reduced total and

individual phospholipid content. Moreover, when exposed to nisin, the resistant cells released smaller amounts of phospholipids than the parental strain. Sensitive cells also appeared to have a higher cell hydrophobicity, as determined by the BATH (bacterial adherence to hydrocarbons) test. All these membrane modifications, both on the level of phospholipids and types of fatty acids, may lead to an impaired association or interaction of nisin with membranes and thus explain nisin resistance of the mutant.

Building on the findings of Ming and Daeschel (1993; 1995), Mazzotta *et al.* (1997) [99] addressed the question of whether nisin resistance could develop at low temperature. Since growth at low temperature requires increased amounts of branched-chain fatty acids to maintain membrane fluidity, this seems to be incompatible with a mechanism of nisin resistance based on reducing the amounts of branched-chain fatty acids and reduced membrane fluidity. Nevertheless, Mazzotta *et al.* (1997) succeeded to isolate mutants with stable nisin-resistance strains from plates containing 1000 IU/ml nisin both at 10 °C and 30 °C. Moreover, mutants generated at 30 °C were resistant when plated in nisin-containing medium at 10 °C and vice-versa. No nisinase activity was found to play a role in the observed resistance of the two isolates. To exclude any role of the cell wall in hindering nisin to reach the cytoplasmic membrane in the resistant strains, protoplasts of a resistant variant were produced. Protoplasts were still resistant to the same concentrations of nisin, while the wild type protoplasts were easily inactivated.

Fatty acid analyses showed no significant differences in fatty acid profile between the wild type strain and both nisin resistant isolates, grown in the absence of nisin and at the same temperature (10 °C or 30 °C), except for a very minor difference in iso-C17:0. More significant differences in fatty acid distribution were observed when cells were grown in the presence of nisin prior to lipid extraction. In comparison to growth in nisin-free medium, the fatty composition of the nisin-resistant strain, isolated at 30 °C, and grown at 30 °C before fatty acid analysis had higher amounts of long chain fatty acids, relatively less short-chain fatty acids, an increase up to 12% in the normally not so abundant unsaturated fatty acids C16:1 and C18:1 and a significant lower ratio C15/C17. The same changes were observed for the resistant strains isolated at 10 °C and grown at 10 °C with and without nisin before fatty acid analysis, with exception of the increase in the unsaturated fatty acids C16:1 and C18:1 which only increased up to 5%. Although all the changes in fatty acid composition are predicted to result

in more rigid membranes, the increase in unsaturated fatty acids will increase fluidity. It is therefore not possible to predict the net effect of these changes. Both mutants showed reduced growth rates at both temperatures, but the difference with the parent strain was equally large at both temperatures. Therefore, there seems to be a fine-tuning adjustment which allows growth in a wide range of temperatures at a reduced rate, but at the same time also restricts the action of nisin as much as possible.

In contrast to the previous studies, Verheul *et al.* (1997) [51] did not find any changes in the fatty acid composition of a nisin-resistant mutant of *L. monocytogenes* Scott A, isolated by stepwise exposure to increasing amounts of nisin in the growth medium at 30 °C. The nature of the mutation was probably different from that in the resistant mutant isolated by Ming and Daeschel (1993) and Mazzotta *et al.* (1997), since the mutant of Verheul *et al.* (1997) still exhibited the same growth characteristics of the parental strain, both at 7 °C and 30 °C. In contrast, the mutant of Verheul *et al.* (1997) had a proportion of phosphatidylglycerol (PG) to diphosphatidylglycerol (DPG), of approximately 7/1 compared to 5/1 in the parental Scott A strain. It was hypothesized that this alteration was caused by decreased activity of DPG synthetase, which forms DPG by condensation of two PG units. The same PG/DPG ratio was observed both in the presence and in the absence of nisin in the growth medium. That the PG/DPG ratio can affect nisin resistance had been previously suggested by Demel *et al.* (1996) [100], who showed that nisin penetrates more deeply into monolayers of DPG than into those with other lipids including PG. Crandall and Montville (1998) [101] also reported nisin-resistant strains of *L. monocytogenes* ATCC 700302 that had modified phospholipids, more specifically decreased amounts of anionic phospholipids (cardiolipin and phosphatidylglycerol) and increased amounts of phosphatidylethanolamine. These modifications result in a decreased net negative charge, and are thus predicted to weaken binding of nisin.

More recently, it was shown that ABC transporters and two-component systems are also involved in susceptibility for nisin. In a study conducted by Collins *et al.* (2010) [102], a non-polar deletion mutant of *arnB* in *L. monocytogenes*, encoding the permease component of a putative multidrug resistance ABC transporter, exhibited increased sensitivity to lantibiotics. Its expression was regulated by the VirRS two-component system. Another two-component signal transduction system of *L. monocytogenes*, LisRK, which plays a role in virulence, also determines nisin sensitivity. A knockout of *lisK*, the histidine kinase sensor component,

enhanced resistance to nisin, which may be explained by the strongly reduced expression of putative penicillin-binding proteins (PBPs) in these mutants [103]. PBPs catalyze peptidoglycan cross-linking, and sometimes also the incorporation of the disaccharide-pentapeptide moiety carried by lipid II into the growing peptidoglycan chain. PBP2229 is hypothesized to shield lipid II and thereby anticipated to reduce nisin sensitivity [104,105].

Furthermore, a few other mechanisms are known to contribute to the innate resistance to nisin in *L. monocytogenes*, including the expression of the glutamate decarboxylase GadD1 [106], the expression of a protein with strong homology to the multiple peptide resistance factor of *Staphylococcus aureus*, that confers resistance to cationic antimicrobial peptides by lysinylation of phospholipids [107], and expression of LiaR [104]. LiaR is a response regulator that is part of the three-component system LiaFSR. LiaR-regulated genes include some that are linked to nisin resistance such as the previously mentioned PPB2229 [105] and *telA*, which encodes a protein involved in toxic ion resistance [102].

Next to direct adaptations by nisin exposure, other environmental stresses such as salt stress have been described to induce cross-resistance to nisin [108]. The cell envelope stress response system LiaFSR, previously linked to nisin resistance, was induced during adaptation to salt at low temperature [109]. Bergholz *et al.* (2013) [108] generated *liaR* mutants in seven different *L. monocytogenes* strains and determined their nisin resistance with and without prior exposure to salt. Nisin resistance increased significantly ($p < 0.0001$) after salt exposure in the wild type strains. The *liaR* mutant cultures were significantly more nisin-sensitive than the wild type, and their nisin resistance also increased significantly less than that of the wild type strains upon exposure to salt.

1.4.6. Plant essential oil compounds

Essential oils (EOs) of plants are predominantly composed of small hydrophobic molecules (see section 1.2). Due to their hydrophobic nature, these compounds partition in the membrane lipid phase where they potentially perturb membrane structure and functionality. A common observation is that essential oils and their compounds cause leakage of cell contents, and this is interpreted as an indication of increased membrane permeability [20]. Yet, detailed molecular evidence and insights in the interactions and events that cause cell leakage remain scarce. More specifically, it remains uncertain whether cell leakage results from direct structural membrane damage or is (also) an indirect consequence of a reduced

cellular energy status or a disturbed homeostasis, leading to disturbance of membrane transport processes. However, besides disturbing membranes, EO compounds may also interfere with the function of proteins, both in the membrane and in the cytoplasm. This is particularly the case for EO compounds with reactive functional groups, like the electrophilic α, β-unsaturated carbonyl compounds and isothiocyanates, which can react with thiol groups. Therefore, the antimicrobial mode of action of most EO compounds cannot just be attributed to a single cellular target, but it rather involves a multiple target mode of action, and it is likely that different compounds have (partly) different targets.

Some studies have investigated the influence of EO compounds on the thermodynamic and physical properties of bacterial membranes, by using *in vitro* model membrane systems. Useful information on the mode of action has also been obtained by investigating changes in membrane composition in response to hydrophobic EO compounds in a variety of food-borne pathogens, including *L. monocytogenes*. Nowotarska *et al.* (2014) [45] studied the interactions between the EO compounds carvacrol, *trans*-cinnamaldehyde (t-CIN) and geraniol and three different Langmuir monolayers composed of the bacterial phospholipids 1,2-dihexadecanoyl-sn-glycero-3-phosphoethanolamine (DPPE, zwitterionic), 1,2-dihexadecanoyl-sn-glycero-3-phospho-(1'-rac-glycerol) (DPPG), and 1,1',2,2'-tetratetradecanoyl cardiolipin (anionic), representing dominant phospholipid fractions of Gram-positive (mostly anionic) and Gram-negative bacteria (mostly zwitterionic and in lesser amounts anionic). Thermodynamic characteristics of the membranes in interaction with the EO compounds were assessed by measuring surface pressure-area and surface potential-area isotherms. Their results indicate that all three compounds modify the three monolayer structures by integrating into the monolayer, forming aggregates of compound-lipid complexes, reducing the packing effectiveness of the lipids, increasing the membrane fluidity and altering the total dipole moment in the monolayer.

Studies of the bacterial response towards EO compounds have reported changes in membrane composition that reflect homeoviscous adaptation. Patrignani *et al.* (2008) [110] reported an increase in saturated fatty acids, predominantly C14:0, C16:0 and C18:0, and a reduction in iso-C14:0, C15:0, iso-C15:0, anteiso-C15:0 and C18:1 ω9c in late-exponential-phase cells of *L. monocytogenes* grown at 37 °C in BHI in the presence of a subinhibitory concentration of 20 ppm *trans*-2-hexenal, an α, β-unsaturated carbonyl compound. These changes are predicted

to reduce membrane fluidity and are thus consistent with the idea of a bacterial response to counteract the membrane fluidizing effect of the compound as reported by Nowotarska *et al.* (2014) [45]. However, remarkably, these authors did not find any anteiso-C17:0 in the control Scott A culture grown in BHI without antimicrobials, although others reported this to be one of the dominant fatty acids in Scott A and other *L. monocytogenes* strains [111,112]. Later work from the same group reported on the effect subinhibitory concentrations (1/2, 1/3 and 1/5 of the MIC) of thymol and carvacrol and the α, β-unsaturated carbonyl compound citral in BHI during growth at 37 °C [113]. Late-exponential cells were collected for fatty acid analysis. In this study, the fatty acid composition of the control Scott A culture corresponded better to the composition reported by others. In the presence of 125 ppm citral, small reductions could be observed in the amounts of anteiso-C15:0, anteiso-C17:0 and iso-C17:0, compensated by increases in C16:0, C18:2 (*cis*-*cis*) and C18:1 ω9c. 50 ppm carvacrol caused a significant reduction in the amounts of iso-C15:0, anteiso-C15:0, iso-C17:0 and anteiso-C17:0 and an increase in the amounts of straight-chain C16:0 and the unsaturated fatty acids C18:2 (*cis*-*cis*) and C18:1 *trans*9. Again, the reduction in the amounts of BCFA and increase in straight-chain fatty acids like C16:0 are predicted to make the membranes more rigid. Remarkably, thymol (40-100 ppm), a structural isomer of carvacrol (2-isopropyl-5-methylphenol and 2-methyl-5-isopropylphenol, respectively), did not induce any changes in membrane composition.

Finally, Di Pasqua *et al.* (2006) [114] investigated adaptive changes in the ratio of saturated to unsaturated fatty acids induced by sublethal concentrations of t-CIN, thymol, carvacrol, limonene and eugenol in various Gram-negative and Gram-positive bacteria. In *E. coli* O157:H7, t-CIN induced a higher degree of unsaturation, and the same was observed for the other compounds tested. However, the effect of t-CIN in different bacteria was not consistent, since it had no significant effect on the degree of saturation in two other Gram-negative bacteria (*Salmonella* enterica serovar Typhimurium and *Pseudomonas fluorescens*), it increased the ratio in one Gram-positive organism (*Brochothrix thermosphacta*) and decreased the ratio in another one (*Staphylococcus aureus*). Also for the other compounds, no consistent trends could be observed that would support the hypothesis of counteraction of a membrane fluidizing effect of the compounds. However, unfortunately, the study did not report changes in cyclopropane fatty acids and BCFAs, which are prominent, if not the major,

players in membrane homeoviscous adaptation in Gram-negative and Gram-positive bacteria, respectively [114].

A different approach to measure the membrane perturbing effect of small antimicrobial molecules was used by Foss *et al.* (2013) [115]. These authors investigated the effect of membrane perturbing compounds on the (mis)localization of membrane associated proteins and the effects on cell division. Many cell division-related proteins are localized at specific sites in the bacterial cell and this localization requires energy. It was previously shown by Strahl and Hamoen (2010) [116] that the membrane potential modulates the localization of cell division proteins such as MinD, FtsA and the bacterial cytoskeletal protein MreB. Disrupting the membrane potential thus leads to mislocalization of cell division proteins. To investigate this mislocalization phenomenon *in vivo* in *Bacillus subtilis*, the investigators used a green fluorescent protein translationally fused to MinD. MinD regulates FtsZ activity and therefore plays a role in bacterial cell division. MinD preferentially binds to anionic phospholipids and the local organization of phospholipids in the membrane is thought to influence the position of MinD *in vivo*. A five-minute exposure of *B. subtilis* to t-CIN at its MIC (2.5 mM), caused a decrease in membrane potential and an increased permeability to propidiumiodide. After 20 min of exposure, MinD was mislocalized in almost 100 % of the analyzed cells. These results demonstrate that t-CIN depolarizes the bacterial membrane, causing a non-specific delocalization of division-related, membrane associated proteins such as MinD and FtsZ. Although it was previously shown by Domadia *et al.* (2007) [117] that t-CIN binds FtsZ, perturbs the cytokinetic Z-ring formation and inhibits its assembly dynamics *in vitro*, the impaired functionality of FtsZ *in vivo* by t-CIN may more likely be due to changes in the physicochemical properties of the membranes brought about by t-CIN [115].

Other membrane perturbing effects were reported by Gill and Holley (2006) [119], who investigated the inhibition of membrane bound ATPases of *E. coli* and *L. monocytogenes* by increasing concentrations (0.1 – 10 mM) of eugenol, carvacrol and t-CIN. ATPase activity was measured in isolated membrane preparations that were treated with suspensions of the compounds at 0.1, 0.5, 1, 5 and 10 mM prepared in Tris buffer. The ATPase reaction was initiated by the addition of ATP and terminated after 10 min by the addition of 10% trichloroacetic acid, after which the ATP content was measured via bioluminescence. Inhibition of *E. coli* membrane ATPase activity was observed starting from 5 mM of carvacrol

or eugenol. t-CIN caused concentration-dependent ATPase inhibition over the entire tested range. In membrane preparations of *L. monocytogenes*, significant inhibition was observed at 5 and 10 mM eugenol and at 10 mM carvacrol or t-CIN. To determine whether or not the observed inhibition is due to a specific interaction with the ATPase enzyme would require a kinetic study using the purified enzyme. The observed effect might as well be caused indirectly by the membrane perturbing effect of the compounds.

An entirely different approach was used by Visvalingam, Hernandez-Doria, and Holley (2013) [46], who examined the genome-wide transcriptional response of *E. coli* O157:H7 after 2 h and 4 h of exposure to a sublethal concentration of 200 mg/l t-CIN at 37 °C. Gene expression changed drastically after 4 h of exposure compared to 2 h. After 2 h of exposure several oxidative stress related genes, encoding superoxide dismutase (*sodA*), catalase (*katE*), glutathione synthetase (*gshA*), Fe-S scaffold protein cluster assembly (sufA), genes for biofilm and cell signaling protein (bhsA) and periplasmic protein (*yhcN*) were also induced. Expression of DNA replication, protein translation, O-antigen and fimbrial synthetic genes were repressed. These results suggest that the electrophilic nature of t-CIN (section 1.3) may result in intracellular oxidative stress. Many enzymes involved in oxidative stress responses have been reported to reduce the intracellular NADPH level in *E. coli*, which not only lowers the reducing power of the cells, but also inhibits cell multiplication by limiting the biosynthetic capability. This might explain the downregulation of biosynthetic genes. After 4 h of exposure, many repressive effects on the gene expression were reversed and the expression of DNA replication, protein translation, and O-antigen and fimbrial synthetic genes increased again by 1.8 to > 5-fold. Also, many genes associated with lipid A biosynthesis, long-chain fatty acid biosynthesis, motility/chemotaxis, cell division cycle/cell shape, F_0F_1-ATP synthase and the global transcriptional regulator Fis were upregulated. The upregulation of these genes at 4 h is consistent with the slightly elevated growth rate observed between 2 and 4 h, indicating that cells were less stressed and started growing again. However, RP-HPLC analysis revealed that the t-CIN concentration was stable at 2 h of incubation, but decreased from 200 mg/l to ≤ 10 mg/l at 4 h, while the concentration of cinnamic alcohol increased to ≥ 120 mg/l. Differential gene expression at 4 h might therefore not be solely caused by t-CIN, but also by cinnamic alcohol. The MIC of cinnamic alcohol was four times higher (400 mg/l) for the same *E. coli* strain. Of the genes upregulated at 2 h, the highest expression (6.1-fold) was observed

for the YqhD gene encoding an alcohol dehydrogenase, followed by a fivefold increase of the 2,5-diketo-D-gluconate reductase (DkgA) gene. At 4 h, these genes were no longer differentially expressed compared to the unexposed control sample. Both enzymes are known to be overexpressed in the presence of aldehydes and have broad substrate specificity. Altogether these observations may indicate that these enzymes convert t-CIN to cinnamic alcohol. In summary, the study of Visvalingam, Hernandez-Doria, and Holley (2013) shows that detrimental effects of t-CIN, and probably also other hydrophobic reactive EO compounds, are not limited to the cell membrane but also involve cytoplasmic targets.

1.5. Conclusion

All discussed compounds target the bacterial membranes, yet the nature of the interactions with the bacterial membrane often differs substantially. This may be caused by a difference in lipophilicity, molecule size, charge or other molecular features like acidity and chemical reactivity. Besides some compound specific adaptation strategies, one common adaptation strategy of bacteria to membrane acting compounds, is altering the membrane fatty acid and/or phospholipid composition in order to counteract the membrane perturbing effect of the compounds. Genetic resistance to these compounds does not emerge quickly or it has not yet been investigated and characterized, with exception for compounds with a specific protein target like triclosan. Because also other characteristic molecular features determine the antimicrobial mode of action of a membrane acting antimicrobial compound, this thesis not only focuses on the membrane disturbing effect of *trans*-cinnamaldehyde and some other lipophilic and thiol-reactive essential oil compounds, but attempts to assess the global impact of these compounds on the metabolism of *L. monocytogenes* by characterizing sensitive transposon mutants.

Scope of the research

Plant essential oils and their major constituents often have pronounced and broad antimicrobial activities. They have been investigated intensively to replace classic 'chemical' food preservatives in response to the increasing demand for minimally processed, nutritionally healthy and fresh foods without artificial preservatives or other technological additives. Essential oil compounds display a wide diversity in chemical structure, reactivity, water and fat solubility, and often have a strong smell and aroma. Many of these compounds show synergistic interactions, in terms of microbial inactivation or growth inhibition, with other natural antimicrobial compounds or with bactericidal processing techniques such as heat or high pressure treatment. They can therefore be incorporated in a hurdle technology concept, which allows the use of lower concentrations of the compounds and less intense processing. This correspondingly leads to better retention of food quality, while maintaining the same microbiological stability and safety. Most of the studies investigating hurdle technology concepts rely on trial and error to find effective synergistic combinations and the antimicrobial mechanism underlying promising individual and combined treatments is rarely investigated. Yet, understanding of these mechanisms would support the rational development of effective food preservation strategies with natural antimicrobial compounds. Therefore, the general goal of this work was to generate insight in the antimicrobial mechanism of two much studied natural antimicrobial compounds, *trans*-cinnamaldehyde (t-CIN) and allyl isothiocyanate (AIT), using a genetic approach. *Listeria monocytogenes* was used as a model organism for this work, because of its importance as a food pathogen in fresh, refrigerated and minimally processed food.

Because bacterial membranes are hypothesized to play a key role in tolerance and adaptation to t-CIN, the current knowledge on stress response and adaptation to membrane perturbing antimicrobial compounds in *L. monocytogenes* and closely related *Firmicutes* have been reviewed in **chapter 1**.

To identify cellular targets of t-CIN and pathways necessary for normal tolerance to t-CIN and AIT, we constructed a whole-genome random *Himar1* transposon mutant library in *L. monocytogenes* Scott A (**chapter 2**). Screening of this library yielded several mutants with increased sensitivity for t-CIN, AIT or both. The growth-inhibitory effect of t-CIN on the wild-

type (WT) strain and the selected mutants was also further characterized and consisted mainly of an elongation of the lag phase. The causes behind this were further investigated in detail on the WT in chapter 2.

One of the most sensitive isolated transposon mutants is disabled in the main production pathway of branched-chain fatty acids, which are the dominant fatty acids in *L. monocytogenes* and of major importance for growth at low temperature. The sensitivity of this mutant for t-CIN was studied in more detail in **chapter 3** by fatty acid analyses, growth assays at 10 °C, and inactivation assays at lethal t-CIN concentrations. The fatty acid composition appeared to be very aberrant compared to WT. Because the results show that membrane composition critically influences t-CIN sensitivity, we also investigated whether cells adapt their membrane fatty acid composition in response to t-CIN exposure.

While studying the *ilvE* mutant, phenotypical revertants were unintentionally found. Since they still carried the intact *ilvE::Himar1* allele, we anticipated that they could potentially improve our understanding of the impact of the IlvE knockout on the cellular metabolism, but also of the mode of action of t-CIN and of the cellular adaptation mechanisms to t-CIN. The analysis of revertants is described in **chapter 4**. A more systematic experiment was set up to investigate the reversion frequency and the spectrum of reversion mutations. Several reversion mutations were identified by whole-genome sequence analysis. Together with the results of some additional targeted experiments, hypotheses were formulated to explain the link between the revertant mutations and t-CIN tolerance.

Chapter 5 zooms in on two other t-CIN sensitive mutants isolated from the *L. monocytogenes* transposon knockout mutant library. One of these has an inactivated PrkC serine/threonine kinase, the other has an inactivated YvcK protein, which is one of the (many) phosphorylation targets of PrkC. The interplay between both proteins and their role in t-CIN tolerance is analyzed. Finally, the most important outcomes and further perspectives of this thesis are discussed in **chapter 6**.

Chapter 2

Isolation and characterization of *trans*-cinnamaldehyde and allyl isothiocyanate sensitive transposon mutants of *Listeria monocytogenes* Scott A

2.1. Introduction

As discussed in chapter 1, antimicrobial compounds from plant essential oils have been investigated intensively in the last ten to fifteen years as potential natural food preservatives. Most studies on essential oils and their active compounds investigate the applicability and the antimicrobial activity against a range of food spoilage bacteria and pathogens in different foods, often in combination with other antimicrobials or processing and preservation methods. The contribution of these studies to the knowledge on the mode of action of these compounds is only limited. The few studies on the antimicrobial mode of action of *trans*-cinnamaldehyde (t-CIN) and allyl isothiocyanate (AIT) discussed in chapter 1, indicate that t-CIN and AIT affect many essential bacterial processes and pathways, but most of these effects are likely to be secondary, and it is not possible to identify the primary target(s) of t-CIN based

on these studies. AIT and t-CIN were chosen as model compounds to study the mode of action in *L. monocytogenes*, because both compounds show promising food application perspectives. The combination of sub-MIC concentrations of both compounds with a high pressure treatment lead to synergistic bacterial inactivation [35], but also combinations with other natural antimicrobials, such as carvacrol and nisin, can lead to synergistic bacterial inactivation [38,39].

A different, complementary approach that has not yet been applied to study t-CIN or AIT, but that may provide additional insights in their mode of action, is the use of genetic analysis to identify genes that affect bacterial t-CIN or AIT sensitivity. Therefore, we have constructed and screened a transposon mutant library in *L. monocytogenes* both for sensitive and resistant mutants for t-CIN and AIT. This chapter describes the isolation and identification of these mutants. In addition, two moderately sensitive mutants (*5'yggS::Himar1* and *5'asnB::Himar1*) are characterized in more detail. The characterization of some other mutants is reported in chapter 3 and 5. Since the major effect of t-CIN is an extension of the lag phase, possible causes of this effect were investigated.

2.2. Materials and methods

2.2.1. Bacterial strains, plasmids and growth conditions

L. monocytogenes Scott A, obtained from the International Life Sciences Institute North America (ILSI NA) *L. monocytogenes* strains collection [120], was used in this work as the wild type (WT) strain. Cultures of both the WT and transposon mutants were routinely grown at 30 °C in Brain Heart Infusion (BHI, Oxoid, Hampshire, UK) broth or on BHI agar (BHI with 15 g/l agar). *E. coli* S17-1 λ*pir* [121] was used as a donor for conjugational plasmid transfer to *L. monocytogenes* Scott A, and was grown in lysogeny broth (LB; 10 g/l tryptone, 5 g/l yeast extract, 5 g/l NaCl) or on LB agar (LB with 15 g/l agar) at 37 °C. Growth media were supplemented with the following antibiotics: chloramphenicol (Cm, 50 µg/ml) for *E. coli* DH5α-pMC38, erythromycin (Em, 50 µg/ml) for *L. monocytogenes* transposon mutants, kanamycin (Km, 50 µg/ml) for *E. coli* S17-1 λ*pir*-pIMK2 and the combination of Em (50 µg/ml) and Km (50 µg/ml) for genetically complemented *L. monocytogenes* transposon mutants. For long-term storage at -80 °C, stationary-phase bacterial cultures were supplemented with 25% glycerol.

Table 2.1. Strains and plasmids used in this chapter

Strain or plasmid	Relevant features	Reference
Strains		
L. monocytogenes		
Scott A	Serovar 4b clinical isolate from the 1983 listeriosis outbreak in Massachusetts	[122]
E. coli		
S17-1 λ*pir*	*pro thi recA hsdR⁻hsdM⁺*RP4: 2-Tc:Mu:Km Tn7 λ*pir*	[121]
DH5-α	F⁻ *endA1 hsdR17* (r_k^-, m_k^+) *supE44 thi⁻1* λ⁻ *recA1 gyrA96 relA1 deoR Δ*(*lacZYA-argF*)U169 Φ80d *lacZ*ΔM15	[123]
Plasmids		
pMC38	Temperature-sensitive *mariner* transposon delivery vector with *B. subtilis* σ^A-dependent promoter P_{mrgA}, with no sequence similarity to the *Listeria* genome, Em^R Km^R	[124]
pIMK2	Site-specific listerial integrative vector, Phelp promoter for constitutive overexpression, 6.2 kb, Km^R	[125]

2.2.2. Mutant library construction via random transposon mutagenesis

Random *Himar1* transposon mutants of *L. monocytogenes* Scott A were generated using the temperature-sensitive pMC38 delivery plasmid as described by Cao, Bitar and Marquis (2007) [124]. After temperature shift, Em-resistant colonies were isolated, purified and stored as BHI cultures in 96-well plates at -80 °C. In about 25 independent experiments, a random transposon mutant library of 7680 mutants, corresponding to a predicted gene coverage of >99% was created and used for screening for t-CIN and AIT sensitivity. Randomness of transposition was verified on about 15 colonies per experiment using a Y-linker PCR protocol (section 2.2.5).

2.2.3. Screening for t-CIN an AIT sensitivity

Stationary microplate cultures of the mutants were diluted a 1000-fold to a final concentration of approximately 10^6 cfu/ml and grown at 30 °C in 200 µL BHI with 4 mM of *trans*-cinnamaldehyde (t-CIN, (2*E*)-3-phenylprop-2-enal, 99%, Acros Organics, New Jersey, USA) or 6 mM of allyl isothiocyanate (AIT, 3-Isothiocyanato-1-propene, 95%, Sigma Aldrich, Steinheim, Germany) in 96-well microplates sealed with an oxygen impermeable cover foil (EASYseal™, Greiner Bio-One, Frickenhausen, Germany). t-CIN and AIT sensitivity was scored based on optical density (OD) measurement at 600 nm after approximately 45 h for t-CIN and after approximately 30 h for AIT. These were the times needed for the WT strain to reach stationary phase (OD ~ 0.6). The incubation time with AIT was selected to be shorter because of its limited chemical stability in aqueous solutions in function of temperature and pH [126].

Mutants were considered t-CIN or AIT sensitive when the OD was below 0.100 after 45 h or 30 h respectively. Sensitivity of selected mutants was subsequently confirmed by growth assays with three independent cultures (section 2.2.4).

2.2.4. Determination of kinetic growth parameters

Growth experiments were conducted in 200 µL BHI cultures in 96-well microplates covered with an oxygen-impermeable cover foil in an automated microplate reader (Multiskan Ascent, Thermo Labsystems, Helsinki, Finland) at 30 °C. Every 15 minutes the plates were shaken at 960 rpm and the OD_{630nm} was measured. The inoculum was prepared by washing stationary overnight cultures once with potassium phosphate buffer (PPB, 10 mM, pH 7.0), resuspending the cells in fresh BHI medium and further diluting them to a start cell concentration of about 10^6 cfu/ml in BHI broth or BHI broth with t-CIN or AIT. Lag phase duration (λ), maximum growth rate (μ_{max}) and maximal OD_{max} value at stationary phase (OD_{max}) were determined by fitting the data according to the model of Baranyi and Roberts [127], using the Excel add-in package DMFit (Quadram Institute Bioscience, Norwich, United Kingdom).

2.2.5. Mutant identification

In mutants with confirmed t-CIN or AIT sensitivity, the transposon insertion sites were identified by PCR amplification of the flanking DNA sequences with the Y-linker protocol of Kwon and Ricke (2000) [128] using primers Y-linker and Marq269 and subsequent sequence analysis with primer Marq269 (primer sequences specified in Table 2.2).

Table 2.2. Oligonucleotide primers used in this chapter

Primer	Sequence (5' – 3')[a]	Reference
asnB_NcoI	GCATCCATGGGATGTGGATTTGTAGGATGCGTAC	This chapter
asnB_SalI	CACTGTCGACTTATTTTCCAAAATCGTATTTATCTGC	This chapter
yggS_NcoI	ACATCCATGGGAACAAAACAAGCTAATTTACAAAAAG	This chapter
yggS_SalI	CACTGTCGACTTACACCTCCATATTATCGTCAC	This chapter
sepF_NcoI	GCATCCATGGGACTATCGAATAAATTTAAGTCATTC	This chapter
yggT_SalI	CACTGTCGACTTAAAATAGCATTGGAATGACATAC	This chapter
pIMK_REV	CCTATCACCTCAAATGGTTCG	This chapter
pIMK_FW	GAGTCAGTGAGCGAGGAAGC	This chapter
NC16	GTCAAAACATACGCTCTTATC	[129]
Ylinker	CTGCTCGAATTCAAGCTTCT	[128]
Marq269	GCTCTGATAAATATGAACATGATGAGTGAT	[124]

[a] Restriction sites are underlined: NcoI (CCATGG) and SalI (GTCGAC)

2.2.6. Genetic complementation

Genetic complementation was performed using the pIMK2 integration plasmid with a strong constitutive promotor [125]. The WT genes were amplified using gene specific primers mentioned in Table 2.2, and cloned as an NcoI - SalI fragment into pIMK2, which was first linearized with the same restriction enzymes. The resulting plasmid was conjugated from *E. coli* S17-1 λ*pir* to *L. monocytogenes Himar1* mutants, using selection for Km (pIMK2 marker) and Em (transposon marker). The pIMK2 plasmid does not replicate in *L. monocytogenes*, but is designed to integrate specifically in the $tRNA^{Arg}$ gene, which is the unique integration site of the phage PSA in the genome of *L. monocytogenes* Scott A [125,129]. Integration in this site was confirmed via PCR using the gene specific primer provided with the NcoI restriction site and primer NC16. The latter anneals just outside the phage integration site [129]. Additionally, the presence of the intact WT copy in the integrants was confirmed via PCR and Sanger sequencing analysis (Macrogen Europe, Amsterdam, Netherlands) using primers pIMK_FW and pIMK_REV, which anneal at both sides just outside the cloning site of the plasmid (Table 2.2). Finally, complemented transposon mutants were phenotypically analyzed by growth assays (section 2.2.4).

2.2.7. Headspace - solid phase micro-extraction - gas chromatography - mass spectrometry (HS-SPME-GC-MS) analysis

For quantification of t-CIN in bacterial cultures, cells were eliminated from the samples by passage over a 0.2 µm cellulose acetate syringe filter (VWR International, Radnor, USA) and the filtrate was frozen with liquid nitrogen and stored at -80 °C. Four hours before HS-SPME-GC-MS analysis, samples were thawed at 4 °C. One ml of the thawed sample was mixed with 1 ml saturated NaCl solution in a 10 ml amber glass vial. The vials were tightly closed using screw-caps with a PTFE/silicon septum seal and 100 µl 0.01 mM ethyl benzoate (≥99%, Sigma Aldrich, Steinheim, Germany) was added to each sample as an internal standard. Headspace fingerprinting was conducted on a gas chromatography system (6890N, Agilent Technologies, Diegem, Belgium), coupled to a mass selective detector (5973N, Agilent Technologies, Diegem, Belgium) and equipped with a CombiPAL auto-sampler (CTC analytics, Zwingen, Switzerland). Volatiles were directly extracted from the headspace with a HS-SPME fiber coated with 30/50 µm divinylbenzene/carboxen/polydimethylsiloxane (DVB/CAR/PDMS) (StableFlex, Supelco, Bellefonte, PA, USA) at 40 °C during 10 min. The SPME fiber was then inserted into the heated (230 °C) GC-injection port for 2 min to thermally desorb the volatiles.

Chromatographic separation was carried out on a HP-5MS capillary column (30 m x 0.25 mm i.d., 0.25 µm film thickness, Agilent Technologies J&W, Santa Clara, CA, USA) having a 5%-phenyl-methylpolysiloxane stationary phase and using a constant helium flow of 1.5 ml/min. The oven temperature was initially 40 °C for 2 min, then ramped to 160 °C at 14 °C/min, to 300 °C at 70 °C/min and held at 300 °C for 2 min before cooling back to 40 °C. Mass spectra were obtained in electron ionization mode at 70 eV with a scanning range of 35 to 400 m/z and a scanning speed of 3.8 scans/s. The selected ions monitored were *m/*z 130.9 (quantifier), 103 and 77 (both qualifier) for t-CIN and *m/*z 104.9 (quantifier) and 77 (qualifier) for ethyl benzoate. MS ion source and quadrupole temperatures were 230 °C and 260 °C, respectively. The experiment was performed for three independent WT cultures (biological replicates). Each sample was analyzed twice (technical repetitions). HS-SPME-GC-MS analyses were performed in cooperation with dr. Biniam T. Kebede at the Lab of Food Technology (KU Leuven).

2.2.8. Selection of t-CIN resistant mutants

The 7680 transposon mutants (section 2.2.2.) were cultured overnight at 30 °C to stationary phase and divided into eight pools of 960 mutants each. The pooled cultures were stored at -80 °C. Before use, the mutant pools were diluted to approximately 10^6 cfu/ml, 100 µl was spread on BHI agar with 3 mM t-CIN and plates were incubated at 30 °C until WT growth was visible. The WT strain and one hypersensitive mutant (*ilvE::Himar1*, see chapter 3) were used as reference and control strains respectively for these experiments. Additionally, six independent cultures, which had just passed through the temperature shift of the protocol for random transposon mutagenesis (section 2.2.2), were also screened for t-CIN resistance via the same protocol.

2.2.9. Statistical analysis

Means of the parameter estimates of the Baranyi and Roberts growth model (λ, μ_{max} and OD_{max} [127]) of each mutant were statistically compared with the WT parameters by a t-test for the experiments in section 2.3.2 and parameter estimates of WT, *asnB* and *yggS* mutants and complemented mutants were statistically compared by Tukey-Kramer HSD test with the JMP® Software (JMP, Version Pro12, SAS Institute Inc., Cary, USA), and considered significantly different when a *p*-value < 0.05 was obtained.

2.3. Results & discussion

2.3.1. Determination of screening conditions to isolate t-CIN or AIT sensitive mutants

Fig. 2.1. shows the growth curves and growth parameter estimates of the WT in increasing amounts of t-CIN (Fig. 2.1a) or AIT (Fig. 2.1b). The effect of both compounds on the WT growth is largely the same, more specifically an elongation of the lag phase (λ), a decrease of the maximum specific growth (μ_{max}) rate and a lower maximum OD value (OD_{max}). These growth parameter estimates are summarized in Fig. 2.1c. Note that the growth curves for both compounds result from different experiments, explaining the difference in lag phase of the control cultures without CIN or AIT. Based on these data, a concentration of 4 mM t-CIN or 5 mM AIT was selected to be used in the growth based screening for sensitive transposon mutants. Mutants were considered t-CIN or AIT sensitive when the OD was below 0.100 after approximately 45 h or 30 h respectively, which is the time needed for the WT to reach stationary phase.

2.3.2. Screening and identification of t-CIN/AIT sensitive transposon mutants

The screening of 7680 transposon mutants resulted in ten mutants (hyper)sensitive to t-CIN and six mutants (hyper)sensitive to AIT, and five mutants were common in both groups. The site of transposon insertion was determined for each of the twelve mutants, and Table 2.3 lists the corresponding genes that were (likely to be) affected.

(a)

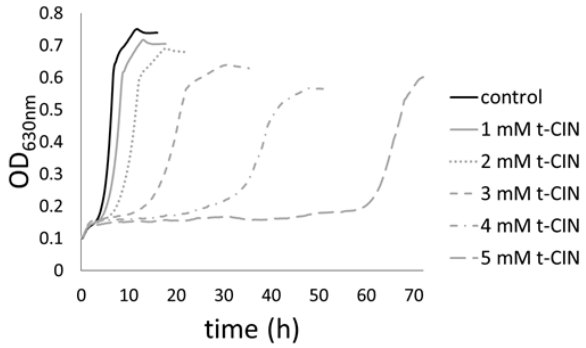

(b)

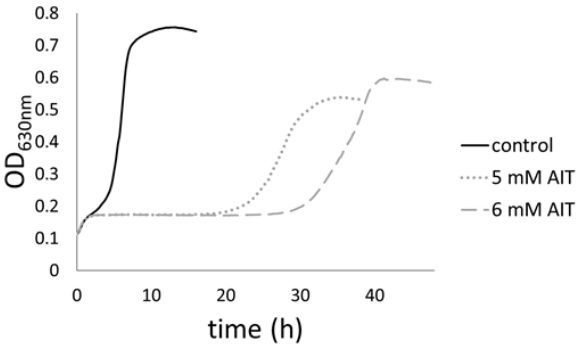

(c)

Sample	λ (h)	μ_{max} (1/h)	OD_{max}
Control (t-CIN)	4.4 ± 0.1	0.187 ± 0.002	0.754 ± 0.020
1 mM t-CIN	5.5 ± 0.2	0.137 ± 0.001	0.718 ± 0.021
2 mM t-CIN	7.9 ± 0.2	0.096 ± 0.001	0.693 ± 0.027
3 mM t-CIN	14.9 ± 0.6	0.054 ± 0.004	0.641 ± 0.018
4 mM t-CIN	31.2 ± 0.2	0.033 ± 0.002	0.568 ± 0.015
5 mM t-CIN	61.8 ± 0.2	0.053 ± 0.001	0.587 ± 0.014
Control (AIT)	4.3 ± 0.2	0.198 ± 0.009	0.741 ± 0.009
5 mM AIT	23.3 ± 1.4	0.049 ± 0.006	0.539 ± 0.039
6 mM AIT	32.9 ± 2.7	0.070 ± 0.005	0.602 ± 0.013

Fig. 2.1. Growth curves of *L. monocytogenes* Scott A in BHI broth (control) and BHI broth with increasing concentrations of t-CIN (a) or AIT (b). All curves are the average of three independent cultures. Standard deviations have been omitted for clarity. (c) Lag phases (λ), growth rates (μ_{max}) and maximum optical densities (OD_{max}) corresponding to the curves in (a) and (b). Values are means ± standard deviation.

Table 2.3. Genes with transposon insertions in mutants of *L. monocytogenes* Scott A with increased sensitivity for t-CIN and/or AIT picked up from the screenings

Gene	Description	t-CIN sensitive	AIT sensitive
5'yggS	UPF001 protein YggS	X	
sepF	FtsZ-interacting protein related to cell division	X	
prkC	Serine/threonine protein kinase	X	X
greA	Transcription elongation factor	X	
oppA	Oligopeptide ABC transporter, periplasmic oligopeptide-binding protein OppA	X	
ilvE	Branched-chain amino acid aminotransferase	X	X
bckd-E1α	Branched-chain α-keto acid dehydrogenase, E1 component, α-subunit	X	X
5'asnB	Asparagine synthetase (glutamine hydrolyzing)	X	
phoH	Phosphate starvation-inducible protein, predicted ATPase		X
yvcK (2x, different insertion sites)	Hypothetical protein, unknown function	X	X
gdpP	Cyclic-di-AMP phosphodiesterase	X	X

5' in front of gene name indicates that the transposon is inserted in the 5' intergenic upstream region of the start codon of the gene

For further confirmation of the sensitivity of the selected mutants, OD-based growth assays were performed of three independent cultures. AIT-sensitivity was also assessed for all mutants detected in the t-CIN screening and vice versa. Analysis of kinetic parameters (Table 2.4 and 2.5) from the growth curves of all mutants in t-CIN and AIT (Supplementary material S1) shows that, with exception of *oppA*, all the mutants have an extended lag phase in t-CIN compared to the WT, and with exception of the *greA*, *5'yggS* and *oppA* mutants, all mutants have an extended lag phase in AIT compared to WT. The μ_{max} and OD_{max} in many cases do not differ significantly from WT. The *oppA* mutant shows the opposite pattern, with a strongly decreased μ_{max} (Table 2.5) but no difference in lag phase. Although standard deviations of the growth parameter estimates for independent replicate cultures of all strains were very small within one experiment, there was much more variation when the experiment was repeated on a different day. Therefore, Scott A was again included in each experiment as a reference strain. A more detailed characterization of selected mutants (underlined in Table 2.4 and 2.5)

is discussed in the next chapters of this dissertation. As can be seen from the growth parameters in Table 2.4 and 2.5, some of the selected mutants also showed growth defects in BHI medium without antimicrobials. Nevertheless, they were retained in the selection because their growth is much more affected by the compounds than is the case for the WT strain.

Table 2.4. Lag phases λ (h) of t-CIN/AIT sensitive mutants compared to the WT

Mutant	**BHI**	**4 mM t-CIN**	**6 mM AIT**
Scott A	4.1 ± 0.3	38.8 ± 0.6	24.4 ± 2.1
5'yggS::Himar1	4.4 ± 0.1	63.1 ± 1.1*	24.6 ± 2.3
greA::Himar1	4.4 ± 0.6	55.8 ± 3.2*	26.9 ± 0.5
oppA::Himar1	3.6 ± 0.3	39.4 ± 1.0	26.8 ± 1.0
ilvE::Himar1	7.6 ± 0.1*	>72*	36.6 ± 2.0*
bckd-E1α::Himar1	10.4 ± 0.1*	65.2 ± 2.1*	34.9 ± 1.6*
5'asnB::Himar1	4.1 ± 0.2	62.5 ± 2.1*	28.2 ± 2.0*
phoH::Himar1	5.0 ± 0.2*	45.2 ± 2.6*	35.5 ± 2.2*
yvcK::Himar1	4.6 ± 0.3*	>72*	35.5 ± 0.2*
gdpP::Himar1	6.9 ± 0.2*	64.9 ± 0.2*	29.1 ± 2.6*
[a]Scott A	5.4 ± 0.1	21.6 ± 0.7	32.4 ± 3.2
[a]*prkC::Himar1*	5.9 ± 0.3*	47.1 ± 1.4*	42.2 ± 3.3*
[a]Scott A	4.4 ± 0.0	37.3 ± 2.2	23.8 ± 0.7
[a]*sepF::Himar1*	4.6 ± 0.1*	68.9 ± 2.6*	24.6 ± 1.2

[a]data for all mutants were obtained in a single experiment for each antimicrobial compound, with exception of the *prkC* and *sepF* mutant of which the sensitivity for both compounds was assessed in separate experiments
* superscript indicates a significant difference ($p < 0.05$) with WT Scott A
Underlined mutants were retained in a smaller selection of mutants to be characterized in more detail further in this work

Table 2.5. Max growth rates (μ_{max}) and max optical densities (OD_{max}) of t-CIN/AIT sensitive mutants compared to the WT

Mutant	BHI		4 mM t-CIN		6 mM AIT	
	μ_{max} (1/h)	**OD_{max}**	**μ_{max} (1/h)**	**OD_{max}**	**μ_{max} (1/h)**	**OD_{max}**
Scott A	0.185 ± 0.009	0.686 ± 0.011	0.052 ± 0.006	0.553 ± 0.028	0.089 ± 0.002	0.560 ± 0.003
5'yggS::Himar1	0.182 ± 0.013	0.665 ± 0.027	0.055 ± 0.015	0.517 ± 0.055	0.085 ± 0.008	0.557 ± 0.021
greA::Himar1	0.174 ± 0.012	0.648 ± 0.033*	0.043 ± 0.014	0.520 ± 0.040	0.079 ± 0.002*	0.556 ± 0.015
oppA::Himar1	0.069 ± 0.003*	0.576 ± 0.009*	0.005 ± 0.000*	0.232 ± 0.009*	0.066 ± 0.001*	0.522 ± 0.018*
ilvE::Himar1	0.083 ± 0.005*	0.490 ± 0.004*	/	/	0.049 ± 0.000*	0.448 ± 0.006*
bckd-E1α::Himar1	0.077 ± 0.005*	0.334 ± 0.011*	0.046 ± 0.006	0.355 ± 0.050*	0.068 ± 0.005*	0.400 ± 0.010*
5'asnB::Himar1	0.152 ± 0.001*	0.577 ± 0.005*	0.047± 0.025	0.443 ± 0.200	0.096 ± 0.004*	0.577 ± 0.004
phoH::Himar1	0.128 ± 0.001*	0.647 ± 0.005*	0.052 ± 0.003	0.531 ± 0.034	0.076 ± 0.003*	0.543 ± 0.003
yvcK::Himar1	0.183 ± 0.002	0.673 ± 0.018	/	/	0.104 ± 0.002*	0.578 ± 0.001
gdpP::Himar1	0.085 ± 0.004*	0.516 ± 0.007*	/	/	0.041 ± 0.003*	0.452 ± 0.020*
[a]Scott A	0.187 ± 0.002	0.722 ± 0.008	0.059 ± 0.002	0.593 ± 0.014	0.060 ± 0.011	0.598 ± 0.019
[a]*prkC::Himar1*	0.169 ± 0.002*	0.695 ± 0.016	0.059 ± 0.005	0.582 ± 0.011	0.069 ± 0.009	0.518 ± 0.049
[a]Scott A	0.188 ± 0.000	0.697 ± 0.008	0.047 ± 0.002	0.541 ± 0.008	0.081 ± 0.004	0.578 ± 0.015
[a]*sepF::Himar1*	0.187 ± 0.002	0.730 ± 0.003*	/	/	0.076 ± 0.002	0.570 ± 0.006

[a, b] data for all mutants were obtained in a single experiment for each antimicrobial compound, with exception of the *prkC* and *sepF* mutant of which the sensitivity for both compounds was assessed in separate experiments; * superscript indicates a significant difference ($p < 0.05$) with WT Scott A; Underlined mutants were retained in a smaller selection of mutants to be characterized in more detail further in this work; "/" means that this growth parameter could not be determined because cultures did not yet reach stationary phase

Cross-testing of all the mutants revealed that some of the mutants picked up in one screen were also hypersensitive to the other compound, although they had not been picked up in that screen. More specifically, the *phoH* mutant was picked up in the AIT screen, but its lag phase in t-CIN was also significantly longer than that of the WT. The same applies for the *asnB* mutant which was isolated in the t-CIN screening, but which also has a significantly longer lag phase than the WT in AIT. In conclusion, it can be stated that the majority of the t-CIN-sensitive mutants are also AIT-sensitive and vice versa. Common physicochemical properties, an electrophilic nature and the similar reactivity towards (cellular) nucleophiles via Michael-type addition reactions can explain these observations. In general, both the WT and the mutants show a significant extension of the lag phase and a significant reduction of μ_{max} and OD_{max} in the presence of t-CIN and AIT (Table 2.4 and 2.5). Similar effects on the growth parameters were also observed by Siroli *et al*. (2015) for *L. monocytogenes* Scott A in BHI supplemented with sub-lethal concentrations of *trans*-2-hexenal and citral, two other small hydrophobic α, β-unsaturated aldehydes like t-CIN [113].

To get a better understanding on the physiological impact of the knocked out gene and the relationship between the observed sensitivity and the genes, a smaller selection of mutants was made based on the sensitivity of the mutants and gene or pathway specificity. These mutants are underlined in Table 2.4 and 2.5. As a first step in the characterization process, mutants were complemented either via constitutive overexpression or induced expression with the intact WT genes. The mutants with a transposon insertion in *5'yggS* and *5'asnB* will be discussed in the remainder of this chapter. Characterization of *ilvE* and *bckd-E1α* mutants will be discussed in chapter 3, *yvcK* and *prkC* mutants in chapter 5.

2.3.3. Characterization of t-CIN/AIT sensitivity

2.3.3.1. *5'yggS::Himar1*

According to the genomic organization represented in Fig. 2.2a, it cannot be excluded that the transposon insertion upstream of *yggS* also disabled the downstream genes *sepF*, *yggT* and *ylmH*. Especially the ORFs of the genes in the cluster *yygS-sepF-yggT* are very close together, with only four base pairs in between *yggS* and *sepF* and twenty-three base pairs in between *sepF* and *yggT*. Although this cannot be concluded with certainty, this short intergenic distance suggests that these genes are part of one operon. To identify which gene(s) were linked to the t-CIN sensitive phenotype, complementation experiments were performed. The

5'yggS mutant was complemented with overexpressed *yggS* (Fig. 2.3, *5'yggS::Himar1*/pIMK2-*yggS*) and *sepF-yggT* (Fig. 2.4, *5'yggS::Himar1*/pIMK2-*sepF-yggT*).

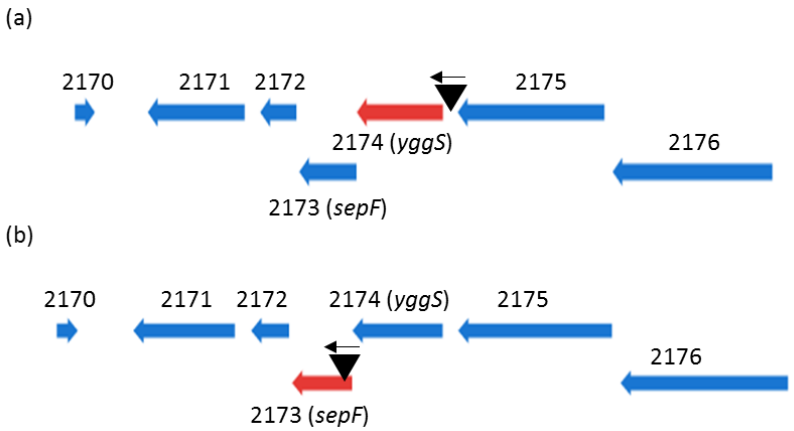

Fig. 2.2. Organization of *yggS-sepF-yggT* gene cluster in *L. monocytogenes* Scott A *yggS::Himar1* (a) and *sepF::Himar1* (b). Genes with transposon inserts are highlighted in red. The *Himar1* transposon is shown as a black triangle and the black arrow indicates the orientation of the erythromycin resistance gene (*ermC*) in the transposon. In the PATRIC database [130] the ORFs are annotated as hypothetical protein (2170), putative RNA-binding protein YlmH (2171), cell division integral membrane protein YggT (2172), FtsZ-interacting protein related to cell division SepF (2173), UPF001 protein YggS (2174), cell division protein FtsZ (EC3.4.24.-) (2175) and cell division protein FtsA (2176).

Fig. 2.3. shows the growth of the WT, *5'yggS* mutant and complemented mutant *5'yggS::Himar1*/pIMK2-*yggS* and the corresponding growth parameter estimates. The data confirm the results from the screening, i.e. that the *5'yggS* mutant is more sensitive than the WT to t-CIN but not to AIT ($p < 0.05$). The hypersensitivity to t-CIN is mainly reflected by an extended lag phase, but also the μ_{max} of the mutant is significantly smaller, which was not the case in the previous experiment (Table 2.5). Complementation of the mutant with overexpressed WT *yggS* reduced the lag phase of the mutant, but did not fully restore it to WT level.

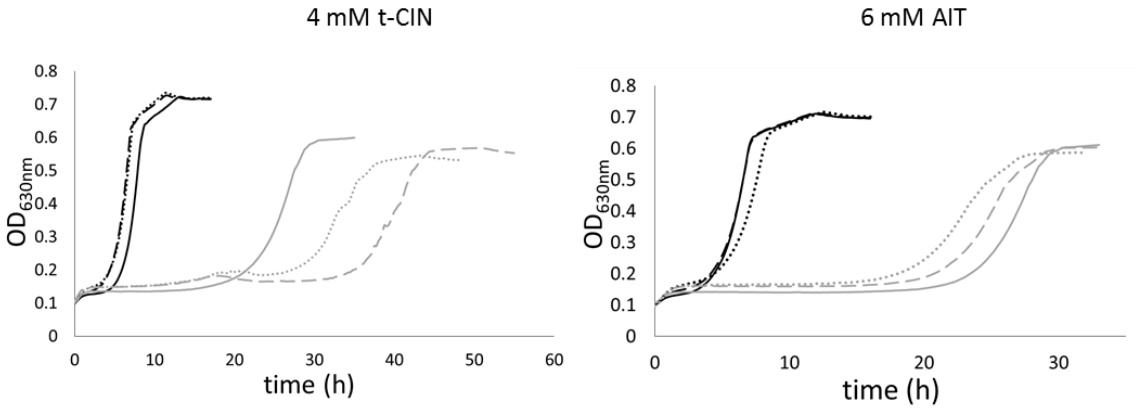

Strain		λ (h)	μmax (1/h)	ODmax	λ (h)	μmax (1/h)	ODmax
			BHI			BHI	
Scott A	——	5.8 ± 0.3^{D}	0.178 ± 0.000^{A}	0.725 ± 0.011^{A}	4.5 ± 0.0^{C}	0.174 ± 0.008^{A}	0.711 ± 0.009^{A}
5'yggS::Himar1	— -	4.5 ± 0.0^{E}	0.176 ± 0.005^{A}	0.727 ± 0.003^{A}	4.4 ± 0.2^{C}	0.166 ± 0.004^{A}	0.714 ± 0.007^{A}
5'yggS::Himar1/ pIMK2-*yggS*	.....	4.6 ± 0.1^{D,E}	0.176 ± 0.002^{A}	0.735 ± 0.010^{A}	5.1 ± 0.2^{C}	0.143 ± 0.002^{B}	0.717 ± 0.005^{A}
			4 mM t-CIN			6 mM AIT	
Scott A	——	21.7 ± 0.7^{C}	0.061 ± 0.002^{B}	0.593 ± 0.014^{B}	23.6 ± 0.7^{A}	0.079 ± 0.007^{C}	0.592 ± 0.035^{B}
5'yggS::Himar1	— -	35.5 ± 0.9^{A}	0.049 ± 0.003^{C}	0.566 ± 0.013^{B,C}	21.8 ± 1.7^{A,B}	0.073 ± 0.002^{C}	0.593 ± 0.022^{B}
5'yggS::Himar1/ pIMK2-*yggS*	.....	28.1 ± 0.2^{B}	0.040 ± 0.001^{D}	0.545 ± 0.021^{C}	19.6 ± 2.0^{B}	0.068 ± 0.005^{C}	0.582 ± 0.028^{B}

Fig. 2.3. Growth curves of *L. monocytogenes* Scott A, its *yggS::Himar1* mutant and the genetically complemented mutant *yggS::Himar1*/pIMK2-*yggS* in BHI broth (black lines) and BHI broth with 4 mM t-CIN or 6 mM AIT (grey lines). All curves are the average of three independent cultures. Standard deviations have been omitted for clarity. Lag phases (λ), maximum growth rates (μ_{max}) and maximum optical densities (OD_{max}) are listed in table below the corresponding growth curves. Values are mean ± standard deviation. ^{A,B,C,D}Different superscripts within one column indicate significant differences ($p < 0.05$).

Interestingly, a mutant with a transposon insert in *sepF* (Fig. 2.2b) was also picked up in the screening for t-CIN sensitivity, and this suggested that knockout of *sepF* and/or *yggT* was responsible for the t-CIN sensitivity rather than *yggS*. To investigate this hypothesis, the *5'yggS* mutant was also complemented with *sepF-yggT,* and this again partially restored the phenotype of the mutant (Fig. 2.4). No PCR amplicon could be obtained of the complete putative operon *yggS-sepF-yggT* and therefore, cloning for complementation was unsuccessful. No further attempts were performed to complement the mutant with *sepF* or *yggT* separately since the combination of both did only partially restore the phenotype.

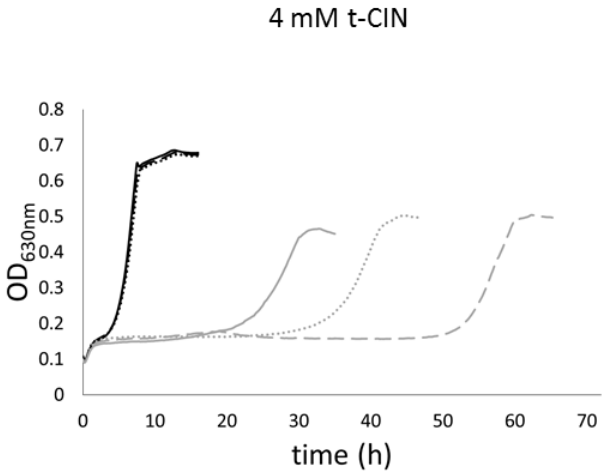

Strain		λ (h)	μ_{max} (1/h)	OD_{max}
			BHI	
Scott A	——	4.5 ± 0.0^{D}	0.165 ± 0.002^{A}	0.686 ± 0.002^{A}
5'yggS::Himar1	— -	4.6 ± 0.2^{D}	0.157 ± 0.007^{A}	0.679 ± 0.012^{A}
5'yggS::Himar1/pIMK2-*sepF-yggT*	·····	4.7 ± 0.2^{D}	0.151 ± 0.008^{A}	0.675 ± 0.007^{A}
			4 mM t-CIN	
Scott A	——	21.6 ± 0.2^{C}	0.032 ± 0.005^{C}	0.466 ± 0.008^{C}
5'yggS::Himar1	— -	53.3 ± 1.7^{A}	0.051 ± 0.004^{B}	0.508 ± 0.009^{B}
5'yggS::Himar1/ pIMK2-*sepF-yggT*	·····	33.4 ± 0.3^{B}	0.037 ± 0.005^{B,C}	0.504 ± 0.005^{B}

Fig. 2.4. Growth curves of *L. monocytogenes* Scott A, its *yggS::Himar1* mutant and the genetically complemented mutant *yggS::Himar1*/pIMK2-*sepF-yggT* in BHI and BHI with 4 mM t-CIN. All curves are the average of three independent cultures. Standard deviations have been omitted for clarity. Lag phases (λ), maximum growth rates (μ_{max}) and maximum optical densities (OD_{max}) are listed in table below the growth curves. Values are mean ± standard deviation. ^{A,B,C,D}Different superscripts within one column indicate significant differences ($p < 0.05$).

It would be interesting to understand from a mechanistic point of view why mutants in this gene cluster are hypersensitive to t-CIN and not to AIT, since both compounds are hydrophobic, electrophilic and thiol-reactive. Therefore, we discuss here what is known about the function of *yggS, sepF* and *yggT*.

YggS and its orthologs are highly conserved pyridoxal-5'-phosphate (PLP) binding proteins that are universally present in Bacteria, Eukaryotes and some Archaea, indicating that it serves an important function. In bacteria *yggS* clusters mostly with *proC* (pyrroline-5-carboxylate reductase), *ftsZ*, or genes involved in PLP metabolism such as *pdxK* and *pdxH* as well as genes

that encode PLP-dependent enzymes such as *glyA*. Its role has only been investigated in *E. coli*, where it is part of a polycistronic operon composed of five poorly characterized genes *yggS-yggT-yggU-yggV-yggW.* To date no functional correlations have been reported between YggS and the other gene products in the cluster. Ito *et al.* (2013) [131] found that a *ΔyggS* mutant excreted strongly increased amounts of valine (0.7 µM for the WT vs 110 µM for the mutant) and somewhat increased levels of α-aminobutyrate in the culture medium during stationary phase. Intracellular amino acid pools of stationary-phase cells confirmed accumulation of valine up to tenfold more than the WT and also leucine, histidine, phenylalanine, tyrosine and α-aminobutyrate were overproduced. Exponential-phase cells showed less accumulation of valine (~2.4-fold), but revealed accumulation of considerable amounts of α-aminobutyrate (~ 4-fold), α-ketobutyrate (~6-fold) and pyruvate (~1.3-fold). The *ΔyggS* mutant also exhibited a 1.3- to 2.6-fold increase in the levels of enzymes of the isoleucine and valine biosynthetic pathways, acetolactate synthase (AHAS), threonine deaminase (IlvA), transaminase B (IlvE) and transaminase C (AvtA). IlvA converts threonine to α-ketobutyrate, which can then undergo a reductive amination catalyzed by AvtA to form α-aminobutyrate. However, α- ketobutyrate is also converted by AHAS to α-ketomethylvalerate. IlvE bidirectionally converts both α-ketoacids to the corresponding branched-chain amino acids (chapter 3, section 3.3.2 Fig. 3.3). Complementation with WT *yggS* fully restored the mutant phenotypes. Therefore, YggS seems to play a role in the amino acid metabolism of *E. coli*, in particular in that of valine. Even though YggS is a highly conserved protein, the genomic organization and location of *yggS* in the chromosome and the (branched-chain) amino acid metabolism differs for *E. coli* and *L. monocytogenes*. It is therefore difficult to hypothesize the impact of a *yggS* mutation on the amino acid metabolism in *L. monocytogenes* based on a single study in *E. coli*.

YggT, which is also part of the putative operon in *L. monocytogenes* Scott A, is an integral membrane protein without a clearly defined function. Ito *et al.* (2009) [132] found that introduction of plasmid-borne *yggT* into an *E. coli* mutant, lacking three major K^+ uptake systems and thus requiring exogenous K^+, restored cell growth at high osmotic pressure.

The function of SepF is much better understood than that of YggS and YggT. SepF is an FtsZ-interacting protein conserved in Gram-positive bacteria. It was first characterized in *Bacillus subtilis* by Hamoen *et al.* (2006) [133] and designated SepF for its role in septum development.

Cell division requires the synchronized action of multimeric enzyme complexes, each with a specific function in Z-ring formation, divisome assembly and septal peptidoglycan synthesis. A key step in bacterial cell division is the polymerization of the tubulin homologue FtsZ into a circular structure at mid-cell, i.e. the Z-ring. The Z-ring serves as a scaffold for all other cell division proteins [134]. Several proteins like FtsA, which binds FtsZ and links the Z-ring to the membrane, and SepF support the assembly of the Z-ring. *B. subtilis sepF* mutants are viable but have a cell division defect, in which septa are formed slowly and with an abnormal morphology. Fluorescence microscopy showed that SepF accumulates at the site of cell division and this localization depends on the presence of FtsZ [133]. More detailed work of Gundogdu *et al.* (2011) [135] using electron microscopy of purified proteins revealed that SepF assembles into very large (~50 nm diameter) rings that are able to bundle FtsZ protofilaments into strikingly long and regular tubular structures. *sepF* mutants are no longer able to align FtsZ filaments *in vitro* and fail to support normal cell division *in vivo*. Therefore Gundogdu *et al.* (2011) proposed that SepF rings are required for the regular arrangement of FtsZ filaments and that absence of this ordered state could lead to the distorted septal morphologies observed in *sepF* mutants. However, via light microscopy we did not observe clear changes in cell shape in stationary-phase cells of our *L. monocytogenes 5'yggS* mutant (data not shown). Since mutations in *sepF* mainly cause distorted septal morphologies, a more detailed analysis via time-lapse microscopy, and using a strain producing fluorescent protein-labeled FtsZ would be useful to look for aberrant cell division or septum morphologies.

A possible link between cell division and t-CIN was reported by Kwon, Yu and Park (2003) [137], who observed filamentation by inhibition of daughter cell separation in *Bacillus cereus* induced by t-CIN. Based on this observation it was later on demonstrated that t-CIN binds with the *E. coli* cell division protein FtsZ *in vitro* with an affinity constant of 1.0 ± 0.2 μM^{-1} and inhibits its GTP-dependent polymerization in a concentration dependent manner. The half maximum inhibitory concentration IC_{50} of t-CIN for FtsZ was found to be 6.86 ± 2.2 µM, for FtsZ GTPase activity 5.81 ± 2.2 µM. t-CIN thus decreases the *in vitro* assembly reaction and bundling of FtsZ at concentrations lower than growth inhibitory concentrations which are in the mM range [117]. Although these *in vitro* experiments demonstrate interaction between t-CIN and FtsZ they should be interpreted carefully. Several phenylpropanoid compounds structurally related to t-CIN but lacking an aldehyde group (e.g. cinnamic acid, caffeic acid,

chlorogenic acid) similarly inhibited FtsZ polymerization under *in vitro* conditions [138]. It would be useful to confirm inhibition of FtsZ ring formation *in vivo*.

Since studies in other bacteria have shown that knockout of *sepF* or *yggS* have pleiotropic effects, affecting not only cell division but also core cellular metabolic pathways such as amino acid and α-ketoacid metabolism, the hypersensitivity of these mutants for t-CIN might be the result of this metabolic disturbance and does not necessarily indicate a specific interaction of t-CIN with components of the cell division machinery. For this reason and because only limited structural and functional information is available for YggS, both mutants were not further studied.

2.3.3.2. *5'asnB::Himar1*

Fig. 2.5 shows the organization of the *asnB* genomic environment and the location of the transposon insertion in the isolated t-CIN hypersensitive mutant. Since the gene downstream of *asnB* is transcribed in the opposite direction, the transposon insertion most probably only affects the expression of *asnB*.

Fig. 2.5. Organization of *asnB* region in *L. monocytogenes* Scott A. The *asnB* gene is highlighted in red and the *Himar1* transposon is shown as a black triangle. The black arrow indicates the orientation of the erythromycin resistance gene (*ermC*) in the transposon. In the PATRIC database [130] the ORFs are annotated as putative rRNA methylase YtqB (1792), asparagine synthetase B (glutamine-hydrolyzing) (EC 6.3.5.4) AsnB (1793) and S-adenosylmethionine synthetase (EC 2.5.1.6) (1794).

Analysis of the growth curves shown in Fig. 2.6 shows that the lag phase of the *asnB* mutant is 1.4-fold longer than the WT lag phase during growth in BHI broth with 4 mM t-CIN, while there is no significant difference in BHI broth. Complementation with overexpressed WT *asnB* (*5'asnB::Himar1*/pIMK2-*asnB*) made the lag phase even slightly shorter than that of the WT. The lag phase of the mutant in 6 mM AIT was not significantly longer in this experiment (p = 0.1678), although it was significantly longer in a previous experiment (Table 2.4). Nevertheless, overexpression of *asnB* in the mutant resulted in a significantly shorter lag phase compared to the WT. We therefore can conclude that the level of *asnB* expression affects sensitivity to both t-CIN and AIT. Generally, only small differences existed between the

μ_{max} and OD_{max} of the WT, *asnB* and complemented *asnB* mutant. Although these differences were statistically significant in some cases, they are unlikely to be biologically meaningful because they occurred only in the genetically complemented strain or could not be complemented if they were observed in the *asnB* mutant.

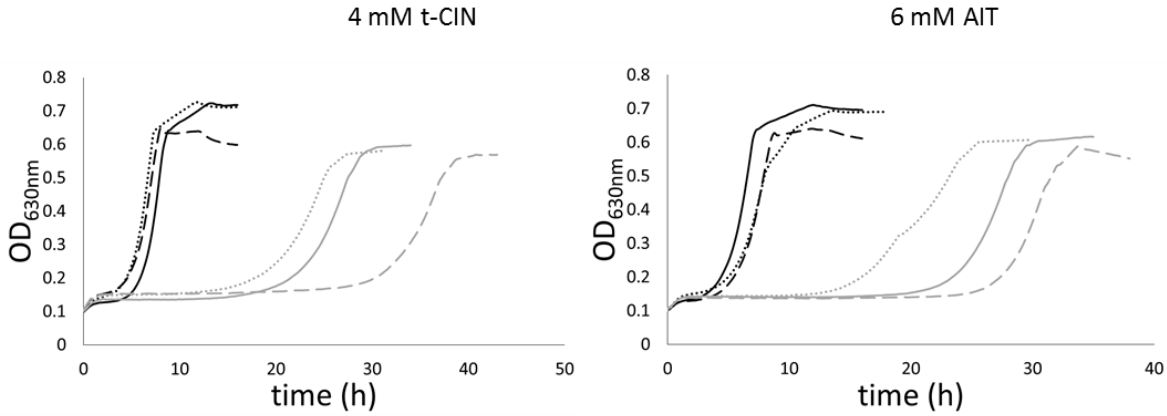

Strain		λ (h)	μ_{max} (1/h)	OD_{max}	λ (h)	μ_{max} (1/h)	OD_{max}
			BHI			**BHI**	
Scott A	——	5.8 ± 0.3^{D}	0.178 ± 0.000^{A}	0.725 ± 0.011^{A}	4.5 ± 0.0^{C}	0.174 ± 0.008^{A}	0.711 ± 0.009^{A}
5'asnB::Himar1	— -	5.0 ± 0.1^{D}	0.170 ± 0.005^{B}	0.648 ± 0.014^{B}	5.5 ± 0.1^{C}	0.157 ± 0.009^{A,B}	0.641 ± 0.026^{A,B}
5'asnB::Himar1/ pIMK2-*asnB*	.....	4.6 ± 0.1^{D}	0.176 ± 0.002^{A,B}	0.727 ± 0.019^{A}	5.5 ± 0.8^{C}	0.132 ± 0.030 ^{B,C}	0.698 ± 0.033^{A}
			4 mM t-CIN			**6 mM AIT**	
Scott A	——	21.7 ± 0.7^{B}	0.061 ± 0.002^{C}	0.593 ± 0.014^{C}	23.6 ± 0.7^{A}	0.079 ± 0.007^{D}	0.592 ± 0.035^{B}
5'asnB::Himar1	— -	31.0 ± 0.9^{A}	0.053 ± 0.002^{D}	0.570 ± 0.009^{C}	27.6 ± 1.3^{A}	0.091 ± 0.007^{C,D}	0.609 ± 0.010^{B}
5'asnB::Himar1/ pIMK2-*asnB*	.....	18.7 ± 0.3^{C}	0.053 ± 0.000^{D}	0.575 ± 0.013^{C}	17.2 ± 4.2^{B}	0.070 ± 0.016^{D}	0.603 ± 0.039^{B}

Fig. 2.6. Growth curves of *L. monocytogenes* Scott A, its *5'asnB::Himar1* mutant and the genetically complemented mutant *5'asnB::Himar1*/pIMK2-*asnB* in BHI broth and BHI broth with 4 mM t-CIN or 6 mM AIT. All curves are the average of three independent cultures. Standard deviations have been omitted for clarity. Lag phases (λ), maximum growth rates (μ_{max}) and maximum optical densities (OD_{max}) are listed in table below the corresponding growth curves. Values are mean ± standard deviation. ^{A,B,C,D}Different superscripts within one column indicate significant differences (*p*-value < 0.05).

Asparagine synthetase B (AsnB) reversibly catalyzes the hydrolysis of glutamine to glutamate according to the following biochemical reaction:

ATP + L-aspartate + L-glutamine + H_2O ⇔ AMP + diphosphate + L-asparagine + L-glutamate

There is no evident link between the enzyme AsnB itself, it substrates, products or biochemical activity and cellular stress caused by hydrophobic and thiol-reactive molecules like t-CIN and AIT. Yet, in a quantitative redox proteomics study on peroxynitrite stress in *E. coli*, Lindemann *et al.* (2013) [139] showed that AsnB (together with FrmA, MaeB and RidA) was one of four proteins that were consistently thiol-modified in cells treated with peroxynitrite. Peroxynitrite ($ONOO^-$) is a highly reactive species that decomposes in aqueous solutions mostly to reactive species $^{\cdot}OH$, $NO^{\cdot}_2$ and O_2^-, causing damage to lipids, DNA and proteins. Proteins are predominantly modified by direct reaction of peroxynitrite with cysteine, methionine and tryptophan or by reaction of the secondary free radicals from peroxynitrite causing tyrosine nitration [140]. After exposure of *E. coli* to peroxynitrite, tyrosine nitration was detected in a major part of *E. coli* proteins and thus seemed to be fairly unspecific, while mass-spectrometry based analysis revealed that only a small subset of the proteins was modified at cysteine residues *in vivo*. In proteins AsnB, FrmA and RidA the affected cysteine was highly conserved. Specifically for AsnB, Cys-2 was identified as the redox-sensitive cysteine. Cys-2 is located in the active site of the N-terminal region. The oxidative modification of Cys-2 blocks the ability of Cys-2 to act as the active-site nucleophile and thus prevents hydrolysis of glutamine to glutamate. Moreover, an *asnB* knockout mutant showed growth defects under peroxynitrite stress. Based on stoichiometric considerations, the authors excluded a role for the four thiol modified proteins as purely sacrificial sinks for peroxynitrite, because the abundance of these proteins in the cytoplasm is too low. It is still possible that these proteins work as a part of a detoxification system for peroxynitrite in a mechanism that re-reduces the cysteines, for example with the help of the glutathione system. In conclusion, although the reaction with virtually any thiol group within the cell with peroxynitrite should be thermodynamically highly favorable, Lindemann *et al.* (2013) demonstrated that most cysteines are not affected by peroxynitrite, showing that these reactions are instead kinetically controlled.

In *L. monocytogenes*, Cys-2 is also present in the active site of the N-terminal region of AsnB. In analogy to *E. coli* AsnB, Cys-2 of *L. monocytogenes* might also be consistently modified due

to reaction with peroxynitrite and potentially other thiol-reactive compounds such as t-CIN and AIT. This might explain the observed sensitivity, at least for t-CIN, of the *5'asnB::Himar1* mutant. Performing similar quantitative redox proteomics experiments with other thiol-reactive compounds and t-CIN and AIT would further clarify the role of Cys-2 in AsnB in a potential detoxification system.

2.3.4. Growth in the presence of t-CIN: an analysis of the WT lag phase

The detailed kinetic growth analyses of both the WT strain and several t-CIN sensitive mutants indicated that t-CIN and AIT primarily affected the lag phase. The μ_{max} and OD_{max} also decreased upon exposure to t-CIN and AIT, but reach lower limits of approximately 0.030-0.050 and 0.500 respectively. The most deviant growth parameter of t-CIN- and AIT-sensitive mutants compared to the WT, is the lag phase while the OD_{max} and μ_{max} mostly do not differ significantly and cannot be unambiguously linked to t-CIN or AIT sensitivity. Therefore, we conducted a more detailed analysis of the underlying causes of the lag phase extension during growth in t-CIN. Several possible explanations can be proposed for this extended lag phase and the subsequent resumption of growth for both WT and mutants: (i) the requirement of cellular adaptation before cells can grow in BHI broth with t-CIN, (ii) chemical or bacterial degradation of t-CIN followed by growth at a lower t-CIN concentration, (iii) the outgrowth of a small subpopulation of mutants with increased t-CIN resistance, or (iv) a combination of these factors.

For growth assays with t-CIN, stationary overnight cultures were diluted to a final cell concentration of approximately 10^6 cfu/ml at the start of the experiment. Since the detection limit of OD measurements at 630 nm is approximately 10^7 cfu/ml, initial inactivation before growth resumption cannot be detected via OD. Therefore, cell concentrations of three independent WT cultures growing in BHI broth with 4 mM t-CIN were determined by plate count (Fig. 2.7). The results showed stable cell numbers at different time points of the lag phase, indicating that no transient inactivation occurred upon exposure to t-CIN.

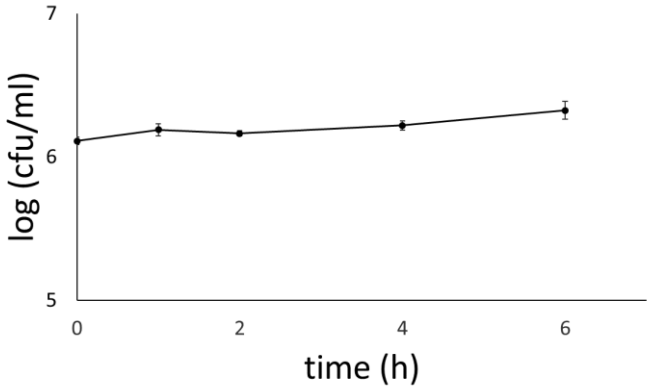

Fig. 2.7. WT growth in BHI broth with 4 mM t-CIN at 30 °C. All curves are the average of three independent cultures. Cell concentrations at each time point are average ± standard deviation.

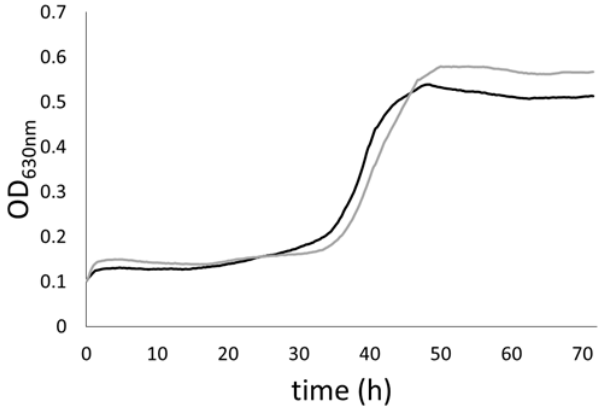

Strain		λ (h)	μ_{max} (1/h)	OD_{max}
Scott A + 4 mM t-CIN	___	36.8 ± 3.5^{A}	0.051 ± 0.002^{A}	0.588 ± 0.010^{A}
Scott A^{4R} + 4 mM t-CIN	___	32.4 ± 2.2^{A}	0.035 ± 0.006^{B}	0.528 ± 0.001^{A}

Fig. 2.8. Growth of regular overnight WT cultures (Scott A, black) in BHI with 4 mM t-CIN compared to the growth of cultures grown for four consecutive times in the same conditions (Scott A^{4R}). All curves are the average of three independent cultures. Standard deviations have been omitted for clarity. Lag phases (λ), maximum growth rates (μ_{max}) and maximum optical densities (OD_{max}) are listed in table below the curves. ^{A,B}Different superscripts for a growth parameter estimate indicate significant differences ($p < 0.05$).

Next, the possibility of outgrowth of a small subpopulation of mutants with increased t-CIN resistance was investigated by reculturing three independent 48-h WT cultures by diluting 1:1000 in fresh BHI broth with 4 mM t-CIN for four consecutive rounds. These cultures are named in Fig. 2.8 as Scott A^{4R}. Afterwards, the growth parameters of both the parent strain Scott A and Scott A^{4R} were compared for growth in BHI broth with 4 mM t-CIN. Because there was no change in the lag phase after four rounds of reculturing, the formation of t-CIN

resistant mutants was excluded, even though there were small but significant differences in μ_{max} and OD_{max}. As mentioned before, these parameter estimates are less valuable to evaluate sensitivity.

Because no initial inactivation occurs upon exposure to t-CIN and more resistant mutants do not seem to arise easily after being recultured in t-CIN, we subsequently investigated the possibility of chemical or bacterial degradation of t-CIN during the lag phase. The t-CIN concentration was analyzed via HS-SPME-GC-MS analysis directly on filter-sterilized culture supernatant. Besides WT cultures growing in t-CIN, control samples with t-CIN but without cells were included to quantify chemical t-CIN degradation (Fig. 2.9). Stationary-phase overnight cultures grown in BHI broth at 30 °C were washed once with PPB (10 mM, pH 7.0), diluted 1000x to approximately 10^6 cfu/ml in 80 ml BHI broth supplemented with t-CIN in a 100 ml Erlenmeyer closed tightly with a screw-cap with teflon seal to avoid evaporative loss of t-CIN, and incubated at 30 °C. Samples from the cultures and controls without cells were taken at several time points during the lag phase and exponential phase. The cell concentration of each sample was determined by plate count on BHI agar. A concentration of 1 mM t-CIN was chosen to perform these experiments to be able to complete the experiment within a timeframe of one day since sampling and sample preparation are quite extensive and laborious. Data from Fig. 2.1 show that the lag phase of the WT at this concentration is extended by approximately 1 h.

The data in Fig. 2.9 show that that there is a slow but steady chemical degradation of t-CIN in the control sample during incubation at 30 °C. After 8 h the concentration dropped to about 90%. Another experiment performed under the same conditions, showed that the concentration dropped further to 66% after 32 h. These results show that t-CIN degrades only slowly during incubation at 30 °C in BHI broth. Degradation may be due to reaction with nucleophiles present in the medium such as thiol groups from peptides.

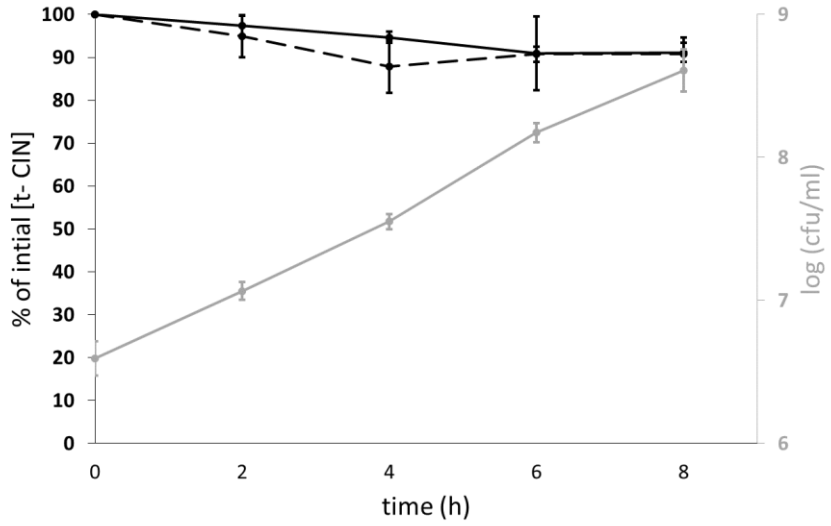

Fig. 2.9. Left axis: evolution of the t-CIN concentration in WT cultures (black solid line) and control samples without cells (black dashed line), expressed as % of the initial t-CIN concentration at the start of the experiment (1 mM). Right axis: cell concentration of the culture in BHI broth with 1 mM t-CIN (grey line). All data points are the average of three independent cultures ± standard deviation.

The evolution of t-CIN concentrations in growing WT cultures did not differ significantly from the cell-free control samples. After 8 h of incubation at 30 °C, there was still about 90% of the initial amount of t-CIN, while the culture already entered stationary phase. Experiments with higher concentrations of t-CIN, that induce longer lag phases, showed similar trends but were not quantified with an internal standard and are therefore not shown in this work.

Since there is no significant bacterial degradation before or during exponential growth, no initial inactivation and resistant mutants do not easily arise, we hypothesize that the resumption of growth after a (long) lag phase results mainly from bacterial adaptation to t-CIN. In chapter 3 at least one of the bacterial adaptation strategies is discussed by detailed characterization of a hypersensitive mutant defective in membrane fatty acid synthesis.

2.3.5. Screening for t-CIN resistance

A transposon gene knockout can potentially lead to increased tolerance instead of hypersensitivity. In an attempt to isolate such mutants, the whole-genome random transposon mutant library was divided in eight pools and plated on BHI agar plates with 3 mM t-CIN. No tolerant mutants could be detected.

2.4. Conclusion

Analysis of the impact of sub-MIC concentrations on the growth parameters of both WT and sensitive transposon mutants, shows that t-CIN primarily exerts its growth inhibitory activity on *L. monocytogenes* by elongating the lag phase in a concentration-dependent manner. Exponential growth rate and maximum OD in stationary phase also decreased, but only up to a certain level of t-CIN, and they did not further decrease at higher levels. At moderate t-CIN concentrations, this extended lag phase, is not due to, or accompanied by inactivation of *L. monocytogenes* or t-CIN degradation. Moreover, mutants of the WT strain with increased tolerance for t-CIN were not detected, even not after four consecutive growth cycles in the presence of t-CIN. Therefore, the lag phase can be considered as an adaptation phase in which cells adapt to become capable to grow in the presence of t-CIN. In chapter 3, at least one of the adaptation strategies is discussed, more specifically membrane fatty acid adaptation in response to the membrane fluidizing effect of t-CIN [45].

The screen for transposon mutants of *L. monocytogenes* Scott A sensitive to t-CIN and/or AIT delivered mutants that are affected in genes encoding proteins with very diverse biochemical functions. The majority of the t-CIN sensitive mutants are also AIT sensitive and vice versa. Only *greA::Himar1* was only sensitive to t-CIN like the *5'yggS* and *sepF* mutants, which showed a remarkably high degree of sensitivity to t-CIN, but not to AIT. The *5'yggS* mutant could be partially complemented both with WT *yggS* and two downstream genes, *sepF* and *yggT*, which reside in a putative operon with *yggS*. Since only limited structural and functional information is available for YggS, this mutant was not further studied. The sensitivity for t-CIN and AIT of the *5'asnB* mutant could be fully restored by complementation with WT *asnB*. Although the enzymatic activity of AsnB is well characterized, its role in t-CIN and AIT sensitivity remains unclear. The remaining selected sensitive transposon mutants are discussed in the next chapters of this dissertation to get a better understanding on the physiological impact of the knocked out gene and the relationship between the observed sensitivity and the genes.

Chapter 3*

Membrane fatty acid composition as a determinant of *Listeria monocytogenes* sensitivity to *trans*-cinnamaldehyde

*This chapter is based on the following publication: Rogiers G, Kebede BT, Van Loey A, Michiels CW. Membrane fatty acid composition as a determinant of *Listeria monocytogenes* sensitivity to trans-cinnamaldehyde. Res Microbiol 2017;168:536–46.

3.1. Introduction

The screening of the 7680 transposon mutants initially yielded several putative t-CIN sensitive mutants (chapter 2). One of the most sensitive mutants, *L. monocytogenes ilvE::Himar1*, with reproducible t-CIN sensitivity is further analyzed and discussed in this chapter. IlvE is a branched-chain amino acid aminotransferase that reversibly catalyzes the deamination of the branched-chain amino acids (BCAAs) L-leucine, L-isoleucine and L-valine to the corresponding α-ketoacids (α-KAs), α-ketoisocaproate (KIC), α-ketomethylvalerate (KMV) and α-ketoisovalerate (KIV), respectively. The latter in turn serve as substrates for the synthesis of branched-chain fatty acids (BCFAs) [52,53]. In the IlvE-catalyzed transamination reaction, the amino group of the BCAA is transferred to 2-ketoglutarate to form glutamate.

3.2. Materials and methods

3.2.1. Bacterial strains, plasmids, oligo's and growth conditions

All strains were routinely cultured under the same conditions as described in chapter 2, section 2.2.1. All strains and plasmids used in this chapter are listed in Table 3.1. All used oligonucleotide primers are listed in Table 3.2.

Table 3.1. Strains and plasmids used in this chapter.

Strain or plasmid	Relevant features	Reference
Strains		
L. monocytogenes		
Scott A	Serovar 4b clinical isolate from the 1983 listeriosis outbreak in Massachusetts	[122]
Scott A *ilvE::Himar1*	Scott A strain with *Himar1* transposon insertion in *ilvE*	Chapter 2
E. coli		
S17-1 λ*pir*	*pro thi recA hsdR*$^-$ *hsdM*$^+$ RP4: 2-Tc:Mu: Km Tn7 λ*pir*	[121]
DH5-α	F$^-$ *endA1 hsdR17* (r_k^-, m_k^+) *supE44 thi*$^-$*1* λ$^-$ *recA1 gyrA96 relA1 deoR* Δ(*lacZYA-argF*)U169 Φ80d *lacZ*ΔM15	[123]
Plasmids		
pIMK2	Site-specific listerial integrative vector, Phelp promoter for constitutive overexpression, 6.2 kb, Km^R	[125]

Table 3.2. Oligonucleotide primers used in this chapter

Primer	Sequence (5' – 3')[a]	Reference
ilvE_NcoI	GCATCCATGGGAAGTAAAGATATTGACTGGAGTAATTTAGG	This chapter
ilvE_SalI	CACTGTCGACTTATTTCACTTTATAAATCCAACCTTC	This chapter
pIMK_REV	CCTATCACCTCAAATGGTTCG	Chapter 2
pIMK_FW	GAGTCAGTGAGCGAGGAAGC	Chapter 2
NC16	GTCAAAACATACGCTCTTATC	[129]
Ylinker	CTGCTCGAATTCAAGCTTCT	[128]
Marq269	GCTCTGATAAATATGAACATGATGAGTGAT	[124]

[a] Restriction sites are underlined: NcoI (CCATGG) and SalI (GTCGAC)

3.2.2. Determination of kinetic growth parameters

Growth assays and determination of kinetic growth parameters were performed as described in chapter 2, section 2.2.4. In some experiments, cultures were supplemented with precursors of branched-chain fatty acid synthesis, including the branched-chain amino acids (BCAAs) L-leucine (Leu, ≥98.5%, Sigma-Aldrich, Steinheim, Germany), L-isoleucine (Ile, 99%, Acros Organics), L-valine (Val, ≥98.5%, Fisher Scientific, Leicestershire, Great-Britain) and the branched-chain α-ketoacids (α-KAs) α-ketoisocaproic acid sodium salt (KIC, ≥98%, Sigma-Aldrich), α-ketomethylvaleric acid sodium salt (KMV, ≥98%, Sigma-Aldrich) and α-ketoisovaleric sodium salt (KIV, ≥98%, Acros Organics).

3.2.3. Genetic complementation

Genetic complementation of *ilvE::Himar1* with the pIMK2 plasmid was performed according to the protocol described in chapter 2, section 2.2.6. WT *ilvE* gene was amplified using primers ilvE_NcoI and ilvE_SalI (Table 3.2) and cloned as a NcoI - SalI fragment into pIMK2, which was first linearized with the same restriction enzymes.

3.2.4. Growth assay at 10 °C

Cells from three independent stationary-phase overnight cultures of each strain were washed once with PPB, diluted to approximately 10^4 cfu/ml in 4 ml of BHI broth in 10 ml glass tubes with loose caps, and incubated shaking at 10 °C. Every 24 h, samples were taken for plate counting on BHI agar.

3.2.5. Whole-cell fatty acid analyses

The whole-cell fatty acid composition was determined for WT and *ilvE* mutant stationary and early exponential phase cultures grown in the absence of t-CIN, and for early exponential phase cultures growing in 2 mM t-CIN. Each analysis was performed with three independent cultures, grown shaken at 200 rpm in 50 ml BHI medium in closed 100 ml Erlenmeyers at 30 °C. At the desired growth stage, cultures were cooled on ice for 10 min, cells were washed three times with sterile cold deionized water, and finally pelleted by centrifugation at 15000 rpm. All manipulations were performed rapidly at 4 °C to avoid any further change in the fatty acid composition. The cell pellets were frozen with liquid nitrogen and finally lyophilized. Lipid extraction and fatty acid methyl ester (FAME) analysis were performed directly on the lyophilized pellets using the method recommended by the commercial Microbial ID System (MIDI Inc., Delaware, USA). Samples were analyzed using an Agilent Technologies 6890N gas chromatograph (Santa Clara, CA, USA) and the peaks were identified using the TSBA50 identification library version 5.0 (MIDI). This analysis was performed by the Belgian Co-Ordinated Collections of Micro-organisms (BCCM/LMG, Ghent, Belgium). The cell concentration of the cultures used for this analysis was determined by colony counts on BHI agar.

3.2.6. Bacterial inactivation by t-CIN

Stationary-phase overnight cultures grown in BHI broth at 30 °C were washed twice with PPB (10 mM, pH 7.0) and diluted to approximately 10^7 cfu/ml in PPB supplemented with 6 mM t-CIN. Cell suspensions were then kept in Eppendorf tubes at 22 °C in a heating/cooling block and sampled every hour for determination of survivors by plate count on BHI agar.

3.2.7. Statistical analysis

Means of the parameter estimates of the Baranyi and Roberts growth model (λ, μ_{max} and OD_{max} [127]), mean percentages of the different fatty acids, mean cell concentrations during growth at 10 °C and mean cell concentrations during the inactivation at different time points, were statistically compared by the Tukey-Kramer HSD test with the JMP® Software (JMP, Version Pro12, SAS Institute Inc., Cary, USA), and considered significantly different when a *p*-value < 0.05 was obtained.

3.3. Results and discussion

3.3.1. Characterization of the *ilvE::Himar1* t-CIN sensitivity

The transposon in one of the most t-CIN-sensitive mutants was found to be located in the *ilvE* gene of this mutant, at 792 base pairs from the start codon (Fig. 3.1). IlvE is a branched-chain amino acid aminotransferase (PATRIC accession number VBILisMon199232_1061 [130], Kegg Enzyme EC 2.6.1.42)

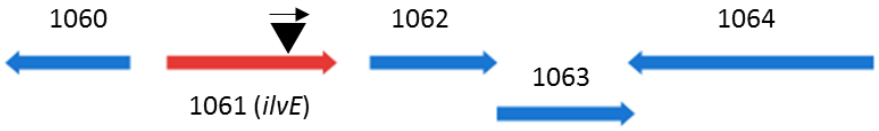

Fig. 3.1. Organization of ilvE region in *L. monocytogenes* Scott A. The *ilvE* gene is highlighted in red, with the *Himar1* transposon at 792 bp from the start codon of *ilvE* shown as a black triangle. The black arrow indicates the orientation of the erythromycin resistance gene (*ermC*) in the transposon. In the PATRIC database [130] the ORFs are annotated as putative acetyl esterase YjcH (EC 3.1.1.-) (1060), branched-chain amino acid aminotransferase (IlvE, EC 2.6.1.42) (1061), ABC transporter, ATP-binding protein (1062), ABC transporter, permease protein (1063) and drug resistance transporter, EmrB/QacA family (1064).

Fig. 3.2 shows the growth curves and the growth parameters of *L. monocytogenes* Scott A and its *ilvE::Himar1* transposon mutant in BHI broth with and without the addition of 4 mM of t-CIN. In absence of t-CIN, the mutant showed a slightly attenuated growth in BHI, with a lower μ_{max} and OD_{max}. Plate counting showed that the stationary-phase cell concentration was about 2.5 times higher for the WT than for the mutant ((4.0 ± 0.5) x 10^9 cfu/ml compared to (1.6 ± 0.2) x 10^9 cfu/ml). Because initial cell concentration may affect the inhibitory effect of t-CIN, the stationary-phase cultures used as inoculum for the growth experiments in the presence of t-CIN were diluted 2.5-fold more for the WT than for the mutant, to ensure that the amount of available t-CIN per cell was equal for both strains. It should be noted that the inoculum may also have been in a somewhat different physiological state because both strains reached stationary phase at different cell density and because the *ilvE* mutation may have altered cellular metabolism. As discussed in chapter 2, the t-CIN sensitivity of the *ilvE* mutant is particularly reflected in the lag phase. While the reduction in μ_{max} and OD_{max} caused by t-CIN were of similar magnitude in the WT and *ilvE* mutant, the lag phase was extended much more in the mutant (8.4-fold) than in the WT (3.6-fold). Just like WT cultures (chapter 2, Fig 2.7), no initial inactivation of *ilvE::Himar1* cultures could be observed upon exposure to inhibitory concentrations used in the growth assays (data not shown).

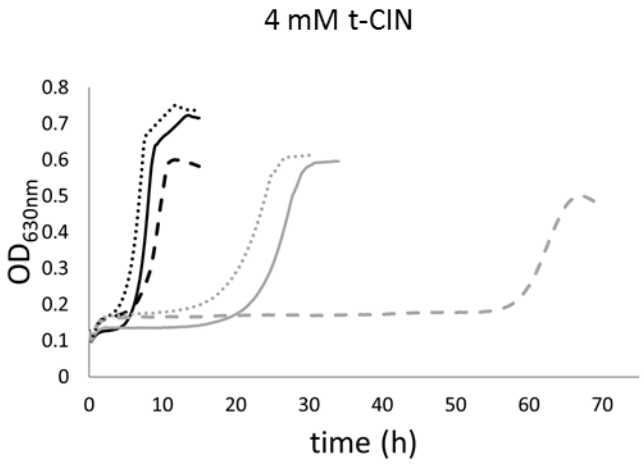

Strain		λ (h)	μ_{max} (1/h)	OD_{max}
			BHI	
Scott A	——	6.1 ± 0.3^{D,E}	0.176 ± 0.001^{A}	0.725 ± 0.011^{B}
ilvE::Himar1	— -	7.0 ± 0.2^{D}	0.110 ± 0.011^{B}	0.602 ± 0.006^{D}
ilvE::Himar1/pIMK2-*ilvE*	·····	4.8 ± 0.1^{E}	0.168 ± 0.003^{A}	0.752 ± 0.009^{A}
			4 mM t-CIN	
Scott A	——	22.1 ± 0.8^{B}	0.062 ± 0.001^{C}	0.614 ± 0.014^{C,D}
ilvE::Himar1	— -	58.5 ± 1.7^{A}	0.047 ± 0.005^{C}	0.512 ± 0.004^{E}
ilvE::Himar1/pIMK2-*ilvE*	·····	18.0 ± 0.2^{C}	0.053 ± 0.001^{C}	0.633 ± 0.005^{C}

Fig. 3.2. Growth curves of *L. monocytogenes* Scott A, its *ilvE::Himar1* mutant and the genetically complemented mutant *ilvE::Himar1*/pIMK2-*ilvE* in BHI and BHI with 4 mM t-CIN. All curves are the average of three independent cultures. Standard deviations have been omitted for clarity. Lag phases (λ), maximum growth rates (μ_{max}) and maximum optical densities (OD_{max}) corresponding to the curves are shown in the table. Values are means ± standard deviation. ^{A,B,C,D,E} Different superscripts indicate significant differences ($p < 0.05$).

As can be seen from Fig. 3.1, it cannot be excluded that *ilvE* is co-transcribed with two downstream ORFs and that the *Himar1* insert in *ilvE* also knocks out the production of the corresponding proteins. However, this is unlikely, since *ilvE* was shown to be separately transcribed in *L. monocytogenes* strain EGD-e, which has the same gene organization in this region [141]. To confirm that it is indeed disruption of *ilvE* that is responsible for t-CIN sensitivity, the mutant was genetically complemented with the *ilvE* gene using the overexpression integration vector pIMK2. This restored the OD_{max} to WT level, and the lag phase even became slightly shorter than that of the WT (Fig. 3.2). These results, together with

the results of chemical complementation below, allow us to conclude that loss of IlvE activity results in increased t-CIN sensitivity in *L. monocytogenes* Scott A.

3.3.2. Chemical complementation of *L. monocytogenes ilvE::Himar1*

IlvE reversibly catalyzes the transamination between the BCAAs Leu, Ile and Val and their corresponding α-ketoacids KIC, KMV and KIV, respectively. As such it has a dual metabolic role (Fig. 3.3). First, it catalyzes an essential step in the biosynthesis of BCAAs when these are in limited supply in the medium. Second, when BCAAs are abundant, IlvE can deaminate them to KIC, KMV and KIV, which are subsequently converted by the branched-chain ketoacid dehydrogenase complex (BCKD) to isovaleryl-CoA, 2-methylbutyryl-CoA and isobutyryl-CoA, which serve as direct precursors for the synthesis of the BCFAs iso-C15:0/iso-C17:0, anteiso-C15:0/anteiso-C17:0 and iso-C14:0/iso-C16:0, respectively [52,53,142].

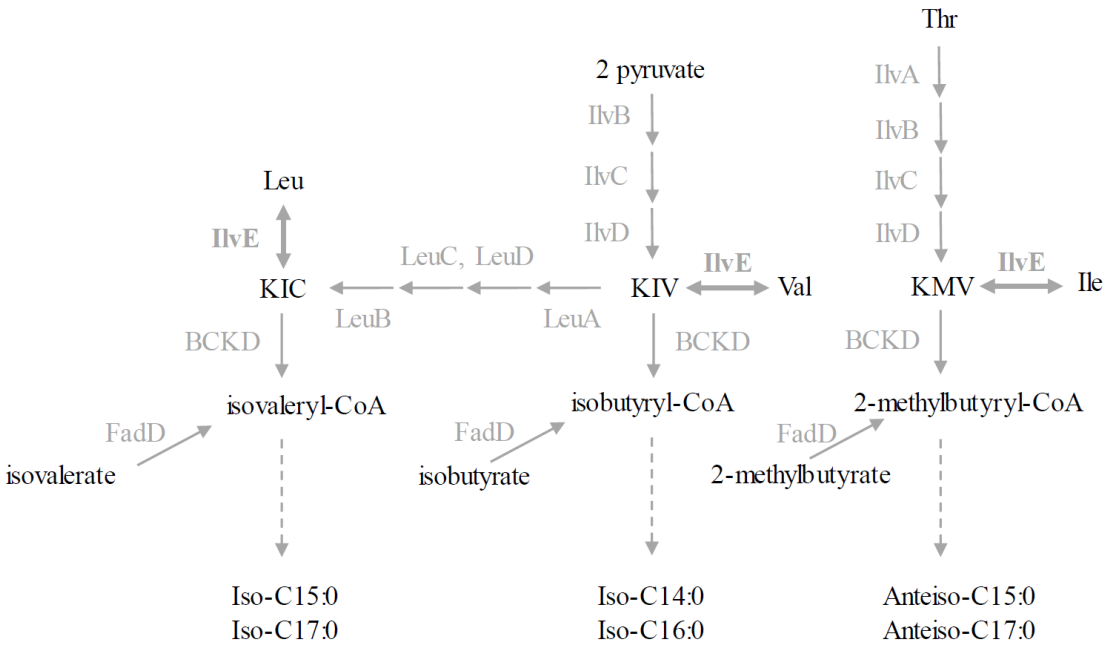

Fig. 3.3. Pathway of branched-chain fatty acid (BCFA) synthesis in *L. monocytogenes*. The central precursors are the α-ketoacids α-ketoisocaproate (KIC), α-ketoisovalerate (KIV) and α-ketomethylvalerate (KMV). These can be derived from the corresponding branched-chain amino acids (BCAAs) Leu, Val or Ile by the transaminase IlvE, but *L. monocytogenes* Scott A also has predicted genes for their *de novo* synthesis from pyruvate (KIC and KIV) or from Thr (KMV). Thr itself can be synthesized *de novo* from oxaloacetate. Pathways are inferred from predicted presence of enzymes based on genome sequence of *L. monocytogenes* Scott A.

To find out whether t-CIN sensitivity of the *ilvE* mutant in BHI broth was due to their inability to synthesize BCAAs or to convert BCAAs from the medium to BCFAs, we supplemented the medium with an equimolar mix (10 mM each) of the above three α-KAs or BCAAs. The α-KAs fully reversed the t-CIN sensitivity of the mutant to WT level, while the BCAAs had no effect (Fig. 3.4a, 3.4c). Supplementation of the WT cultures with α-KAs also significantly shortened the lag phase in the presence of t-CIN.

a.

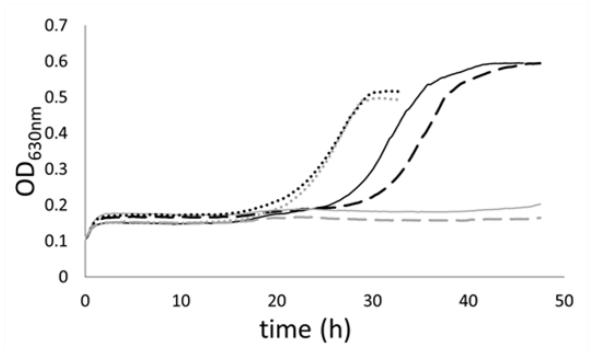

b.

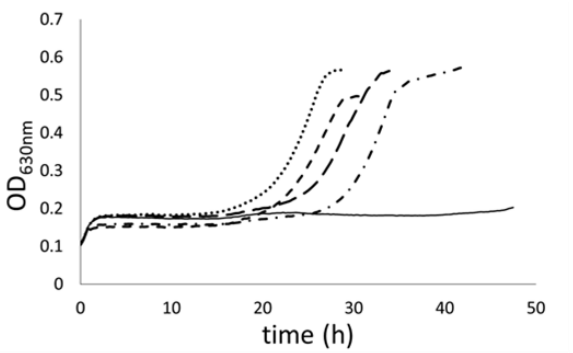

c.

Growth parameter	Scott A			*ilvE::Himar1*					
	No	BCAAs	α-KAs	No	BCAAs	α-KAs	KIC	KIV	KMV
λ (h)	26.8 ± 2.4^{A,B}	30.3 ± 1.6^{A}	20.9 ± 1.4^{D}	> 47.5^{E}	> 47.5^{E}	21.0 ± 0.4^{C,D}	24.9 ± 1.9^{B,C}	20.1 ± 0.6^{D}	28.0 ± 0.3^{A,B}
μ_{max} (1/h)	0.046 ± 0.004^{B,C}	0.045 ± 0.002^{C}	0.039 ± 0.002^{D}	/	/	0.043 ± 0.001^{C,D}	0.054 ± 0.001^{A}	0.054 ± 0.001^{A}	0.051 ± 0.001^{A,B}
OD_{max}	0.601 ± 0.006^{A}	0.595 ± 0.004^{A,B}	0.522 ± 0.009^{D,E}	/	/	0.506 ± 0.017^{E}	0.592 ± 0.011^{A,B}	0.569 ± 0.009^{B,C}	0.544 ± 0.015^{C,D}

Fig. 3.4. (a) Growth of *L. monocytogenes* Scott A (black) and its *ilvE::Himar1* mutant (grey) in BHI + 4 mM t-CIN. Full, dashed and dotted lines represent cultures without supplements, with 10 mM each of all three BCAAs, and with 10 mM each of all three α-KAs, respectively. (b) Growth of the *ilvE::Himar1* mutant in BHI + 4 mM t-CIN (——), supplemented with 10 mM each of all three α-KAs (– – –), 10 mM α-ketoisovalerate (KIV, ••••••), 10 mM α-ketoisocaproate (KIC, — —) or 10 mM α-ketomethylvalerate (KMV, — •). All curves are the average of three independent experiments. Standard deviations have been omitted for clarity. (c) Lag phases (λ), maximum growth rates (μ_{max}) and maximum optical densities (OD_{max}) corresponding to the curves in (a) and (b). Values are means ± standard deviation. ^{A,B,C,D,E} Different superscripts indicate significant differences ($p < 0.05$).

These results lead us to conclude that the t-CIN sensitivity of the *ilvE* mutant is due to its inability to use BCAAs from the medium for the production of BCFAs. It should be noted that the full pathway to synthesize BCFAs *de novo* without IlvE (Fig. 3.3) is predicted to be present in *L. monocytogenes* Scott A based on its genome sequence, and the fatty acid analysis of the *ilvE* mutant indicates this (see section 3.3.3). Therefore, our results suggest that BCFA production via this pathway may be kinetically limited. This would also explain the much

reduced growth rate of the *ilvE* mutant at 10 °C (Fig. 3.5), since *L. monocytogenes* requires BCFAs for maintaining its membrane fluidity under these conditions [52]. The growth defect at 10 °C rate was also completely restored by genetic complementation (Fig. 3.5).

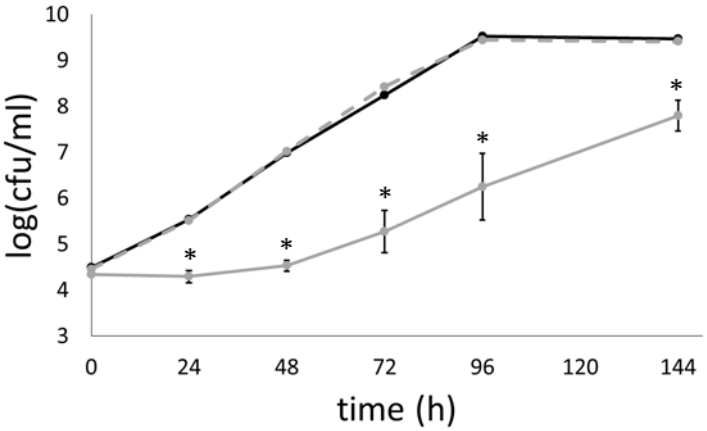

Fig. 3.5. Growth of *L. monocytogenes* Scott A (black), its *ilvE::Himar1* mutant (full grey line) and the genetically complemented mutant *ilvE::Himar1*/pIMK2-*ilvE* (dashed grey line) in BHI at 10 °C. The asterisk indicates significant differences with the WT and genetically complemented strain at the same time point.

Next, we investigated whether there is a difference in the ability of the three α-KAs to neutralize the t-CIN sensitive phenotype of the *ilvE* mutant (Fig. 3.4b, 3.4c). All three α-KAs significantly reduced the lag phase, but only KIV restored the t-CIN tolerance to the same level as the WT supplemented by all three α-KAs. Since KIV supports the synthesis of iso-fatty acids (especially C14:0 and C16:0, see Fig. 3.3), it could be that this type of BCFAs is most effective in generating t-CIN tolerance. However, this cannot be concluded with certainty, since there may be additional factors influencing the response to α-KAs, like the uptake efficiency from the medium.

3.3.3. Membrane fatty acid analysis

3.3.3.1. Stationary-phase cells cultured in absence of t-CIN

The previous results suggest that the t-CIN sensitivity of the *ilvE* mutant may be due to an altered membrane composition. To provide more direct evidence for this hypothesis, we first compared the whole-cell fatty acid composition of stationary-phase cultures of the WT and the *ilvE* mutant after growth in BHI at 30 °C (Table 3.3).

Table 3.3. Percentage of total whole-cell fatty acids of cultures grown in BHI at 30 °C with and without 2 mM t-CIN. Summary data are shown at the bottom of the table. Values are means ± standard deviation from three independent experiments, except for the analysis of the mutant grown in t-CIN where means are from two independent experiments. Exponential cultures were harvested at the same OD_{600nm}. Most dominant FA fractions in both stationary and exponential Scott A are framed grey.

	BHI		BHI		BHI + t-CIN	
	Stationary phase		Exponential phase		Exponential phase	
Fatty acid	**Scott A**	***ilvE::Himar1***	**Scott A**	***ilvE::Himar1***	**Scott A**	***ilvE::Himar1***
C10:0	0.1 ± 0.1^{A}	0.0 ± 0.0^{A}	0.0 ± 0.0^{A}	0.0 ± 0.0^{A}	0.0 ± 0.0^{A}	0.3 ± 0.0^{B}
C12:0	1.4 ± 0.2^{C}	4.1 ± 0.5^{B}	0.9 ± 0.0^{C}	1.8 ± 0.2^{C}	7.0 ± 1.3^{A}	3.7 ± 0.2^{B}
Iso-C13:0	0.0 ± 0.0^{B}	0.4 ± 0.0^{A}	0.0 ± 0.0^{B}	0.6 ± 0.2^{A}	0.0 ± 0.0^{B}	0.0 ± 0.0^{B}
Anteiso-C13:0	0.0 ± 0.0^{A}	0.0 ± 0.0^{A}	0.0 ± 0.0^{A}	0.1 ± 0.1^{A}	0.0 ± 0.0^{A}	0.0 ± 0.0^{A}
Iso-C14:0	0.6 ± 0.0^{C}	9.9 ± 1.6^{B}	0.8 ± 0.0^{C}	19.9 ± 2.9^{A}	7.5 ± 0.6^{B}	11.5 ± 0.0^{B}
C14:1 ω5c	0.0 ± 0.0^{B}	0.1 ± 0.2^{B}	0.0 ± 0.0^{B}	0.4 ± 0.4^{B}	2.2 ± 0.4^{A}	0.4 ± 0.1^{B}
C14:0	0.5 ± 0.1^{E}	11.6 ± 0.8^{B}	1.3 ± 0.1^{E}	6.4 ± 0.4^{C}	4.0 ± 0.7^{D}	18.2 ± 0.8^{A}
Iso-C15:0	$10.9 \pm 0.4^{B,C}$	17.1 ± 3.9^{A}	$12.6 \pm 0.2^{A,B}$	$12.5 \pm 0.8^{A,B}$	7.4 ± 0.2^{C}	1.8 ± 0.9^{D}
Anteiso-C15:0	29.9 ± 1.0^{B}	2.6 ± 0.2^{E}	36.6 ± 0.2^{A}	7.6 ± 0.7^{D}	22.4 ± 1.0^{C}	3.5 ± 0.6^{E}
Iso-C16:0	2.8 ± 0.1^{B}	16.7 ± 1.6^{A}	2.0 ± 0.1^{B}	16.9 ± 2.4^{A}	16.0 ± 1.9^{A}	14.1 ± 0.2^{A}
C16:0	2.1 ± 0.1^{E}	27.6 ± 1.3^{B}	5.5 ± 0.2^{D}	12.0 ± 1.1^{C}	10.8 ± 0.3^{C}	42.8 ± 0.7^{A}
Iso-C17:0	9.2 ± 0.5^{A}	5.5 ± 0.8^{B}	4.8 ± 0.1^{B}	1.8 ± 0.1^{D}	3.0 ± 0.3^{C}	0.7 ± 0.2^{D}
Anteiso-C17:0	41.0 ± 0.9^{A}	1.4 ± 0.2^{D}	26.8 ± 0.4^{B}	1.9 ± 0.5^{D}	10.5 ± 0.4^{C}	1.8 ± 0.6^{D}
C18:1 ω9c	0.2 ± 0.2^{D}	0.3 ± 0.4^{D}	6.3 ± 0.3^{B}	9.8 ± 2.0^{A}	3.4 ± 0.6^{C}	0.0 ± 0.0^{D}
C18:1 ω6c	0.0 ± 0.0^{A}	0.0 ± 0.0^{A}	0.0 ± 0.0^{A}	0.6 ± 0.8^{A}	0.0 ± 0.0^{A}	0.0 ± 0.0^{A}
C18:0	0.5 ± 0.1^{D}	$2.0 \pm 0.2^{B,C}$	1.0 ± 0.1^{D}	3.5 ± 0.6^{A}	$2.8 \pm 0.3^{A,B}$	$1.1 \pm 0.3^{C,D}$
Anteiso-C19:0	0.6 ± 0.1^{A}	0.0 ± 0.0^{B}	0.0 ± 0.0^{B}	0.0 ± 0.0^{B}	0.0 ± 0.0^{B}	0.0 ± 0.0^{B}
Iso-C17:1 ω5c	0.0 ± 0.0^{A}	0.2 ± 0.3^{A}	0.0 ± 0.0^{A}	0.0 ± 0.0^{A}	0.0 ± 0.0^{A}	0.0 ± 0.0^{A}
C18:1 ω7c	0.0 ± 0.0^{A}	0.0 ± 0.0^{A}	0.0 ± 0.0^{A}	0.5 ± 0.8^{A}	0.0 ± 0.0^{A}	0.0 ± 0.0^{A}
BCFAs	95.0 ± 1.2	53.7 ± 3.8	83.5 ± 0.4	61.0 ± 3.2	66.8 ± 1.9	33.3 ± 0.9
Anteiso-BCFAs	71.5 ± 1.1	4.1 ± 0.2	63.4 ± 0.3	9.5 ± 0.8	32.9 ± 0.8	5.3 ± 0.6
Iso-BCFAs	23.5 ± 0.5	49.6 ± 3.7	20.1 ± 0.2	51.5 ± 3.1	33.9 ± 1.7	28.0 ± 0.7
Iso/Anteiso	0.3	12.2	0.3	5.4	1.0	5.3
CA <15	2.6 ± 0.2	26.1 ± 1.5	2.9 ± 0.1	29.1 ± 2.4	20.7 ± 1.3	34.0 ± 0.6
Weighted mean CA*	15.1	14.7	14.8	14.2	14.3	14.9
Weighted mean B-CA*	15.1	14.4	14.8	14.1	14.5	14.2
Weighted mean UB-CA*	14.8	15.2	16.6	16.2	15.1	15.2

$^{A, B, C, D, E}$ Different superscripts indicate significant differences (p-value < 0.05); * CA = carbon atoms; B = branched-chain; UB = unbranched-chain.

The most notable feature of the fatty acid composition of the WT strain is the high level of BCFAs (~ 95%), mainly anteiso-BCFAs (~ 71.5%). This prominent presence of BCFAs has been reported before for the same strain, grown in buffered BHI at 30 °C to mid-log phase [111]. In comparison, and as expected, the *ilvE* mutant had strongly reduced BCFA levels (53.7%). This reduction was entirely accounted for by the anteiso fraction, which decreased from 71.5% to only 4.1%, while the iso-BCFAs even increased from 23.5% to 49.6%. The reduced anteiso-BCFA content is further balanced by an increase in unbranched saturated fatty acids, predominantly C14:0 and C16:0. Furthermore there is a clear shift to fatty acids with lower molecular mass (< C15) in the mutant. Since the *ilvE* mutant can no longer convert BCAAs to BCFAs, its BCFAs must be derived from *de novo* synthesis or from alternative substrates from the medium like α-KAs or branched-chain carboxylic acids (Fig. 3.3). The increased level of iso- but not anteiso-BCFAs in this mutant may therefore indicate that BHI medium is a good source of alternative iso-BCFAs precursors (i.e. KIV, KIC, isobutyrate and isovalerate) but less so for anteiso-BCFAs precursors (KMV and 2-methylbutyrate). Alternatively, the increased iso/anteiso ratio of the mutant may reflect a kinetic limitation of the anteiso biosynthesis pathway, possibly because this pathway is much longer than the iso biosynthesis pathway and starts from another precursor, threonine instead of pyruvate (Fig. 3.3).

From a functional perspective, the membranes of the *ilvE* mutant are predicted to be more rigid, predominantly due to the almost complete loss of the anteiso-BCFAs. Despite the small structural difference, anteiso-BCFAs have a much lower phase-transition temperature than iso-BCFAs with the same number of carbon atoms (iso-C15:0, 52.2 °C; anteiso-C15:0, 25.8 °C; anteiso-C17:0, 30.0 °C; iso-C17:0, 60.5 °C) [142,143], and this explains why anteiso-BCFAs are much more critical for maintaining membrane fluidity and supporting growth of *L. monocytogenes* at low temperature [52,143,144]. Therefore, in the *ilvE* mutant, the increase of iso-BCFAs and the shift towards less carbon atoms apparently could not fully compensate for the loss of anteiso-BCFAs in maintaining membrane fluidity, since the mutant showed a severe growth defect at 10 °C (Fig. 3.5). Finally, the shift towards less carbon atoms in the mutant may reflect an adaptation to maintain membrane thickness, because the replacement of BCFAs by unbranched fatty acids would otherwise lead to increased chain length, since the methyl side chain in BCFAs does not contribute to chain length.

Although our study is the first to document the role of IlvE in BCFA synthesis in *L. monocytogenes*, mutants in the branched-chain α-KA dehydrogenase complex (BCKD), which are unable to convert the branched-chain α-KAs to the corresponding acyl-CoA derivatives (Fig. 3.3) have been previously isolated as being cold-sensitive, and showed a similar decrease in total and anteiso-BCFAs as our *ilvE* mutant [53]. As opposed to *ilvE* mutants, *bckd* mutants fully depend on exogenous branched-chain carboxylic acid precursors for BCFA synthesis.

Interestingly, during the screen for t-CIN/AIT sensitivity, we also identified a mutant with a transposon in one of the genes of the BCKD complex, more specifically *bckd-E1α::Himar1.* This gene encodes the α-subunit of the E1 component of the BCKD enzyme complex and is the fourth gene in an operon of six co-transcribed genes: *ptb* (branched-chain phosphotransacylase), *buk* (butyrate kinase), *lpd* (dihydrolipoamide dehydrogenase), *bckd-E1α*, *bckd-E1β* and *bckd-E2* (dihydrolipoamide acyltransferase component). This mutant has a lag phase of 65.2 h in 4 mM t-CIN and 28.2 h in AIT (Table 2.4, chapter 2), which is significantly longer than the WT lag phases in the presence of these compounds (38.8 h and 24.4 h respectively). However, this mutant also shows a severe growth defect in BHI without antimicrobial compounds, with a longer lag phase and lower μ_{max} and OD_{max} than the WT strain. Complementation via constitutive overexpression with the WT gene *bckd-E1α* did not restore the phenotype, while complementation with *bckd-E1α* together with the downstream genes *bckd-E1β* and *bckd-E2* caused aberrant cell morphology (enlarged cells) and did not restore normal growth in BHI. Therefore, and because the biochemical function of the BCKD enzyme complex has been previously well studied in *L. monocytogenes* [52,53], we did not further characterize the biochemical role of this enzyme complex or its relation to the antimicrobial activity of t-CIN.

3.3.3.2. Exponential-phase cells cultured in the presence of t-CIN

While the above findings clearly indicate that the modified membrane fatty acid composition is at the basis of the increased t-CIN sensitivity of the *ilvE* mutant, the growth curve in Fig. 3.2 shows that also *ilvE* mutant cells eventually start growing in the presence of t-CIN after a long lag phase. To investigate whether adaptation of the fatty acid composition during the lag phase in the presence of t-CIN could play a role in this, we analyzed the whole-cell fatty acid composition of early-exponential phase WT and mutant cells grown both in the absence and in the presence of 2 mM t-CIN. This concentration induces a lag phase in the WT of 11.0 h and

in the mutant a lag phase of 24.8 h. Early-exponential phase cells were chosen for this experiment, because if resumption of growth in t-CIN depends on an adaptation of membrane composition, it is expected to be best visible shortly after the lag phase. In addition, HS-SPME-GC-MS analysis indicated that the concentration of t-CIN in the WT culture had only slightly decreased by 5.3 ± 1.4% until this stage of growth (chapter 2, Fig 2.9). This decrease was not significantly different (p = 0.13) from that in control medium without cells (12.2 ± 6.1%), suggesting that it was due to chemical degradation or reaction with medium compounds rather than to bacterial metabolism. Note that exponential-phase cultures were harvested at the same OD_{600nm} and not at the same time of incubation, because lag times differ between WT and *ilvE* mutant in BHI (Fig. 3.2), but also between both strains during growth in BHI compared to BHI with t-CIN.

The results of the fatty acid analyses of the exponential cultures are presented in Table 3.3. Compared to stationary phase, exponential-phase cells of the WT strain had less BCFAs (-12%), and within the BCFAs there was a shift towards shorter chain length (C17 to C15). Also notable was the appearance of the unsaturated C18:1 ω9c (6.3%). In the *ilvE* mutant, there was a similar shift towards shorter BCFAs (C15 but also C14 in this case) and the appearance of C18:1 ω9c (9.8%). However, unlike in the WT, the proportion of BCFAs was higher in exponential than in stationary phase (+ 14%), mainly due to an increase in the anteiso fraction. Possibly, this is because the branched-ketoacid or acid precursors for BCFA synthesis in the BHI medium are not yet limiting during the initial stages of growth, while they get progressively exhausted later during growth. The presence of t-CIN induced some marked changes in the fatty acid profiles of both strains. There was a decrease in BCFAs both in the WT (from 83.5% to 66.8%) and in the *ilvE* mutant (from 61.0% to 33.3%). However, whereas in the WT this net effect was the result of a decrease of the anteiso fraction (from 63.4% to 32.9%) and an increase in the iso fraction (from 20.1% to 33.9%), both fractions declined in the mutant (from 9.5% to 5.3% and from 51.5% to 28.0%, respectively). The unsaturated C18:1 ω9c also decreased in both strains. These decreases are balanced by an increase in unbranched saturated fatty acids in both strains. Finally, both strains show a shift towards fatty acids with less carbons (< C15) in the presence of t-CIN. This shift is considerable in the WT strain (from 2.9% to 20.7%), and less marked in the *ilvE* mutant (from 29.1% to 34.0%), possibly because the level in the mutant is already elevated even in absence of t-CIN.

Although the changes in fatty acid composition induced by t-CIN differ in some aspects between the WT and the mutant, they are expected to result in higher phase-transition temperatures (i.e. reduced membrane fluidity) in both cases. For the WT, this is mainly because of the reduction of the anteiso-BCFA fraction, while in the mutant the decrease in the iso-BCFAs and unsaturated FA fractions are likely to also play a role. Since small hydrophobic molecules like t-CIN partition into the membrane and have a fluidizing effect [45], the changes in fatty acid composition may be considered as a response of the bacteria to counteract this effect.

Some previous studies have investigated the effect of other hydrophobic α, β-unsaturated carbonyl compounds on the membrane composition of *L. monocytogenes* Scott A in similar conditions. Patrignani *et al*. (2008) [110] reported an increase in saturated fatty acids, predominantly C14:0, C16:0 and C18:0, and a reduction in iso-C14:0, C15:0, iso-C15:0, anteiso-C15:0 and C18:1 ω9c in late-exponential-phase cells grown at 37 °C in BHI when 20 ppm (~ 0.2 mM) *trans*-2-hexenal was added [110]. Even though this concentration was reported to be subinhibitory (while we used growth-inhibitory concentrations of t-CIN), these changes are also predicted to reduce membrane fluidity and are thus consistent with the idea of a bacterial response to counteract the membrane fluidizing effect of the compound. However, remarkably, these authors did not find any anteiso-C17:0 in the control Scott A culture grown in BHI without antimicrobials, although we and others found this to be one of the dominant fatty acids in Scott A and other *L. monocytogenes* strains [111,112]. Later work from the same group reported on the effect of sub-lethal concentrations of citral (50, 85, 125 ppm) in BHI during growth at 37 °C [113]. In this study, the fatty acid composition of the control Scott A culture corresponded better to the composition reported in our work and that of others. Interestingly, much like t-CIN in our work, citral primarily affected growth by extending the lag phase. Although the changes in the membrane fatty acid composition were less pronounced than for t-CIN, there was a small reduction, for cultures grown with 125 ppm citral, in the amount of anteiso-C15:0, anteiso-C17:0 and iso-C17:0, compensated by a increases in C16:0, C18:2 (cis-cis) and C18:1 ω9c. Again, these changes in the fatty acid composition are predicted to make the membranes more rigid.

Finally, Di Pasqua *et al*. (2006) [114] investigated adaptive changes in the ratio of saturated to unsaturated fatty acids induced by sublethal concentrations of t-CIN and other essential oil compounds in various Gram-negative and Gram-positive bacteria. In *Escherichia coli* O157:H7, t-CIN induced more unsaturation, and the same was observed for the other compounds tested. However, the effect of t-CIN in different bacteria was not consistent, since it had no significant effect on the degree of saturation in two other Gram-negative bacteria (*Salmonella enterica* serovar Typhimurium and *Pseudomonas fluorescens*), increased the ratio in one Gram-positive organism (*Brochothrix thermosphacta*) and decreased the ratio in another one (*Staphylococcus aureus*). Also for the other compounds, no consistent trends could be observed that would support the hypothesis of counteraction of a membrane fluidizing effect of the compounds. However, unfortunately, the study did not report changes in cyclopropane fatty acids and BCFAs, which are prominent, if not the major, players in membrane homeoviscous adaptation in Gram-negative and Gram-positive bacteria, respectively.

3.3.4. The role of IlvE in survival of lethal t-CIN concentrations

The effect of antimicrobial compounds can be either bacteriostatic or bactericidal depending on the applied concentration, and the effects do not necessarily rely on the same mode of action. Therefore, the elongated lag phase of the *ilvE* mutant during growth in the presence of t-CIN does not necessarily imply a higher sensitivity of this mutant to bactericidal concentrations of t-CIN. More specifically, we here investigated whether the aberrant membrane fatty acid composition of the *ilvE* mutant would result in a different inactivation rate for stationary-phase cells in 6 mM t-CIN in potassium phosphate buffer without added nutrients (Fig. 3.6). Inactivation of both WT, *ilvE* mutant and the genetically complemented mutant (*ilvE::Himar1*/pIMK2-*ilvE*) cells started after 1 h of exposure to t-CIN, but proceeded significantly faster for the mutant. Furthermore, when the mutant was grown in BHI with an equimolar mix (1 mM) of the three α-KA, resistance was restored to WT level. Supplementation with α-KA did not affect the inactivation of WT cells. These results indicate that the faster inactivation of the *ilvE* mutant at lethal t-CIN concentrations, similar to its retarded growth at sublethal t-CIN concentrations, is caused by their altered membrane composition rather than to their inability to synthesize BCAAs. This may lead to increased diffusion of t-CIN through the membrane into the cytoplasm, where it can react with cellular nucleophiles (mainly thiol and amino groups) based on its electrophilic properties, giving rise

to DNA damage, malfunctioning enzymes, depletion of CoA-SH, and disturbance of redox homeostasis. The increased intracellular damage expected to occur in the mutant can in turn explain its increased sensitivity to lethal as well as to sublethal concentrations of t-CIN. In the latter case, the increased damage will require more time to be repaired, and thus a longer lag phase at sublethal concentrations of t-CIN. However, additional effects may play a role. For example, the altered membrane composition in the mutant may affect the amount of t-CIN that accumulates in the membrane and/or the interaction of t-CIN with membrane proteins. As a result, it could be that the functionality or permeability of the membrane is more sensitive to disturbance by t-CIN in the mutant than in the WT.

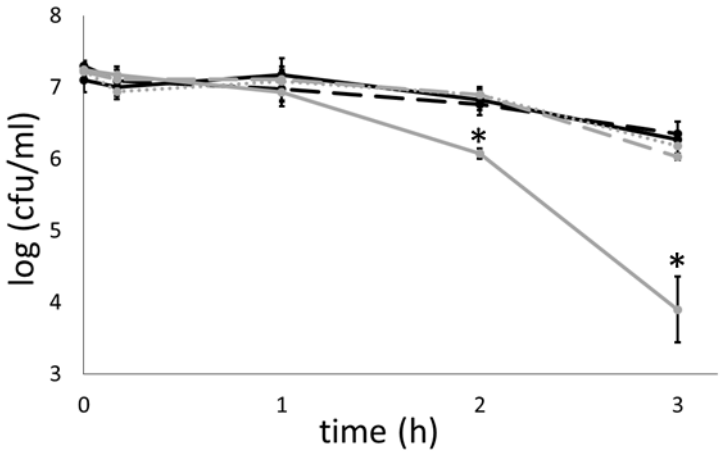

Fig. 3.6. Inactivation of WT (black lines) and *ilvE::Himar1* (grey lines) diluted stationary cultures by 6 mM t-CIN in 10 mM potassium phosphate buffer. Solid lines represent cultures grown overnight without supplementation of 1 mM each of all three α-KAs, dashed lines with supplementation. The grey dotted line represents the complemented mutant *ilvE::Himar1*/pIMK2-*ilvE* without supplementation of α-KAs. The asterisk indicates significant differences with the WT and genetically complemented strain at the same time point.

3.4. Conclusion

The isolation and characterization of an IlvE deficient mutant in this work has provided novel information on the production of BCFAs and on the role of membrane composition on t-CIN sensitivity in *L. monocytogenes* Scott A. Although this strain appears to have an intact pathway for the biosynthesis of BCFAs from Krebs cycle intermediates, our experiments indicate that most BCFAs are produced from branched-chain intermediates (BCAAs, α-KAs, organic acids) acquired from the growth medium. Only limited amounts of BCFAs (especially the anteiso fraction) can be synthesized when these intermediates are not available or cannot be used, as is the case for BCAAs in the IlvE mutant. Further, our results show that *L. monocytogenes* modulates its membrane fatty acid composition in response to sub-MIC concentrations of t-CIN, confirming similar observations for t-CIN and other small hydrophobic α, β-unsaturated carbonyl compounds in a range of bacteria [110,113,114]. The observed changes suggest an adaptation to compensate for the fluidizing effect of t-CIN on the membrane. Our work also provides direct evidence that membrane fatty acid composition is a critical determinant of t-CIN sensitivity. Further work will be required to determine whether this sensitivity results from an increased diffusion rate of t-CIN towards the cytosol or from an increased accumulation of t-CIN in the membrane itself.

Chapter 4

Isolation and characterization of *ilvE::Himar1* revertants with partially restored *trans*-cinnamaldehyde tolerance

4.1. Introduction

During characterization experiments of the *ilvE* mutant we observed that the colonies of this mutant were paler white than those of the Scott A WT strain, and that they became transparent after a few days of storage at 4 °C. In one specific experiment where cultures were grown in BHI with t-CIN and subsequently spread-plated on BHI agar plates, colonies with reverted WT-like morphology were detected. After confirmation of the presence of the *Himar1* transposon, these "revertants" of the *ilvE* mutant additionally showed a reduced lag phase during growth in t-CIN, suggesting that one or more mutations had suppressed the t-CIN sensitive phenotype. Whole-genome sequence analysis of two independent revertants revealed two different single nucleotide substitution mutations in the transcriptional regulator CodY. Because identifying suppressor mutations in a hypersensitive mutant can contribute to a better understanding of the mode of action of t-CIN but also the impact of the *ilvE* knockout on the metabolism, we used a more standardized approach to isolate and characterize additional revertants in this chapter.

4.2. Materials and methods

4.2.1. Bacterial strains, plasmids, oligo's and growth conditions

All bacterial strains were routinely cultured under the same conditions mentioned in chapter 2, section 2.2.1. All used strains and plasmids are mentioned in Table 4.1. All used oligonucleotide primers are listed in Table 4.2. Strains 10403S and its *codY* deletion mutant were obtained from A. Herskovits (Tel Aviv University). Kinetic growth parameters were determined as described in chapter 2, section 2.2.4. To study the role of the transcriptional regulator ArgR, 5 mM L-arginine (Merck, Darmstadt, Germany) was supplemented to growing cultures. Growth assays at 10 °C were performed according to the protocol described in chapter 3, section 3.2.4.

Table 4.2. Oligonucleotide primers used in this chapter

Primer	Sequence (5' – 3')[a]	Reference
codY_seq_F	GAAGCACCAGAAATCAATATGG	This chapter
codY_seq_R	CATTTGATCGGTTTCTGCATAG	This chapter
argR_seq_F	GTGATGTTTTCCGGTTTTTGC	This chapter
argR_seq_R	CGCATCAATAATAATTGATTTACCAGC	This chapter
ack_seq_F	AAGTCTGAACAAGCACGAAAAAGC	This chapter
ack_seq_R	CGCTGTAGAACGTTTGTTAATTGG	This chapter
argR_NcoI	CATCCATGGGAAATAAAGGTCATCGTCATATTATTATTCG	This chapter
argR_SalI	CACTGTCGACTTAAAGCATATCTATAAAACGATCTGTTAATG	This chapter
ack_Klenow_F	/5'Phos/GAAGGAATTGACAAAAACAAAATGG	This chapter
ack_Klenow_R	/5'Phos/TTAGTGATTGTTTTTAATTGTTTCTACATCACG	This chapter
pIMK_REV	CCTATCACCTCAAATGGTTCG	This chapter
pIMK_FW	GAGTCAGTGAGCGAGGAAGC	This chapter
NC16	GTCAAAACATACGCTCTTATC	[129]

[a] Restriction sites are underlined: NcoI (CCATGG) and SalI (GTCGAC)

Table 4.1. Strains and plasmids used in this chapter.

Strain or plasmid	Relevant features	Reference
Strains		
L. monocytogenes		
Scott A	Serovar 4b clinical isolate from the 1983 listeriosis outbreak in Massachusetts	[122]
Scott A *ilvE::Himar1*	*Himar1* transposon insertion in *ilvE*	Chapter 2
ilvE::Himar1 codY1	CodY Phe98Ser	This chapter
ilvE::Himar1 codY2	CodY Arg167Ser	This chapter
ilvE::Himar1 codY3	CodY Arg214Leu	This chapter
ilvE::Himar1 argR1	GA insertion in *argR*	This chapter
ilvE::Himar1 argR2	TTGA deletion in *argR*	This chapter
ilvE::Himar1 argR3	G → T substitution, premature stop codon	This chapter
ilvE::Himar1 argR4	T deletion in *argR*	This chapter
ilvE::Himar1 ack1	4339 bp deletion among which *ack*	This chapter
ilvE::Himar1 ack2	Ack Arg346Cys	This chapter
ilvE::Himar1 ack3	T deletion in *ack*	This chapter
10403S	Serovar 1/2a, streptomycin resistant derivative of 10403, isolated from human skin lesions	[145]
10403S *ΔcodY*	*codY* deletion mutant	[146]
E. coli		
S17-1 λ*pir*	*pro thi recA hsdR*$^-$ *hsdM*$^+$ RP4: 2-Tc:Mu: Km Tn7 λ*pir*	[121]
DH5-α	F$^-$ *endA1 hsdR17* (r_k^-, m_k^+) *supE44 thi*$^-$*1* λ$^-$ *recA1 gyrA96 relA1 deoR* Δ(*lacZYA-argF*)U169 Φ80d *lacZ*ΔM15	[123]
Plasmids		
pIMK2	Site-specific listerial integrative vector, Phelp promoter for constitutive overexpression, 6.2 kb, Km^R	[125]
pIMK3	Site-specific listerial integrative vector, consensus lacOid sequence inserted between P_{CP25} promoter (containing -35 and -10 regions) and the downstream 5' untranslated region of the *hlyA* gene for high-level IPTG controlled gene expression, 7.5 kb, Km^R	[125]

4.2.2. Whole-genome sequencing

After confirmation of the reverted phenotype of revertants of *ilvE::Himar1* via growth assays with t-CIN (chapter 2, section 2.2.4), the gDNA from the revertants was isolated from overnight cultures using the GeneJET Genomic DNA purification kit (Thermo Scientific). DNA purity and concentration was assessed by Nanodrop analysis, gel electrophoresis and Qubit (Thermo Scientific) analysis. Paired-end libraries were constructed using the NEBNext Ultra

gDNA library prep protocol with an average insert size of 240 bp, and analyzed on the Agilent BioAnalyzer (VIB nucleomics core, Belgium). Sequencing was performed on an Illumina MiSeq sequencer, resulting in on average 1.05 million reads per sample. Reads were analyzed with Qiagen's CLC Genomics Workbench (v.7) (CLC Bio, Aarhus, Denmark), and included standard quality control, read trimming and filtering (reads < 15 nucleotides were discarded, quality score limit=0.01, ambiguous nucleotides trim limit = 2), read mapping to *L. monocytogenes* Scott A reference (NCBI accession number CM001159-1) using parameters: mismatch cost=2, insertion cost=3, deletion cost=3, length fraction=0.8, similarity fraction=0.8). Lists of mutations were obtained by combining CLC's tools: 'Fixed Ploidy Variant Detection' for point mutations and small INDELs and 'Coverage Analysis' and 'InDels and structural variants' for larger structural rearrangements. Called SNPs were filtered using a minimum coverage of 10 and a presence frequency of a specific mutation of 75%. Structural variations like insertions and deletions were identified using coverage and breakpoint analysis tools. In addition, all potential mutations were manually inspected in the mapping.

4.2.3. Colony PCR and sanger sequencing

Some revertants that were not analyzed by WGS were subjected to targeted colony PCR's using primer pairs codY_seq_F and codY_seq_R, argR_seq_F and argR_seq_R or ack_seq_F and ack_seq_R. These primers anneal 100 – 150 bp away from the start codon (seq_F primers) or stop codon (seq_R primers) from the targeted gene. PCR products were sequenced via Sanger sequencing using the seq_F and seq_R primers in two different sequencing samples (Macrogen Europe, Amsterdam, Netherlands).

4.2.4. Whole-cell fatty acid analysis

The whole-cell fatty acid compositions of stationary-phase *ilvE::Himar1* revertants cultured at 30 °C in BHI broth were determined as described in chapter 3, section 3.2.5.

4.2.5. Genetic complementation

Genetic complementation of revertant *ilvE::Himar1 argR1*, *ack1* and *ack2* was performed using the pIMK3 integration plasmid with a high level IPTG controlled promoter [125]. The WT *argR* gene was amplified using gene specific primers mentioned in Table 4.2, and cloned as an NcoI-SalI fragment into pIMK3, which was first linearized with the same restriction enzymes. For cloning of the WT *ack* gene, the pIMK3 plasmid was cut with NcoI, resulting in 5' overhangs which were filled in using DNA Polymerase I, Large (Klenow) Fragment. The WT *ack* gene was

amplified using the 5' phosphorylated primers mentioned in Table 4.2 and cloned into cut pIMK3 via blunt-end ligation. The resulting plasmids were conjugated from *E. coli* S17-1 λ*pir* to *L. monocytogenes ilvE::Himar1 argR1* or *ilvE::Himar1 ack1 and ack2*, using selection for Km (pIMK3 marker) and Em (transposon marker). The pIMK3 plasmid does not replicate in *L. monocytogenes*, but, like pIMK2, is designed to integrate specifically in the $tRNA^{Arg}$ gene, which is the unique integration site of the phage PSA in the genome of *L. monocytogenes* Scott A [125,129]. Integration in this site was confirmed via PCR using the gene specific primer provided with the NcoI restriction site and primer NC16. The latter anneals just outside the phage integration site [129]. Additionally, the presence of the intact WT copy in the integrants was confirmed via PCR and Sanger sequencing analysis (Macrogen Europe, Amsterdam, Netherlands) using primers pIMK_FW and pIMK_REV, which anneal at both sides just outside the cloning site of the plasmid (Table 4.2).

4.2.6. Motility assay

Four independent colonies of each strain were stab-inoculated in BHI soft agar plates with 0.2% agar with a toothpick. Plates were incubated at 30 °C for 24 h. Diameters of the bacterial growth zones were measured using a standard ruler to determine the motility of the strains. Pictures were taken with an automatic colony counter (IUL Countermat Flash).

4.2.7. Voges-Proskauer (VP) test and culture pH measurements

The VP test was carried out to evaluate the production of acetoin in stationary-phase cultures, grown anaerobically in a microplate at 30 °C. 100 µl of culture was mixed with 30 µl of 5% α-naphtol and 10 µl of 40% potassium hydroxide in a well of a microtiter plate. After one hour incubation at room temperature, the intensity of the red color that develops in the presence of acetoin was measured spectrophotometrically by absorption at 495 nm in an automated microplate reader (Multiskan Ascent, Thermo lab systems, Helsinki, Finland). The pH of the same cultures used for the VP-test was measured in a microtiter plate with a Double Pore™ Hamilton electrode (FALC Instruments, Treviglio, Italy).

4.2.8. Statistical analysis

Means of the parameter estimates of the Baranyi and Roberts growth model (λ, μ_{max} and OD_{max} [127]), mean percentages of the different fatty acids, mean OD_{495nm} values of the VP-test and the corresponding pH-values were statistically compared by the Tukey-Kramer HSD test with

the JMP® Software (JMP, Version Pro12, SAS Institute Inc., Cary, USA), and considered significantly different when a *p*-value < 0.05 was obtained.

4.3. Results & discussion

4.3.1. Identification of suppressor mutations

Compared to WT, *ilvE* mutants form colonies on BHI agar that are paler white and become more transparent during storage at 4 °C. During a particular experiment, two colony appearance revertants of the *ilvE* mutant were picked up by happenstance after spread-plating an *ilvE::Himar1* culture that was cultured in BHI broth with t-CIN. These revertants were found in only one of three biological replicate cultures. Besides the reverted colony morphology, these revertants also exhibited increased t-CIN tolerance, as documented further on in this chapter. Since these revertants still carried the intact *ilvE::Himar1* allele, we attempted to detect other mutations in the revertants by whole-genome sequence (WGS) analysis. The only mutations found in both revertants were two different single nucleotide substitution mutations in *codY*. These mutants are designated *ilvE::Himar1 codY1* and *ilvE::Himar1 codY2* in the remainder of this chapter.

The identification of suppressor mutations in the *ilvE::Himar1* mutant that lead to a reversal of the mutant phenotype can potentially improve our understanding of the impact of the IlvE knockout on the cellular metabolism, but also of the mode of action of t-CIN and of the cellular adaptation mechanisms to t-CIN. Therefore, a more systematic experiment was set up to investigate (i) the frequency at which revertants emerge and (ii) the spectrum of mutations that lead to increased t-CIN resistance and/or a change in colony morphology in an *ilvE::Himar1* background. The workflow followed to conduct this experiment is presented in Fig. 4.1.

Six biological replicates of *ilvE* mutant cultures were routinely cultured overnight at 30 °C. Each culture was subsequently diluted 1000-fold and cultured both in BHI and BHI with t-CIN. This allows us to determine if revertants also arise in absence of t-CIN. After these first-round cultures reached stationary phase, a part of the cultures was spread-plated on BHI-agar ((1) in Fig. 4.1), while another part was diluted and cultured again in the same conditions ((2) in Fig. 4.1). When these second-round cultures reached stationary phase, they were also spread-plated on BHI agar. Afterwards eight colonies per culture from the spread plates from both the first- and second-round cultures were purified based on colony morphology,

corresponding to a total of 192 colonies. Colony morphologies were categorized in white (WT-like), pale-white (slightly more white than *ilvE::Himar1*) and transparent (*ilvE::Himar1*-like). At least one colony from each morphology type present on the spread plates, was purified from each culture. Afterwards, t-CIN sensitivity of at least one representative purified culture per morphology type was assessed by diluting an overnight BHI culture 1:1000 in BHI with 2 mM t-CIN and monitoring growth at 30 °C (chapter 2, section 2.2.4).

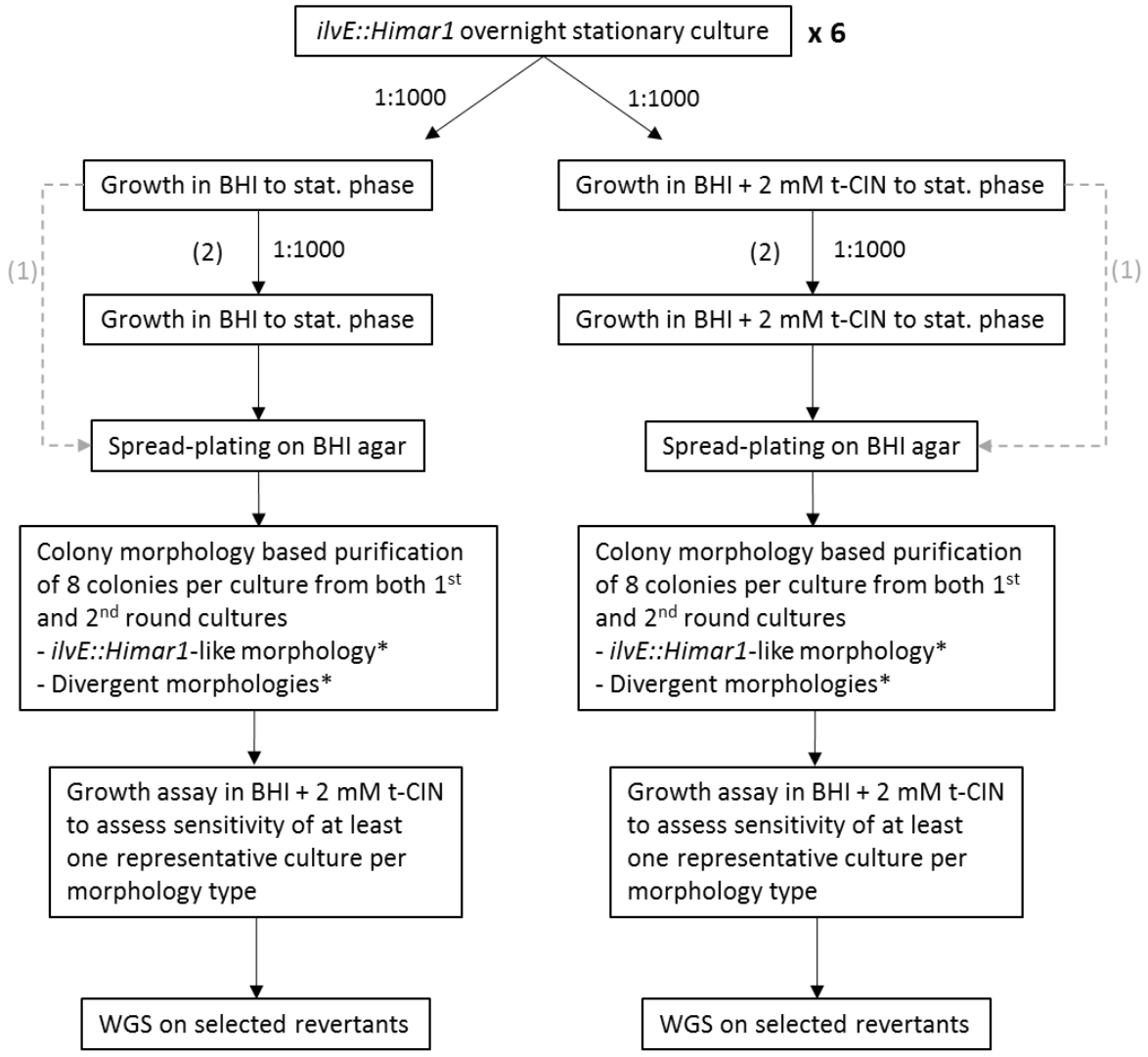

Fig. 4.1. Workflow of the *ilvE::Himar1* revertants isolation experiment. (1) First- round cultures grown in BHI or BHI + 2 mM t-CIN were spread-plated on BHI and (2) recultured in the same medium. * *ilvE::Himar1*-like morphology is transparent, divergent morphologies are white (WT), or intermediate (pale-white).

Table 4.3. shows the percentage of colonies with a morphology divergent from *ilvE::Himar1*, i.e. WT or intermediate colony morphology, from both the first- and second-round cultures grown in BHI with and without t-CIN. Colony counts of these different morphologies were

performed on spread plates with the same dilution. Mutants with a more WT-like morphology emerged in both media and occurred even at higher frequency in the absence than in the presence of t-CIN. Of course, these are not necessarily the same mutants as those emerging in BHI with t-CIN. The mutation frequency in the *ilvE* mutant appears to be high, but it should be noted that the experiment was not designed to determine mutation frequency and may give a false impression. This is because mutants may already have been enriched in the overnight culture, used as inoculum for this experiment and may have been further enriched in the first- and second-round cultures if they had a growth advantage. Therefore, we have determined growth parameter estimates only for second-round cultures (Table 4.4 and 4.5). Strain codes of second-round cultures in BHI are provided with "B", in BHI with t-CIN with "BC". The corresponding growth curves are presented in Supplementary material S2.

Table 4.3. Percentage of colonies from the first- and second-round cultures grown in BHI or BHI + 2 mM t-CIN on BHI agar, showing an *ilvE::Himar1* divergent morphology

Culture nr.	1st round BHI	2nd round BHI	1st round BHI + t-CIN	2nd round BHI + t-CIN
1	0	6.5	0	5.1
2	29.5	68.6	0	0
3	5.3	57.1	0	0
4	0	5.6	5.6	ND*
5	0	0	0	47.3
6	28.4	86.2	0	68.0

*ND: not determined due to technical failure with the spread plate of the specific dilution used for colony count. Yet, colonies with different morphology types could be isolated and purified from other dilutions of culture nr. 4 and were used in further experiments (Table 4.5)

Based on the curves, but particularly on reduced lag phases (λ, Table 4.4 and 4.5), five reverted mutants (marked with an asterisk in Table 4.4 and 4.5) as well as the two revertants picked up earlier (*ilvE::Himar1 codY1* and *ilvE::Himar1 codY2)*, were selected to be analyzed by WGS on an Illumina Miseq sequencer, together with the original *ilvE::Himar1* mutant for comparison.

Table 4.4. Growth parameter estimates in BHI + 2 mM t-CIN of colonies picked up from the second-round cultures of *ilvE::Himar1* grown in BHI (see experiment represented in Fig. 4.1; strain code preceded with B). Colonies were selected based on morphology type: white (wild-type); transparent (*ilvE::Himar1*). Values are means ± standard deviation of three independent biological replicates. All the strains were tested simultaneously on the same day. Curves are presented in Supplementary material S2a.

Strain code	Colony morphology	λ (h)	μ_{max} (1/h)	OD_{max}
B-1.4[a,*]	White	15.4 ± 0.7[B]	0.072 ± 0.001	0.608 ± 0.014
B-1.7	Transparent	24.8 ± 0.6[A]	0.061 ± 0.001	0.556 ± 0.002
B-2.2	Transparent	26.2 ± 0.3[A]	0.059 ± 0.002	0.514 ± 0.031
B-2.6	White	15.7 ± 0.1[B]	0.072 ± 0.000	0.579 ± 0.015
B-3.3*	White	15.4 ± 0.5[B]	0.071 ± 0.002	0.605 ± 0.017
B-3.6	Transparent	24.5 ± 0.8[A]	0.058 ± 0.002	0.549 ± 0.002
B-4.7	Transparent	27.1 ± 0.3[A]	0.059 ± 0.000	0.510 ± 0.028
B-4.8	White	15.2 ± 0.7[B]	0.072 ± 0.003	0.585 ± 0.019
B-5.4	Transparent	24.9 ± 1.0[A]	0.056 ± 0.002	0.529 ± 0.014
B-6.4	Transparent	24.6 ± 0.9[A]	0.059 ± 0.002	0.527 ± 0.009
B-6.7	White	15.5 ± 1.2[B]	0.069 ± 0.001	0.560 ± 0.014
ilvE::Himar1[b]	Transparent	25.5 ± 3.0[A]	0.057 ± 0.002	0.495 ± 0.042
Scott A[b]	White	10.8 ± 0.4[C]	0.082 ± 0.004	0.688 ± 0.043

*mutants selected for WGS analysis; [a] first number before dot is the culture number (1-6), second number after dot is the purified colony (1-8); [b] cultures of *ilvE::Himar1* and Scott A used for this experiment were regular overnight cultures. [A,B,C]Different superscripts for lag phases (λ) indicate significant differences ($p < 0.05$).

Table 4.5. Growth parameter estimates in BHI + 2 mM t-CIN of colonies picked up from second-round cultures of *ilvE::Himar1* grown in BHI + 2 mM t-CIN (see experiment represented in Fig. 4.1; strain code preceded with BC). Colonies were selected based on morphology type: white (Wild-type); pale-white (intermediate); transparent (*ilvE::Himar1*). Values are means ± standard deviation of three independent biological replicates. All the strains were tested simultaneously on the same day. Curves are presented in Supplementary material S2b.

Strain code	Colony morphology	λ (h)	μ_{max} (1/h)	OD_{max}
BC-1.1[a]	Pale-white	$24.2 \pm 1.4^{D,E}$	0.063 ± 0.001	0.501 ± 0.015
BC-1.3	Pale-white	22.1 ± 1.4^{E}	0.055 ± 0.001	0.485 ± 0.005
BC-1.5	Transparent	$28.2 \pm 2.1^{A,B}$	0.059 ± 0.000	0.498 ± 0.007
BC-2.1	Transparent	28.7 ± 0.6^{A}	0.060 ± 0.001	0.501 ± 0.004
BC-3.8	Transparent	$27.1 \pm 1.5^{A,B,C}$	0.062 ± 0.000	0.512 ± 0.010
BC-4.2	Transparent	$25.7 \pm 0.6^{B,C,D}$	0.062 ± 0.000	0.522 ± 0.008
BC-4.4*	Pale-white	18.7 ± 0.6^{F}	0.064 ± 0.001	0.551 ± 0.008
BC-5.2*	Pale-white	19.2 ± 0.3^{F}	0.064 ± 0.003	0.556 ± 0.013
BC-5.7	Pale-white	17.2 ± 0.6^{F}	0.068 ± 0.000	0.555 ± 0.004
BC-6.4	Transparent	17.5 ± 0.7^{F}	0.066 ± 0.001	0.556 ± 0.019
BC-6.5	Transparent	17.5 ± 0.7^{F}	0.066 ± 0.001	0.567 ± 0.003
BC-6.7*	White	22.1 ± 1.0^{E}	0.049 ± 0.001	0.449 ± 0.004
BC-6.8	Transparent	$24.2 \pm 0.7^{D,E}$	0.059 ± 0.004	0.496 ± 0.030
ilvE::Himar1[b]	Transparent	$24.9 \pm 0.5^{C,D,E}$	0.061 ± 0.000	0.537 ± 0.002
Scott A[b]	White	10.3 ± 0.1^{G}	0.089 ± 0.003	0.729 ± 0.050

*mutants selected for WGS; [a] first number before dot is the culture number (1-6), second number after dot is the purified cfu (1-8); [b]cultures of *ilvE::Himar1* and Scott A used for this experiment were regular overnight cultures. ^{A,B,C,D,E}Different superscripts for lag phases (λ) indicate significant differences ($p < 0.05$).

After whole-genome sequencing, sequences of all reverted mutants were mapped to the reference genome of *L. monocytogenes* Scott A and compared to the whole-genome sequences of *ilvE::Himar1*. Table 4.6 shows the identified mutations in the different revertants. All identified revertants harboured only one mutation, in either of three genes: *codY*, *argR* or *ack*.

Table 4.6. Mutational changes in *L. monocytogenes ilvE::Himar1* induced by two rounds of growth in BHI with or without t-CIN. Mutations of strains listed under the grey line are determined via Sanger sequencing; these strains are not analyzed via WGS.

Strain[1]	Isolation medium	Strain code [2]	Mutation	Predicted protein	Protein/gene modification	Location [3]	Locus taq [3]
ilvE::Himar1 codY1	BHI + t-CIN	/	T → C	Transcriptional repressor CodY	Phe98Ser	1362406	LMOSA_22040
ilvE::Himar1 codY2	BHI + t-CIN	/	C → A	Transcriptional repressor CodY	Arg167Ser	1362612	LMOSA_22040
ilvE::Himar1 codY3	BHI + t-CIN	BC-6.7	G → T	Transcriptional repressor CodY	Arg214Leu	1362754	LMOSA_22040
ilvE::Himar1 argR1	BHI	B-1.4	Insertion GA	Arginine repressor ArgR	Frameshift	1445335^1445336	LMOSA_22880
ilvE::Himar1 argR2	BHI	B-3.3	Deletion TTGA	Arginine repressor ArgR	Frameshift	1445516-1445519	LMOSA_22880
ilvE::Himar1 ack1	BHI + t-CIN	BC-4.4	4349 bp deletion	Multiple proteins[4], including acetate kinase Ack	Deletion multiple genes	1674804-1679152	Multiple[4]
ilvE::Himar1 ack2	BHI + t-CIN	BC-5.2	G → A	Acetate kinase Ack	Arg346Cys	1678330	LMOSA_25030
ilvE::Himar1 argR3	BHI	B-4.8	G → T	Arginine repressor ArgR	Premature stop codon	1445623	LMOSA_22880
ilvE::Himar1 argR4	BHI	B-6.7	Deletion T	Arginine repressor ArgR	Frameshift	1445303	LMOSA_22880
ilvE::Himar1 ack3	BHI + t-CIN	BC-5.7	Deletion T	Acetate kinase Ack	Frameshift	1678047	LMOSA_25030

Mean read lengths were estimated to be 150 bp. Total read counts varied between 898761 and 1139615 bp. The average genome coverage varied between 43.42-fold and 55.2-fold coverage. [1]All sequenced mutants originate from *L. monocytogenes* Scott A *ilvE::Himar1* and are designated with a new name according to the protein that is affected by the mutation; [2]strain codes mentioned in Table 4.4 (BHI) and 4.5 (BHI + t-CIN) [3]in parental *L. monocytogenes* Scott A; [4]Universal stress protein family protein, alanine dehydrogenase, proline dipeptidase, acetate kinase and metal dependent hydrolase

The *codY, argR* and *ack* genes of all other revertants, that showed increased t-CIN resistance based on lag phase reduction, but that were not analyzed via WGS (strains B-2.6, B-4.8 and B-6.7 from Table 4.4, and strains BC-5.7, BC-6.4 and BC-6.5 from Table 4.5), were determined by Sanger sequencing of PCR amplicons. This yielded three more mutants, listed in Table 4.6 underneath the grey line. Two of these mutants which were isolated after two rounds of growth in BHI, harboured mutations in *argR* (strains B-4.8 and B-6.7 from Table 4.4). The third additional mutant which was cultured for two rounds in BHI with t-CIN, had a mutation in the *ack* gene (strain BC-5.7 from Table 4.5). For strains BC-6.4 and BC-6.5, no mutations were found in *codY, argR* or *ack*, and these strains may therefore have a different reversion mutation. Strain B-2.6 did not have mutations in *codY* or *ack*, but its *argR* gene did not produce a PCR product, indicating that at least part of the gene and its flanking region may be deleted. The phenotype of this revertant is therefore probably caused by *argR* knockout.

Interestingly, the results suggest that different mutations emerge in cultures grown in BHI or BHI with t-CIN. *ilvE::Himar1 argR* revertants were only isolated after growth in BHI without t-CIN, while *ilvE::Himar1 codY and ilvE::Himar1 ack* revertants only appeared in the presence of t-CIN.

Moreover, all mutations in *codY* and *argR* are accompanied by a reverted colony morphology type to WT level, while all *ilvE::Himar1 ack* revertants have a slightly more white, but still very *ilvE::Himar1*-like transparent morphology. An intriguing observation relates to the type of mutations. The mutations in *codY* are all amino acid substitution mutations, while the mutations in *argR* are either frameshifts or premature stop codons. The mutations in *ack* are of different types. The number of analyzed mutants is perhaps too small to exclude coincidence, but it is tempting to speculate that the CodY mutations do not result in complete loss of function but modulate the function of CodY in a subtle way. Additional analysis of these mutants supports this idea (see section 4.3.3).

4.3.2. Detailed phenotypical analysis of *ilvE::Himar1* revertants

To evaluate the impact of the different suppressor mutations in the *ilvE::Himar1* revertants, two phenotypes were analyzed for all whole-genome sequenced revertants: growth in BHI with t-CIN and growth in BHI at 10 °C without t-CIN. Growth in the presence of t-CIN and at 10 °C require cells to adapt the membrane fatty acid composition and were used to characterize the *ilvE* mutant in chapter 3. Because the *ilvE* transposon knockout mainly impairs the BCFA synthesis in *L. monocytogenes*, repressor mutations are predicted to result in at least partial recovered capacity of BCFAs biosynthesis.

4.3.2.1. Growth in t-CIN

Growth of the WGS-analyzed revertants in BHI without and with t-CIN was compared with growth of WT and *ilvE* mutant in one single experiment with three biological replicates of each strain. This allows us to mutually compare the sensitivity for t-CIN of all revertants with each other and the WT and *ilvE* mutant. Because initial cell concentration may affect the inhibitory effect of t-CIN, the stationary-phase cultures, used as inoculum for the growth assays with t-CIN, were diluted and brought to the same cell concentration of approximately 10^6 cfu/ml to ensure that the amount of available t-CIN per cell was equal for all strains. Therefore, the results shown in this paragraph contain new information compared to the data in Table 4.4 and 4.5 where differences in cell numbers were not taken into account during the screening for revertants. Growth curves and growth parameter analysis of the *ilvE::Himar1 codY, argR* and *ack* revertants cultured in BHI and BHI with t-CIN of are shown in Fig. 4.2, 4.3 and 4.4 respectively.

Lag phases of revertants *ilvE::Himar1 codY1* (25.2 h) and *ilvE::Himar1 codY2* (28.9 h) have become much shorter than the lag phase of the *ilvE* mutant (45.8 h), but they are still significantly longer than the WT lag phase (16.7 h) (Fig. 4.2). The lag phase of *ilvE::Himar1 codY3* (40.6 h) is also reduced compared to the *ilvE* mutant, but less so than in the *ilvE::Himar1 codY1 and codY2* revertants. Moreover, the lag phase of *ilvE::Himar1 codY3* is even longer than that of the *ilvE* mutant in BHI without t-CIN, while those of *ilvE::Himar1 codY1 and codY2* do not differ significantly from the *ilvE* mutant. For growth in t-CIN, the μ_{max} and OD_{max} of the *ilvE::Himar1 codY* revertants do not differ significantly from the *ilvE* mutant. Consequently, growth of *ilvE::Himar1 codY* revertants in t-CIN is only characterized by partially reverted lag phases.

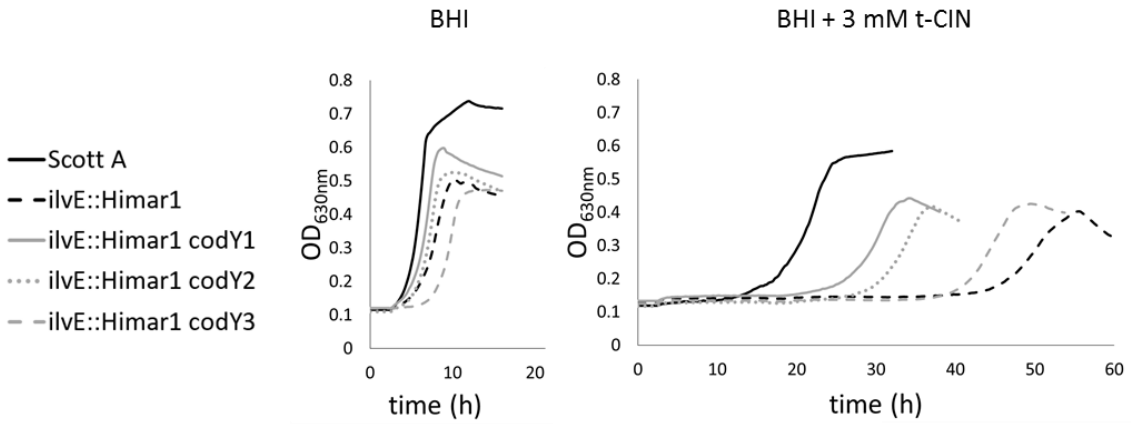

Strain	BHI			BHI + 3 mM t-CIN		
	λ (h)	μ_{max} (1/h)	OD_{max}	λ (h)	μ_{max} (1/h)	OD_{max}
Scott A	4.2 ± 0.0^{C}	0.198 ± 0.002^{A}	0.729 ± 0.010^{A}	16.7 ± 0.6^{E}	0.054 ± 0.004^{A}	0.566 ± 0.015^{A}
ilvE::Himar1	5.2 ± 0.0^{B}	0.090 ± 0.005^{C}	0.506 ± 0.015^{C}	45.8 ± 2.4^{A}	0.036 ± 0.001^{B}	0.432 ± 0.010^{B}
ilvE::Himar1 codY1	4.8 ± 0.1^{B}	0.143 ± 0.015^{B}	0.599 ± 0.006^{B}	25.2 ± 0.6^{D}	0.038 ± 0.001^{B}	0.446 ± 0.005^{B}
ilvE::Himar1 codY2	5.0 ± 0.4^{B}	0.120 ± 0.021^{B,C}	0.525 ± 0.008^{C}	28.9 ± 0.9^{C}	0.039 ± 0.001^{B}	0.424 ± 0.012^{B}
ilvE::Himar1 codY3	7.6 ± 0.2^{A}	0.111 ± 0.001^{C}	0.470 ± 0.008^{D}	40.6 ± 1.6^{B}	0.046 ± 0.001^{B}	0.425 ± 0.008^{B}

Fig. 4.2. Growth curves of *L. monocytogenes* Scott A, its *ilvE::Himar1* mutant and the *ilvE::Himar1 codY* revertants in BHI and BHI with 3 mM t-CIN. All curves are the average of three independent cultures. Standard deviations have been omitted for clarity. Lag phases (λ), maximum growth rate (μ_{max}) and maximal optical densities (OD_{max}) corresponding to the curves above are mentioned in the table. Values are means ± standard deviation. ^{A,B,C,D,E} different superscripts indicate significant differences ($p < 0.05$).

Revertants *ilvE::Himar1 argR1 and argR2* also have a reduced lag phase in BHI with t-CIN, 30.3 h and 28.4 h respectively (Fig. 4.3). In comparison to the *ilvE::Himar1 codY and ack* revertants (Fig. 4.4), the growth curve shape of the *ilvE::Himar1 argR* revertants resembles again much more the WT curve shape, both in BHI and BHI with t-CIN. In particular, they reach higher OD_{max}-values compared to the *ilvE* mutant and the *ilvE::Himar1 codY* and *ack* revertants in both growth media.

Of all revertants, *ilvE::Himar1 ack1* and *ack2* have the shortest lag phase for growth in t-CIN, 20.2 h and 23.1 h respectively (Fig. 4.4). Remarkably, the lag phases of both *ilvE::Himar1 ack* revertants in BHI without t-CIN is slightly but significantly longer than that of the *ilvE* mutant.

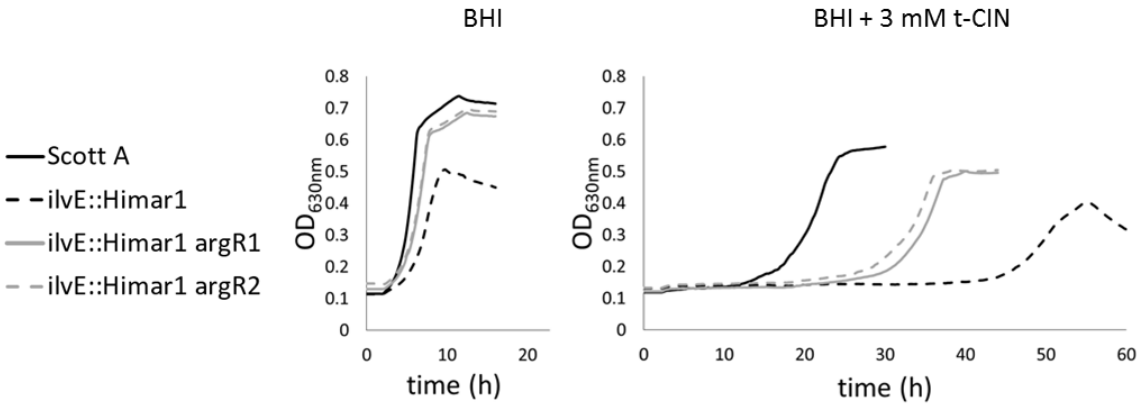

Strain	BHI			BHI + 3 mM t-CIN		
	λ (h)	μ_{max} (1/h)	OD_{max}	λ (h)	μ_{max} (1/h)	OD_{max}
Scott A	4.2 ± 0.0^{A}	0.198 ± 0.002^{A}	0.729 ± 0.010^{A}	16.7 ± 0.6^{A}	0.054 ± 0.004^{A}	0.566 ± 0.015^{A}
ilvE::Himar1	5.2 ± 0.0^{C}	0.090 ± 0.005^{C}	0.506 ± 0.015^{C}	45.8 ± 2.4^{C}	0.036 ± 0.001^{C}	0.432 ± 0.010^{C}
ilvE::Himar1 argR1	4.8 ± 0.0^{B}	0.141 ± 0.001^{B}	0.685 ± 0.011^{B}	30.3 ± 0.1^{B}	0.045 ± 0.002^{B}	0.502 ± 0.011^{B}
ilvE::Himar1 argR2	4.8 ± 0.0^{B}	0.142 ± 0.000^{B}	0.699 ± 0.006^{B}	28.4 ± 0.6^{B}	0.040 ± 0.003^{B,C}	0.508 ± 0.001^{B}

Fig. 4.3. Growth curves of *L. monocytogenes* Scott A, its *ilvE::Himar1* mutant and the *ilvE::Himar1 argR* revertants in BHI and BHI with 3 mM t-CIN. All curves are the average of three independent cultures. Standard deviations have been omitted for clarity. Lag phases (λ), maximum growth rate (μ_{max}) and maximal optical densities (OD_{max}) corresponding to the curves above are mentioned in the table. Values are means ± standard deviation. ^{A,B,C} different superscripts indicate significant differences ($p < 0.05$).

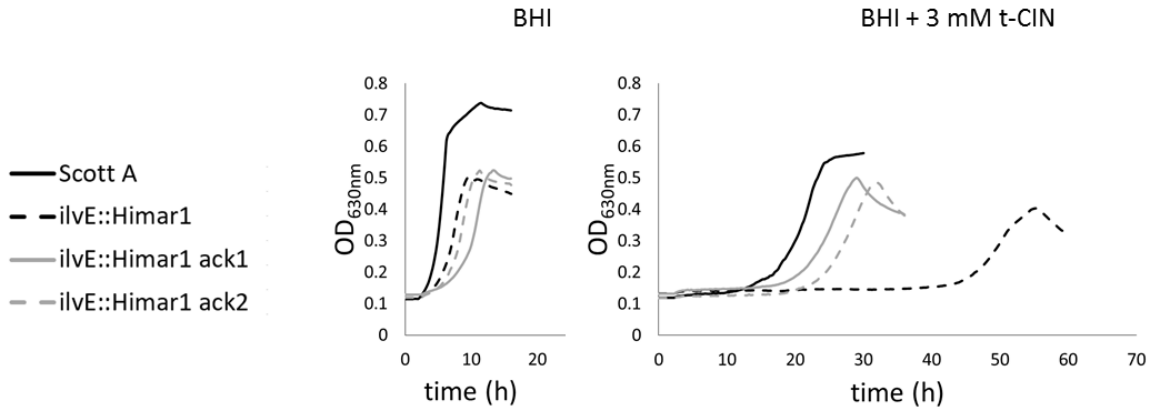

Strain	BHI			BHI + 3 mM t-CIN		
	λ (h)	μ_{max} (1/h)	OD_{max}	λ (h)	μ_{max} (1/h)	OD_{max}
Scott A	4.2 ± 0.0^{A}	0.198 ± 0.002^{A}	0.729 ± 0.010^{A}	16.7 ± 0.6^{A}	0.054 ± 0.004^{A}	0.566 ± 0.015^{A}
ilvE::Himar1	5.2 ± 0.0^{B}	0.090 ± 0.005^{B}	0.506 ± 0.015^{B}	45.8 ± 2.4^{C}	0.036 ± 0.001^{C}	0.432 ± 0.010^{B}
ilvE::Himar1 ack1	7.7 ± 0.4^{C}	0.074 ± 0.002^{C}	0.527 ± 0.008^{B}	20.2 ± 0.3^{B}	0.041 ± 0.001^{B,C}	0.503 ± 0.003^{C}
ilvE::Himar1 ack2	6.0 ± 0.3^{D}	0.086 ± 0.006^{B}	0.524 ± 0.016^{B}	23.1 ± 0.7^{B}	0.043 ± 0.001^{B}	0.496 ± 0.009^{C}

Fig. 4.4. Growth curves of *L. monocytogenes* Scott A, its *ilvE::Himar1* mutant and the *ilvE::Himar1 ack* revertants in BHI and BHI with 3 mM t-CIN. All curves are the average of three independent cultures. Standard deviations have been omitted for clarity. Lag phases (λ), maximum growth rate (μ_{max}) and maximal optical densities (OD_{max}) corresponding to the curves above are mentioned the table. Values are means ± standard deviation. ^{A,B,C} different superscripts indicate significant differences ($p < 0.05$).

4.3.2.2. Growth at 10 °C

The *ilvE* mutant also showed strongly impaired growth in BHI at 10 °C compared to the WT because of the nearly complete loss of anteiso-BCFAs (Fig. 3.5 and Table 3.3, chapter 3). Here, we evaluated the growth at 10 °C of the revertants because this may indicate that they had regained the ability to incorporate BCFAs in their membrane. Growth at 10 °C was assessed for all revertants in one experiment, but is shown in three different figures for improved clarity. The growth curves for WT and *ilvE* mutant are the same in Fig. 4.5 (a-c).

(a)

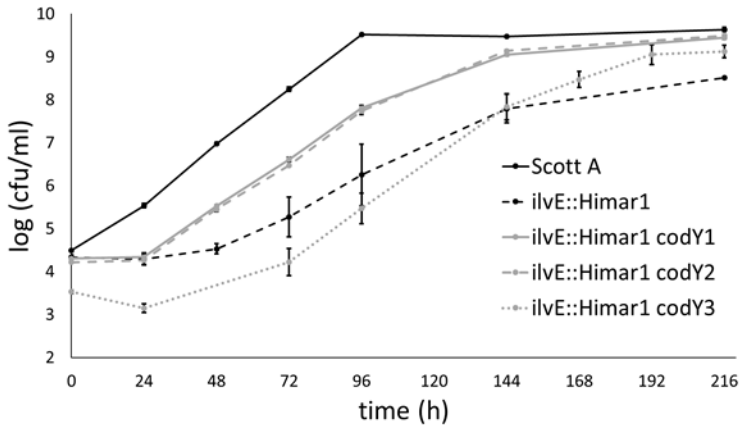

(b)

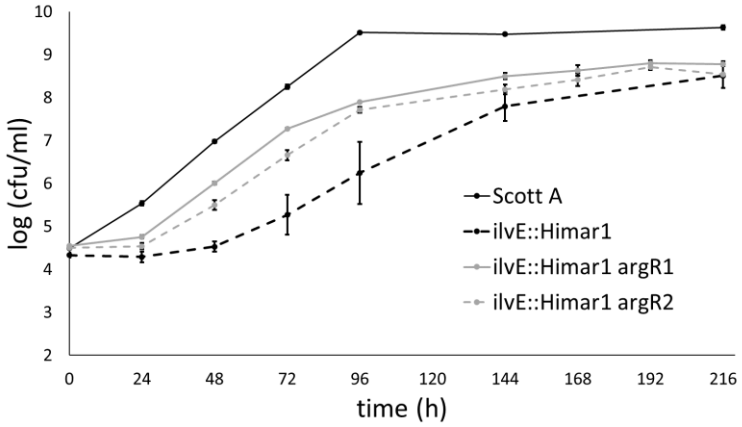

(c)

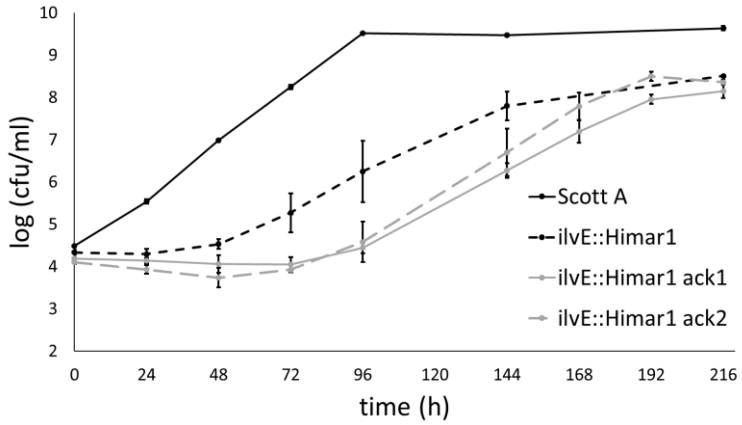

Fig. 4.5. Growth of *L. monocytogenes* Scott A, its *ilvE::Himar1* mutant, the *ilvE::Himar1 codY* revertants (a), the *ilvE::Himar1 argR* revertants (b) and *ilvE::Himar1 ack* revertants (c) in BHI broth at 10 °C. Growth curves of Scott A and the *ilvE* mutant are the same in each graph.

All *ilvE::Himar1 codY* revertants showed faster exponential growth and reached higher cell concentrations in stationary phase than the *ilvE* mutant in BHI broth at 10 °C. Revertants *ilvE::Himar1 codY1* and *codY2* also had a shorter lag phase. Remarkably, the initial cell concentration of *ilvE::Himar1 codY3* is lower than for all other strains (Fig. 4.5a). Because all cultures are equally diluted before the start of the growth assay at 10 °C, this means that *ilvE::Himar1 codY3* overnight stationary cultures, grown at 30 °C, reach lower cell concentrations. Therefore, we can conclude that all *codY* mutations in *ilvE::Himar1* result in improved growth at 10 °C, even though mutations in *ilvE::Himar1 codY1* and *codY2* appear to be more advantageous.

Revertants *ilvE::Himar1 argR1* and *argR2* also appear to have a shorter lag phase than the *ilvE* mutant (Fig. 4.5b), but reach remarkably lower cell concentrations in stationary phase compared to the WT and the *ilvE::Himar1 codY* revertants. Yet *ilvE::Himar1* argR1 and *argR2* reach the same stationary-phase cell concentration as the WT after overnight growth in the same BHI broth at 30 °C. This can be derived from the equal initial inoculum concentrations at the start of this growth experiment.

In contrast to the *ilvE::Himar1 codY* and *argR* revertants, the *ilvE::Himar1 ack1* and *ack2* revertants show decreased growth performance at 10 °C (Fig. 4.5c), with even longer lag phases than the *ilvE* mutant. The exponential growth rate and stationary-phase cell concentrations seem to be unchanged.

4.2.2.3. Whole-cell fatty acid analyses

Fatty acid compositions of stationary-phase cultures, cultured in BHI broth at 30 °C, of the WT Scott A, the *ilvE* mutant and its revertants *ilvE::Himar1 codY1, argR1, ack1* and *ack2* are listed in Table 4.7. Only a subset of the revertants was analyzed because fatty acid analysis is relatively expensive.

In *ilvE::Himar1 codY1* the total amount of BCFAs is similar to that in the *ilvE* mutant, but there is a shift from iso to anteiso-BCFA resulting in an iso/anteiso ratio of 1.5 compared to 12.2 in the *ilvE* mutant. As discussed in chapter 3, especially anteiso-BCFA are very important determinants of membrane fluidity because their phase-transition temperature is twice as low as that of the iso forms of the same chain length. Membranes of *ilvE::Himar1 codY1* are therefore predicted to have partly regained the fluidity of the WT membrane, and this most likely explains the improved growth at 10 °C. The shift of the membrane composition of

ilvE::Himar1 codY1 may also be the reason for the partly regained resistance to t-CIN. The way in which CodY mutations affect the BCFA synthesis pathway is further discussed in part 4.3.3.

In *ilvE::Himar1 argR1* the total amount of BCFAs increased from 53.7% in the *ilvE* mutant to 79.7% in the revertant. This increase is completely attributed to the increase in odd-numbered iso-BCFA, especially iso-C15:0, and to a lesser extent also iso-C13:0 and iso-C17:0 . The even-numbered iso-BCFAs slightly decreased. Together this leads to an increase in iso-BCFAs from 53.7% to 79.7%. This causes the iso/anteiso ratio to shift to an even higher value. The amounts of anteiso-BCFA remain unchanged, just like the amounts of FA with C < 15. Therefore the increase of 26% in total BCFA is predicted to make the membranes more fluid than those of the *ilvE* mutant, and this may explain the increased growth rate at 10 °C. These alterations in fatty acid composition may also contribute to increased t-CIN resistance.

Similar to *ilvE::Himar1 argR1*, the group of iso-BCFAs has increased in *ilvE::Himar1 ack1*, though this time mainly the even numbered iso-BCFA iso-C14:0 and iso-C16:0 are responsible. These increases are at the expense of reduced amounts of straight-chain fatty acids C14:0 and C16:0. Again, the increased amounts of iso-BCFAs could be the reason for increased t-CIN resistance of *ilvE::Himar1 ack1*. However, the fatty acid composition of *ilvE::Himar1 ack2* remains virtually unchanged compared to that of the *ilvE* mutant, while *ilvE::Himar1 ack1* and *ack2* have very similar phenotypes for growth in the presence of t-CIN and at 10 °C. This means that the increase in iso-C14:0 and iso-C16:0 does not improve *ilvE::Himar1 ack1* growth at 10 °C, but it interestingly also implies that the *ack* mutations render the *ilvE* mutant more resistant to t-CIN without clear changes in the membrane fatty composition and fluidity.

In summary, mutations in *ilvE::Himar1 codY1* and *argR* lead to clear changes in the membrane fatty acid composition that most probably contribute to increased growth performance at 10 °C and increased resistance towards t-CIN. However, since increased t-CIN resistance is uncoupled from membrane fatty acid composition and growth at 10 °C in the *ilvE::Himar1 ack* revertants, a different mechanism must be at the basis of the increased t-CIN resistance of this mutant, and it will be interesting to investigate this further.

Table 4.7. Percentage of total whole-cell fatty acids of stationary cultures of Scott A, *ilvE::Himar1* and its revertants *codY1, argR1, ack1* and , cultured in BHI at 30 °C. Summary data are shown at the bottom of the table. Values are mean ± standard deviation. Means are calculated from the whole-cell fatty acid analysis of three independent cultures. Most dominant FA fractions in Scott A are framed in grey.

Fatty acid	Scott A	*ilvE::Himar1*	*ilvE::Himar1 codY1*	*ilvE::Himar1 argR1*	*ilvE::Himar1 ack1*	*ilvE::Himar1 ack2*
C10:0	0.1 ± 0.1^{B}	0.0 ± 0.0^{C}	0.0 ± 0.0^{C}	0.2 ± 0.0^{A}	0.0 ± 0.0^{C}	0.0 ± 0.0^{C}
Iso-C11:0	0.0 ± 0.0^{B}	0.0 ± 0.0^{B}	0.0 ± 0.0^{B}	0.2 ± 0.1^{A}	0.0 ± 0.0^{B}	0.0 ± 0.0^{B}
C12:0	1.4 ± 0.2^{C}	4.1 ± 0.5^{A}	2.4 ± 0.2^{B}	2.6 ± 0.1^{B}	5.1 ± 0.9^{A}	2.9 ± 0.1^{B}
Iso-C13:0	0.0 ± 0.0^{B}	0.4 ± 0.0^{B}	0.3 ± 0.3^{B}	4.7 ± 0.2^{A}	0.2 ± 0.2^{B}	0.5 ± 0.0^{B}
Anteiso-C13:0	0.0 ± 0.0^{A}	0.0 ± 0.0^{A}	0.1 ± 0.2^{A}	0.0 ± 0.1^{A}	0.0 ± 0.0^{A}	0.0 ± 0.0^{A}
C13:0	0.0 ± 0.0^{B}	0.0 ± 0.0^{B}	0.7 ± 0.1^{A}	0.0 ± 0.0^{B}	0.0 ± 0.0^{B}	0.1 ± 0.1^{B}
Iso-C14:0	0.6 ± 0.0^{D}	9.9 ± 1.6^{B}	7.9 ± 0.1^{B,C}	4.6 ± 0.2^{C}	15.9 ± 2.6^{A}	8.5 ± 0.6^{B}
C14:1 ω5c	0.0 ± 0.0^{B}	0.1 ± 0.2^{B}	0.1 ± 0.1^{B}	0.2 ± 0.2^{B}	0.7 ± 0.2^{A}	0.5 ± 0.1^{A,B}
C14:0	0.5 ± 0.1^{D}	11.6 ± 0.8^{B}	20.3 ± 1.7^{A}	5.7 ± 0.1^{C}	6.2 ± 0.6^{C}	12.4 ± 0.4^{B}
Iso-C15:0	10.9 ± 0.4^{D}	17.1 ± 3.9^{B,C}	9.0 ± 1.0^{D}	53.3 ± 0.5^{A}	13.9 ± 2.2^{C,D}	19.2 ± 0.6^{B}
Anteiso-C15:0	29.9 ± 1.0^{A}	2.6 ± 0.2^{C}	12.9 ± 3.9^{B}	2.4 ± 0.3^{C}	3.2 ± 0.6^{C}	2.6 ± 0.2^{C}
Iso-C16:0	2.8 ± 0.1^{E}	16.7 ± 1.6^{B}	9.2 ± 0.9^{C}	5.9 ± 0.1^{D}	28.5 ± 1.9^{A}	11.9 ± 1.0^{C}
C16:0	2.1 ± 0.1^{C}	27.6 ± 2.3^{A}	28.3 ± 3.7^{A}	10.1 ± 0.1^{B}	14.6 ± 3.3^{B}	30.0 ± 0.8^{A}
Iso-C17:0	9.2 ± 0.5^{A}	5.5 ± 0.8^{B,C}	2.0 ± 0.1^{D}	7.9 ± 0.4^{A}	4.0 ± 0.8^{C,D}	6.4 ± 0.5^{A,B}
Anteiso-C17:0	41.0 ± 0.9^{A}	1.4 ± 0.2^{C,D}	5.5 ± 0.7^{B}	0.6 ± 0.1^{D}	2.2 ± 0.5^{C}	1.3 ± 0.1^{C,D}
C17:0	0.0 ± 0.0^{B}	0.0 ± 0.0^{B}	0.3 ± 0.2^{A}	0.0 ± 0.0^{B}	0.0 ± 0.0^{B}	0.0 ± 0.0^{B}
C18:1 ω9c	0.2 ± 0.2^{C}	0.3 ± 0.4^{C}	0.4 ± 0.4^{C}	0.8 ± 0.1^{B,C}	2.0 ± 0.5^{A}	1.7 ± 0.2^{A,B}
C18:0	0.5 ± 0.1^{D}	2.0 ± 0.2^{A,B}	0.8 ± 0.2^{C,D}	0.6 ± 0.1^{D}	2.7 ± 0.7^{A}	1.7 ± 0.2^{B,C}
Anteiso-C19:0	0.6 ± 0.1^{A}	0.0 ± 0.0^{B}	0.0 ± 0.0^{B}	0.0 ± 0.0^{B}	0.0 ± 0.0^{B}	0.0 ± 0.0^{B}
Iso-C17:1 ω5c	0.0 ± 0.0^{A}	0.2 ± 0.3^{A}	0.0 ± 0.0^{A}	0.0 ± 0.0^{A}	0.0 ± 0.0^{A}	0.0 ± 0.0^{A}
BCFA (%)	95.0 ± 1.2	53.7 ± 3.8	46.9 ± 4.2	79.7 ± 0.7	67.9 ± 4.1	50.3 ± 1.4
Anteiso-BCFA (%)	71.5 ± 1.1	4.1 ± 0.2	18.5 ± 4.0	3.1 ± 0.3	5.4 ± 0.8	3.9 ± 0.2
Iso-BCFA (%)	23.5 ± 0.5	49.6 ± 3.7	28.3 ± 1.4	76.6 ± 0.7	62.5 ± 4.0	46.4 ± 1.4
iso/anteiso	0.3	12.2	1.5	24.9	11.5	11.8
C-atoms <15 (%)	2.6 ± 0.2	26.1 ± 1.5	31.6 ± 1.8	18.4 ± 0.3	28.1 ± 3.2	24.8 ± 0.1
Weighted mean CL*	15.1	14.7	14.7	14.3	14.5	14.8
Weighted mean B-CL*	15.1	14.4	14.3	14.1	15.3	14.3
Weighted mean UB-CL*	14.8	15.2	15.1	14.9	15.2	15.4

*CL = chain length; B = branched; UB = unbranched; ^{A,B,C,D} Different superscripts within one row indicate significant differences (p < 0.05). Percentages of fatty acids of Scott A and *ilvE::Himar1* cultures are the result from the analysis performed in Chapter 3.

4.2.2.4. Genetic complementation

Complementation of *ilvE::Himar1 codY1* with WT *codY* was unsuccessful because the transconjugants showed very weak growth, both upon constitutive overexpression via the pIMK2 plasmid and upon induced expression via the pIMK3 plasmid.

The identified *argR* mutations are either introducing a frameshift or a premature stop codon, and are therefore predicted to be loss-of-function mutations. Complementation of *ilvE::Himar1 argR1* with WT *argR* was successful both via overexpression via pIMK2 (data not shown) and via IPTG controlled expression with the pIMK3 plasmid (Fig. 4.6). The pIMK3 integration vector has a strong IPTG controlled promoter showing limited leaky expression (personal communication Patrick Studer, ETH, Switzerland). Induction of the *ilvE::Himar1 argR1*/pIMK3-*argR* cultures growing in BHI with 3 mM t-CIN with IPTG clearly elongated the lag phase, from 31.9 to 61.0 h, completely nullifying the reverted phenotype of *ilvE::Himar1 argR1*. The lag phase of complemented *ilvE::Himar1 argR1* becomes even longer than that of the original *ilvE* mutant (48.7 h). This confirms that (some of) the activities controlled by ArgR make the *ilvE* mutant sensitive t-CIN.

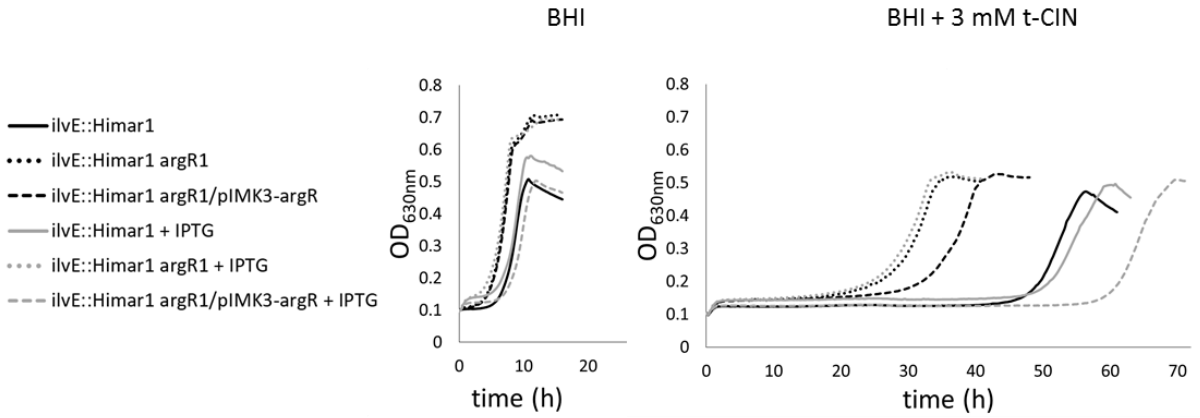

Strain	BHI			BHI + 3 mM t-CIN		
	λ (h)	μ_{max} (1/h)	OD_{max}	λ (h)	μ_{max} (1/h)	OD_{max}
ilvE::Himar1	6.5 ± 0.1^{B}	0.102 ± 0.002^{C}	0.510 ± 0.009^{C}	48.7 ± 2.0^{B}	0.059 ± 0.003^{B}	0.501 ± 0.008^{B}
ilvE::Himar1 argR1	5.0 ± 0.0^{C,D}	0.148 ± 0.002^{A}	0.707 ± 0.006^{A}	25.9 ± 0.7^{D}	0.041 ± 0.002^{C}	0.525 ± 0.006^{A,B}
ilvE::Himar1 argR1 /pIMK3-*argR*	5.1 ± 0.0^{C}	0.146 ± 0.001^{A}	0.690 ± 0.002^{A}	31.9 ± 0.6^{C}	0.040 ± 0.000^{C}	0.530 ± 0.003^{A}
ilvE::Himar1 + IPTG	6.7 ± 0.1^{B}	0.121 ± 0.002^{B}	0.584 ± 0.007^{B}	51.5 ± 2.6^{B}	0.060 ± 0.002^{A,B}	0.547 ± 0.021^{A}
ilvE::Himar1 argR1 + IPTG	4.8 ± 0.0^{D}	0.151 ± 0.001^{A}	0.700 ± 0.002^{A}	24.8 ± 0.4^{D}	0.040 ± 0.001^{C}	0.535 ± 0.003^{A}
ilvE::Himar1 argR1 /pIMK3-*argR* + IPTG	7.6 ± 0.1^{A}	0.100 ± 0.005^{C}	0.505 ± 0.027^{C}	61.0 ± 2.4^{A}	0.065 ± 0.002^{A}	0.525 ± 0.007^{A,B}

Fig. 4.6. Growth curves of *L. monocytogenes ilvE::Himar1* mutant, the *ilvE::Himar1 argR1* revertant and complemented *ilvE::Himar1 argR1*/pIMK3-*argR* strain in BHI and BHI with 3 mM t-CIN at 30 °C. Grey curves represent cultures supplemented with 1 mM IPTG, black without. All curves are the average of three independent cultures. Standard deviations have been omitted for clarity. Lag phases (λ), maximum growth rate (μ_{max}) and maximal optical densities (OD_{max}) corresponding to the curves above the table. Values are means ± standard deviation. ^{A,B,C,D} different superscripts indicate significant differences ($p < 0.05$).

ArgR is a transcriptional regulator using arginine as a ligand [66,147]. Therefore, we investigated whether t-CIN sensitivity would also be influenced by L-arginine. The effect of arginine supplementation on growth in t-CIN was studied on Scott A, *ilvE::Himar1* and its revertants *ilvE::Himar1 argR1* and *codY1* (Fig. 4.7). Arginine did not affect growth in BHI without t-CIN in any of the investigated strains. However, in the presence of t-CIN, the lag phase of the *ilvE* mutant gets extended from 44.2 h to > 61 h with arginine supplementation. The effect of arginine supplementation is therefore similar to the expression of WT *argR* in *ilvE::Himar1 argR1*. The t-CIN sensitivity of Scott A cultures was not affected by arginine supplementation, suggesting that loss of ArgR activity only relieves t-CIN sensitivity in an *ilvE::Himar1* background. The t-CIN sensitivity (lag phase) of *ilvE::Himar1 argR1* slightly but significantly increased upon arginine supplementation, which is unexpected since ArgR is

assumed to be non-functional in *ilvE::Himar1 argR1*. Finally and remarkably, growth of *ilvE::Himar1 codY1* in t-CIN remained unaffected by exogenous arginine. This indicates that the mutation in *ilvE::Himar1 codY1* makes *ilvE* mutant cells insensitive for the regulatory activity of ArgR during growth in t-CIN and implies that regulatory interactions between ArgR and CodY may exist. The impact of the mutations in both transcriptional regulators is discussed in the remainder of this chapter.

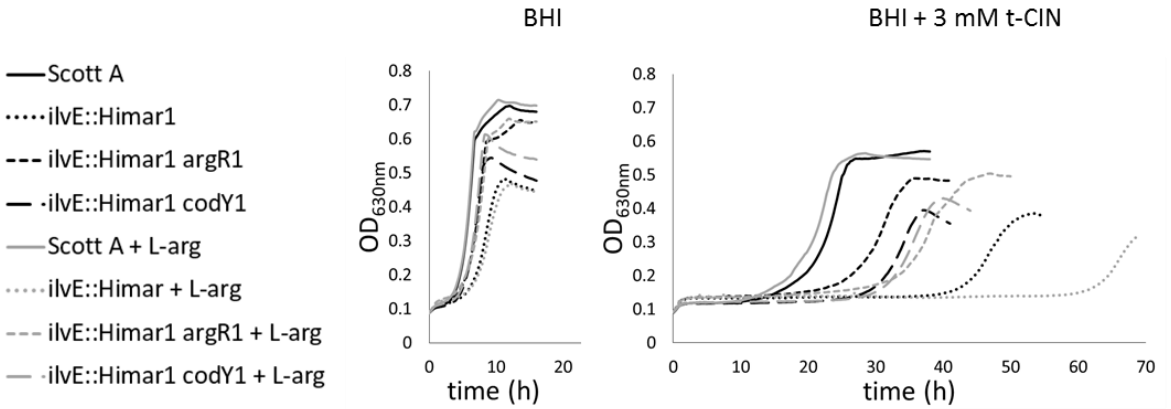

	BHI			BHI + 3 mM t-CIN		
Strain	**λ (h)**	**μ_{max} (1/h)**	**OD_{max}**	**λ (h)**	**μ_{max} (1/h)**	**OD_{max}**
Scott A	4.3 ± 0.0^{C}	0.183 ± 0.006^{B}	0.700 ± 0.019^{A}	19.1 ± 0.4^{D}	0.059 ± 0.001^{A}	0.572 ± 0.013^{A}
ilvE::Himar1	6.2 ± 0.3^{A}	0.089 ± 0.002^{E}	0.487 ± 0.010^{E}	44.2 ± 2.9^{A}	0.044 ± 0.001^{C}	0.442 ± 0.010^{C}
ilvE::Himar1 argR1	5.3 ± .0.0^{B}	0.142 ± 0.002^{D}	0.655 ± 0.007^{B}	26.0 ± 1.3^{C}	0.042 ± 0.003^{C,D}	0.497 ± 0.011^{B}
ilvE::Himar1 codY1	5.1 ± 0.1^{B}	0.140 ± 0.003^{D}	0.538 ± 0.005^{D}	29.3 ± 0.5^{B,C}	0.037 ± 0.001^{D}	0.397 ± 0.015^{D}
Scott A + L-arg	4.4 ± 0.1^{C}	0.197 ± 0.002^{A}	0.715 ± 0.006^{A}	16.7 ± 0.5^{D}	0.052 ± 0.003^{B}	0.567 ± 0.010^{A}
ilvE::Himar1 + L-arg	6.4 ± 0.3^{A}	0.077 ± 0.002^{F}	0.463 ± 0.010^{E}	> 61^{E}	/	/
ilvE::Himar1 argR1 + L-arg	5.6 ± 0.1^{B}	0.139 ± 0.001^{D}	0.661 ± 0.006^{B}	33.5 ± 2.6^{B}	0.042 ± 0.002^{C,D}	0.504 ± 0.015^{B}
ilvE::Himar1 codY1 + L-arg	5.3 ± 0.1^{B}	0.164 ± 0.002^{C}	0.618 ± 0.010^{C}	31.3 ± 1.4^{B}	0.042 ± 0.001^{C,D}	0.440 ± 0.017^{C}

Fig. 4.7. Growth curves of *L. monocytogenes* Scott A, its *ilvE::Himar1* mutant and the *ilvE::Himar1* revertants *ilvE::Himar1 argR1* and *codY1* in BHI and BHI with 3 mM t-CIN at 30 °C. Grey curves represent cultures supplemented with 5 mM L-arginine. All curves are the average of three independent cultures. Standard deviations have been omitted for clarity. Lag phases (λ), maximum growth rate (μ_{max}) and maximal optical densities (OD_{max}) corresponding to the curves above the table. Values are means ± standard deviation. ^{A,B,C,D,E,F} different superscripts indicate significant differences ($p < 0.05$).

The identified *ack* mutations are of different types (amino acid substitution, deletion or frameshift). Complementation of *ilvE::Himar1 ack1* and *ack2* with WT *ack* was successful via IPTG controlled expression with the pIMK3 plasmid (Fig. 4.8). Induction of the *ilvE::Himar1 ack1*/pIMK3-*ack* and *ilvE::Himar1 ack2*/pIMK3-*ack* cultures (grey curves) growing in BHI restored the lag phase, μ_{max} and OD_{max} to *ilvE* mutant level. Induction of *ilvE::Himar1 ack1*/pIMK3-*ack* and *ilvE::Himar1 ack2*/pIMK3-*ack*, growing in BHI with 3 mM t-CIN clearly elongated the lag phase from 21.9 to 44.3 h and 31.3 to 48.3 h respectively. Expression of WT *ack* in these *ilvE::Himar1 ack* revertants thus completely nullifies the reverted phenotype. The lag phase of complemented *ilvE::Himar1 ack1* and *ack2* becomes even longer than that of the original *ilvE* mutant (38.5 h), confirming that the enzymatic activity of Ack influences the sensitivity of the *ilvE* mutant for t-CIN.

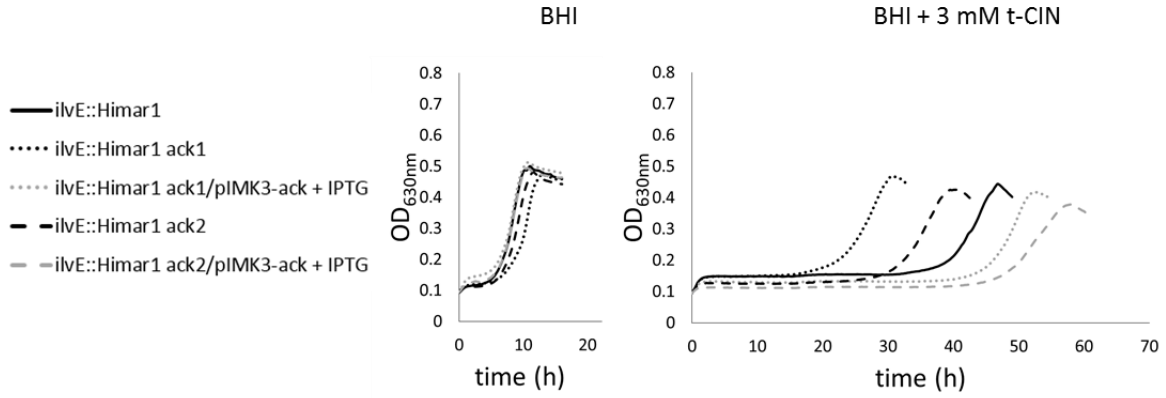

	BHI			BHI + 3 mM t-CIN		
Strain	**λ (h)**	**(μ_{max}) (1/h)**	**OD_{max}**	**λ (h)**	**(μ_{max}) (1/h)**	**OD_{max}**
ilvE::Himar1	6.1 ± 0.1^{C}	0.096 ± 0.002^{A}	$0.496 \pm 0.005^{A,B}$	38.5 ± 0.2^{B}	0.035 ± 0.001^{B}	$0.445 \pm 0.012^{A,B}$
ilvE::Himar1 ack1	7.7 ± 0.1^{A}	0.073 ± 0.001^{B}	0.469 ± 0.007^{B}	21.9 ± 0.4^{D}	$0.037 \pm 0.001^{A,B}$	0.473 ± 0.013^{A}
ilvE::Himar1 ack2	6.6 ± 0.2^{B}	$0.083 \pm 0.006^{A,B}$	$0.484 \pm 0.009^{A,B}$	31.3 ± 2.2^{C}	0.040 ± 0.001^{A}	0.457 ± 0.012^{A}
ilvE::Himar1 ack1/pIMK3-*ack*	5.9 ± 0.2^{C}	0.090 ± 0.007^{A}	0.513 ± 0.003^{A}	44.3 ± 0.7^{A}	$0.036 \pm 0.002^{A,B}$	$0.418 \pm 0.004^{B,C}$
ilvE::Himar1 ack2/pIMK3-*ack*	6.0 ± 0.1^{C}	0.088 ± 0.003^{A}	$0.493 \pm 0.027^{A,B}$	48.3 ± 3.0^{A}	$0.036 \pm 0.003^{A,B}$	0.398 ± 0.0189^{C}

Fig. 4.8. Growth curves of *L. monocytogenes ilvE::Himar1* mutant, the *ilvE::Himar1 ack1* and *ack2* revertants and complemented *ilvE::Himar1 ack1*/pIMK3-*ack* and *ilvE::Himar1 ack2*/pIMK3-*ack* strain in BHI and BHI with 3 mM t-CIN at 30 °C. Grey curves represent cultures supplemented with 1 mM IPTG, black without. All curves are the average of three independent cultures. Standard deviations have been omitted for clarity. Lag phases (λ), maximum growth rate (μ_{max}) and maximal optical densities (OD_{max}) corresponding to the curves above the table. Values are means ± standard deviation. ^{A,B,C,D} different superscripts indicate significant differences ($p < 0.05$).

4.3.3. Impact of the reversion mutations in CodY on its role as a transcriptional regulator

CodY is a global transcriptional regulator with a high degree of conservation within the group of *Firmicutes*, and has been well studied in *B. subtilis* and *L. monocytogenes*. It controls the expression of stationary-phase metabolic pathways, such as BCAAs synthesis, and of pathways involved in adaptation to nutrient depletion [148]. CodY acts as a repressor upon binding with isoleucine, but not or hardly with the other branched chain amino acids valine and leucine [149].

In *B. subtilis* GTP has been shown to be a second effector in addition to isoleucine, even though the effect of the interaction is not completely understood [150]. With isoleucine and GTP being the main effectors, CodY has always been considered to be a repressor especially under nutrient-rich conditions. As the concentrations of BCAAs and GTP drop under nutrient limitation, CodY will dissociate from the target DNA, leading to derepression of genes that are required for adaptation to nutrient-poor conditions. Nonetheless, using genome-wide RNA-Seq and ChIP-Seq analysis, Lobel and Herskovits (2016) [146] recently demonstrated that CodY in *L. monocytogenes* binds DNA both in nutrient-rich and minimal growth medium (i.e. in absence of BCAAs), suggesting that it acts both as an activator and repressor under both conditions. The RNA-Seq data further revealed that CodY affects the expression of hundreds of genes related to metabolism, stress response, motility and virulence. Therefore, CodY can be considered a central regulator of *L. monocytogenes*.

Fig. 4.9 shows the amino acid sequence of *L. monocytogenes* Scott A CodY and the amino acid substitutions in the three *ilvE::Himar1 codY* revertants identified in our screen: F98S in *ilvE::Himar1 codY1*, R167S in *ilvE::Himar1 codY2* and R214L in *ilvE::Himar1 codY3*. The CodY protein consists of two functional domains. The N-terminal effector region is a GAF domain (residues 1-155), named after its discovery on the basis of sequence analysis in cGMP-specific phosphodiesterases, adenyl cyclases and a bacterial transcription regulator FhlA [151]. GAF domains are commonly found in signaling and sensory proteins [152]. The C-terminal fragment is a DNA-binding domain with a winged helix-turn-helix (wHTH) fold. Residues 156-167 (in italic in Fig. 4.9) have a α-helical confirmation and link the GAF-domain to the wHTH domain. This inter-domain linker has an unusual sequence with nine out of twelve residues possessing ionizable side chains, including five glutamates (E) in a string of six residues. As

such the isoleucine-binding GAF domain and wHTH domain are remote from one another and exist as discrete entities [153]. This is clearly visualized in the ribbon diagram of *Staphylococcus aureus* dimeric CodY (Fig. 4.10), based on the crystal structures determined by Han *et al.* (2016) [154]. CodY crystal structures of *L. monocytogenes* are unavailable, but the amino acid sequences of CodY of members of the *Firmicutes* phylum are very conserved [148]. *L. monocytogenes* CodY shows 61% amino acid sequence identity with *S. aureus* CodY and all functionally important residues, including the mutated residues in the *ilvE::Himar1 codY* revertants, are conserved.

MTLLEKTRKINAMLQNAAGKTVNFKEMADTLTDVIEANTYIVSRKGKLLGYSEALPIENDRMKQMLTER
QFPEEYTQSLFNVGETSSNLEVSSQYTAFPIENSELFTKGLTTIVPIVGGGERLGTLILSRLESNFTDDDLLLAE
YGGTVVGMEIL*HEKAEEIEEEA**R**SRAVVQMAISSLSYSELEAIEHIFDELNGKEGLLVASKIADRVGITRSVI
VNALRKLESAGVIDSRSLGMKGTFIRVLNDKFLVELEKLKNN

Fig. 4.9. Amino acid sequence of CodY in *L. monocytogenes* Scott A. Mutated amino acid residues in *L. monocytogenes ilvE::Himar1 codY1* (F98S), *ilvE::Himar1 codY2* (R167S) and *ilvE::Himar1 codY3* (R214L) are framed. Grey residues represent the GAF domain (residues 1-155), black residues the DNA-binding domain (residues 168-259), and underlined residues the HTH motif. Residues 156-167 (italic) link the GAF domain to the DNA-binding domain.

X-ray crystallography has shown CodY to exist in a dimeric or tetrameric state [153,154]. Because the DNA-binding motif and GTP-binding site are occluded in the tetrameric state, this state was proposed to be the inactive repressor state which occurs under low nutrient conditions. Upon binding to isoleucine, the tetramer dissociates into two dimers with repressor activity. However, there is still discussion about this model, since size-exclusion chromatography with multi-angle laser light scattering (SEC-MALLS) revealed only dimer forms, even at protein concentrations higher than those found *in vivo* [153]. Thus, it remains questionable whether the tetrameric state, observed in crystallography studies, is physiologically relevant.

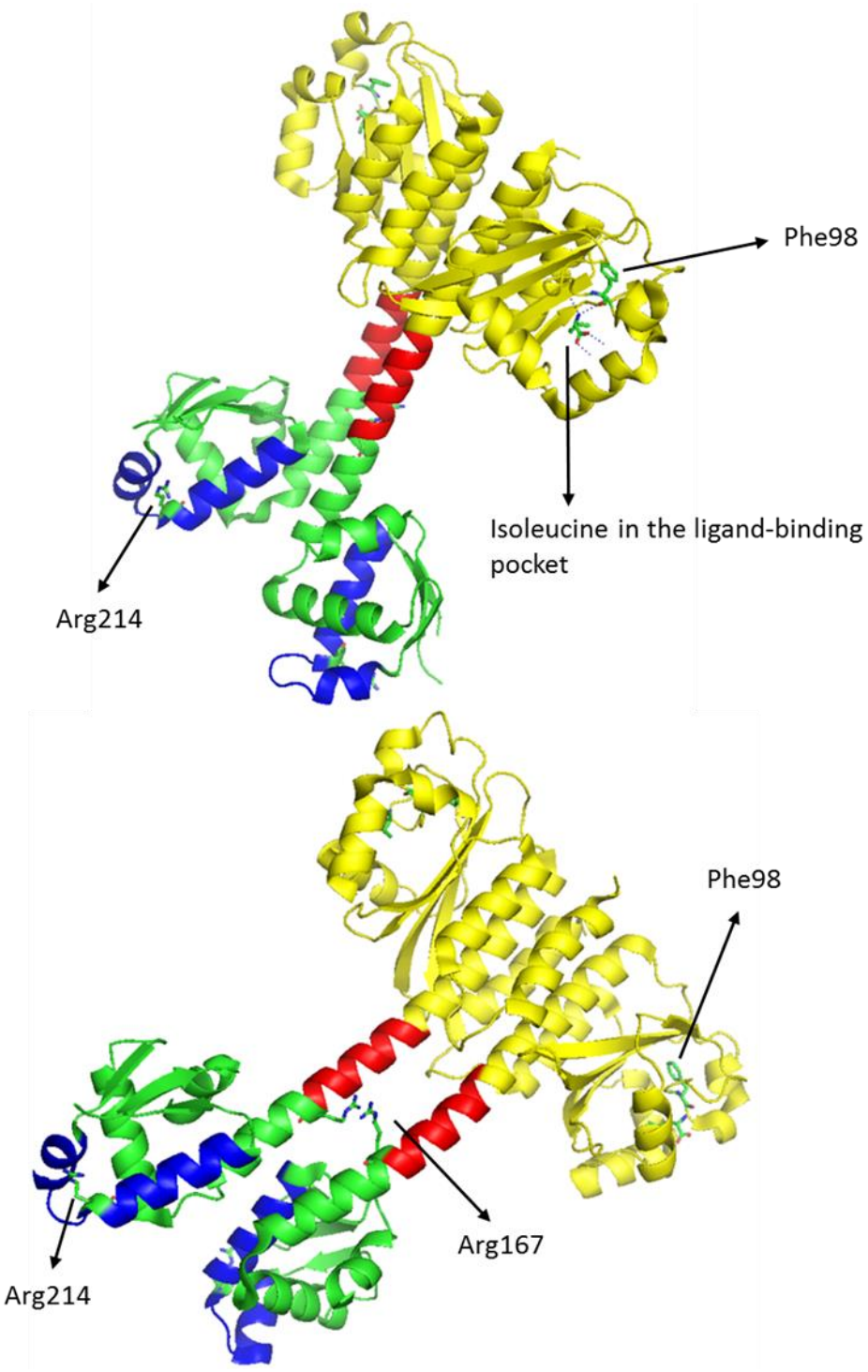

Fig. 4.10. Ribbon diagrams of *Staphylococcus aureus* dimeric CodY visualized with Pymol (The PyMOL Molecular Graphics System, Version 1.8 Schrödinger, LLC.) and based on the protein structure determined by Han *et al.* (2016) [154] . The GAF domain is colored yellow, the linker between the GAF and DNA-binding domain red and DNA binding domain green. Within the DNA-binding domain the HTH domain is colored blue. The residues which are mutated in the *L. monocytogenes* Scott A *ilvE::Himar1 codY* revertants and isoleucine in the ligand-binding pocket are visualized as stick models.

The GAF domain of CodY contains a hydrophobic pocket within which the effector isoleucine (and to a lesser extent valine) is bound. This pocket is composed of the residues M62, M65, F71, P72, Y75 and P99. The α-amino group of the effector forms charge-dipole interactions with the main chain carbonyl groups of T96 and F98, and the α-carboxylate group forms ion pairing interactions with the guanidinium group of R61. All these residues are highly conserved in CodY homologs from bacteria within the genera *Bacillus, Listeria* and *Staphylococcus* [148].

Revertant *ilvE::Himar1 codY1* (F98S) is affected in one of these residues assumed to be involved in effector binding. In a systematic site-directed mutagenesis study, Villapakkam *et al.* (2009) [155] investigated the functional importance of several residues in the binding pocket on interaction with BCAAs and GTP and on the expression of the *ilv-leu* operon and *yhdG*, which are under negative control of CodY in nutrient-rich medium. One of the constructed mutants was F98A, and this caused a strong derepression of the *ilv-leu* operon and *yhdG* in a medium containing BCAAs. Because F98 interacts with isoleucine through a charge-dipole interaction via its main-chain carbonyl group, it was somewhat unexpected that the F98A substitution leads to derepression because alanine should also be able to interact with its main-chain carbonyl group. However, it has been shown that F98 undergoes a 10-15 Å movement upon ligand binding [156], and possibly this conformational change is hindered by the F98A mutation.

We hypothesize that the F98S substitution in the *ilvE::Himar1 codY1* revertant has a similar effect as the F98A mutation and leads to derepression of the *ilv-leu* operon in *L. monocytogenes*. This allows the production of α-keto acids as substrates for BCFA production (see Fig. 3.3 in chapter 3). The increase in anteiso-C15:0 in *ilvE::Himar1 codY1* compared to the *ilvE* mutant (12.9 vs. 2.6%) and anteiso-C17:0 (5.5 vs. 1.4%) support this mechanism. Derepression results in increased synthesis of α-ketomethylvalerate from threonine via the IlvA, IlvB, IlvC and IlvD enzymes (Fig. 3.3, chapter 3). α-ketomethylvalerate serves as precursor for anteiso-C15:0 and anteiso-17:0. Yet, the fatty acid profile of *ilvE::Himar1 codY1* is not entirely restored to WT level, possibly because of kinetic limitations due to restricted availability of intracellular threonine and/or pyruvate. It should also be noted that stationary-phase cells were used for the fatty acid analysis, and that the fatty acid profile of exponential-phase cells may be more similar to the WT profile due to higher availability of pyruvate and threonine.

Revertant *ilvE::Himar1 codY2* has a R167S mutation (Fig. 4.11). R167 is the last residue of the 12-residue α-helical linker connecting the GAF-domain to the DNA-binding wHTH domain. According to the crystallography analysis of Han *et al.* (2016) [154], R167 has a role in the dimer-dimer interaction in the tetrameric state of CodY. However, since the existence of a tetrameric form *in vivo* has been questioned [153], it is difficult to predict how exactly the R167S mutation affects CodY functionality. Yet from both the growth curves in t-CIN at 30 °C and in BHI without t-CIN at 10 °C, it can be seen that *ilvE::Himar1 codY1* (F98S) and *ilvE::Himar1 codY2* (R167S) have a similar reverted phenotype. Only during growth in t-CIN, *ilvE::Himar1 codY1* has a slightly shorter lag phase (25.2 vs. 28.9 h). The membrane fatty acid profile of *ilvE::Himar1 codY2* was not determined, but based on the similar growth profile in t-CIN at 30 °C and in BHI without t-CIN at 10 °C as the *ilvE::Himar1 codY1* revertant, we anticipate that a similar increase in anteiso-FA may have occurred in *ilvE::Himar1 codY2* as in *codY1*, compared to the *ilvE* mutant.

The *ilvE::Himar1 codY3* revertant finally, has an amino acid substitution in the HTH motif (R214L). This HTH motif is highly conserved in CodY homologs ≥ 80% identity [148], suggesting that CodY homologs recognize and bind target promoters in a similar way. To investigate the importance of amino acids within this motif that are important for DNA recognition and binding, Joseph *et al.* (2005) [157] targeted specific residues, that were expected to contact DNA or to form hydrophobic interactions between helix 1 and 2, for specific site-directed mutagenesis. Amongst these residues is arginine-214 (R214), the amino acid that is mutated into leucine in revertant *ilvE::Himar1 codY3*.

In a site-directed mutagenesis study of this HTH motif, Joseph *et al.* (2005) substituted R214 by either a similar positively charged residue (R214K) or by a negatively charged residue (R214E). The effect of the mutations on DNA binding *in vitro* and on the *in vivo* expression of two target promoters, *dpp* and *ilvB* from the *ilv-leu* operon*,* was investigated. CodY(R214K) bound to the two promoters with four- to eightfold reduced affinity *in vitro*, and repression of the *dpp and ilvB* promoters was only partially affected *in vivo*. In contrast, CodY(R214E) did not bind to either promoter even at very high protein concentrations, and caused a 30- to 48-fold derepression of expression from *dpp* and *ilvB* promoters. In our work, the phenotype of the *ilvE::Himar1 codY3* revertant (R214L) is not as much restored to WT level compared to *ilvE::Himar1 codY1* and *ilvE::Himar1 codY2*, both for growth in the presence of t-CIN and at

10 °C (Fig. 4.2 and 4.5 respectively). Moreover, *ilvE::Himar1 codY3* stationary overnight cultures grow to lower cell counts than the *ilvE* mutant, *ilvE::Himar1 codY1* and *ilvE::Himar1 codY2*. As discussed above, CodY is a global regulator of metabolism in *L. monocytogenes*, and it acts both as an activator and a repressor [146]. Therefore, a possible explanation of the lower general fitness of the *ilvE::Himar1 codY3* revertant is that the R214L mutation in the DNA binding domain affects the expression of other key metabolic pathways, but still increases resistance towards t-CIN and increases growth rate at 10 °C by derepression of the *ilv-leu* operon.

The central role of CodY as a regulator of many important pathways [146] may also explain why the revertant screen only resulted in amino acid substitutions and not CodY knockout mutations. It seems to indicate that CodY knockout would be deleterious or non-viable, at least in the *ilvE::Himar1* mutant background. A *codY* deletion mutant has not been described in *L. monocytogenes* Scott A so far, but has been studied in strain 10403S [146]. Deletion of *codY* severely impaired motility, and CodY was shown to act as an activator of the flagellar biosynthesis genes both in minimal medium and nutrient rich BHI medium. To investigate whether the CodY variants in our revertants can still activate the flagellar biosynthesis operon, we performed motility assays with the revertant strains.

4.3.3.1 Motility assays

Motility assays in soft agar were performed at 30 °C as described by Lobel and Herskovits (2016) [146] (Table 4.8). Photographs of the motility assays can be found in Supplementary material S2. The motility of the *ilvE* mutant and its *codY* revertants was compared to that of the WT strain Scott A. Since we did not have a *codY* deletion mutant in a Scott A background, we included *L. monocytogenes* 10403S Δ*codY* and its WT strain 10403S. The diameters of the growth zones of the two WT strains, Scott A and 10403S, are very similar, which facilitates comparison between the Δ*codY* strain and the *ilvE::Himar1 codY* revertants.

The results confirm the finding of Lobel *et al.* (2016) that deletion of *codY* impairs motility. Unexpectedly, the *ilvE* mutant appeared to be even less motile than the Δ*codY* strain, although this conclusion has to be made with some caution, since we are comparing mutants of a different strain. This makes it difficult to compare the motility of the *ilvE::Himar1 codY* revertants (which are in an *ilvE::Himar1* background) with the *codY* deletion mutant.

Therefore, we attempted to neutralize the effect of the *ilvE* knockout by supplementing α-KAs in the growth medium. As demonstrated in chapter 3 (section 3.3.2), this restores the membrane fatty acid composition and all the associated phenotypes of the *ilvE* mutant. Supplementation with α-KAs also restored motility of the *ilvE* mutant to WT level (Scott A). Addition of α-KAs did not influence motility of the WT strains Scott A and 10403S or of the Δ*codY* strain, because they still possess intact IlvE to convert BCAAs to the corresponding α-KAs. Interestingly, in the presence of α-KAs, the three *ilvE::Himar1 codY* revertants had larger growth diameters than the Δ*codY* strain. For the *ilvE::Himar1 codY3* revertant, the diameter was even undistinguishable from WT level. These results suggest that the CodY variants have retained at least some functionality as positive regulators of the flagellar synthesis operon. The results also support the idea that complete loss of CodY function is deleterious in an *ilvE* knockout background. To confirm the partial functionality of the CodY variants, it will be necessary to construct a *codY* deletion strain in the Scott A background and complement it with the CodY variants.

Table 4.8. Growth zone diameter (cm) of *L. monocytogenes* strains stabbed in BHI 0.2% agar plates and grown for 24 h at 30 °C, with or without supplementation of an equimolar mix of 1 mM α-KAs as precursors for BCFA synthesis.

Strain	BHI	BHI + 1 mM α-KA
Scott A (WT)	3.0	2.9
10403S (WT)	2.9	2.9
ilvE::Himar1	1.0	2.9
10403S Δ*codY*	1.8	1.8
ilvE::Himar1 codY1	2.0	2.5
ilvE::Himar1 codY2	2.0	2.6
ilvE::Himar1 codY3	1.5	2.9

4.3.4. Impact of the mutations in ArgR on its role as a transcriptional regulator

ArgR is a transcriptional regulator belonging to the ArgR/AhrC arginine repressor family that is mainly known to tune the arginine metabolism under acidic conditions. ArgR functions as a classical repressor providing feedback inhibition of the arginine biosynthetic pathway in the presence of arginine. In *L. monocytogenes*, the arginine biosynthetic genes are organized in two operons, *argGH* and *argCJBDF*, which are both repressed in the presence of 10 mM arginine both in neutral (pH 7.0) and acidic (pH 5.5) conditions [147].

ArgR also acts as an activator of the arginine deiminase (ADI) system at low pH and in the presence of arginine. ArcA, one of the ADI system enzymes, converts arginine to citrulline and ammonia (NH_3). Ammonia then reacts with intracellular protons to form the ammonium cation, and therefore the ADI system is an important mechanism to cope with acid stress [66,147].

In our study, four revertants with presumably a loss of function mutation were isolated after repeated growth in BHI without t-CIN. To see whether the appearance of these revertants could be related to an acidification-related stress, end-point measurements of the pH of stationary cultures of Scott A, *ilvE::Himar1* and *ilvE::Himar1 argR1* revertant, grown under the same conditions as those of the isolation experiment, were conducted (Fig 4.13). The pH of *ilvE::Himar1 argR1* cultures (5.81) was slightly but significantly lower than that of the *ilvE* mutant (6.09), and is thus unlikely to be the selective pressure that drives the appearance of the ArgR revertants.

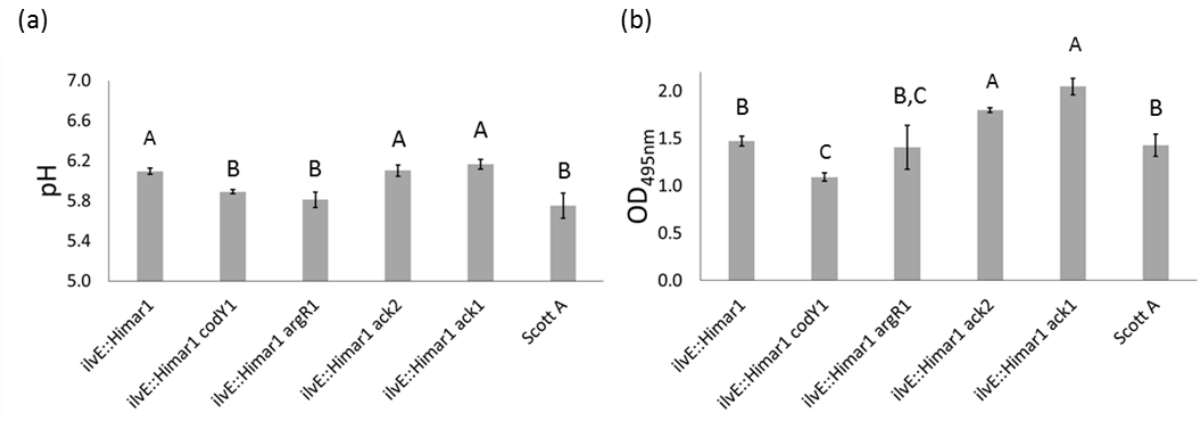

Fig. 4.11. Stationary-phase cultures grown anaerobically in BHI at 30 °C: (a) culture pH; (b) Relative amounts of acetoin, expressed as OD_{495nm} values from VP test. Values are mean ± standard deviation. Different letters (A, B, C) above bars indicate significant differences ($p < 0.05$).

On the other hand, loss of ArgR function in the *ilvE* mutant clearly affected the membrane fatty acid composition (Table 4.7). Revertant *ilvE::Himar1 argR1* is characterized by strong elevation of iso-C15:0 and a more moderate increase in iso-C17:0. The increased levels of these BCFAs suggests that the supply of α-ketoisocaproic acid is increased (see pathway Fig. 3.3, chapter 3). The only route to produce α-ketoisocaproic acid is from pyruvate via the *ilv-leu* operon which is, as discussed in section 4.3.3, repressed by CodY in BHI [146]. This repression is expected to be particularly strong in an *ilvE* mutant, because isoleucine imported from the medium is not deaminated by IlvE in this background. Since the *ilvE::Himar1 argR1* revertant did not have elevated amounts of anteiso-BCFA, and since both iso- and anteiso-BCFA are synthesized via the *ilv-leu* operon, it seems unlikely that the *ilv-leu* operon is derepressed in the *ilvE::Himar1 argR1* revertant. Nevertheless, our results suggest a functional link between the arginine pathway and BCFA synthesis, although it remains unclear how the synthesis of iso-C15:0 and iso-C17:0 can be derepressed without simultaneous derepression of the synthesis of the other BCFAs.

4.3.5. Impact of the *ack* mutations on the central carbon metabolism

Acetate kinase (Ack), often annotated as acetate kinase A, catalyzes the reversible conversion of acetyl phosphate to acetate, generating ATP. Since acetyl phosphate is directly produced from pyruvate, loss of Ack activity in the *ack* revertants may increase pyruvate flux into other pathways, such as BCAA biosynthesis, the TCA cycle, and the production of lactate and acetoin [146,158] (Fig. 4.12).

To verify if the pyruvate flux towards these pathways is different in strains Scott A, *ilvE::Himar1* and its revertants, the pH and production of acetoin were measured in stationary overnight cultures grown anaerobically in BHI at 30 °C in a microplate (Fig. 4.11). The higher the $OD_{495\ nm}$-value, the higher the concentration of acetoin in the growth medium.

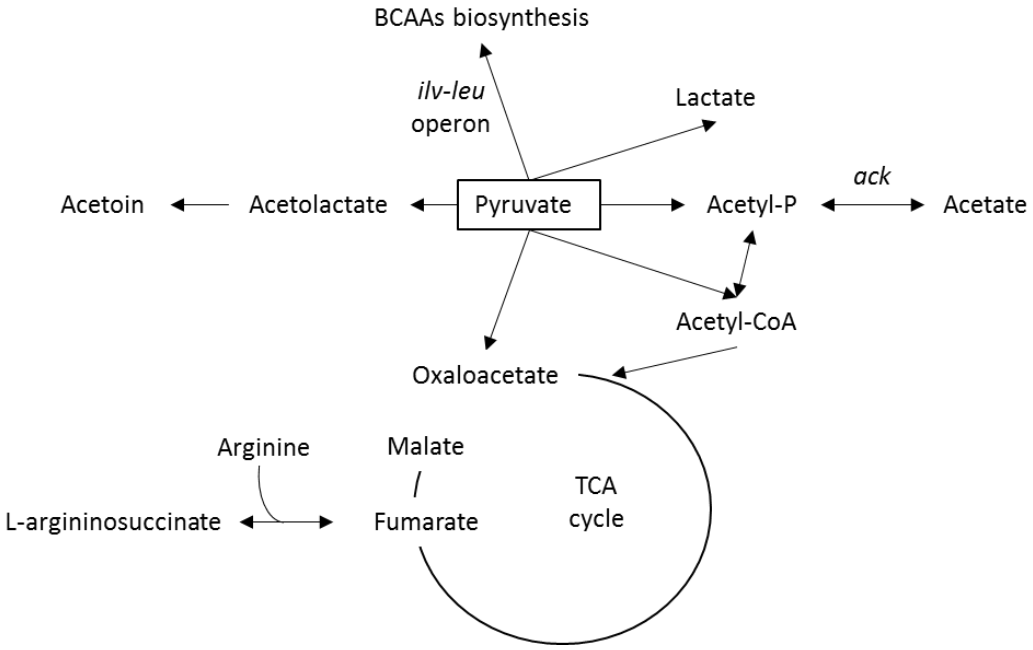

Fig. 4.12. Generalized scheme of the pyruvate and central carbon flow of *L. monocytogenes*. Pathways are inferred from predicted presence of enzymes based on genome sequence of *L. monocytogenes* Scott A.

Both *ilvE::Himar1 ack1* and *ilvE::Himar1 ack2* produced significantly higher amounts of acetoin compared to WT, *ilvE* mutant, *ilvE::Himar1 codY1 and ilvE::Himar1 argR1*. Elevated acetoin production is predicted to result in higher culture pH values, because production of acetoin is accompanied by the consumption of intracellular protons. The pH reached in the *ilvE::Himar1 ack1* and *ilvE::Himar1 ack2* cultures was indeed higher than that of the other cultures, although the difference with the *ilvE* mutant was not significant. A more detailed metabolite analysis could clarify the rerouting of pyruvate in the *ack* revertants.

Besides Ack, CodY also has a regulatory function in the pathways of the central carbon metabolism. In BHI medium, CodY represses BCAA biosynthesis and the oxidation of pyruvate to acetyl phosphate, but it activates the transcription of critical enzymes of the TCA cycle and the arginine biosynthetic genes at the same time [146]. This is in contrast to what was shown in *B. subtilis* and *Lactococccus lactis* where CodY was found to repress the expression of these genes in nutrient rich medium [159,160]. It is important to note in this context that *L. monocytogenes* has an incomplete TCA cycle. The first missing enzyme is the one that converts 2-oxoglutarate to succinate which is by-passed in *L. monocytogenes* by the production of glutamate from 2-oxoglutarate and the GABA shunt. The other missing key enzyme is malate dehydrogenase that converts malate to oxaloacetate. This means that the conversion of

fumarate to malate is a dead-end reaction. According to Lobel and Herskovits (2016) [146], the activated expression of the arginine biosynthesis genes, which are also controlled by ArgR, during growth in BHI may serve as an alternative pathway to consume fumarate through a reversed arginine pathway, generating carbamoyl phosphate that can be used further downstream in the nitrogen and pyrimidine metabolism. In minimal medium CodY does not upregulate the expression of the TCA cycle or arginine metabolism genes, but diverts the flux of pyruvate to the production of BCAAs. Other regulators such as ArgR might influence the activity of CodY and promote or inhibit transcription which makes it very hard to predict the impact of regulator mutations or knockouts on the central carbon metabolism.

4.4. Conclusion

Mutations in three different genes were found to revert the t-CIN sensitive phenotype of the *ilvE* mutant. All *ilvE::Himar1 codY* revertants were isolated from consecutive growth in BHI with t-CIN and all carry single nucleotide substitutions leading to single amino acid substitutions in structurally and functionally important regions of the global transcriptional regulator CodY. In contrast, all identified mutations in *ilvE::Himar1 argR* revertants are predicted to result in loss-of-function of ArgR, while the mutations in the *ilvE::Himar1 ack* revertants are very diverse. Two analyzed revertants of *ilvE::Himar1*, *ilvE::Himar1 codY1* and *ilvE::Himar1 argR1* were found to have an altered fatty acid composition. We propose that the ability of these revertants to bypass the blocked BCFA-biosynthesis in the *ilvE* knockout, leads to increased t-CIN resistance and increased growth rate at 10 °C.

Interestingly, the *ilvE::Himar1 ack* revertants have no clear alterations in the fatty acid composition and even grow slower at 10 °C. This leads to the conclusion that, besides adaptation of membrane fatty acid composition, other mechanisms can render increased resistance towards t-CIN in the *ilvE* mutant. Ack has a direct impact on central carbon flow and energy generation, and consequently also on the generation of reducing power. This may possibly explain the regained t-CIN tolerance in the *ilvE::Himar1 ack* revertants, because t-CIN is a thiol-reactive compound predicted to disturb the intracellular redox homeostasis.

Chapter 5

Characterization of *yvcK::Himar1 and prkC::Himar1* and the interaction between both proteins

5.1. Introduction

This chapter zooms in on two other t-CIN sensitive mutants isolated from the *L. monocytogenes* Scott A transposon knockout mutant library from chapter 2. The first mutant is *prkC::Himar1*, characterized by a moderate sensitivity to t-CIN. PrkC is a serine/threonine kinase that reversibly phosphorylates numerous effector proteins [161]. A mutant of one of these phosphorylation targets, *yvcK::Himar1*, was also picked up in the screening as being hypersensitive to t-CIN. Although knockout mutants of *yvcK* show some very clear phenotypes [162], its biochemical function in *L. monocytogenes* and other Gram-positive bacteria remains largely unidentified. Both mutants are characterized in more detail in this chapter.

5.2. Materials and methods

5.2.1. Bacterial strains, plasmids and growth conditions

L. monocytogenes and *E. coli* strains were routinely cultured under the conditions specified in chapter 2 section 2.2.1. Strains and plasmids, and oligonucleotide primers used in this chapter are listed in Table 5.1 and Table 5.2, respectively. *L. monocytogenes* 10403S and its mutants were obtained from J.D. Sauer, Department of Medical Microbiology and Immunology at the University of Wisconsin-Madison. Kinetic growth parameters were determined as described in chapter 2 section 2.2.4.

Table 5.1. Strains and plasmids used in this chapter

Strain or plasmid	Relevant features	Reference
Strains		
L. monocytogenes		
Scott A	Serovar 4b clinical isolate from the 1983 listeriosis outbreak in Massachusetts	[122]
Scott A *prkC::Himar1*	*Himar1* transposon insertion in *prkC*	Chapter 2
Scott A *yvcK::Himar1*	*Himar1* transposon insertion in *yvcK*	Chapter 2
10403S	Serovar 1/2a, streptomycin resistant derivative of 10403, isolated from human skin lesions	[162,163]
10403S Δ*yvcK*	10403S *yvcK* deletion mutant	[162]
10403S YvcK T252A/T256A	10403S *yvcK* double substitution mutant	[162]
10403S YvcK T252E/T256E	10403S *yvcK* double substitution mutant	[162]
E. coli		
S17-1 λ*pir*	*pro thi recA hsdR*$^-$ *hsdM*$^+$ RP4: 2-Tc:Mu: Km Tn7 λ*pir*	[121]
Plasmids		
pIMK2	Site-specific listerial integrative vector, Phelp promoter for constitutive overexpression, 6.2 kb, Km^R	[125]
pIMK3	Site-specific listerial integrative vector, consensus lacOid sequence inserted between P_{CP25} promoter (containing -35 and -10 regions) and the downstream 5' untranslated region of the *hlyA* gene, for high-level IPTG controlled gene expression 7.5 kb, Km^R	[125]

Table 5.2. Oligonucleotide primers used in this chapter

Primer	Sequence (5' – 3')[a]	Reference
prkC_NcoI	GCATCCATGGGAATGATTGGTAAGCGATTAAGTGATCG	This chapter
prkC_SalI	CACTGTCGACTTAATTTGGATAAGGGACTGTACCTTCATC	This chapter
yvcK_NcoI	GCATCCATGGGAAAAAAGGAAATGAAACC	This chapter
yvcK_SalI	CACTGTCGACTCACTCCTTTTCAATAG	This chapter
nfor_NcoI	ACATCCATGGGATCCAAATTATTTTCAGAATATAAATTAAAAG	This chapter
nfor_SalI	CACTGTCGACTTATTTCCACGCGCGTGAA	This chapter
chp_NcoI	GCATCCATGGGATCATTTGCATCGGAAACCAAGAAAG	This chapter
nfoR_SalI(2)	CACTGTCGACTTATTTCCACGCGCGTGAATATTG	This chapter
pIMK_REV	CCTATCACCTCAAATGGTTCG	This chapter
pIMK_FW	GAGTCAGTGAGCGAGGAAGC	This chapter
NC16	GTCAAAACATACGCTCTTATC	[129]

[a] Restriction sites are underlined: NcoI (CCATGG) and SalI (GTCGAC)

5.2.2. Genetic complementation

WT genes were amplified using gene specific primers mentioned in Table 5.2, and cloned as an NcoI-SalI fragment into pIMK2 or pIMK3, which were first linearized with the same restriction enzymes. Genetic complementations of strain *L. monocytogenes yvcK::Himar1* were performed with the pIMK2 (constitutive overexpression) or pIMK3 (high level IPTG-controlled expression) plasmid [125]. Genes cloned into pIMK2 were *yvcK*, *nfor* and *chp-nfor*, using primers yvcK_NcoI & yvcK_SalI, nfor_NcoI & nfor_SalI, chp_NcoI & nfor_SalI(2) respectively. *yvcK* was also cloned in pIMK3 using primers yvcK_NcoI and yvcK_SalI. *L. monocytogenes prkC::Himar1* was complemented with *prkC* amplified with primers prkC_NcoI and prkC_SalI and cloned in plasmid pIMK2. Plasmids for complementation were conjugated from *E. coli* S17-1 λ*pir* to the *L. monocytogenes* transposon mutants, using selection for Km (pIMK2 and pIMK3 marker) and Em (transposon marker). The pIMK2 and pIMK3 plasmids do not replicate in *L. monocytogenes*, but are designed to integrate specifically in the $tRNA^{Arg}$ gene, which is the unique integration site of the phage PSA in the genome of *L. monocytogenes* Scott A [125,129]. Correct integration in this site was confirmed via PCR using the gene specific primer provided with the NcoI restriction site and primer NC16, which anneals just outside the phage integration site [129]. Additionally, the presence of the intact WT copy of the introduced gene in the integrants was confirmed via PCR and Sanger sequencing analysis

(Macrogen Europe, Amsterdam, Netherlands) using primers pIMK_FW and pIMK_REV, which anneal at both sides just outside the cloning site of the plasmid (Table 5.2).

5.2.3. Headspace - solid phase micro-extraction - gas chromatography - mass spectrometry (HS-SPME-GC-MS) analysis

HS-SPME-GC-MS analysis was performed as described in chapter 2 section 2.2.7. Stationary-phase overnight cultures grown in BHI at 30 °C were washed once with PPB (10 mM, pH 7.0), diluted a 1000-fold to approximately 10^6 cfu/ml in 80 ml BHI supplemented with 1 mM t-CIN in a 100 ml Erlenmeyer closed tightly with a screw-cap and incubated at 30 °C. At several time points, the concentration of cells and of t-CIN were determined by BHI plate count and by HS-SPME-GC-MS, respectively. The experiment was performed for both the WT and *yvcK* mutant at the same day with the same t-CIN stock solution and growth media. In order to be able to perform the sample preparation for HS-SPME-GC-MS analysis at a certain time point of three biological replicates from one strain and their respective control sample as quickly as possible, both strains were not sampled simultaneously, but with a one-hour difference. At each sampling time point, a cell-free control sample that had been incubated in the same conditions was also analyzed and a separate control sample for each strain was used. Identification of t-CIN degradation products was performed by comparing the deconvoluted mass spectrum with the reference mass spectra from the NIST14 spectral library (version 2.2, National Institute of Standards and technology, Gaithersburg, Maryland, USA). For identification, a threshold of 90% was taken into account. Concentrations of these degradation products were not quantified.

5.2.4. Growth at 10 °C

Cells from three independent stationary-phase overnight cultures of Scott A and *prkC::Himar1* were washed once with PPB, diluted to approximately 10^4 cfu/ml in 4 ml of BHI broth in 10 ml glass tubes with loose caps, and incubated shaking at 10 °C. At several time points, 200 µl samples were taken for OD measurement at 600 nm in a microplate reader.

5.2.5. Fatty acid analysis

The whole-cell fatty acid compositions of stationary-phase *prkC::Himar1* and its complemented strain *prkC::Himar1*/pIMK2-*prkC*, cultured at 30 °C in BHI broth were determined as described in chapter 3, section 3.2.5. The fatty acid compositions of both strains are compared with the composition of stationary WT cultures determined in chapter 3 section 3.3.4.1.

5.2.6. Statistical analysis

Means of the parameter estimates of the Baranyi and Roberts growth model (λ, μ_{max} and OD_{max} [127]), and mean percentages of the different fatty acids were statistically compared by the Tukey-Kramer HSD test with the JMP® Software (JMP, Version Pro12, SAS Institute Inc., Cary, USA), and considered significantly different when a *p*-value < 0.05 was obtained. Mean relative t-CIN concentrations in WT and *yvcK::Himar1* cultures measured via HS-SPME-GC-MS were statistically compared by a t-test with the JMP® Software and also considered significantly different when a *p*-value < 0.05 was obtained.

5.3. Results and discussion

5.3.1. Characterization of *L. monocytogenes prkC::Himar1*

In one of the selected t-CIN sensitive transposon mutants (chapter 2, Table 2.4 and 2.5), the transposon was found to be located in the *prkC* gene. PrkC is a serine/threonine kinase that reversibly phosphorylates numerous effector proteins [161]. Fig. 5.1 shows the organization of the genomic *prkC* region in *L. monocytogenes* Scott A.

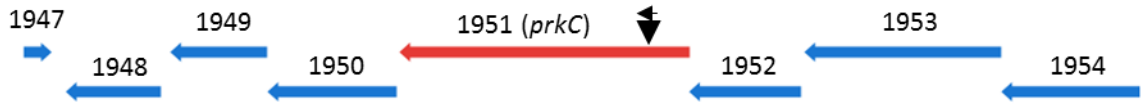

Fig. 5.1. Organization of the *prkC* region in *L. monocytogenes* Scott A. The *prkC* gene is highlighted in red, with the *Himar1* transposon at 271 bp from the start codon of *prkC* shown as a black triangle. The black arrow indicates the orientation of the erythromycin resistance gene (*ermC*) in the transposon. In the PATRIC database [130] the different ORF's are annotated as LSU ribosomal protein L28p, zinc-independent (1947), Thiamine pyrophosphokinase (EC 2.7.6.2) (1948), Ribulose phosphate 3-epimerase (EC 5.1.3.1) (1949), Ribosome small subunit biogenesis RbfA-release protein RsgA (1950), Serine/threonine protein kinase PrkC, regulator of stationary phase (1951), Protein serine/threonine phosphatase PrpC, regulation of stationary phase (1952), 16S rRNA (cytosine(967)-C(5))-methyltransferase (EC 2.1.1.176) (1953), Helicase PriA essential for oriC/DnaA-independent DNA replication (1954).

Fig. 5.2 shows the growth curves and growth parameters of the WT and its *prkC::Himar1* transposon mutant in BHI broth with and without 4 mM t-CIN. In absence of t-CIN, the mutant grew almost like the WT strain. Lag phases were equally long, only μ_{max} and OD_{max} were slightly lower for the *prkC* mutant compared to WT. In BHI with 4 mM t-CIN, the lag phase of the *prkC* mutant (47.0 h) was much more extended compared to WT (21.6 h), confirming the mutant's increased sensitivity to t-CIN. OD_{max} and μ_{max} were similar for mutant and WT for growth in the presence of t-CIN. As can be seen from Fig. 5.1, it cannot be excluded that *prkC* is co-transcribed with one or more downstream genes and that the *Himar1* insert also knocks out the production of these proteins. To confirm that t-CIN sensitivity is due to disruption of *prkC*, the mutant was genetically complemented with the WT *prkC* gene using the overexpression integration vector pIMK2 (Table 5.1). Complementation shortened the lag phase in the presence of t-CIN to WT-level and restored the OD_{max} reached in BHI without t-CIN. It can thus be concluded that the loss of PrkC activity results in increased t-CIN sensitivity.

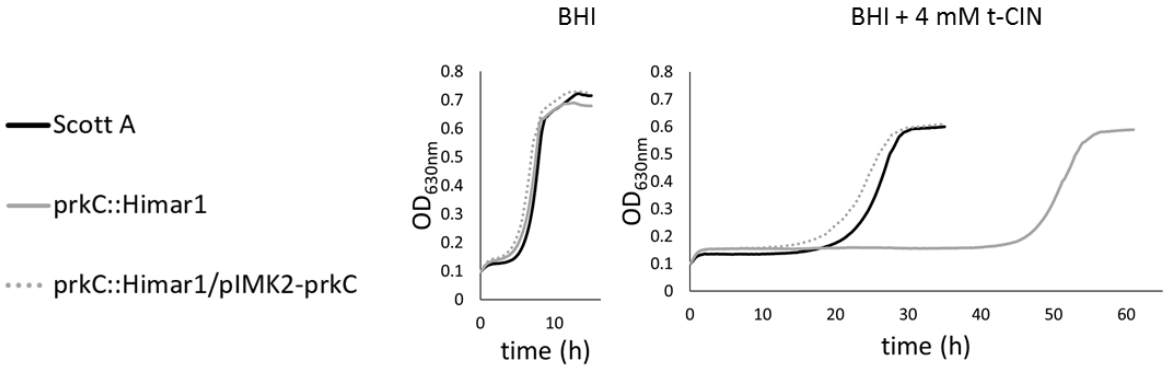

	BHI			BHI + 4 mM t-CIN		
Strain	**λ (h)**	**μ_{max} (1/h)**	**OD_{max}**	**λ (h)**	**μ_{max} (1/h)**	**OD_{max}**
Scott A	5.9 ± 0.3^{A}	0.181 ± 0.000^{A}	0.725 ± 0.011^{A}	21.6 ± 0.8^{B}	0.059 ± 0.002^{A}	0.592 ± 0.013^{A}
prkC::Himar1	5.3 ± 0.1^{A}	0.167 ± 0.002^{C}	0.695 ± 0.016^{B}	47.0 ± 1.3^{A}	0.058 ± 0.007^{A}	0.560 ± 0.021^{A}
prkC::Himar1/ pIMK2-*prkC*	4.9 ± 0.7^{A}	0.174 ± 0.003^{B}	0.735 ± 0.011^{A}	19.3 ± 1.8^{B}	0.051 ± 0.003^{A}	0.592 ± 0.020^{A}

Fig. 5.2. Growth curves of *L. monocytogenes* Scott A, its *prkC::Himar1* mutant and the genetically complemented mutant *prkC::Himar1*/pIMK2-*prkC* in BHI broth and BHI broth with 4 mM t-CIN. All curves are the average of three independent cultures. Standard deviations have been omitted for clarity. Lag phases (λ), maximum growth rates (μ_{max}) and maximum optical densities (OD_{max}) are listed in table below the corresponding growth curves. Values are mean ± standard deviation. ^{A,B,C}Different superscripts within one column indicate significant differences ($p < 0.05$).

Besides being sensitive to t-CIN, the *prkC* mutant was also characterized by attenuated growth in BHI at 10 °C (Fig. 5.3). To investigate whether the growth deficiency at 10 °C was caused by an altered membrane fatty acid composition, as for the *ilvE* mutant (chapter 3), stationary-phase cells of the WT strain, the *prkC* mutant and the complemented mutant cultured in BHI at 30 °C were subjected to whole-cell fatty acid compositional analysis (Table 5.3). The proportion of BCFAs as well as the ratio of iso to anteiso BCFA were unaltered in the mutant. However, the *prkC* mutant and complemented mutant had significantly higher amounts of anteiso-C15:0 (44.3% and 43.4%, respectively) than the WT (29.9%), and, correspondingly, significantly lower amounts of anteiso-C17:0 (27.7 % and 26.2 %, respectively) than the WT (41.0 %). Despite the small difference in phase-transition temperature of anteiso-C15:0 (25.8 °C) compared to that of anteiso-C17:0, (30.0 °C) [50,142], the altered anteiso-C15:0/anteiso-C17:0 ratio and its impact on membrane fluidity are unlikely to be the cause of the reduced growth rate at 10 °C. The modified fatty acid composition in the mutants is remarkable, because both anteiso fatty acids are produced from the same precursor, α-ketomethylvalerate. In general, the membranes of the *prkC* mutant, complemented mutant and WT can be regarded as very similar, as shown by the summarized features at the bottom of Table 5.3.

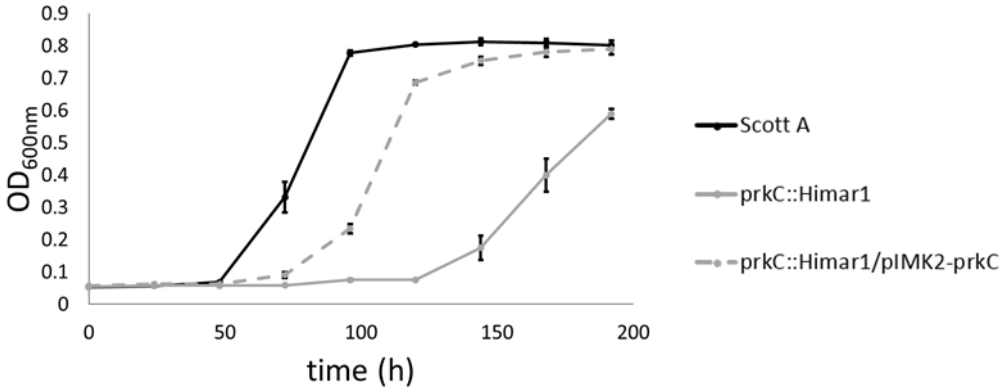

Fig. 5.3. Growth of *L. monocytogenes* Scott A, its mutant *prkC::Himar1* and complemented mutant *prkC::Himar1/*pIMK2-*prkC* at 10 °C in BHI broth.

The metabolic role of PrkC in *L. monocytogenes* in relation to the observed phenotypes of the *prkC* mutant is further discussed in section 5.3.5.

Table 5.3. Whole-cell fatty acid composition (%) of stationary cultures of *L. monocytogenes* Scott A, *prkC::Himar1* and its complemented mutant *prkC::Himar1*/pIMK2-*prkC* grown in BHI at 30 °C. Summary data are shown at the bottom of the table. Values are mean ± standard deviation from three independent cultures. Most dominant FA fractions in Scott A are framed grey.

Fatty acid	Scott A	*prkC::Himar1*	*prkC::Himar1*/pIMK2-*prkC*
C10:0	0.1 ± 0.1^{B}	$0.2 \pm 0.1^{A,B}$	0.3 ± 0.0^{A}
Iso-C11:0	0.0 ± 0.0^{A}	0.0 ± 0.0^{A}	0.0 ± 0.0^{A}
C12:0	1.4 ± 0.2^{B}	2.1 ± 0.5^{A}	$2.0 \pm 0.1^{A,B}$
Iso-C13:0	0.0 ± 0.0^{A}	0.0 ± 0.0^{A}	0.1 ± 0.1^{A}
Anteiso-C13:0	0.0 ± 0.0^{A}	0.0 ± 0.0^{A}	0.0 ± 0.0^{A}
C13:0	0.0 ± 0.0^{A}	0.0 ± 0.0^{A}	0.0 ± 0.0^{A}
Iso-C14:0	0.6 ± 0.0^{B}	0.8 ± 0.1^{A}	0.7 ± 0.0^{A}
C14:1 ω5c	0.0 ± 0.1^{A}	0.2 ± 0.1^{A}	0.2 ± 0.1^{A}
C14:0	0.5 ± 0.1^{B}	0.7 ± 0.1^{A}	$0.6 \pm 0.0^{A,B}$
Iso-C15:0	10.9 ± 0.4^{C}	12.9 ± 0.4^{B}	15.6 ± 0.1^{A}
Anteiso-C15:0	29.9 ± 1.0^{B}	44.3 ± 0.9^{A}	43.4 ± 0.3^{A}
C15:0	0.0 ± 0.0^{A}	0.0 ± 0.0^{A}	0.0 ± 0.0^{A}
Iso-C16:0	2.8 ± 0.1^{A}	2.5 ± 0.2^{A}	2.5 ± 0.1^{A}
C16:0	2.1 ± 0.1^{B}	2.9 ± 0.2^{A}	2.4 ± 0.1^{B}
Iso-C17:0	9.2 ± 0.5^{A}	4.8 ± 0.6^{B}	5.1 ± 0.2^{B}
Anteiso-C17:0	41.0 ± 0.9^{A}	27.7 ± 0.9^{B}	26.2 ± 0.4^{B}
C17:0	0.0 ± 0.0^{A}	0.0 ± 0.0^{A}	0.0 ± 0.0^{A}
C18:1 ω9c	0.2 ± 0.2^{A}	0.1 ± 0.3^{A}	0.1 ± 0.2^{A}
C18:1 ω6c	0.0 ± 0.0^{A}	0.0 ± 0.0^{A}	0.0 ± 0.0^{A}
C18:0	0.5 ± 0.1^{A}	0.6 ± 0.1^{A}	0.5 ± 0.1^{A}
Anteiso-C19:0	0.6 ± 0.1^{A}	0.0 ± 0.0^{B}	0.0 ± 0.0^{B}
Iso-C17:1 ω5c	0.0 ± 0.0^{A}	0.0 ± 0.0^{A}	0.0 ± 0.0^{A}
C18:1 ω7c	0.0 ± 0.0^{A}	0.0 ± 0.0^{A}	0.0 ± 0.0^{A}
BCFA (%)	95.0 ± 1.2	93.0 ± 1.5	93.5 ± 0.5
Anteiso-BCFA (%)	71.5 ± 1.1	72.0 ± 1.3	69.6 ± 0.5
Iso-BCFA (%)	23.5 ± 0.5	20.9 ± 0.7	23.9 ± 0.2
iso/anteiso	0.3	0.3	0.3
C-atoms <15 (%)	2.6 ± 0.2	4.0 ± 0.5	3.8 ± 0.1
Weighted mean CL*	15.1	14.7	14.6
Weighted mean B-CL*	15.1	14.7	14.7
Weighted mean UB-CL*	14.8	14.5	14.4

*CL = chain length; B = branched; UB = unbranched; ^{A,B,C} Different superscripts indicate significant differences ($p < 0.05$).

5.3.2. Characterization of *L. monocytogenes yvcK::Himar1*

One of the most sensitive strains detected during the screen for t-CIN sensitive transposon mutants, was *yvcK::Himar1*. Fig. 5.4 shows the genomic region surrounding the *yvcK* gene. The biochemical function and cellular role of *yvcK* and the two downstream genes with which it is predicted to form an operon, are poorly characterized [162,164]. The first downstream gene of *yvcK* (2606) is annotated in the Scott A genome in the PATRIC database as a cytoplasmic hypothetical protein, abbreviated in this work as Chp, while in other *L. monocytogenes* strains it is often annotated as DNA-binding protein WhiA. The second downstream gene (2607) is annotated as a NADH:flavin oxidoreductase, in this work abbreviated as Nfor.

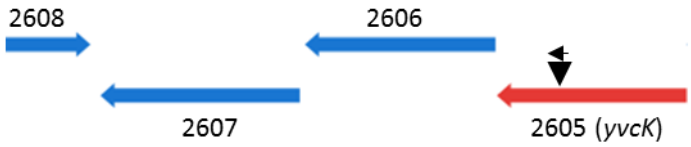

Fig. 5.4. Organization of the *yvcK* region in *L. monocytogenes* Scott A. The *yvcK* gene (2605) is highlighted in red. The *Himar1* transposon is located at 655 bp from the start codon of *yvcK*, and is shown as a black triangle. The black arrow indicates the orientation of the erythromycin resistance gene (*ermC*) in the transposon. In the PATRIC database [130], the downstream ORF's are annotated as Cytoplasmic hypothetical protein (2606), NADH:flavin oxidoreductase (2607) and internalin-like protein Lmo2470 homolog (2608).

Fig. 5.5 shows the growth curves and growth parameters of the WT and the *yvcK::Himar1* mutant in BHI broth with and without 2 mM t-CIN. In absence of t-CIN, the *yvcK* mutant grew almost like the WT. Only the lag phase was slightly (0.7 h) longer compared to WT. In BHI with 2 mM t-CIN, the lag phase of the *yvcK* mutant (63.9 h) was much longer compared to WT (9.8 ± 0.1 h). This very long lag phase, despite the low concentration of t-CIN, indicates that this is one of the most sensitive mutants. As can be seen from Fig. 5.4, the transposon insertion could have a polar effect on one or both of the genes downstream of *yvcK*. To confirm that *yvcK* is responsible for t-CIN sensitivity, we attempted to genetically complement the mutant with the WT *yvcK* gene using the overexpression integration vector pIMK2, but this was unsuccessful because no transconjugants could be isolated after conjugation with *E. coli* S17-1 λ*pir* harboring the pIMK2-*yvcK* vector. Complementation attempts were also performed with the downstream genes cloned in pIMK2. The growth curves and growth parameters of these constructs are shown in Fig. 5.5.

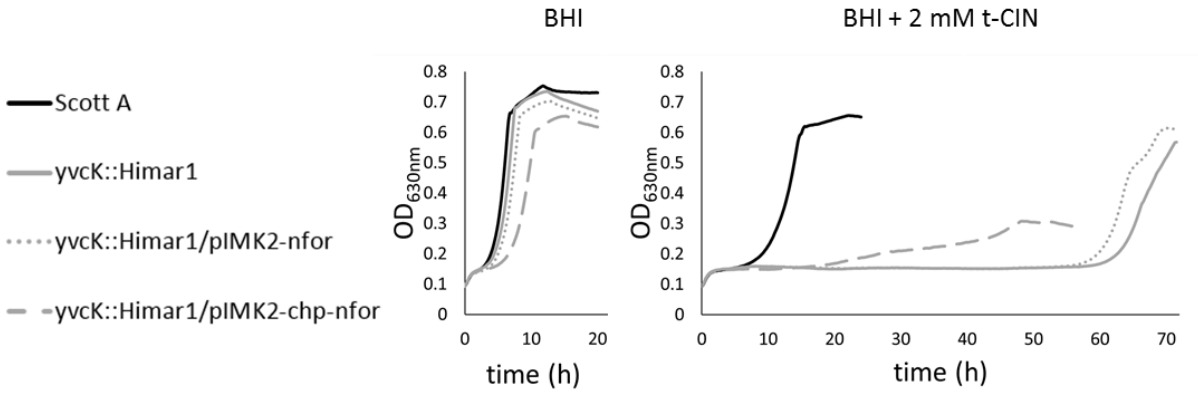

Strain	BHI			BHI + 2 mM t-CIN		
	λ (h)	μ_{max} (1/h)	OD_{max}	λ (h)	μ_{max} (1/h)	OD_{max}
Scott A	4.3 ± 0.0^{D}	0.185 ± 0.001^{A}	0.753 ± 0.005^{A}	9.8 ± 0.1^{C}	0.086 ± 0.002^{A}	0.643 ± 0.005^{A}
yvcK::Himar1	5.0 ± 0.1^{C}	0.189 ± 0.002^{A}	0.735 ± 0.004^{A}	63.9 ± 2.8^{A}	0.079 ± 0.012^{A}	0.579 ± 0.015^{B}
yvcK::Himar1/ pIMK2-*nfor*	5.5 ± 0.0^{B}	0.165 ± 0.002^{B}	0.704 ± 0.004^{B}	61.2 ± 2.6^{A}	0.088 ± 0.014^{A}	0.623 ± 0.004^{A}
yvcK::Himar1/ pIMK2-*chp-nfor*	7.0 ± 0.1^{A}	0.116 ± 0.011^{C}	0.622 ± 0.013^{C}	17.1 ± 1.4^{B}	0.005 ± 0.000^{B}	0.311 ± 0.009^{C}

Fig. 5.5. Growth curves of *L. monocytogenes* Scott A, its *yvcK::Himar1* mutant and the complemented mutants *yvcK::Himar1*/pIMK2-*nfor* and *yvcK::Himar1*/pIMK2-*chp-nfor* in BHI broth and BHI broth with 2 mM t-CIN. All curves are the average of three independent cultures. Standard deviations have been omitted for clarity. Lag phases (λ), maximum growth rates (μ_{max}) and maximum optical densities (OD_{max}) are listed in the table. Values are mean ± standard deviation. ^{A,B,C,D}Different superscripts within one column indicate significant differences ($p < 0.05$).

Complementation with the downstream genes did not restore the phenotype of the *yvcK* mutant. Although the lag phase of *yvcK::Himar1*/pIMK2-*chp* was significantly shorter than that of the *yvcK* mutant, its phenotype is clearly not restored as evidenced by its very low exponential growth rate and OD in stationary phase.

5.3.3. t-CIN degradation by *L. monocytogenes*

Analysis of the amino acid sequence of the NADH:flavin oxidoreductase (Nfor) encoded by ORF2607 downstream of *yvcK* (Fig. 5.4), shows a 63% amino acid sequence identity with *B. subtilis* strain 168 YqjM (Fig. 5.6).

Bacillus YqjM is related to yeast Old Yellow Enzyme (OYE), belonging to the family of flavoprotein oxidoreductases. Like OYE, YqjM tightly but noncovalently binds FMN and utilizes NADPH as the preferred reductant, to reduce the double bond or an array of α, β-unsaturated aldehydes and ketones such as cyclohex-2-enone, but also nitroester and nitroaromatic compounds such as N-ethylmaleimide [165]. Fitzpatrick *et al.* (2003) showed induction of YqjM synthesis *in vivo* upon exposure to the toxic compound trinitrotoluene and in response to hydrogen peroxide, indicating a role in detoxification and oxidative stress response. Based on this information, we hypothesized that the NADH:flavin oxidoreductase encoded by ORF2607 could possibly reduce the double carbon bond of the α, β-unsaturated aldehyde of t-CIN.

Score	Expect	Method	Identities	Positives	Gaps
435 bits(1119)	1e-158	Compositional matrix adjust.	210/335(63%)	253/335(75%)	0/335(0%)

L. mono ORF2607	KLFTPITIKDMTLKNRIVMSPMCMYSSHEKDGKLTPFHMAHYISRAIGQVGLIIVEASAV	63
	KLF+ +KD+TLKNRIVMSPMCMYS KDG T FH AHY+SRA G GL+I+EA+AV	
B. subt YqjM	KLFSEYKLKDVTLKNRIVMSPMCMYSVENKDGIATDFHFAHYVSRAAGGTGLVILEATAV	62
L. mono ORF2607	NPQGRITDQDLGIWSDEHIEGFAKLTEQVKEQGSKIGIQLAHAGRKAELEGDIFAPSAIA	123
	GRI++ DLG+W+DE + KL + + G+K GIQLAHAGRKA L G+I APSAIA	
B. subt YqjM	QEVGRISEFDLGLWNDEQVPALKKLVDGLHYHGAKAGIQLAHAGRKAVLPGEIVAPSAIA	122
L. mono ORF2607	FDEQSATPVEMSAEKVKETVQEFKQAAARAKEAGFDVIEIHAAHGYLIHEFLSPLSNHRT	183
	FDE+S PVE++ E +KE V +FK+AA RAKEAGFDVIEIHAAHGYLIH+FLSP++N R	
B. subt YqjM	FDEKSDKPVELTKEAIKEVVADFKRAAYRAKEAGFDVIEIHAAHGYLIHQFLSPITNRRE	182
L. mono ORF2607	DEYGGSPENRYRFLREIIDEVKQVWDGPLFVRVSASDYTDKGLDIADHIGFAKWMKEQGV	243
	D YGG NRY+ L +II VK+VWDGP+ VRVSA+DY GL + DHI FAKWMK GV	
B. subt YqjM	DNYGGPAGNRYKILSDIIKAVKEVWDGPIIVRVSATDYAHGGLQLEDHIPFAKWMKADGV	242
L. mono ORF2607	DLIDCSSGALVHADINVFPGYQVSFAEKIREQADMATGAVGMITDGSMAEEILQNGRADL	303
	+LID S+G LV+ VFPGYQV FA++IR A +ATGA+G+IT G AEEIL N RADL	
B. subt YqjM	ELIDVSTGGLVNVAPPVFPGYQVPFADEIRRGAGIATGALGLITRGEQAEEILCNERADL	302
L. mono ORF2607	IFIGRELLRDPFFARTAAKQLNTEIPAPVQYERGW	338
	I +GRELLR+P+FA+ AAKQL I P QY R W	
B. subt YqjM	IIVGRELLRNPYFAKDAAKQLGETIEGPKQYSRAW	337

Fig. 5.6. Alignment of amino acid sequences via Protein BLAST of *L. monocytogenes* Scott A ORF2607 (Fig. 5.4) encoding NADH:flavin oxidoreductase and *B. subtilis* subsp. *subtilis* str. 168 *yqjM* gene encoding NADH dependent flavin oxidoreductase. BLAST sequence alignment parameters: max score 435, total score 435, query cover 99%, E-value $1x10^{-158}$, identity 63%.

Therefore, we investigated whether cultures of *L. monocytogenes* Scott A growing in BHI degrade t-CIN and whether such degradation was affected by the transposon insertion in *yvcK.* Reduced t-CIN detoxification could be a potential explanation for the hypersensitivity to t-CIN

of the *yvcK* mutant. Fig. 5.7 shows the evolution of the t-CIN concentration as measured by HS-SPME-GC-MS in WT and *yvcK* mutant cultures grown in BHI in the presence of 1 mM t-CIN. Note that the sample preparation for HS-SPME-GC-MS analysis was performed with the same culture medium and the same t-CIN stock on the same day, but that the experiment for WT and *yvcK* mutant cultures started with a one-hour difference, to be able to process samples as quickly as possible. Therefore, a separate control sample for WT and *yvcK::Himar1* was used.

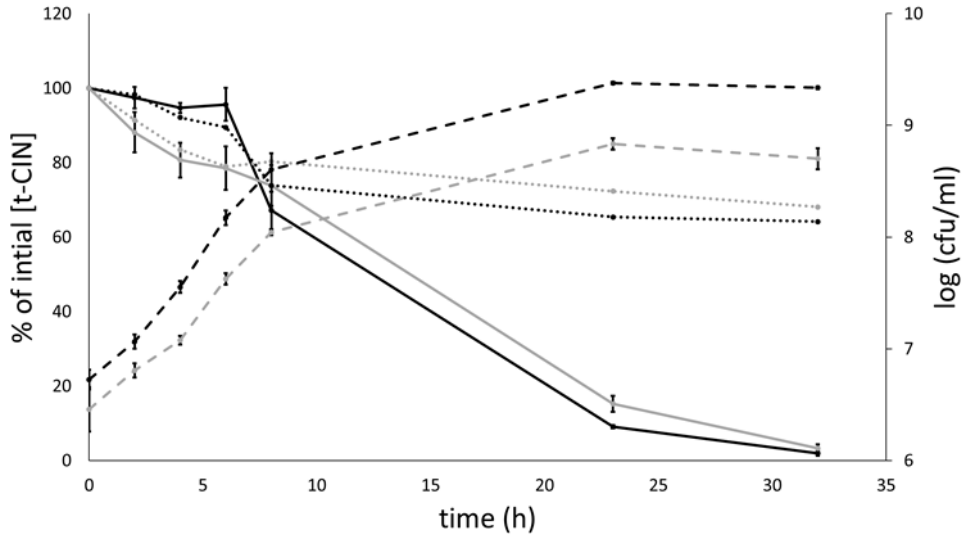

Fig. 5.7. Degradation of t-CIN in WT (black solid line) and *yvcK::Himar1* (grey solid line) cultures grown in BHI with 1 mM t-CIN. Dotted lines represent chemical degradation of t-CIN in cell-free samples, sampled at the same time points as the WT (black) or *yvcK::Himar1* (grey) culture. Cell numbers of the WT (black dashed line) and *yvcK::Himar1* (grey dashed line) cultures at the same time points were determined by plating on BHI agar (right axis). All values are means of three independent cultures ± standard deviation, with exception of the cell-free control samples, for which two single measurements are shown.

The data show that t-CIN gets almost completely broken down after 32 h in culture samples. Biological degradation of t-CIN appears to proceed faster in the *yvcK* mutant compared to WT during the first 6 h. However, when chemical degradation in the corresponding control samples is considered and t-CIN degradation in culture samples is expressed relatively to chemical degradation in control samples (data not shown), then there is only a significant difference ($p < 0.05$) in t-CIN degradation between both strains after 24 h. However, the difference was small and may be related to the higher cell numbers reached in the WT compared to the *yvcK* mutant. Interestingly, compared to chemical degradation of t-CIN in cell-free control samples, biological degradation only starts when the cells reach the late-

exponential phase or early-stationary phase. Based on these observations, it can be concluded that t-CIN degradation does not depend on *yvcK* or the downstream NADH:flavin oxidoreductase, at least if the oxidoreductase is indeed part of the same operon as *yvcK* as has been previously suggested [164].

After 23 h of growth, 3-phenylpropanal, phenyl-2-propen-1-ol and 3-phenyl-1-pronanol were detected in culture samples of both the WT and *yvcK* mutant, but not in the cell-free control samples. These compounds appear to be degradation products produced by a two-step reduction of t-CIN (Fig. 5.8). The concentration of these compounds in the growth media was not determined, because calibration curves of degradation products in relation to the internal standard were not determined since we had only limited access to the HS-SPME-GC-MS. MIC assays for the WT strain with pure compounds showed that the MIC of 3-phenylpropanal is about 2.5 times higher than for t-CIN. Phenyl-2-propen-1-ol and 3-phenyl-1-pronanol showed no growth inhibitory effect up to 12 mM, which was the highest concentration tested. The t-CIN derivatives 3-phenylpropanal, phenyl-2-propen-1-ol and 3-phenyl-1-propanol have $\log P_{oct}$ values of 2.04, 1.70 and 1.88 respectively, and thus are only slightly less lipophilic than t-CIN ($\log P_{oct}$ = 2.12) (PubChem). On the other hand, reduction of the C=C double bond and/or reduction of the aldehyde to an alcohol group reduces the electrophilic nature of t-CIN, and this is probably the major reason for the reduced antimicrobial activity of the degradation products. It can be concluded that the electrophilic nature of the α, β-unsaturated aldehyde functional group, possibly in combination with a lipophilic nature, is an essential feature for the antimicrobial activity of t-CIN.

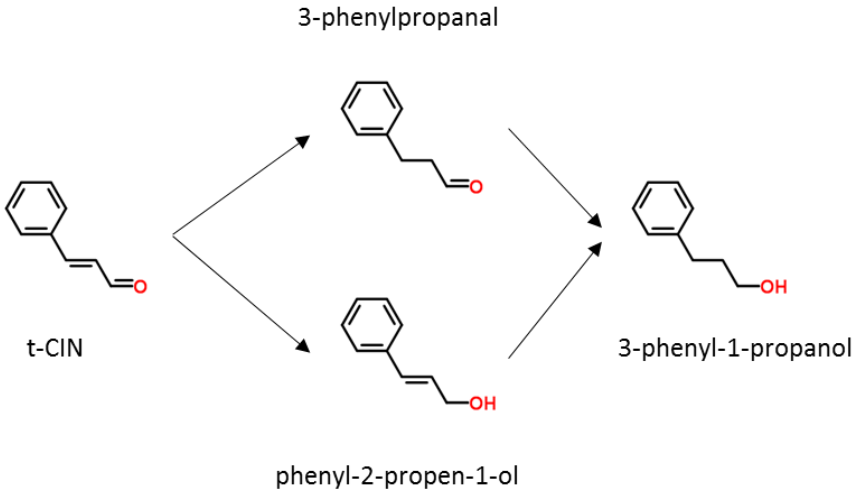

Fig. 5.8. Degradation of t-CIN in cultures of *L. monocytogenes* Scott A and its *yvcK:Himar1* mutant.

5.3.4. Complementation with *yvcK* via controlled expression

Since attempts to reintroduce the WT *yvcK* gene in the yvcK mutant on an overexpression vector were unsuccessful, and the *yvcK* downstream genes did not restore the mutant's phenotype, we attempted to complement the *yvcK* mutant with the WT gene via the IPTG-controlled pIMK3 integration vector (see Table 5.1). Introduction and integration of the complementation plasmid was successful, and induced expression of the WT *yvcK* gene in the *yvcK* mutant resulted in an almost completely restored phenotype (Fig. 5.9). The lag phase of the *yvcK* mutant in BHI with 2 mM t-CIN diminished from 43.4 h to 12.3 h upon expression of intact *yvcK*, which is only slightly longer than that of the WT (9.3 h). These results finally confirm that knockout of *yvcK* causes t-CIN sensitivity, and they suggest that its overexpression may be lethal.

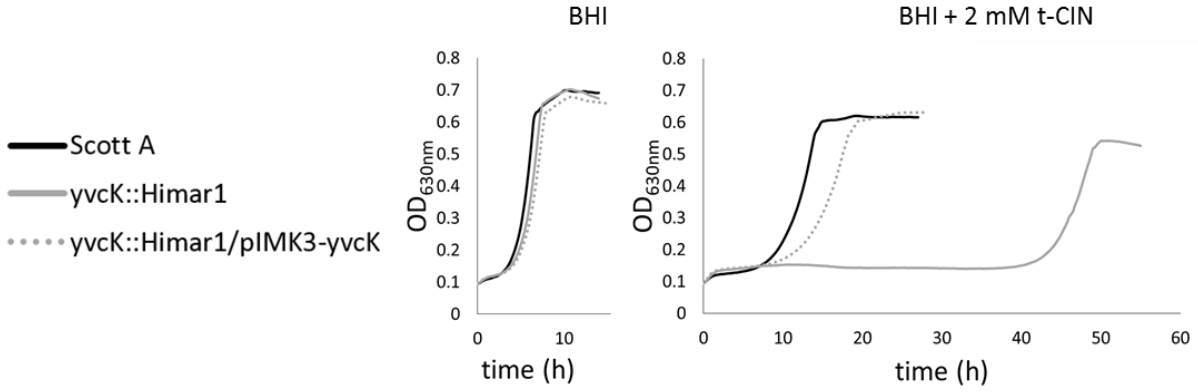

	BHI			BHI + 2 mM t-CIN		
Strain	**λ (h)**	**μ_{max} (1/h)**	**OD_{max}**	**λ (h)**	**μ_{max} (1/h)**	**OD_{max}**
Scott A	4.1 ± 0.1^{B}	0.194 ± 0.002^{A}	0.700 ± 0.003^{A}	9.3 ± 0.2^{C}	0.088 ± 0.001^{A}	0.621 ± 0.010^{A}
yvcK::Himar1	4.8 ± 0.1^{A}	0.199 ± 0.002^{A}	0.703 ± 0.005^{A}	43.4 ± 1.8^{A}	0.071 ± 0.028^{A}	0.543 ± 0.099^{A}
yvcK::Himar1/ pIMK3-*yvcK*	5.0 ± 0.1^{A}	0.177 ± 0.008^{B}	0.681 ± 0.023^{A}	12.3 ± 0.3^{B}	0.067 ± 0.003^{A}	0.617 ± 0.009^{A}

Fig. 5.9. Growth curves of *L. monocytogenes* Scott A, its *yvcK::Himar1* mutant and the genetically complemented mutant *yvcK::Himar1*/pIMK3-*yvcK* in BHI broth and BHI broth with 2 mM t-CIN. All curves are the average of three independent cultures. Standard deviations have been omitted for clarity. Lag phases (λ), maximum growth rates (μ_{max}) and maximum optical densities (OD_{max}) are listed in table. Values are mean ± standard deviation. ^{A,B,C}Different superscripts within one column indicate significant differences ($p < 0.05$).

5.3.5. Metabolic role of YvcK and PrkC in *L. monocytogenes*

To date, the biochemical role of YvcK in *L. monocytogenes* is poorly understood. In *Bacillus subtilis*, growth of *yvcK* deletion mutants is impaired on carbon sources which are substrates of the TCA cycle or the pentose phosphate pathway. Moreover, these mutants show media-dependent filamentous (on malate) or L-form shape morphologies (on gluconate). Addition of magnesium ions (25 mM $MgCl_2$) restored normal growth rate and cell morphology. Because it was previously reported that abnormal cell morphologies due to cell wall deficiency, caused by mutations in the pathway for production of teichoic acids or due to a *mreB* null mutation, can be corrected by addition of magnesium [166,167], Görke *et al.* (2005) [168] suggested that the cell wall biosynthesis is affected in the *yvcK* deletion mutant. In contrast, the t-CIN sensitive phenotype of our *yvcK* mutant could not be restored by supplementation of magnesium chloride (data not shown). Since *L. monocytogenes* has an incomplete TCA cycle and even WT strains cannot utilize TCA cycle intermediates as primary carbon sources [169], the YvcK homologue may not have the same biochemical function in *L. monocytogenes*.

Sauer *et al.* (2010) [164] were the first to report on a potential biochemical role of *L. monocytogenes* YvcK, after a genetic screen performed to identify *L. monocytogenes* mutants that induced altered levels of host cell death after infection. YvcK appeared to be required for cytosolic survival and evasion of the AIM2 inflammasome. Moreover, *yvcK* deletion mutants were hypersusceptible to lysozyme [162,170] and had significantly lower MIC values for cell wall targeting agents such as ampicillin, bacitracin, ceftriaxone and LL-37, a human antimicrobial peptide. *yvcK* deletion mutants showed normal growth in rich and minimal media with glucose-6-phosphate as the primary carbon source, but exhibited severe growth and morphology defects in minimal media with glycerol as the primary carbon source. Glucose-6-phosphate and glycerol are the two primary carbon sources used by *L. monocytogenes* during intracellular growth [171,172]. All phenotypes could be restored via complementation with the WT gene [162].

L. monocytogenes has evolved from a saprophyte to a food-borne human intracellular pathogen able to access the cytosol and spread from cell to cell, thereby evading the immune system. As such, *L. monocytogenes* has the capacity to adapt to very diverse environmental, food and host related hostile environments. Given this lifestyle, the organism requires the ability to sense changing environments and transduce these signals to consequently adapt its

metabolism. Classically, signal transduction in prokaryotes is thought to be predominantly accomplished by two-component systems, composed of two dedicated proteins, a sensor and a regulator [173]. However, it has recently become clear that many Gram-positive bacteria respond to a changing environment through one-component sensor kinases that reversibly phosphorylate effector proteins, such as the Penicillin-Binding Protein And Serine/Threonine Kinase-Associated Protein (PASTA) kinases that phosphorylate proteins to regulate diverse cellular processes ranging from cell wall synthesis [174,175] and cell division [176], to central metabolism [177], biofilm formation [178] and virulence [179]. PASTA kinases consist of an extracellular penicillin-binding domain that can also bind peptidoglycan fragments, and an intracellular serine/threonine kinase domain. Upon binding of peptidoglycan fragments, the intracellular kinase domains dimerize leading to autophosphorylation and ultimately phosphorylation of effector proteins [180].

Lima *et al.* (2011) [161] identified, via affinity chromatography and proteomic approaches, 62 proteins in *L. monocytogenes* EGD-e as putative interaction partners that interact directly or indirectly with the catalytic domain of PrkC. These proteins play a role in very diverse metabolic pathways such as cell wall synthesis, membrane bioenergetics, carbohydrate metabolism (e.g. acetate kinase), membrane synthesis (e.g. IlvE and the branched-chain α-keto acid dehydrogenase E2 subunit), DNA and RNA metabolism and detoxification systems such as superoxide dismutase and thiol peroxidase. Yet, direct evidence that these proteins are real phosphorylation substrates of PrkC was not provided. More specific phenotypic and interaction experiments were performed by Pensinger *et al.* (2014, 2016) [162,181] with a *prkC* deletion mutant. PrkC of *L. monocytogenes* 10403S appeared to be required for β-lactam tolerance, because pharmacological inhibition of PrkC by the PASTA kinase inhibitor staurosporine resulted in enhanced susceptibility to β-Lactam antibiotics. A Δ*prkC* mutant also showed ~100-fold increased susceptibility to tunicamycin, which prevents the attachment of peptidoglycan and wall teichoic acid precursors to their lipid carrier. Furthermore, increased sensitivity of this deletion mutant was observed for the same cell wall acting agents for which *ΔyvcK* showed increased sensitivity, i.e. ampicillin, bacitracin, ceftriaxone, LL-37 and lysozyme. Also like *ΔyvcK*, Δ*prkC* showed no defects in bacterial morphology or growth in rich medium or minimal medium with glucose-6-phosphate, but a severe growth defect in minimal medium with glycerol as the main carbon source. Thus, the phenotypic characteristics of the Δ*prkC*

mutant, including sensitivity to t-CIN as observed in our work, are very similar to those of the Δ*yvcK* mutant.

Interestingly, YvcK was shown to be one of the many (putative) substrates of PrkC in *Mycobacterium tuberculosis* [176] and *B. subtilis* [182]. However, YvcK was not detected by Lima *et al.* (2011) as a putative interacting protein with PrkC in *L. monocytogenes*. More recently, Pensinger *et al.* (2016) provide direct evidence that YvcK is phosphorylated by PrkC in *L. monocytogenes* on amino acid residues T252 and/or T256. To investigate the cellular functions and phenotypes regulated by YvcK via phosphorylation by PrkC, Pensinger *et al.* (2016) generated a phosphoablative T252A/T256A and a phosphomimetic T252E/T256E mutant in the native *yvcK* locus. Neither of these variant proteins can still be phosphorylated, and the YvcK T252A/T256A variant mimics a fully unphosphorylated (uncharged) state of YvcK, while the T252E/T256E variant induces a permanent negative charge which mimics the fully phosphorylated state of YvcK.

MIC-values for cell wall targeting agents remained unchanged for both double mutants, with exception of lysozyme, for which the phosphomimetic strain had a significantly lower MIC-value (2048 µg/ml) than the WT and the phosphoablative mutant (both > 4096 µg/ml). This MIC was still higher than for the *yvcK* deletion mutant (1195 µg/ml). For growth in minimal medium with glycerol as carbon source, the phosphomimetic strain showed a moderate growth defect, though not to the level of a *yvcK* or *prkC* deletion mutant, while the phosphoablative strain phenocopied the WT. Furthermore, the phosphoablative mutant appeared indistinguishable from WT when cytosolic survival, inflammasome avoidance or virulence *in vivo* was assessed, whereas the phosphomimetic mutant phenocopied a *yvcK* deletion mutant. Therefore, phosphorylation appears to inhibit the function of YvcK such that phosphomimetic YvcK mutants are highly attenuated *in vivo*. Although phosphorylation of YvcK clearly influences a number of biochemical functions in *L. monocytogenes*, the conditions under which phosphorylation is beneficial remain to be determined.

To investigate the role of YvcK phosphorylation in sensitivity to t-CIN, growth assays in t-CIN were performed with the same strains used by Pensinger *et al.* (2016) and compared with growth of WT Scott A and its *yvcK::Himar1* mutant (Fig. 5.10). The mutants of Pensinger *et al.* (2016) are constructed in a *L. monocytogenes* 10403S WT background, but the WT strains Scott A and 10403S are equally sensitive to t-CIN since their lag phases in 2 and 3 mM t-CIN

are not statistically different. The lag phase of Scott A *yvcK::Himar1* and 10403S *ΔyvcK* is also elongated roughly to the same extent by t-CIN. Similar to the observations in the assays performed by Pensinger *et al.* (2016), the mutant with the phosphoablative variant of YvcK (T252A/T256A) was indistinguishable from the WT strain and thus equally sensitive to t-CIN. The phosphomimetic strain had intermediate sensitivity between the WT and the *yvcK* knockout strains. It had an extended lag phase compared to the WT and the phosphoablative strain at 3 mM t-CIN, but less so than the *yvcK* knockout strains. However, its sensitivity did not differ from the WT and the phosphoablative strain at 2 mM t-CIN.

Since the *prkC* knockout causes inability to phosphorylate YvcK, and the phosphoablative YvcK mutant mimics a constitutively unphosphorylated YvcK, phenotypes that depend on YvcK would be expected to be similar in both mutants. However, the *prkC* knockout was very sensitive to t-CIN, while the phosphoablative YvcK mutant retained WT t-CIN tolerance. Therefore, we conclude that the t-CIN sensitivity of the *prkC* mutant does not depend on YvcK, but probably on one or more of the other numerous effector proteins of PrkC [161].

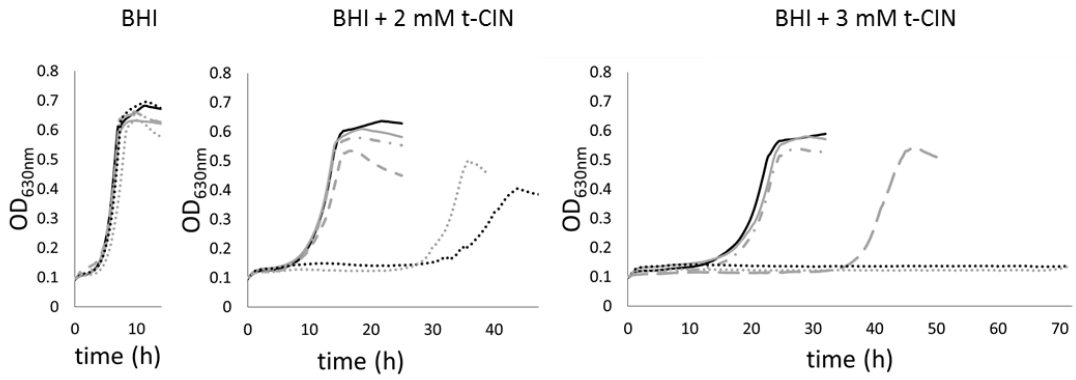

Strain		BHI			BHI + 2 mM t-CIN			BHI + 3 mM t-CIN		
		λ (h)	μ_{max} (1/h)	OD_{max}	λ (h)	μ_{max} (1/h)	OD_{max}	λ (h)	μ_{max} (1/h)	OD_{max}
Scott A	——	4.4 ± 0.0^{D}	0.184 ± 0.002^{A}	0.683 ± 0.012^{A,B}	9.6 ± 0.2^{C}	0.088 ± 0.001^{C}	0.627 ± 0.012^{A}	16.8 ± 0.2^{C}	0.061 ± 0.001^{B}	0.589 ± 0.010^{A}
10403S	——	4.7 ± 0.0^{B,C}	0.185 ± 0.003^{A}	0.632 ± 0.007^{D}	9.5 ± 0.2^{C}	0.087 ± 0.001^{C}	0.610 ± 0.004^{A}	17.8 ± 0.2^{C}	0.058 ± 0.002^{B}	0.579 ± 0.004^{A,B}
Scott A *yvcK::Himar1*	·····	4.9 ± 0.0^{B,C}	0.190 ± 0.004^{A}	0.698 ± 0.016^{A}	33.8 ± 3.2^{A}	0.031 ± 0.007^{A}	0.416 ± 0.021^{C}	>72^{A}	/	/
10403S Δ*yvcK*	·····	5.4 ± 0.2^{A}	0.167 ± 0.005^{B}	0.634 ± 0.015^{C,D}	29.3 ± 0.8^{B}	0.057 ± 0.006^{B}	0.506 ± 0.012^{B}	>72^{A}	/	/
10403S T252A/T256A	— ·	4.7 ± 0.0^{C}	0.191 ± 0.002^{A}	0.652 ± 0.006^{C,D}	9.6 ± 0.2^{C}	0.087 ± 0.001^{C}	0.580 ± 0.006^{A}	17.9 ± 0.4^{C}	0.057 ± 0.002^{B}	0.538 ± 0.020^{C}
10403S T252E/T256E	— —	4.7 ± 0.0^{C}	0.191 ± 0.001^{A}	0.663 ± 0.006^{B,C}	9.7 ± 0.0^{C}	0.065 ± 0.001^{C}	0.532 ± 0.004^{B}	38.2 ± 2.2^{B}	0.077 ± 0.005^{A}	0.550 ± 0.018^{B,C}

Fig. 5.10. Growth curves of *L. monocytogenes* Scott A and its *yvcK::Himar1* mutant, and of *L. monocytogenes* 10403S, its Δ*yvcK* mutant, YvcK phosphoablative mutant (T252A/T256A) and YvcK phosphomimetic mutant (T252E/T256E) in BHI broth and BHI broth with 2 and 3 mM t-CIN. All curves are the average of three independent cultures. Standard deviations have been omitted for clarity. Lag phases (λ), maximum growth rates (μ_{max}) and maximum optical densities (OD_{max}) are listed in the table. Values are mean ± standard deviation. ^{A,B,C,D}Different superscripts within one column indicate significant differences ($p < 0.05$).

5.4. Conclusion

Both the *prkC* and *yvcK* mutant are hypersensitive to t-CIN. The biochemical role of PrkC cannot be directly linked to the mode of action of t-CIN, as this serine/threonine PASTA kinase putatively interacts, directly or indirectly, with more than 62 proteins in *L. monocytogenes* [161]. Despite the numerous phenotypes of *yvcK* knock-out mutants, the biochemical role of YvcK remains unknown. Yet, our data and the results of Pensinger *et al.* (2016) [162] suggest that the phosphorylation state of YvcK is important to regulate the stress response induced by specific environmental conditions or antimicrobials. Yet, the conditions and dynamics of YvcK phosphorylation, and its precise cellular function and relation to t-CIN sensitivity require further investigation.

NADH:flavin oxidoreductase (NfoR), a predicted reductase of α, β-unsaturated aldehydes, resides in a putative operon with *yvcK* [164]. Yet, we could not detect less biological degradation of t-CIN in the *yvcK* mutant compared to WT, indicating that NfoR has no major contribution in the reduction of t-CIN. Interestingly, the HS-SPME-GC-MS analysis showed that biological reduction only starts in late-exponential phase and that degradation to less or non-reactive t-CIN derivatives proceeds to undetectable levels during stationary phase. These results indicate that biological degradation of t-CIN is not a prerequisite for the onset of bacterial exponential growth in the presence of t-CIN.

Chapter 6

General conclusions & future perspectives

Natural antimicrobial food preservatives have been investigated for over a decade, driven by a consumers' demand for foods that are more natural and less processed, but maintain the highest safety standard. Plant extracts such as EOs constitute a vast reservoir of potential antimicrobial compounds that can be used to meet these challenges and suppress the growth of food-borne pathogens [20]. Although many EO compounds have a wide activity spectrum including Gram-positive and Gram-negative bacteria and yeasts and molds, their application as food preservatives is often limited by their low water solubility and strong sensory impact. An attractive approach to overcome the limitations of essential oil based antimicrobials is the use of hurdle technology, which combines two or more processing and preservation factors at mild intensity to obtain maximal control of microbial safety and stability with a minimal loss of food quality [22]. Hurdle technology is most effective when it combines hurdles that act synergistically. Currently, such synergistic applications are developed by trial and error.

Knowledge on the mode of action of individual hurdles could provide insight in the mechanisms underlying synergistic interactions and as such support the development of novel effective hurdle combinations, but such knowledge remains rather scarce.

Therefore, we used a molecular-genetic approach to investigate the mode of action of *trans*-cinnamaldehyde (t-CIN), as a model for small hydrophobic and thiol-reactive compounds of plant EOs. This work focused on *Listeria monocytogenes* as one of the most important food pathogens in minimally treated and refrigerated ready-to-eat foods, which is one of the strongest growing and innovative segments in the food industry.

6.1. Impact of subinhibitory concentrations of t-CIN on *L. monocytogenes* growth

Analysis of the impact of sub-MIC concentrations on the growth parameters of both WT and sensitive transposon mutants, shows that t-CIN primarily exerts its growth inhibitory activity on *L. monocytogenes* by elongating the lag phase in a concentration-dependent manner (chapter 2). The lag phase can be considered as an adaptation phase in which cells adapt to become capable to grow in the presence of t-CIN. In chapter 3, at least one of the adaptation strategies is discussed, more specifically membrane fatty acid adaptation in response to the membrane fluidizing effect of t-CIN [45]. Lag phases of independent biological replicates of all investigated strains generally show very little variability within one experiment. It would be interesting to further investigate the effect of t-CIN on the lag phase distribution within the cell populations, for example via time-lapse microscopy or growth assays with more diluted cultures.

6.2. Screen for t-CIN and AIT sensitive transposon mutants

To gain insight in the cellular mode of action of t-CIN we constructed a whole-genome random transposon mutant library in *L. monocytogenes* Scott A and screened it for t-CIN sensitivity (chapter 2). The library was also screened for mutants sensitive to allyl isothiocyanate (AIT), a compound with a different chemical functional group, that is however also thiol-reactive and lipophilic. The screen delivered mutants that are affected in genes encoding proteins with very diverse biochemical functions. Some of these mutations are predicted to have pleiotropic detrimental consequences on the metabolism and cannot be directly linked to the mode of action of t-CIN. An example of this type of t-CIN sensitive mutants is *L. monocytogenes prkC::Himar1*. PrkC is a serine/threonine PASTA kinase that putatively interacts, directly or

indirectly, with more than 62 proteins in *L. monocytogenes* [161]. Among these interacting proteins are YvcK [162] and IlvE [161], of which the production was knocked out in two other mutants picked up in the screen.

Since t-CIN and AIT are both lipophilic and thiol-reactive, we had expected that the screen would yield mutants affected in membrane synthesis and membrane processes on the one hand, but also in redox homeostasis on the other hand. However, no mutants directly linked to redox homeostasis or thiol-disulfide balance were found. Genes involved in such processes in *L. monocytogenes* include *spx* and *gshF*. Spx is a global regulator that senses oxidative stress through a conserved cysteine-X-X-cysteine motif that is reduced under normal growth conditions and that can activate or repress transcription in response to oxidative stress via direct interaction with RNA polymerase [183]. GshF is the sole *L. monocytogenes* glutathione synthase. Glutathione is a thiol-bearing tripeptide (γ-glutamyl cysteinyl glycine) present at millimolar concentrations in the cytoplasm, that contributes to maintaining a reducing environment in bacteria [184,185]. Only the moderately sensitive mutant *L. monocytogenes 5'asnB::Himar1* could be indirectly linked to redox stress. In *E. coli*, Cys-2 of AsnB is one of the first cellular thiol groups to be consistently modified upon exposure to peroxynitrite, indicating a potential role in sensing redox stress [139]. Screening conditions may be partially responsible for the fact that no genes related to redox homeostasis were detected. However, inactivating one gene of the redox homeostasis system does not necessarily imbalance the system to such an extent that mutants show increased sensitivity for t-CIN.

To investigate the role of proteins linked to thiol-redox balance, directed gene deletion mutants such as Δ*gshF* or *Δspx* should be constructed and assessed for t-CIN sensitivity. Also, a quantitative redox proteomics approach, as previously used by Lindemann *et al.* (2013) [139] could uncover which cytosolic proteins are consistently thiol-modified by t-CIN, and to which extent they are modified. Monitoring real-time redox variations at single cell level via time-lapse microscopy with fluorescent protein-based FRET (Förster resonance energy transfer) sensors [186], would deliver even more detailed insights in the dynamics of the redox status from initial exposure to t-CIN, during the t-CIN induced lag phase and during exponential growth.

The screening with t-CIN and AIT yielded some identical, but also some different mutants. This suggests that these compounds, although they are both lipophilic and thiol-reactive, may still

have somewhat different cellular targets. Although the identified mutations that cause hypersensitivity do not immediately reveal the mode of action, it is a powerful approach for comparing different compounds to reveal if there are differences in the mode of action. As such, it will be interesting to test the t-CIN and AIT sensitive mutants identified in this work against other low-molecular weight compounds that differ in either lipophilicity or thiol reactivity. More specifically, testing the mutants against lipophilic, but not thiol-reactive compounds such as carvacrol (logP = 3.28), and hydrophilic and electrophilic compounds such as reuterin (logP = -1.11), could generate insight in the properties of the compounds that contribute to their antimicrobial action. Additionally, the transposon mutant library can be screened with the latter compounds and with any other compounds of interest. This would allow to group compounds based on their 'mutant profile'. When this information is subsequently overlaid with results from inhibition tests with pairs of compounds, groups of compounds can be mapped according to synergistic, additive or antagonistic interactions. This would generate insight in how different antimicrobials interact, and would also support the development of effective combinations of compounds for applications.

6.3. Membrane fatty acid composition as a determinant of t-CIN sensitivity

Within the diverse set of identified t-CIN sensitive mutants, we choose to first characterize the *ilvE::Himar1* mutant in more detail (chapter 3), because IlvE has a very specific and well documented biochemical role in the biosynthesis of membrane fatty acids in *L. monocytogenes*. IlvE reversibly catalyzes the conversion of BCAAs to corresponding α-ketoacids that are subsequently used as precursors for the BCFA synthesis. Moreover, while it is widely assumed that membrane properties play an important role in the sensitivity for hydrophobic antimicrobials, the influence of fatty acid composition on the tolerance for EO compounds had not been investigated in detail.

The results of chapter 3 indicate that fatty acid synthesis and membrane composition play a key role in tolerance for t-CIN. In line with the biochemical function of IlvE, the membranes of the *ilvE* mutant had almost completely lost the anteiso BCFAs, which are the major fatty acid fraction in WT *L. monocytogenes*. In addition, both the WT and its *ilvE* mutant adapted their membrane composition in response to subinhibitory concentrations of t-CIN, in a way that the membranes are predicted to become more rigid. Such an adaptation could possibly counteract the described membrane fluidizing effect of t-CIN [45]. Although exponential cells growing in

the presence of t-CIN already possess adapted membranes, it remains unclear whether this adaptation takes already place during the lag phase and would therefore be a prerequisite to initiate growth in the presence of t-CIN.

However, because the impact of shifts in fatty acid composition on membrane fluidity are not always easy to predict, it would be useful to conduct direct measurements of membrane fluidity. Further, the altered membrane composition is also likely to affect the diffusion of t-CIN through the membranes and the accumulation of t-CIN in the membranes, but our results do not allow to make predictions on these effects. Increased diffusion may lead to increased cytoplasmic redox stress, and increased membrane accumulation may compromise membrane associated functions. Both effects may thus contribute to the hypersensitivity of the *ilvE* mutant. Passage of t-CIN through the membranes could be investigated using C^{13}-labeled t-CIN via nuclear magnetic resonance and/or mass spectrometry. In addition, membrane fluidity can be determined via fluorescent anisotropy measurements using fluorescent hydrophobic probes like DPH (1,6-diphenyl 1,3,5-hexatriene). DPH incorporates into the lipid bilayer and exhibits strong fluorescence when intercalated into lipid membranes. Relative increases or decreases of the membrane fluidity can then be determined by exciting cell suspensions with polarized light and measuring the degree of polarization of emitted light, which is inversely related to the fluidity, because the probe molecules will be more mobile and less ordered in a fluid membrane [187]. To assign a real value to membrane fluidity, fluorescent molecular rotors like phenyl-BODIPY are more valuable. Its fluorescence lifetime is sensitive to the viscosity of the membrane and measurements are made using fluorescence lifetime microscopy which allows quantitative mapping of viscosity in microscopically heterogeneous environments [188,189].

6.4. Regulation of fatty acid synthesis and the relation of IlvE to central metabolic pathways

Although its biochemical activity is well documented, the role of IlvE in BCFA synthesis and its relation to central metabolic pathways has not been described in detail in *L. monocytogenes*. The isolation of suppressor mutations in *codY, argR* and *ack* in the *ilvE::Himar1* mutant led to novel insights in these aspects (chapter 4).

CodY is one of the major transcriptional regulators in the *Firmicutes*. Transcriptome analysis of a *L. monocytogenes* 10403S WT and *codY* knockout has recently revealed that CodY controls

amino acid biosynthesis (mainly BCAAs and histidine), certain carbon and nitrogen metabolism genes, critical enzymes of the TCA cycle, arginine metabolism, purine and riboflavin biosynthesis, motility and virulence [146]. Interestingly, each of the three identified CodY revertants with increased t-CIN tolerance had a single amino acid substitution, suggesting subtle changes in the regulatory function of CodY instead of loss-of-function mutations. As an example, the Phe98Ser mutation causes a well-documented change in affinity for its ligand isoleucine, thereby derepressing the *ilv-leu* operon [155], allowing WT-like fatty acid synthesis in an IlvE-independent manner. Since no *codY* loss-of-function revertants were found, it seems that complete loss of CodY may reduce tolerance for t-CIN rather than increasing it, possibly because of its impact on the regulation of other pathways in *L. monocytogenes.* Moreover, each of the three substituted amino acid residues (Phe-98, Arg-167 and Arg-214) are found to be invariant residues in CodY orthologues of twelve different *Firmicutes* species, highlighting their importance for the function or structure of CodY [148]. However, a *codY* deletion mutant in *L. monocytogenes* 10403S has been described and is viable, but impaired in motility and cell adhesion [146]. To further investigate the functionality of the single substitution CodY variants, a *codY* deletion mutant in an *ilvE::Himar1* background could be made and phenotypically compared with the substitution mutants. Alternatively, a *codY* deletion mutant of the WT strain could be complemented with the CodY variant proteins. Subsequently, the performance of these strains could be assessed for the different CodY-regulated phenotypes such as motility, as well as for t-CIN sensitivity. In addition, transcriptome studies of the WT, its *ilvE* mutant and the revertants in absence or presence of t-CIN would fully elucidate the regulatory role of CodY under these stressful conditions and the functionality of mutated CodY proteins.

In contrast to the subtle mutations identified in CodY, the four mutations found in the ArgR revertants all abort translation and are thus probably loss-of-function mutations (chapter 4). The ArgR regulon in *L. monocytogenes* is so far unknown. ArgR was shown to tune the arginine metabolism especially during acid stress in *L. monocytogenes* [66,147] and in other *Firmicutes* including *Bacillus* [190,191], *Lactobacillus* [192], *Lactococcus* [193,194] and *Streptococcus* [195] species. So far, no regulatory roles of ArgR in other metabolic pathways have been documented, and transcriptome analysis in *Lactococcus lactis* revealed no involvement of ArgR in pathways other than arginine metabolism [196]. Our results indicate that ArgR may

additionally control the expression of genes related to BCFA biosynthesis in *L. monocytogenes*, because the *ilvE::Himar1 argR* revertants have strongly increased amounts of iso-C15:0 compared to the *ilvE* mutant. In line with these observations, the *ilvE* mutant became even more sensitive to t-CIN upon supplementation of the ArgR effector molecule, arginine. Transcriptome analysis of an *argR* knockout in comparison with its WT could confirm its putative role in fatty acid synthesis, possibly via interaction with CodY, as well as other possible functions.

In contrast to the suppression mutations identified in *ilvE::Himar1 codY* and *argR* revertants, suppression mutations in acetate kinase (Ack) are very diverse and resulted in greatly increased t-CIN tolerance without major changes in membrane fatty composition. This implies that the membrane itself is not the major or only target of the antimicrobial action of t-CIN and that t-CIN also disturbs metabolic homeostasis. The *ilvE::Himar1 ack* revertants will prove very useful to investigate the nature of this disturbance in more detail. Mutations in acetate kinase are predicted to influence the central carbon metabolism, and this is reflected by the increased production of acetoin in the revertants (chapter 4). They are also likely to affect the generation of energy and reducing power. Reducing power in turn is essential for thiol-redox homeostasis, which is one of the possible targets of t-CIN in view of its thiol reactivity. Therefore, further work should focus on the assessment of redox stress in the WT, *ilvE* mutant and its *ack* revertants, for example by the use of redox-sensitive fluorescent reporter proteins as mentioned earlier in this chapter. In addition, it would be interesting to see if the same mutations in acetate kinase also increase t-CIN tolerance in a WT background.

6.5. Membrane fluidity as a determinant for cell motility

Some interesting observations, although not related to the main focus of this work on antimicrobial mode of action, relate to the effect of IlvE and of the CodY variant proteins on motility. As mentioned earlier, a *codY* deletion mutant shows reduced motility in swimming assays [146]. However, we found that the *ilvE::Himar1* mutant of *L. monocytogenes* Scott A is even less motile than the *codY* deletion mutant of *L. monocytogenes* 10403S, and that its motility can be fully restored by α-ketoacid supplementation in the medium. This may indicate that motility depends on the physical state of the membrane, a link that has also been proposed for swarming in *Serratia marcescens* [197]. *S. marcescens* swarms in complex medium at 30 °C, but not at 37 °C. However, swarming at 30 °C could be inhibited by

exogenous provision of the saturated fatty acids lauric and myristic acid. In addition, swarming also occurred at 37 °C when a defined medium free of fatty acid traces was used. The study also identified a mutant defective in a two-component signal transduction system that showed constitutive swarming unaffected by exogenous saturated fatty acid addition. Further analysis showed that swarming correlated with a 'low' ratio of saturated to unsaturated fatty acids (~ 2.0), whereas swarming was inhibited when this ratio was 'high' (~ 5 or more).

Whether the effect of reduced motility due to changed fatty acid profiles in our mutants is due to the failure to assemble a functional flagellar apparatus or due to malfunctioning of this apparatus remains to be investigated. A link between membrane fluidity and motility can potentially also explain some other observations, like the finding that subinhibitory concentrations of several plant essential oil compounds inhibit motility [23,198,199]. Finally, the loss of motility in the *ilvE* mutant was also partially restored in the *ilvE::Himar1 codY* revertants, and it was further restored to WT level by α-ketoacid supplementation. This supports the earlier hypothesis that the CodY variants are still partly functional. Indeed, although they appear to have lost the ability to inhibit the *ilvE* operon (BCFA synthesis), they are still able to activate the flagellar synthesis operons.

6.6. General conclusion

The experimental approach used in this PhD work, starting with a classical screening of a whole-genome random transposon mutant library, mutant characterization and subsequent isolation and analysis of revertants, appears to be a powerful approach that can be applied to investigate the mode of action of antimicrobial compounds in general. This method not only allowed us to identify genes and pathways that are required for normal t-CIN tolerance in *L. monocytogenes*, it also resulted in novel basic insights in the biochemical activity of proteins like IlvE and YvcK, and in the regulatory network of key metabolic pathways such as the BCFA biosynthesis and carbon metabolism. The approach of isolating revertants has only been applied to the *ilvE* knockout mutant in this work, but is anticipated to be useful to further investigate the biochemical role of YvcK, which remains unclear despite –or because of- the numerous phenotypes of *L. monocytogenes yvcK* knockout strains (chapter 5, [162]).

In conclusion, this PhD work contributes to a better understanding of the mode of action of t-CIN in *L. monocytogenes*, as a model for small thiol-reactive and lipophilic compounds that are abundant in plant EOs. In-depth knowledge on the mode of action of antimicrobial compounds

remains scarce, but will support the understanding of the basis of synergistic interactions between compounds, and the design of effective hurdle technology applications that the food industry is pursuing to provide safer, more natural, fresher and tastier foods.

References

[1] Doganay M. Listeriosis: Clinical presentation. FEMS Immunol Med Microbiol 2003;35:173–5. doi:10.1016/S0928-8244(02)00467-4.

[2] The European Union summary report on trends and sources of zoonoses, zoonotic agents and food-borne outbreaks in 2015. EFSA J 2016;14. doi:10.2903/j.efsa.2016.4634.

[3] Walker SJ, Archer P, Banks JG. Growth of *Listeria monocytogenes* at refrigeration temperatures. J Appl Bacteriol 1990;68:157–62. doi:10.1111/j.1365-2672.1990.tb02561.x.

[4] Junttila JR, Niemelä SI, Hirn J. Minimum growth temperatures of *Listeria monocytogenes* and non-haemolytic *Listeria*. J Appl Bacteriol 1988;65:321–7. doi:10.1111/j.1365-2672.1988.tb01898.x.

[5] Tienungoon S, Ratkowsky DA, McMeekin TA, Ross T. Growth limits of *Listeria monocytogenes* as a function of temperature, pH, NaCl, and lactic acid. Appl Environ Microbiol 2000;66:4979–87. doi:10.1128/AEM.66.11.4979-4987.2000.

[6] Petran RL, Zottola EA. A Study of factors affecting growth and recovery of *Listeria monocytogenes* Scott A. J Food Sci 1989;54:458–60. doi:10.1111/j.1365-2621.1989.tb03105.x.

[7] Nolan DA, Chamblin DC, Troller JA. Minimal water activity levels for growth and survival of *Listeria monocytogenes* and *Listeria innocua*. Int J Food Microbiol 1992;16:323–35. doi:10.1016/0168-1605(92)90034-Z.

[8] McClure P., Roberts T., Otto Oguru P. Comparison of the effects of sodium chloride , pH and temperature on the growth of *Listeria monocytogenes* on gradient plates and in liquid medium. Lett Appl Microbiol 1989;9:95–9. doi:10.1111/j.1472-765X.1989.tb00299.x.

[9] Sleator RD, Gahan CGM, Abee T, Hill C. Identification and disruption of BetL, a secondary glycine betaine transport system linked to the salt tolerance of *Listeria monocytogenes* LO28. Appl Environ Microbiol 1999;65:2078–83.

[10] Bayles DO, Wilkinson BJ. Osmoprotectants and cryoprotectants for *Listeria monocytogenes*. Lett Appl Microbiol 2000;30:23–7. doi:doi:10.1046/j.1472-765x.2000.00646.x.

[11] McClure PJ, Kelly TM, Roberts TA. The effects of temperature, pH, sodium chloride and sodium nitrite on the growth of *Listeria monocytogenes*. Int J Food Microbiol 1991;14:77–91. doi:10.1016/0168-1605(91)90039-R.

[12] Buchanan RL, Stahl HG, Whiting RC. Effects and interactions of temperature, pH, atmosphere, sodium chloride, and sodium nitrite on the growth of *Listeria monocytogenes*. J Food Prot 1989;52:844–51.

[13] Autio T. Tracing the sources of *Listeria monocytogenes* contamination and listeriosis using molecular tools. University of Helsinki, 2003.

[14] Gudbjörnsdóttir B, Suihko ML, Gustavsson P, Thorkelsson G, Salo S, Sjöberg AM, et al. The incidence of *Listeria monocytogenes* in meat, poultry and seafood plants in the Nordic countries. Food Microbiol 2004;21:217–25. doi:10.1016/S0740-0020(03)00012-1.

[15] Ferreira V, Wiedmann M, Teixeira P, Stasiewicz MJ. *Listeria monocytogenes* persistence in food-associated environments: epidemiology, strain characteristics, and implications for public health. J Food Prot 2014;77:150–70. doi:10.4315/0362-028X.JFP-13-150.

[16] Truelstrup Hansen L, Vogel BF. Desiccation of adhering and biofilm *Listeria monocytogenes* on stainless steel: Survival and transfer to salmon products. Int J Food Microbiol 2011;146:88–93. doi:10.1016/j.ijfoodmicro.2011.01.032.

[17] Lundén JM, Miettinen MK, Autio TJ, Korkeala HJ. Persistent *Listeria monocytogenes* strains show enhanced adherence to food contact surface after short contact times. J Food Prot 2000;63:1204–7.

[18] Wulff G, Gram L, Ahrens P, Vogel BF. One group of genetically similar *Listeria monocytogenes* strains frequently dominates and persists in several fish slaughter- and smokehouses. Appl Environ Microbiol 2006;72:4313–22. doi:10.1128/AEM.02288-05.

[19] Mackey BM, Bratchell N. The heat resistance of *Listeria monocytogenes*. Lett Appl Microbiol 1989;9:89–94. doi:10.1111/j.1472-765X.1989.tb00298.x.

[20] Burt S. Essential oils: their antibacterial properties and potential applications in foods—a review. Int J Food Microbiol 2004;94:223–53. doi:doi:10.1016/j.ijfoodmicro.2004.03.022.

[21] Gyawali R, Ibrahim SA. Natural products as antimicrobial agents. Food Control 2014;46:412–29. doi:10.1016/j.foodcont.2014.05.047.

[22] Leistner L. Basic aspects of food preservation by hurdle technology. Int J Food Microbiol 2000;55:181–6. doi:10.1016/S0168-1605(00)00161-6.

[23] Hyldgaard M, Mygind T, Meyer RL. Essential oils in food preservation: Mode of action, synergies, and interactions with food matrix components. Front Microbiol 2012;3:1–24.

doi:10.3389/fmicb.2012.00012.

[24] Dufour V, Alazzam B, Ermel G, Thepaut M, Rossero A, Tresse O, et al. Antimicrobial activities of isothiocyanates against *Campylobacter jejuni* isolates. Front Cell Infect Microbiol 2012;2:53. doi:10.3389/fcimb.2012.00053.

[25] Fenwick GR, Heaney RK. Glucosinolates and their breakdown products in cruciferous crops, foods and feedingstuffs. Food Chem 1983;11:249–71. doi:10.1016/0308-8146(83)90074-2.

[26] Donsì F, Ferrari G. Essential oil nanoemulsions as antimicrobial agents in food. J Biotechnol 2016;233:106–20. doi:10.1016/j.jbiotec.2016.07.005.

[27] Zhang Z, Vriesekoop F, Yuan Q, Liang H. Effects of nisin on the antimicrobial activity of d-limonene and its nanoemulsion. Food Chem 2014;150:307–12. doi:10.1016/j.foodchem.2013.10.160.

[28] Li W, Chen H, He Z, Han C, Liu S, Li Y. Influence of surfactant and oil composition on the stability and antibacterial activity of eugenol nanoemulsions. LWT - Food Sci Technol 2015;62:39–47. doi:10.1016/j.lwt.2015.01.012.

[29] Donsì F, Annunziata M, Sessa M, Ferrari G. Nanoencapsulation of essential oils to enhance their antimicrobial activity in foods. LWT - Food Sci Technol 2011;44:1908–14. doi:10.1016/j.lwt.2011.03.003.

[30] Terjung N, Löffler M, Gibis M, Hinrichs J, Weiss J. Influence of droplet size on the efficacy of oil-in-water emulsions loaded with phenolic antimicrobials. Food Funct 2012;3:290–301. doi:10.1039/c2fo10198j.

[31] Shah B, Davidson PM, Zhong Q. Nanodispersed eugenol has improved antimicrobial activity against *Escherichia coli* O157:H7 and *Listeria monocytogenes* in bovine milk. Int J Food Microbiol 2013;161:53–9. doi:10.1016/j.ijfoodmicro.2012.11.020.

[32] Espina L, Somolinos M, Lorán S, Conchello P, García D, Pagán R. Chemical composition of commercial citrus fruit essential oils and evaluation of their antimicrobial activity acting alone or in combined processes. Food Control 2011;22:896–902. doi:10.1016/j.foodcont.2010.11.021.

[33] Karatzas AK, Kets EPW, Smid EJ, Bennik MHJ. The combined action of carvacrol and high hydrostatic pressure on *Listeria monocytogenes* Scott A. J Appl Microbiol 2001;90:463–9. doi:10.1046/j.1365-2672.2001.01266.x.

[34] Espina L, García-Gonzalo D, Laglaoui A, Mackey BM, Pagán R. Synergistic combinations of high hydrostatic pressure and essential oils or their constituents and their use in preservation of fruit juices. Int J Food Microbiol 2013;161:23–30. doi:10.1016/j.ijfoodmicro.2012.11.015.

[35] Feyaerts J, Rogiers G, Corthouts J, Michiels CW. Thiol-reactive natural antimicrobials and high pressure treatment synergistically enhance bacterial inactivation. Innov Food Sci Emerg Technol 2015;27:26–34.

[36] Amslinger S, Al-Rifai N, Winter K, Wörmann K, Scholz R, Wild PB and M. Reactivity assessment of chalcones by a kinetic thiol assay. Org Biomol Chem 2012:2–5. doi:10.1039/b000000x.

[37] Janzowski C, Glaab V, Mueller C, Straesser U, Kamp HG, Eisenbrand G. Alpha,beta-unsaturated carbonyl compounds: induction of oxidative DNA damage in mammalian cells. Mutagenesis 2003;18:465–70. doi:10.1093/mutage/geg018.

[38] Ye H, Shen S, Xu J, Lin S, Yuan Y, Jones GS. Synergistic interactions of cinnamaldehyde in combination with carvacrol against food-borne bacteria. Food Control 2013;34:619–23. doi:10.1016/j.foodcont.2013.05.032.

[39] Field D, Daly K, O'Connor PM, Cotter PD, Hill C, Paul Ross R. Efficacies of nisin a and nisin V semipurified preparations alone and in combination with plant essential oils for controlling *Listeria monocytogenes*. Appl Environ Microbiol 2015;81:2762–9. doi:10.1128/AEM.00070-15.

[40] Tajima H, Kimoto H, Taketo A. Specific antimicrobial synergism of synthetic hydroxy isothiocyanates with aminoglycoside antibiotics. Biosci Biotechnol Biochem 2001;65:1886–8. doi:10.1271/bbb.65.1886.

[41] Tajima H, Kimoto H, Taketo A. Paradoxical effect of synthetic hydroxy isothiocyanates on antimicrobial action of aminoglycosides. Biosci Biotechnol Biochem 2003;67:1844–6.

[42] Saavedra MJ, Borges A, Dias C, Aires A, Bennett RN, Rosa ES, et al. Antimicrobial activity of phenolics and glucosinolate hydrolysis products and their synergy with streptomycin against pathogenic bacteria. Med Chem 2010;6:174–83. doi:10.2174/1573406411006030174.

[43] Little DR, Masjedizadeh MR, Wallquist O, McLoughlin JI. The intramolecular Michael reaction. Org React 1995:316–543. doi:10.1002/0471264180.or047.02.

[44] Sikkema J, de Bont JA, Poolman B. Mechanisms of membrane toxicity of hydrocarbons. Microbiol Rev 1995;59:201–22. doi:0146-0749/95/$04.00+0.

[45] Nowotarska S, Nowotarski K, Friedman M, Situ C. Effect of structure on the interactions

between five natural antimicrobial compounds and phospholipids of bacterial cell membrane on model monolayers. Molecules 2014;19:7497–515. doi:10.3390/molecules19067497.

[46] Visvalingam J, Hernandez-Doria JD, Holley RA. Examination of the genome-wide transcriptional response of *Escherichia coli* O157:H7 to cinnamaldehyde exposure. Appl Environ Microbiol 2013;79:942–50. doi:10.1128/AEM.02767-12.

[47] Schaefer L, Auchtung TA, Hermans KE, Whitehead D, Borhan B, Britton RA. The antimicrobial compound reuterin (3-hydroxypropionaldehyde) induces oxidative stress via interaction with thiol groups. Microbiology 2010;156:1589–99. doi:10.1099/mic.0.035642-0.

[48] Sinensky M. Homeoviscous adaptation--a homeostatic process that regulates the viscosity of membrane lipids in *Escherichia coli*. Proc Natl Acad Sci U S A 1974;71:522–5. doi:10.1073/pnas.71.2.522.

[49] Zhang YM, Rock CO. Membrane lipid homeostasis in bacteria. Nat Rev Microbiol 2008;6:222–33. doi:10.1038/nrmicro1839.

[50] Suutari M, Laakso S. Microbial fatty acids and thermal adaptation. vol. 20. 1994. doi:10.3109/10408419409113560.

[51] Verheul A, Russell NJ, Hof RVT, Rombouts FM, Abee T, Rombouts FM, et al. Modifications of membrane phospholipid composition in nisin-resistant *Listeria* modifications of membrane phospholipid composition in nisin-resistant *Listeria monocytogenes* Scott A. Appl Environ Microbiol 1997;63:3451–7.

[52] Annous BA, Becker LA, Bayles DO, Labeda DP, Wilkinson BJ. Critical role of anteiso-C(15:0) fatty acid in the growth of *Listeria monocytogenes* at low temperatures. Appl Environ Microbiol 1997;63:3887–94.

[53] Zhu K, Bayles DO, Xiong A, Jayaswal RK, Wilkinson BJ. Precursor and temperature modulation of fatty acid composition and growth of *Listeria monocytogenes* cold-sensitive mutants with transposon-interrupted branched-chain alpha-keto acid dehydrogenase. Microbiology 2005;151:615–23. doi:10.1099/mic.0.27634-0.

[54] Poger D, Caron B, Mark AE. Effect of methyl-branched fatty acids on the structure of lipid bilayers. J Phys Chem B 2014;118:13838–48. doi:10.1021/jp503910r.

[55] Chan YC, Wiedmann M. Physiology and genetics of *Listeria monocytogenes* survival and growth at cold temperatures. Crit Rev Food Sci Nutr 2009;49:237–53. doi:10.1080/10408390701856272.

[56] Salmond C V, Kroll RG, Booth IR. The effect of food preservatives on pH homeostasis in *Escherichia coli*. J Gen Microbiol 1984;130:2845–50. doi:10.1099/00221287-130-11-2845.

[57] Ter Beek A, Keijser BJF, Boorsma A, Zakrzewska A, Orij R, Smits GJ, et al. Transcriptome analysis of sorbic acid-stressed *Bacillus subtilis* reveals a nutrient limitation response and indicates plasma membrane remodeling. J Bacteriol 2008;190:1751–61. doi:10.1128/JB.01516-07.

[58] Heavin SB, Brennan OM, Morrissey JP, O'Byrne CP. Inhibition of *Listeria monocytogenes* by acetate, benzoate and sorbate: Weak acid tolerance is not influenced by the glutamate decarboxylase system. Lett Appl Microbiol 2009;49:179–85. doi:10.1111/j.1472-765X.2009.02634.x.

[59] Stratford M, Anslow P a. Evidence that sorbic acid does not inhibit yeast as a classic "weak acid preservative". Lett Appl Microbiol 1998;27:203–6. doi:10.1046/j.1472-765X.1998.00424.x.

[60] Freese E, Sheu CW, Galliers E. Function of lipophilic acids as antimicrobial food additives. Nature 1973;241:321–5. doi:10.1038/241321a0.

[61] Golden DA, Beuchat LR, Lary Hitchcock H. Changes in fatty acid composition of various lipid components of *Zygosaccharomyces rouxii* as influenced by solutes, potassium sorbate and incubation temperature. Int J Food Microbiol 1994;21:293–303. doi:10.1016/0168-1605(94)90059-0.

[62] Mastronicolis SK, Berberi A, Diakogiannis I, Petrova E, Kiaki I, Baltzi T, et al. Alteration of the phospho- or neutral lipid content and fatty acid composition in *Listeria monocytogenes* due to acid adaptation mechanisms for hydrochloric, acetic and lactic acids at pH 5.5 or benzoic acid at neutral pH. Antonie van Leeuwenhoek, Int J Gen Mol Microbiol 2010;98:307–16. doi:10.1007/s10482-010-9439-z.

[63] Diakogiannis I, Berberi A, Siapi E, Arkoudi-Vafea A, Giannopoulou L, Mastronicolis SK. Growth and membrane fluidity of food-borne pathogen *Listeria monocytogenes* in the presence of weak acid preservatives and hydrochloric acid. Front Microbiol 2013;4:1–6. doi:10.3389/fmicb.2013.00152.

[64] Cotter PD, Gahan CGM, Hill C. A glutamate decarboxylase system protects *Listeria monocytogenes* in gastric fluid. Mol Microbiol 2001;40:465–75. doi:10.1046/j.1365-2958.2001.02398.x.

[65] Cotter PD, Ryan S, Gahan CGM, Hill C. Presence of GadD1 glutamate decarboxylase in selected *Listeria monocytogenes* strains is associated with an ability to grow at low pH. Appl Environ Microbiol 2005;71:2832–9. doi:10.1128/AEM.71.6.2832-2839.2005.

[66] Ryan S, Begley M, Gahan CGM, Hill C. Molecular characterization of the arginine deiminase system in *Listeria monocytogenes*: regulation and role in acid tolerance. Environ Microbiol 2009;11:432–45.

[67] Wiedmann M, Arvik TJ, Hurley RJ, Boor KJ. General stress transcription factor sigmaB and its role in acid tolerance and virulence of *Listeria monocytogenes*. J Bacteriol 1998;180:3650–6.

[68] Nes IF, Eklund T. The effect of parabens on DNA, RNA and protein synthesis in *Escherichia coli* and *Bacillus subtilis*. J Appl Bacteriol 1983;54:237–42. doi:0021-8847/83/0400-0237.

[69] Ma Y, Marquis RE. Irreversible paraben inhibition of glycolysis by *Streptococcus mutans* GS-5. Lett Appl Microbiol 1996;23:329–33.

[70] Valkova N, Lépine F, Valeanu L, Dupont M, Labrie L, Bisaillon JG, et al. Hydrolysis of 4-hydroxybenzoic acid esters (parabens) and their aerobic transformation into phenol by the resistant *Enterobacter cloacae* strain EM. Appl Environ Microbiol 2001;67:2404–9. doi:10.1128/AEM.67.6.2404-2409.2001.

[71] Gilbert P, Moore LE. Cationic antiseptics: Diversity of action under a common epithet. J Appl Microbiol 2005;99:703–15. doi:10.1111/j.1365-2672.2005.02664.x.

[72] Kastbjerg VG. The effect of disinfectants on *Listeria monocytogenes*-phenotypic, physiological and genetic response. Technical University of Denmark, 2009.

[73] Holah JT, Taylor JH, Dawson DJ, Hall KE. Biocide use in the food industry and the disinfectant resistance of persistent strains of *Listeria monocytogenes* and *Escherichia coli*. J Appl Microbiol Symp Suppl 2002;92:111S–120S. doi:10.1046/j.1365-2672.92.5s1.18.x.

[74] Martinez-Suarez J V., Ortiz S, López-Alonso V. Potential impact of the resistance to quaternary ammonium disinfectants on the persistence of *Listeria monocytogenes* in food processing environments. Front Microbiol 2016;7:1–8. doi:10.3389/fmicb.2016.00638.

[75] To MS, Favrin S, Romanova N, Griffiths MW. Postadaptational resistance to benzalkonium chloride and subsequent physicochemical modifications of *Listeria monocytogenes*. Appl Environ Microbiol 2002;68:5258–64. doi:10.1128/AEM.68.11.5258-5264.2002.

[76] Bisbiroulas P, Psylou M, Iliopoulou I, Diakogiannis I, Berberi A, Mastronicolis SK. Adaptational

changes in cellular phospholipids and fatty acid composition of the food pathogen *Listeria monocytogenes* as a stress response to disinfectant sanitizer benzalkonium chloride. Lett Appl Microbiol 2011;52:275–80. doi:10.1111/j.1472-765X.2010.02995.x.

[77] Mereghetti L, Quentin R, Marquet-Van Der Mee N, Audurier A. Low sensitivity of *Listeria monocytogenes* to quaternary ammonium compounds. Appl Environ Microbiol 2000;66:5083–6. doi:10.1128/AEM.66.11.5083-5086.2000.

[78] Fox EM, Leonard N, Jordan K. Physiological and transcriptional characterization of persistent and nonpersistent *Listeria monocytogenes* isolates. Appl Environ Microbiol 2011;77:6559–69. doi:10.1128/AEM.05529-11.

[79] Casey A, Fox EM, Schmitz-Esser S, Coffey A, McAuliffe O, Jordan K. Transcriptome analysis of *Listeria monocytogenes* exposed to biocide stress reveals a multi-system response involving cell wall synthesis, sugar uptake, and motility. Front Microbiol 2014;5:68. doi:10.3389/fmicb.2014.00068.

[80] Aase B, Sundheim G, Langsrud S, R??rvik LM. Occurrence of and a possible mechanism for resistance to a quaternary ammonium compound in *Listeria monocytogenes*. Int J Food Microbiol 2000;62:57–63. doi:10.1016/S0168-1605(00)00357-3.

[81] Mata MT, Baquero F, Pérez-Díaz JC. A multidrug efflux transporter in *Listeria monocytogenes*. FEMS Microbiol Lett 2000;187:185–8. doi:10.1016/S0378-1097(00)00199-3.

[82] Godreuil S, Galimand M, Gerbaud G, Jacquet C, Courvalin P. Efflux pump Lde is associated with fluoroquinolone resistance in *Listeria monocytogenes*. Antimicrob Agents Chemother 2003;47:704–8. doi:10.1128/AAC.47.2.704.

[83] Romanova NA, Wolffs PFG, Brovko LY, Griffiths MW. Role of efflux pumps in adaptation and resistance of *Listeria monocytogenes* to benzalkonium chloride. Appl Environ Microbiol 2006;72:3498–503. doi:10.1128/AEM.72.5.3498-3503.2006.

[84] Chindera K, Mahato M, Kumar Sharma A, Horsley H, Kloc-Muniak K, Kamaruzzaman NF, et al. The antimicrobial polymer PHMB enters cells and selectively condenses bacterial chromosomes. Sci Rep 2016;6:23121. doi:10.1038/srep23121.

[85] Nielsen L, Larsen M, Skovgaard S, Kastbjerg V, Westh H, Gram L, et al. *Staphylococcus aureus* but not *Listeria monocytogenes* adapt to triclosan and adaptation correlates with increased fabI expression and agr deficiency. BMC Microbiol 2013;13:177. doi:10.1186/1471-2180-13-177.

[86] McMurry LM, Oethinger M, Levy SB. Triclosan targets lipid synthesis. Nature 1998;394:531–2. doi:10.1038/28970.

[87] Bergler H, Wallner P, Ebeling A, Leitinger B, Fuchsbichler S, Aschauer H, et al. Protein EnvM is the NADH-dependent enoyl-ACP reductase (FabI) of *Escherichia coli*. J Biol Chem 1994;269:5493–6. doi:10.1007/s40256-015-0128-1.

[88] Kater MM, Koningstein GM, Nijkamp HJJ, Stuitje AR. The use of a hybrid genetic system to study the functional relationship between prokaryotic and plant multi-enzyme fatty acid synthetase complexes. Plant Mol Biol 1994;25:771–90. doi:10.1007/BF00028873.

[89] Bergler H, Fuchsbichler S, Högenauer G, Turnowsky F. The enoyl-[acyl-carrier-protein] reductase (FabI) of *Escherichia coli*, which catalyzes a key regulatory step in fatty acid biosynthesis, accepts NADH and NADPH as cofactors and is inhibited by palmitoyl-CoA. Eur J Biochem 1996;242:689–94. doi:10.1111/j.1432-1033.1996.0689r.x.

[90] Heath RJ, Rubin JR, Holland DR, Zhang E, Snow ME, Rock CO. Mechanism of triclosan inhibition of bacterial fatty acid synthesis. J Biol Chem 1999;274:11110–4. doi:10.1074/jbc.274.16.11110.

[91] Levy CW, Roujeinikova a, Sedelnikova S, Baker PJ, Stuitje a R, Slabas a R, et al. Molecular basis of triclosan activity. Nature 1999;398:383–4. doi:10.1038/18803.

[92] Mcmurry LM, Oethinger ' M, Levy SB. Overexpression of marA, soxS, or acrAB produces resistance to triclosan in laboratory and clinical strains of *Escherichia coli*. Microbiol Lett FEMS Microbiol Lett 1998;166:305–9. doi:10.1111/j.1574-6968.1998.tb13905.x.

[93] Morvan C, Halpern D, Kénanian G, Hays C, Anba-Mondoloni J, Brinster S, et al. Environmental fatty acids enable emergence of infectious *Staphylococcus aureus* resistant to FASII-targeted antimicrobials. Nat Commun 2016;7:12944. doi:10.1038/ncomms12944.

[94] Christensen EG, Gram L, Kastbjerg VG. Sublethal triclosan exposure decreases susceptibility to gentamicin and other aminoglycosides in *Listeria monocytogenes*. Antimicrob Agents Chemother 2011;55:4064–71. doi:10.1128/AAC.00460-11.

[95] Kastbjerg VG, Hein-Kristensen L, Gram L. Triclosan-induced aminoglycoside-tolerant *Listeria monocytogenes* isolates can appear as small-colony variants. Antimicrob Agents Chemother 2014;58:3124–32. doi:10.1128/AAC.02266-13.

[96] Zhou H, Fang J, Tian Y, Lu XY. Mechanisms of nisin resistance in Gram-positive bacteria. Ann Microbiol 2014;64:413–20. doi:10.1007/s13213-013-0679-9.

[97] Ming X, Daeschel MA. Nisin resistance of food-borne bacteria and the specific resistance responses of *Listeria monocytogenes*. J Food Prot 1993;56:944–8.

[98] Ming X, Daeschel MA. Correlation of Cellular Phospholipid Content with Nisin Resistance of *Listeria monocytogenes* Scott A. J Food Prot 1995;58:416–20.

[99] Mazzotta AS, Montville TJ. Nisin induces changes in membrane fatty acid composition of *Listeria monocytogenes* nisin-resistant strains at 10°C and 30°C. J Appl Microbiol 1997;82:32–8. doi:10.1111/j.1365-2672.1997.tb03294.x.

[100] Demel R a, Peelen T, Siezen RJ, De Kruijff B, Kuipers OP. Nisin Z, mutant nisin Z and lacticin 481 interactions with anionic lipids correlate with antimicrobial activity. A monolayer study. Eur J Biochem 1996;235:267–74. doi:10.1111/j.1432-1033.1996.00267.x.

[101] Crandall AD, Montville TJ. Nisin resistance in *Listeria monocytogenes* ATCC 700302 is a complex phenotype. Appl Environ Microbiol 1998;64:231–7.

[102] Collins B, Curtis N, Cotter PD, Hill C, Ross RP. The ABC transporter AnrAB contributes to the innate resistance of *Listeria monocytogenes* to nisin, bacitracin, and various beta-lactam antibiotics. Antimicrob Agents Chemother 2010;54:4416–23. doi:10.1128/AAC.00503-10.

[103] Cotter PD, Guinane CM, Hill C. The LisRK signal transduction system determines the sensitivity of *Listeria monocytogenes* to nisin and cephalosporins. Antimicrob Agents Chemother 2002;46:2784–90. doi:10.1128/AAC.46.9.2784-2790.2002.

[104] Gravesen A. Spontaneous nisin-resistant *Listeria monocytogenes* mutantswith increased expression of a putative penicilin-binding protein and their sensitivity to various antibiotics. Microb Drug Resist 2001;7:127–35.

[105] Gravesen A, Kallipolitis B, Holmstrøm K, Høiby PE, Ramnath M, Knøchel S. pbp2229-mediated nisin resistance mechanism in *Listeria monocytogenes* confers cross-protection to class IIa bacteriocins and affects virulence gene expression. Appl Environ Microbiol 2004;70:1669–79. doi:10.1128/AEM.70.3.1669-1679.2004.

[106] Begley M, Cotter PD, Hill C, Ross RP. Glutamate decarboxylase-mediated nisin resistance in *Listeria monocytogenes*. Appl Environ Microbiol 2010;76:6541–6. doi:10.1128/AEM.00203-10.

[107] Thedieck K, Hain T, Mohamed W, Tindall BJ, Nimtz M, Chakraborty T, et al. The MprF protein is required for lysinylation of phospholipids in listerial membranes and confers resistance to cationic antimicrobial peptides (CAMPs) on *Listeria monocytogenes*. Mol Microbiol 2006;62:1325–39. doi:10.1111/j.1365-2958.2006.05452.x.

[108] Bergholz TM, Tang S, Wiedmann M, Boor KJ. Nisin resistance of *Listeria monocytogenes* is increased by exposure to salt stress and is mediated via liaR. Appl Environ Microbiol 2013;79:5682–8. doi:10.1128/AEM.01797-13.

[109] Bergholz TM, Bowen B, Wiedmann M, Boor KJ. *Listeria monocytogenes* shows temperature-dependent and -independent responses to salt stress, including responses that induce cross-protection against other stresses. Appl Environ Microbiol 2012;78:2602–12. doi:10.1128/AEM.07658-11.

[110] Patrignani F, Iucci L, Belletti N, Gardini F, Guerzoni ME, Lanciotti R. Effects of sub-lethal concentrations of hexanal and 2-(E)-hexenal on membrane fatty acid composition and volatile compounds of *Listeria monocytogenes*, *Staphylococcus aureus*, *Salmonella* enteritidis and *Escherichia coli*. Int J Food Microbiol 2008;123:1–8. doi:10.1016/j.ijfoodmicro.2007.09.009.

[111] Li J, Chikindas ML, Ludescher RD, Montville TJ. Temperature- and surfactant-induced membrane modifications that alter *Listeria monocytogenes* nisin sensitivity by different mechanisms. Appl Environ Microbiol 2002;68:5904–10. doi:10.1128/AEM.68.12.5904-5910.2002.

[112] Chihib NE, Ribeiro Da Silva M, Delattre G, Laroche M, Federighi M. Different cellular fatty acid pattern behaviours of two strains of *Listeria monocytogenes* Scott A and CNL 895807 under different temperature and salinity conditions. FEMS Microbiol Lett 2003;218:155–60. doi:10.1016/S0378-1097(02)01116-3.

[113] Siroli L, Patrignani F, Gardini F, Lanciotti R. Effects of sub-lethal concentrations of thyme and oregano essential oils, carvacrol, thymol, citral and trans-2-hexenal on membrane fatty acid composition and volatile molecule profile of *Listeria monocytogenes*, *Escherichia coli* and *Salmonella* enteritidis. Food Chem 2015;182:185–92. doi:10.1016/j.foodchem.2015.02.136.

[114] Pasqua RD, Hoskins N, Betts G, Mauriello G. Changes in membrane fatty acids composition of microbial cells induced by addiction of thymol, carvacrol, limonene, cinnamaldehyde,and eugenol in the growing media. J Agric Food Chem 2006;54:2745–2749.

[115] Foss MH, Eun Y-J, Grove CI, Pauw D a., Sorto N a., Rensvold JW, et al. Inhibitors of bacterial tubulin target bacterial membranes in vivo. Medchemcomm 2013;4:112–9. doi:10.1039/c2md20127e.

[116] Strahl H, Hamoen LW. Membrane potential is important for bacterial cell division. Proc Natl Acad Sci 2010;107. doi:10.1073/pnas.1005485107.

[117] Domadia P, Swarup S, Bhunia A, Sivaraman J, Dasgupta D. Inhibition of bacterial cell division protein FtsZ by cinnamaldehyde. Biochem Pharmacol 2007;74:831–40. doi:10.1016/j.bcp.2007.06.029.

[118] Gill AO, Holley RA. Inhibition of membrane bound ATPases of *Escherichia coli* and *Listeria monocytogenes* by plant oil aromatics. Int J Food Microbiol 2006;111:170–4. doi:10.1016/j.ijfoodmicro.2006.04.046.

[119] Gill AO, Holley RA. Disruption of *Escherichia coli*, *Listeria monocytogenes* and *Lactobacillus sakei* cellular membranes by plant oil aromatics. Int J Food Microbiol 2006;108:1–9. doi:10.1016/j.ijfoodmicro.2005.10.009.

[120] Fugett E, Fortes E, Nnoka C. *Listeria monocytogenes* strain collection: development of standard *Listeria monocytogenes* strain sets for research and validation studies. J Food Prot 2006;69:2929–38.

[121] Simon R, Priefer U, Pühler A. A broad host range mobilization system for in vivo genetic engineering: transposon mutagenesis in Gram-negative bacteria. Bio/Technology 1983;1:784–91. doi:10.1038/nbt1183-784.

[122] Fleming DW, Cochi SL, MacDonald KL, Brondum J, Hayes PS, Plikaytis BD, et al. Pasteurized milk as a vehicle of infection in an outbreak of listeriosis. N Engl J Med 1985;312:404–7. doi:10.1056/NEJM198502143120704.

[123] Grant SGN, Jessee J, Bloom FR, Hanahan D. Differential plasmid rescue from transgenic mouse DNAs into *Escherichia coli* methylation-restriction mutants. Proc Natl Acad Sci U S A 1990;87:4645–9. doi:10.1073/pnas.87.12.4645.

[124] Cao M, Bitar AP, Marquis H. A mariner-based transposition system for *Listeria monocytogenes*. Appl Environ Microbiol 2007;73:2758–61. doi:10.1128/AEM.02844-06.

[125] Monk IR, Gahan CGM, Hill C. Tools for functional postgenomic analysis of *Listeria monocytogenes*. Appl Environ Microbiol 2008;74:3921–34. doi:10.1128/AEM.00314-08.

[126] Olaimat AN, Holley RA. Effects of changes in pH and temperature on the inhibition of *Salmonella* and *Listeria monocytogenes* by Allyl isothiocyanate. Food Control 2013;34:414–9. doi:10.1016/j.foodcont.2013.05.014.

[127] Baranyi J, Roberts TA. A dynamic approach to predicting bacterial growth in food. Int J Food Microbiol 1994;23:277–94. doi:10.1016/0168-1605(94)90157-0.

[128] Kwon YM, Ricke SC. Efficient amplification of multiple transposon-flanking sequences. J Microbiol Methods 2000;41:195–9. doi:10.1016/S0167-7012(00)00159-7.

[129] Lauer P, Chow MYN, Loessner MJ, Portnoy a, Calendar R. Construction, characterization, and use of two *Listeria monocytogenes* site-specific pahge integration vectors. J Bacteriol 2002;184:4177–86. doi:10.1128/JB.184.15.4177.

[130] Wattam AR, Abraham D, Dalay O, Disz TL, Driscoll T, Gabbard JL, et al. PATRIC, the bacterial bioinformatics database and analysis resource. Nucleic Acids Res 2014;42. doi:10.1093/nar/gkt1099.

[131] Ito T, Iimori J, Takayama S, Moriyama A, Yamauchi A, Hemmi H, et al. Conserved pyridoxal protein that regulates ile and val metabolism. J Bacteriol 2013;195:5439–49. doi:10.1128/JB.00593-13.

[132] Ito T, Uozumi N, Nakamura T, Takayama S, Matsuda N, Aiba H, et al. The implication of YggT of *Escherichia coli* in osmotic regulation. Biosci Biotechnol Biochem 2009;73:2698–704. doi:10.1271/bbb.90558.

[133] Hamoen LW, Meile JC, De Jong W, Noirot P, Errington J. SepF, a novel FtsZ-interacting protein required for a late step in cell division. Mol Microbiol 2006;59:989–99. doi:10.1111/j.1365-2958.2005.04987.x.

[134] Errington J, Daniel RA, Scheffers D-J. Cytokinesis in bacteria. Microbiol Mol Biol Rev 2003;67:52–65. doi:10.1128/MMBR.67.1.52-65.2003.

[135] Gundogdu ME, Kawai Y, Pavlendova N, Ogasawara N, Errington J, Scheffers DJ, et al. Large ring polymers align FtsZ polymers for normal septum formation. Embo J 2011;30:617–26. doi:10.1038/emboj.2010.345.

[136] Kwon JA, Yu CB, Park HD. Bacteriocidal effects and inhibition of cell separation of cinnamic aldehyde on *Bacillus cereus*. Lett Appl Microbiol 2003;37:61–5.

[137] Kwon JA, Yu CB, Park HD. Bacteriocidal effects and inhibition of cell separation of cinnamic aldehyde on *Bacillus cereus.* Lett Appl Microbiol 2003;37:61–5. doi:10.1046/j.1472-765X.2003.01350.x.

[138] Hemaiswarya S, Soudaminikkutty R, Narasumani ML, Doble M. Phenylpropanoids inhibit protofilament formation of *Escherichia coli* cell division protein FtsZ. J Med Microbiol 2011;60:1317–25. doi:10.1099/jmm.0.030536-0.

[139] Lindemann C, Lupilova N, Müller A, Warscheid B, Meyer HE, Kuhlmann K, et al. Redox proteomics uncovers peroxynitrite-sensitive proteins that help *Escherichia coli* to overcome nitrosative stress. J Biol Chem 2013;288:19698–714. doi:10.1074/jbc.M113.457556.

[140] Alvarez B, Radi R. Peroxynitrite reactivity with amino acids and proteins. Amino Acids 2003;25:295–311. doi:10.1007/s00726-003-0018-8.

[141] Toledo-Arana A, Dussurget O, Nikitas G, Sesto N, Guet-Revillet H, Balestrino D, et al. The Listeria transcriptional landscape from saprophytism to virulence. Nature 2009;459:950–6. doi:10.1038/nature08080.

[142] Kaneda T. Iso- and anteiso-fatty acids in bacteria: biosynthesis, function, and taxonomic significance. Microbiol Rev 1991;55:288–302.

[143] Suutari M, Laakso S. Microbial fatty acids and thermal adaptation. Crit Rev Microbiol 1994;20:285–328. doi:10.3109/10408419409113560.

[144] Jones SL, Drouin P, Wilkinson BJ, Morse PD. Correlation of long-range membrane order with temperature-dependent growth characteristics of parent and a cold-sensitive, branched-chain-fatty-acid-deficient mutant of *Listeria monocytogenes*. Arch Microbiol 2002;177:217–22. doi:10.1007/s00203-001-0380-4.

[145] Bécavin C, Bouchier C, Lechat P, Archambaud C, Creno S, Gouin E. Variations in pathogenicity. MBio 2014;5:1–12. doi:10.1128/mBio.00969-14.Editor.

[146] Lobel L, Herskovits AA. Systems level analyses reveal multiple regulatory activities of CodY controlling metabolism, motility and virulence in *Listeria monocytogenes*. PLoS Genet 2016;12:1–27. doi:10.1371/journal.pgen.1005870.

[147] Cheng C, Dong Z, Han X, Sun J, Wang H, Jiang L, et al. *Listeria monocytogenes* 10403S arginine repressor ArgR finely tunes arginine metabolism regulation under acidic conditions. Front Microbiol 2017;8:145. doi:10.3389/fmicb.2017.00145.

[148] Levdikov VM, Blagova E, Joseph P, Sonenshein AL, Wilkinson AJ. The structure of CodY, a GTP- and isoleucine-responsive regulator of stationary phase and virulence in gram-positive bacteria. J Biol Chem 2006;281:11366–73. doi:10.1074/jbc.M513015200.

[149] Shivers RP, Sonenshein AL. Activation of the *Bacillus subtilis* global regulator CodY by direct interaction with branched-chain amino acids. Mol Microbiol 2004;53:599–611. doi:10.1111/j.1365-2958.2004.04135.x.

[150] Handke LD, Shivers RP, Sonenshein AL. Interaction of *Bacillus subtilis* CodY with GTP. J Bacteriol 2008;190:798–806. doi:10.1128/JB.01115-07.

[151] Aravind L, Ponting CP. The GAF domain: an evolutionary link between diverse phototransducing proteins. Trends Biochem Sci 1997;22:458–9.

[152] Hurley JH. GAF domains: cyclic nucleotides come full circle. Sci STKE 2003;2003:PE1. doi:10.1126/stke.2003.164.pe1.

[153] Levdikov VM, Blagova E, Young VL, Belitsky BR, Lebedev A, Sonenshein AL, et al. Structure of the branched-chain amino acid and GTP-sensing global regulator, CodY, from *Bacillus subtilis.* J Biol Chem 2017;292:2714–28. doi:10.1074/jbc.M116.754309.

[154] Han AR, Kang HR, Son J, Kwon DH, Kim S, Lee WC, et al. The structure of the pleiotropic transcription regulator CodY provides insight into its GTP-sensing mechanism. Nucleic Acids Res 2016;44:9483–93. doi:10.1093/nar/gkw775.

[155] Villapakkam AC, Handke LD, Belitsky BR, Levdikov VM, Wilkinson AJ, Sonenshein AL. Genetic and biochemical analysis of the interaction of *Bacillus subtilis* CodY with branched-chain amino acids. J Bacteriol 2009;191:6865–76. doi:10.1128/JB.00818-09.

[156] Levdikov VM, Blagova E, Colledge VL, Lebedev AA, Williamson DC, Sonenshein AL, et al. Structural rearrangement accompanying ligand binding in the GAF domain of CodY from *Bacillus subtilis.* J Mol Biol 2009;390:1007–18. doi:10.1016/j.jmb.2009.05.077.

[157] Joseph P, Ratnayake-Lecamwasam M, Sonenshein AL. A region of *Bacillus subtilis* CodY protein required for interaction with DNA. J Bacteriol 2005;187:4127–39. doi:10.1128/JB.187.12.4127-4139.2005.

[158] Shivers RP, Dineen SS, Sonenshein AL. Positive regulation of *Bacillus subtilis* ackA by CodY and CcpA: Establishing a potential hierarchy in carbon flow. Mol Microbiol 2006;62:811–22. doi:10.1111/j.1365-2958.2006.05410.x.

[159] Den Hengst CD, Van Hijum SAFT, Geurts JMW, Nauta A, Kok J, Kuipers OP. The *Lactococcus lactis* CodY regulon: Identification of a conserved cis-regulatory element. J Biol Chem 2005;280:34332–42. doi:10.1074/jbc.M502349200.

[160] Molle V, Nakaura Y, Shivers RP, Yamaguchi H, Losick R, Fujita Y, et al. Additional targets of the *Bacillus subtilis* global regulator codY identified by chromatin immunoprecipitation and genome-wide transcript analysis. J Bacteriol 2003;185:1911–22. doi:10.1128/JB.185.6.1911-1922.2003.

[161] Lima A, Durán R, Schujman GE, Marchissio MJ, Portela MM, Obal G, et al. Serine/threonine protein kinase PrkA of the human pathogen *Listeria monocytogenes*: Biochemical characterization and identification of interacting partners through proteomic approaches. J Proteomics 2011;74:1720–34. doi:10.1016/j.jprot.2011.03.005.

[162] Pensinger DA, Boldon KM, Chen GY, Vincent WJB, Sherman K, Xiong M, et al. The *Listeria monocytogenes* PASTA kinase PrkA and its substrate YvcK are required for cell wall homeostasis, metabolism, and virulence. PLoS Pathog 2016;12. doi:10.1371/journal.ppat.1006001.

[163] Bécavin C, Bouchier C, Lechat P, Archambaud C, Creno S, Gouin E, et al. Comparison of widely used *Listeria monocytogenes* strains EGD, 10403S, and EGD-e highlights genomic variations underlying differences in pathogenicity. MBio 2014;5:e00969-14. doi:10.1128/mBio.00969-14.

[164] Sauer JD, Witte CE, Zemansky J, Hanson B, Lauer P, Portnoy DA. *Listeria monocytogenes* triggers AIM2-mediated pyroptosis upon infrequent bacteriolysis in the macrophage cytosol. Cell Host Microbe 2010;7:412–9. doi:10.1016/j.chom.2010.04.004.

[165] Fitzpatrick TB, Amrhein N, Macheroux P. Characterization of YqjM, an old yellow enzyme homolog from *Bacillus subtilis* involved in the oxidative stress response. J Biol Chem 2003;278:19891–7. doi:10.1074/jbc.M211778200.

[166] Lazarevic V, Soldo B, Medico N, Pooley H, Bron S, Karamata D. *Bacillus subtilis* alpha-phosphoglucomutase is required for normal cell morphology and biofilm formation. Appl Environ Microbiol 2005;71:39–45. doi:10.1128/AEM.71.1.39-45.2005.

[167] Formstone A, Errington J. A magnesium-dependent *mreB* null mutant: implications for the role of *mreB* in *Bacillus subtilis*. Mol Microbiol 2005;55:1646–57. doi:10.1111/j.1365-2958.2005.04506.x.

[168] Gorke B, Foulquier E, Galinier A. YvcK of *Bacillus subtilis* is required for a normal cell shape and for growth on Krebs cycle intermediates and substrates of the pentose phosphate pathway. Microbiology 2005;151:3777–91. doi:10.1099/mic.0.28172-0.

[169] Trivett TL, Meyer EA. Citrate cycle and related metabolism of *Listeria monocytogenes*. J Bacteriol 1971;107:770–9.

[170] Burke TP, Loukitcheva A, Zemansky J, Wheeler R, Boneca IG, Portnoy DA. *Listeria monocytogenes* is resistant to lysozyme through the regulation, not the acquisition, of cell wall-modifying enzymes. J Bacteriol 2014;196:3756–67. doi:10.1128/JB.02053-14.

[171] Joseph B, Przybilla K, Stühler C, Schauer K, Slaghuis J, Fuchs TM, et al. Identification of *Listeria monocytogenes* genes contributing to intracellular replication by expression profiling and mutant screening. J Bacteriol 2006;188:556–68. doi:10.1128/JB.188.2.556-568.2006.

[172] Eylert E, Schär J, Mertins S, Stoll R, Bacher A, Goebel W, et al. Carbon metabolism of *Listeria monocytogenes* growing inside macrophages. Mol Microbiol 2008;69:1008–17. doi:10.1111/j.1365-2958.2008.06337.x.

[173] Casino P, Rubio V, Marina A. The mechanism of signal transduction by two-component systems. Curr Opin Struct Biol 2010;20:763–71. doi:10.1016/j.sbi.2010.09.010.

[174] Dasgupta A, Datta P, Kundu M, Basu J. The serine/threonine kinase PknB of *Mycobacterium tuberculosis* phosphorylates PBPA, a penicillin-binding protein required for cell division. Microbiology 2006;152:493–504. doi:10.1099/mic.0.28630-0.

[175] Parikh A, Verma SK, Khan S, Prakash B, Nandicoori VK. PknB-mediated phosphorylation of a novel substrate, N-acetylglucosamine-1-phosphate uridyltransferase, modulates its acetyltransferase activity. J Mol Biol 2009;386:451–64. doi:10.1016/j.jmb.2008.12.031.

[176] Kang C-M, Abbott DW, Park ST, Dascher CC, Cantley LC, Husson RN. The *Mycobacterium tuberculosis* serine/threonine kinases PknA and PknB: substrate identification and regulation of cell shape. Genes Dev 2005;19:1692–704. doi:10.1101/gad.1311105.

[177] Pietack N, Becher D, Schmidl SR, Saier MH, Hecker M, Commichau FM, et al. In vitro phosphorylation of key metabolic enzymes from *Bacillus subtilis*: PrkC phosphorylates enzymes from different branches of basic metabolism. J Mol Microbiol Biotechnol 2010;18:129–40. doi:10.1159/000308512.

[178] Liu Q, Fan J, Niu C, Wang D, Wang J, Wang X, et al. The eukaryotic-type serine/threonine protein kinase Stk is required for biofilm formation and virulence in *Staphylococcus epidermidis.* PLoS One 2011;6:e25380. doi:10.1371/journal.pone.0025380.

[179] Echenique J, Kadioglu A, Romao S, Andrew PW, Trombe M-C. Protein serine/threonine kinase StkP positively controls virulence and competence in *Streptococcus pneumoniae*. Infect Immun 2004;72:2434–7. doi:10.1128/iai.72.4.2434-2437.2004.

[180] Ruggiero A, De Simone P, Smaldone G, Squeglia F, Berisio R. Bacterial cell division regulation by Ser/Thr kinases: a structural perspective. Curr Protein Pept Sci 2012;13:756–66.

[181] Pensinger DA, Aliota MT, Schaenzer AJ, Boldon KM, Ansari IUH, Vincent WJB, et al. Selective pharmacologic inhibition of a PASTA kinase increases *Listeria monocytogenes* susceptibility to

β-lactam antibiotics. Antimicrob Agents Chemother 2014;58:4486–94. doi:10.1128/AAC.02396-14.

[182] Foulquier E, Pompeo F, Freton C, Cordier B, Grangeasse C, Galinier A. PrkC-mediated phosphorylation of overexpressed YvcK protein regulates PBP1 protein localization in *Bacillus subtilis* mreB mutant cells. J Biol Chem 2014;289:23662–9. doi:10.1074/jbc.M114.562496.

[183] Whiteley AT, Ruhland BR, Edrozo MB, Reniere ML. A Redox-Responsive Transcription factor Is critical for pathogenesis and aerobic growth of *Listeria monocytogenes*. Infect Immun 2017;85:e00978-16. doi:10.1128/IAI.00978-16.

[184] Reniere ML, Whiteley AT, Portnoy DA. An In Vivo Selection Identifies *Listeria monocytogenes* Genes Required to Sense the Intracellular Environment and Activate Virulence Factor Expression. PLoS Pathog 2016;12:e1005741. doi:10.1371/journal.ppat.1005741.

[185] Masip L, Veeravalli K, Georgiou G. The many faces of glutathione in bacteria. Antioxid Redox Signal 2006;8:753–62. doi:10.1089/ars.2006.8.753.

[186] George Abraham B, Sarkisyan KS, Mishin AS, Santala V, Tkachenko N V., Karp M. Fluorescent Protein Based FRET Pairs with Improved Dynamic Range for Fluorescence Lifetime Measurements. PLoS One 2015;10:e0134436. doi:10.1371/journal.pone.0134436.

[187] Najjar MB, Chikindas M, Montville TJ. Changes in *Listeria monocytogenes* membrane fluidity in response to temperature stress. Appl Environ Microbiol 2007;73:6429–35. doi:10.1128/AEM.00980-07.

[188] Vu TT, Méallet-Renault R, Clavier G, Trofimov BA, Kuimova MK, Belijonne D, et al. Tuning BODIPY molecular rotors into the red: sensitivity to viscosity vs. temperature. J Mater Chem C 2016;4:2828–33. doi:10.1039/C5TC02954F.

[189] Loison P, Hosny NA, Gervais P, Champion D, Kuimova MK, Perrier-Cornet JM. Direct investigation of viscosity of an atypical inner membrane of *Bacillus* spores: A molecular rotor/FLIM study. Biochim Biophys Acta - Biomembr 2013;1828:2436–43. doi:10.1016/j.bbamem.2013.06.028.

[190] Maghnouj A, de Sousa Cabral TF, Stalon V, Vander Wauven C. The arcABDC gene cluster, encoding the arginine deiminase pathway of *Bacillus licheniformis,* and its activation by the arginine repressor *argR*. J Bacteriol 1998;180:6468–75.

[191] Czaplewski LG, North AK, Smith MC, Baumberg S, Stockley PG. Purification and initial characterization of AhrC: the regulator of arginine metabolism genes in *Bacillus subtilis*. Mol

Microbiol 1992;6:267–75.

[192] Nicoloff H, Arsene-Ploetze F, Malandain C, Kleerebezem M, Bringel F. Two Arginine Repressors Regulate Arginine Biosynthesis in *Lactobacillus plantarum.* J Bacteriol 2004;186:6059–69. doi:10.1128/JB.186.18.6059-6069.2004.

[193] Larsen R, Buist G, Kuipers OP, Kok J. ArgR and AhrC are both required for regulation of arginine metabolism in *Lactococcus lactis.* J Bacteriol 2004;186:1147–57.

[194] Larsen R, Kok J, Kuipers OP. Interaction between ArgR and AhrC Controls Regulation of Arginine Metabolism in *Lactococcus lactis*. J Biol Chem 2005;280:19319–30. doi:10.1074/jbc.M413983200.

[195] Fulde M, Willenborg J, de Greeff A, Benga L, Smith HE, Valentin-Weigand P, et al. ArgR is an essential local transcriptional regulator of the arcABC operon in *Streptococcus suis* and is crucial for biological fitness in an acidic environment. Microbiology 2011;157:572–82. doi:10.1099/mic.0.043067-0.

[196] Larsen R, Van Hijum SAFT, Martinussen J, Kuipers OP, Kok J. Transcriptome analysis of the *Lactococcus lactis* ArgR and AhrC regulons. Appl. Environ. Microbiol., vol. 74, American Society for Microbiology (ASM); 2008, p. 4768–71. doi:10.1128/AEM.00117-08.

[197] Lai HC, Soo PC, Wei JR, Yi WC, Liaw SJ, Horng YT, et al. The RssAB two-component signal transduction system in *Serratia marcescens* regulates swarming motility and cell envelope architecture in response to exogenous saturated fatty acids. J Bacteriol 2005;187:3407–14. doi:10.1128/JB.187.10.3407-3414.2005.

[198] Burt SA, van der Zee R, Koets AP, de Graaff AM, van Knapen F, Gaastra W, et al. Carvacrol induces heat shock protein 60 and inhibits synthesis of flagellin in *Escherichia coli* O157:H7. Appl Environ Microbiol 2007;73:4484–90. doi:10.1128/AEM.00340-07.

[199] Amalaradjou MAR, Kim KS, Venkitanarayanan K. Sub-inhibitory concentrations of trans-cinnamaldehyde attenuate virulence in *Cronobacter sakazakii* in vitro. Int J Mol Sci 2014;15:8639–55. doi:10.3390/ijms15058639.

Databases

Biocyc Database Collection (https://biocyc.org)

PubChem (https://pubchem.ncbi.nlm.nih.gov/)

Legislation

European Union (2012). Commission implementing regulation (EU) No 872/2012 of 1 October 2012 adopting the list of flavouring substances provided for by Regulation (EC) No 2232/96 of the European Parliament and of the Council, introducing it in Annex I to Regulation (EC) No 1334/2008 of the European Parliament and of the Council and repealing Commission Regulation (EC) No 1565/2000 and Commission Decision 1999/217/EC. *Official Journal of the European Union*, 55(L267): 1-161.

Web pages

Conjugate addition reactions, Chemistry Libretexts. Last visisted on 12/05/2017. https://chem.libretexts.org/?title=Core/Organic_Chemistry/Aldehydes_and_Ketones/Reactivity_of_Aldehydes_%26_Ketones/Conjugate_Addition_Reactions.

Supplementary material

Supplementary material S1a, b, c: Growth curves of WT Scott A and *Himar1* transposon mutants in BHI (1a), BHI with 4 mM t-CIN (1b) and BHI with 6 mM AIT (1c), corresponding to the growth parameters listed in Table 2.4 and Table 2.5 in chapter 2. Transposon inserted genes are mentioned above the corresponding curve. Black lines represent WT growth, grey lines mutant growth. All curves are the average of three independent cultures. Standard deviations have been ommitted for clarity.

S1a. Growth in BHI

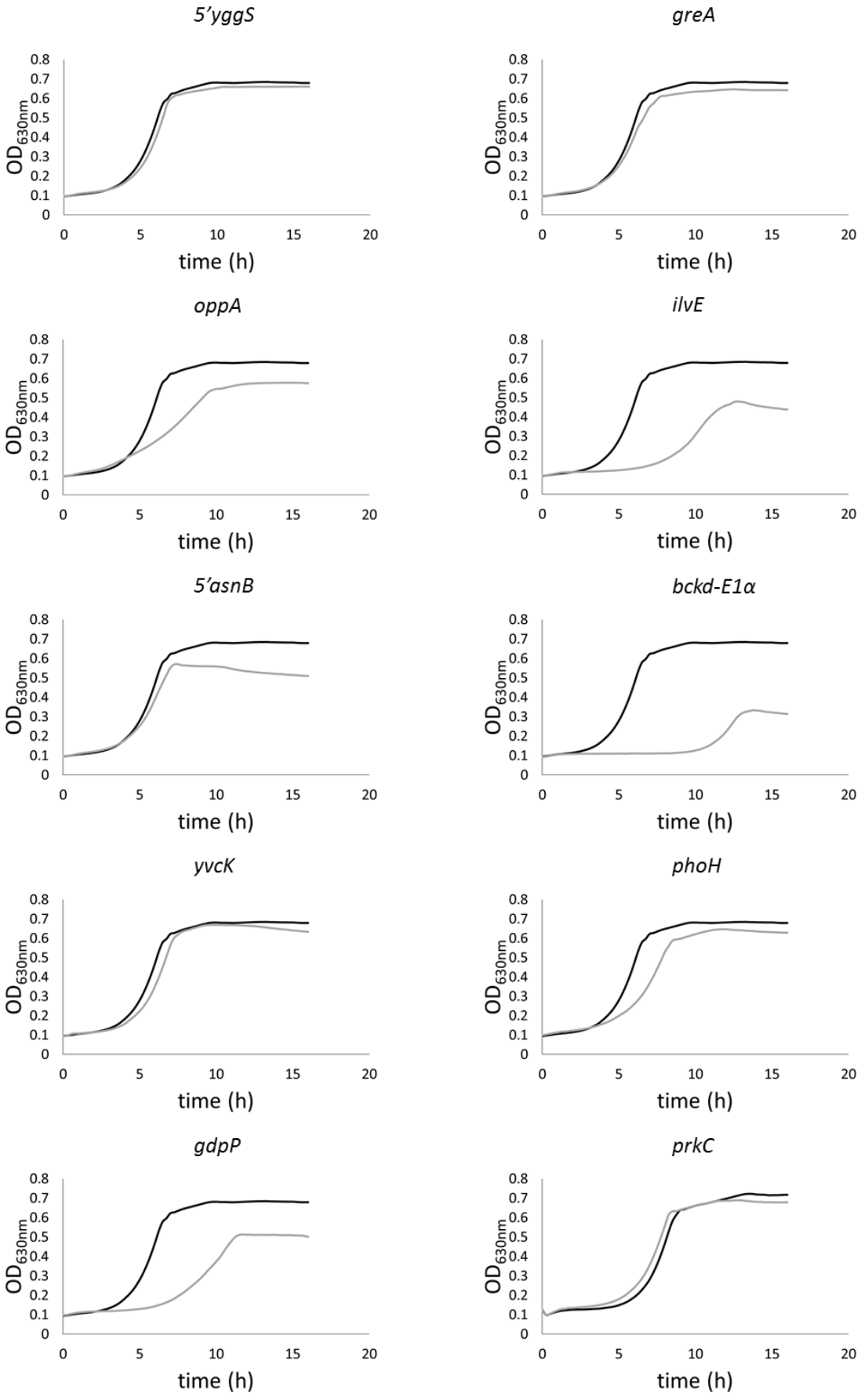

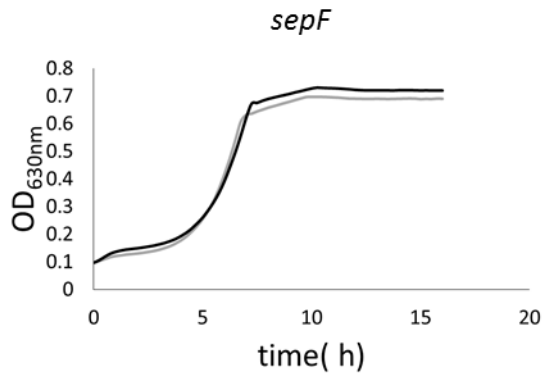
sepF
0.8
0.7
0.6
0.5
0.4
0.3
0.2
0.1
0
OD630nm
0
5
10
15
20
time(h)

S1b. Growth in BHI with 4 mM t-CIN

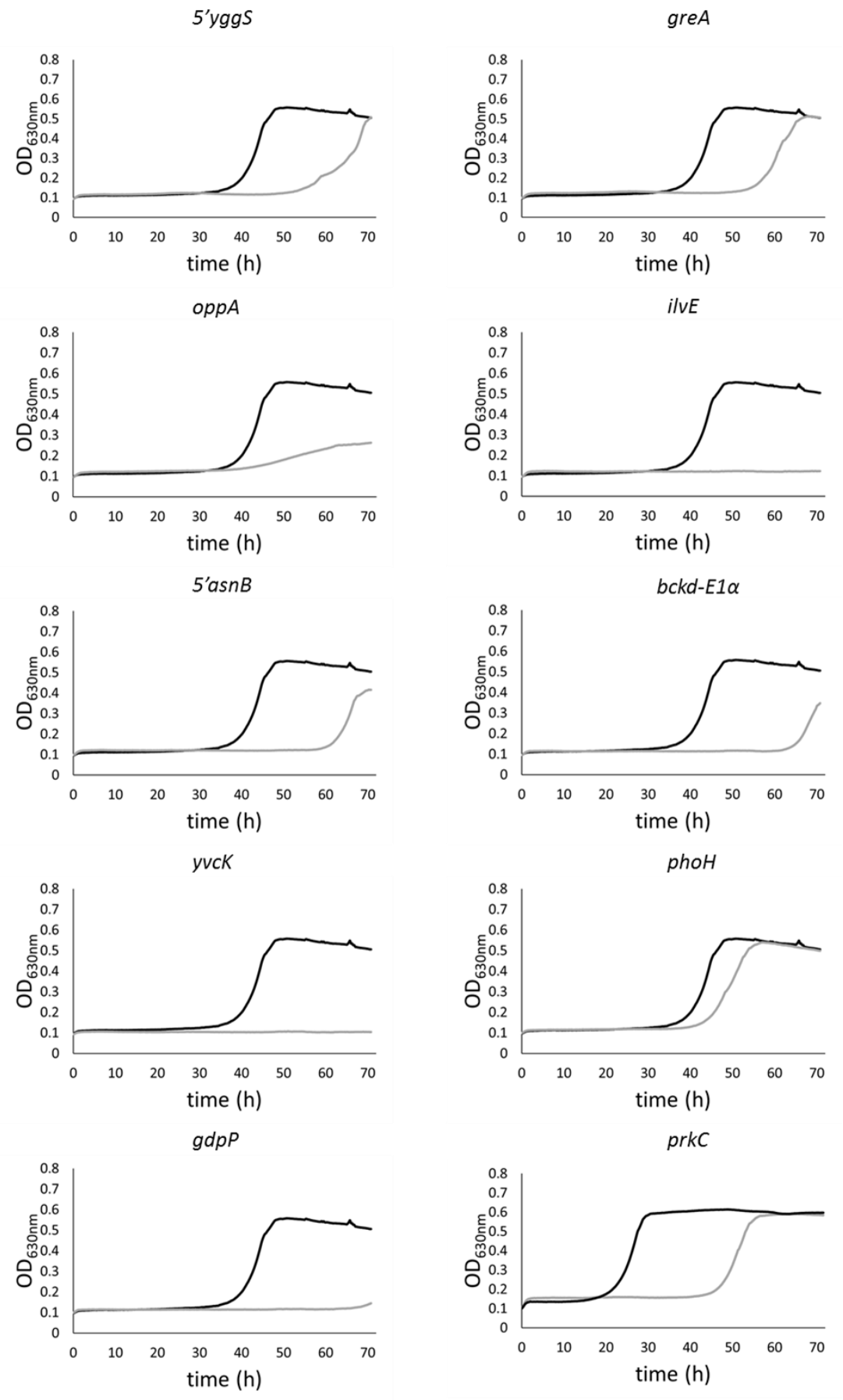

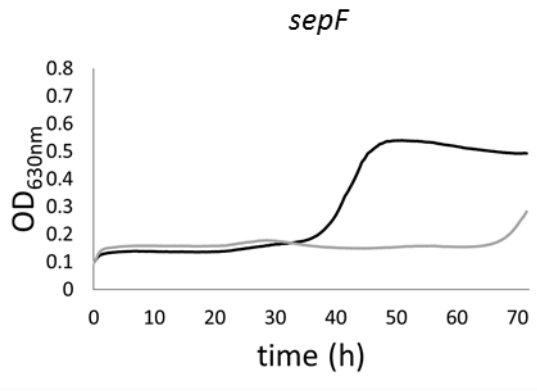
sepF
0.8
0.7
0.6
0.5
0.4
0.3
0.2
0.1
0
OD630nm
0
10
20
30
40
50
60
70
time (h)

S1c. Growth in BHI with 6 mM AIT

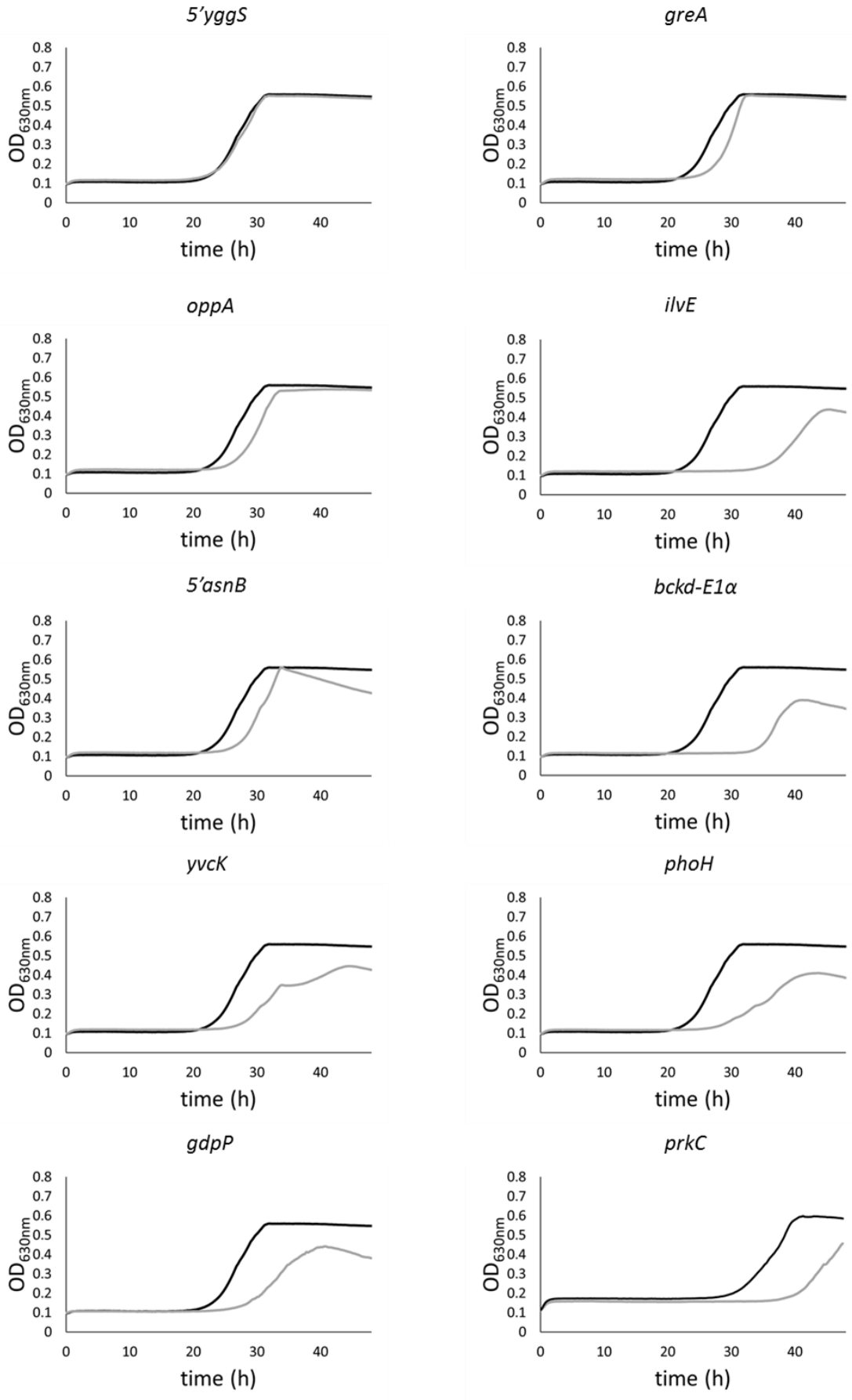

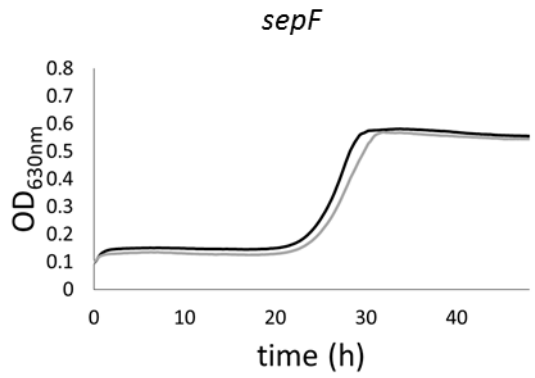
sepF
0.8
0.7
0.6
0.5
0.4
0.3
0.2
0.1
0
OD630nm
0
10
20
30
40
time (h)

Supplementary material S2. Growth curves in BHI + 2 mM t-CIN of revertants obtained from *L. monocytogenes ilvE::Himar1*, cultured in BHI as listed in Table 4.4 (2a) and in BHI + t-CIN as listed in Table 4.5 (2b). All curves are the average of three independent cultures. Standard deviations have been ommitted for clarity.

2a.

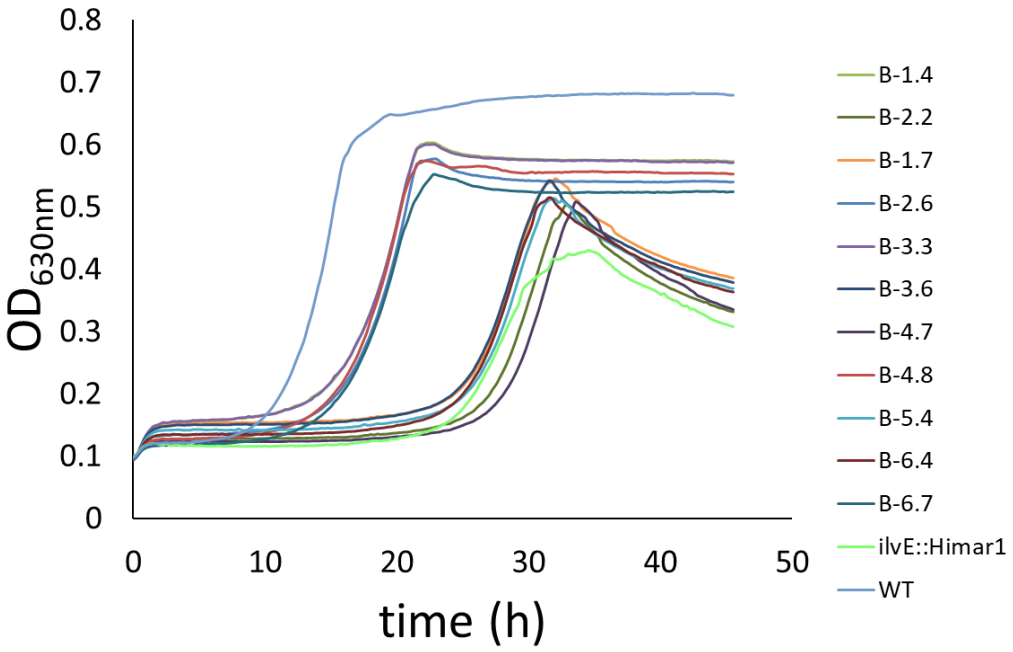

2b.

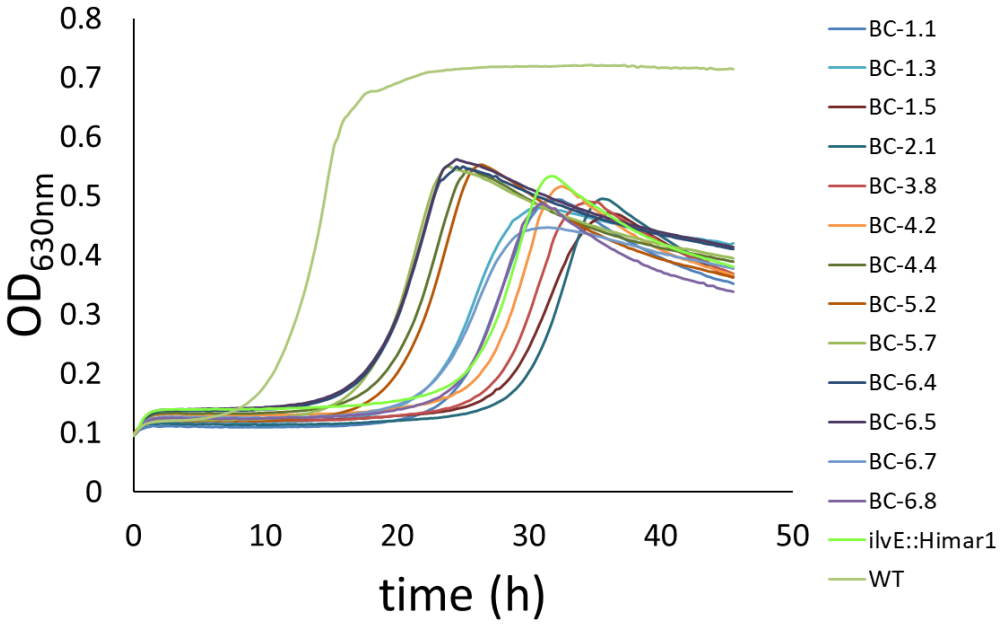

Supplementary material S3. Photographs corresponding to the motility assay (chapter 4, section 4.3.3.1). Colonies were stabbed in soft agar and grown for 24 h at 30°C. Colony diameters are presented in Table 4.8.

Scott A

BHI 0.2% agar | BHI 0.2% agar + 1 mM α-keto acids

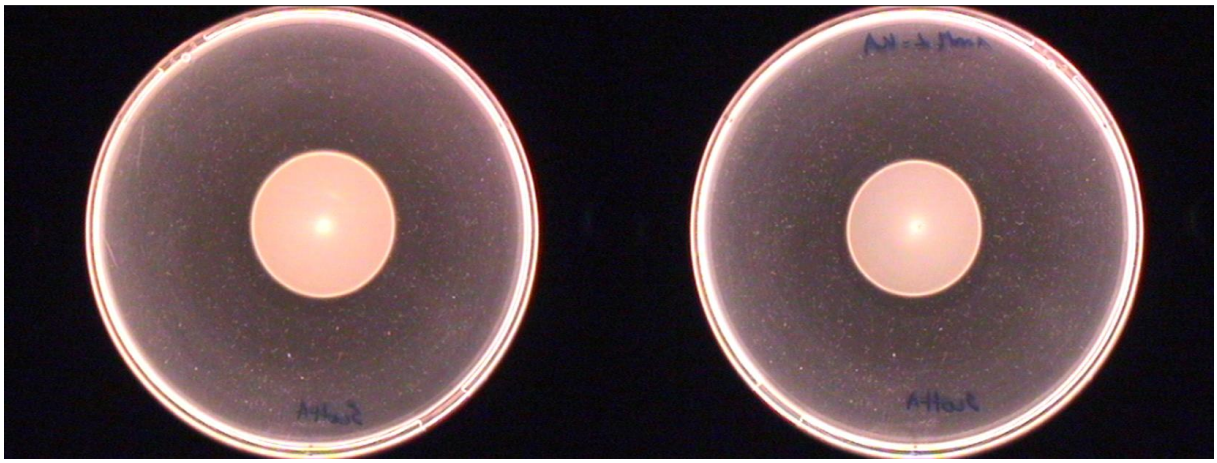

10403S

BHI 0.2% agar | BHI 0.2% agar + 1 mM α-keto acids

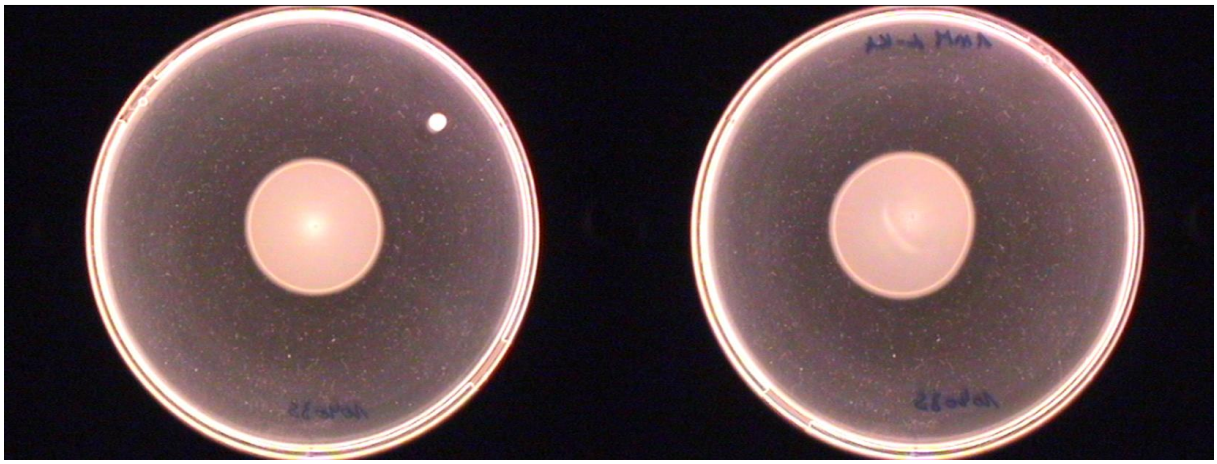

Scott A *ilvE::Himar1*

BHI 0.2% agar

BHI 0.2% agar + 1 mM α-keto acids

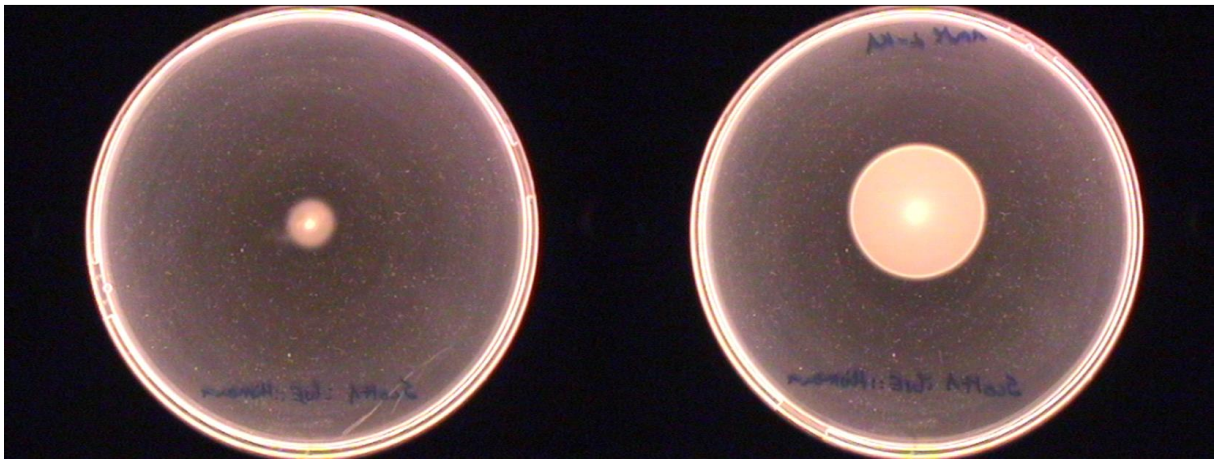

10403S Δ*codY*

BHI 0.2% agar

BHI 0.2% agar + 1 mM α-keto acids

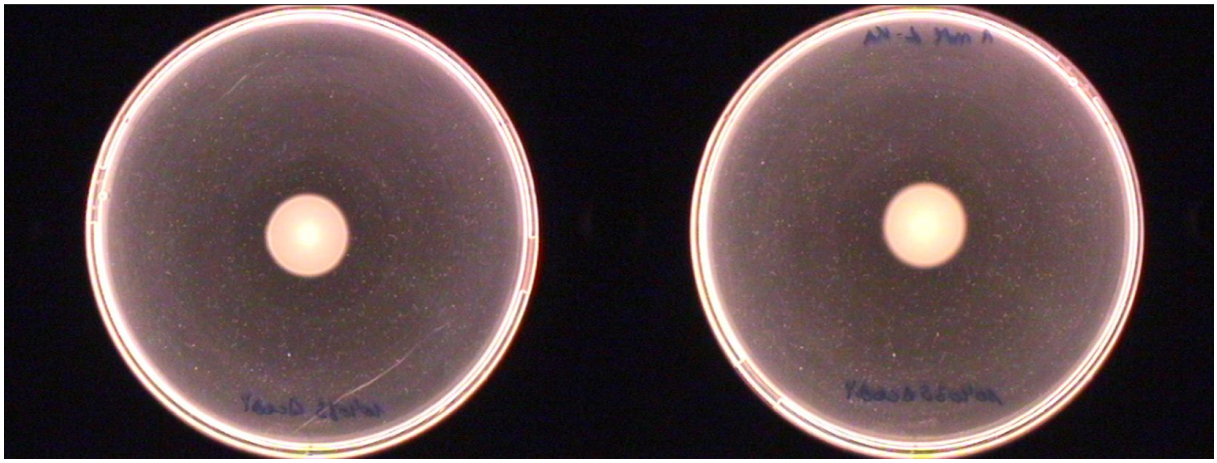

Scott A *ilvE::Himar1 codY1* (Phe98Ser)

BHI 0.2% agar | BHI 0.2% agar + 1 mM α-keto acids

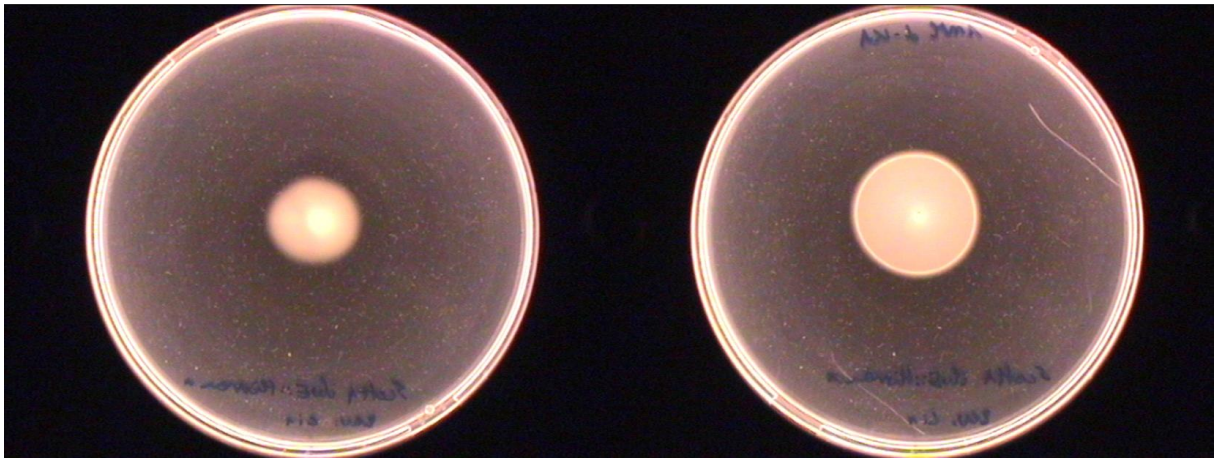

Scott A *ilvE::Himar1 codY2* (Arg167Ser)

BHI 0.2% agar | BHI 0.2% agar + 1 mM α-keto acids

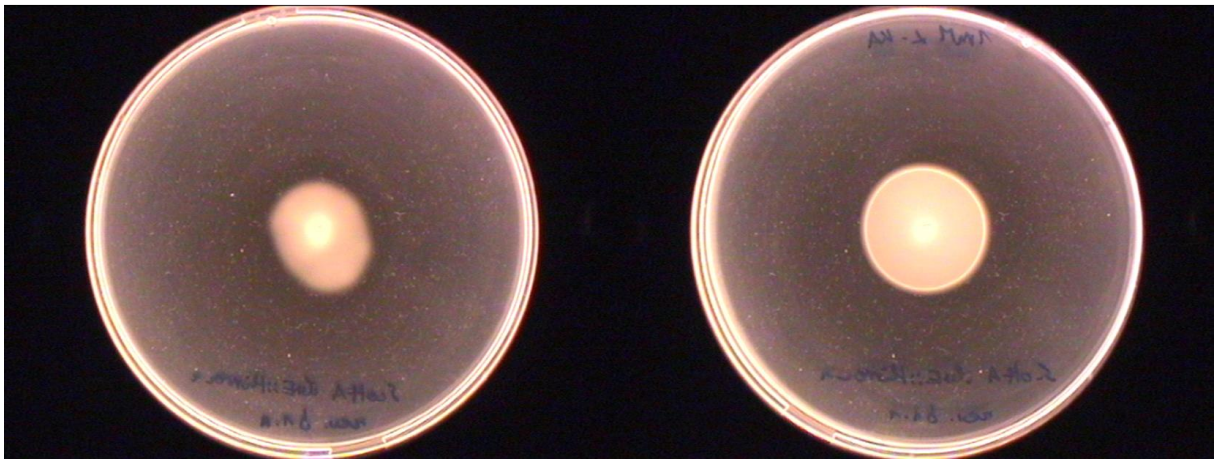

Scott A *ilvE::Himar1 codY3* (Arg214Leu)

BHI 0.2% agar | BHI 0.2% agar + 1 mM α-keto acids

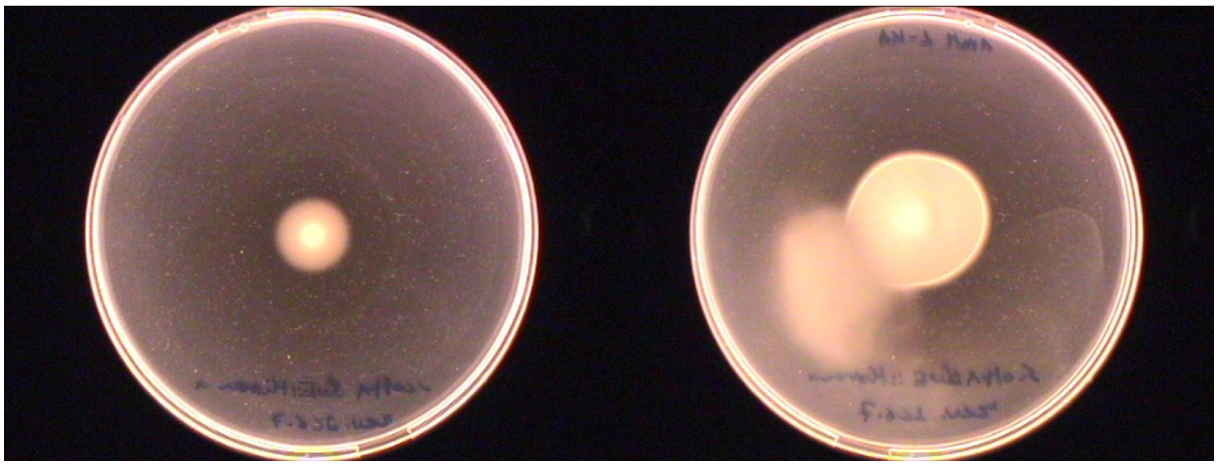

List of publications

Rogiers G, Kebede BT, Van Loey A, Michiels CW. Membrane fatty acid composition as a determinant of *Listeria monocytogenes* sensitivity to trans-cinnamaldehyde. Res Microbiol 2017;168:536–46. doi:10.1016/j.resmic.2017.03.001

Feyaerts J, Rogiers G, Corthouts J, Michiels CW. Thiol-reactive natural antimicrobials and high pressure treatment synergistically enhance bacterial inactivation. Innov Food Sci Emerg Technol 2015;27:26–34.